Investigation of branched and linear polymers as oral delivery systems of antimalarial drugs

Elisabet Martí Coma-Cros

INVESTIGATION OF BRANCHED AND LINEAR POLYMERS AS ORAL DELIVERY SYSTEMS OF ANTIMALARIAL DRUGS

Elisabet Martí Coma-Cros

Cover design by Mar Martí Coma-Cros

'*Stories matter. Many stories matter. Stories have been used to dispossess and to malign, but stories can also be used to empower and to humanize. Stories can break the dignity of a people, but stories can also repair that broken dignity… When we reject the* ***single story****, when we realize that there is never a single story about any place, we regain a kind of paradise*.' Chimamanda Ngozi Adichie

There is never a single story, and the cover is one example of it.

Tesi Doctoral

UNIVERITAT DE BARCELONA

FACULTAT DE FARMÀCIA I CIÈNCIES DE L'ALIMENTACIÓ

Programa de doctorat

BIOTECNOLOGIA

Títol de la tesi

INVESTIGATION OF BRANCHED AND LINEAR POLYMERS AS ORAL DELIVERY SYSTEMS OF ANTIMALARIAL DRUGS

Tesi presentada per ELISABET MARTÍ COMA-CROS per optar al títol de doctora per la Universitat de Barcelona

Director de la Tesi

DR. XAVIER FARNÀNDEZ BUSQUETS

Tutor de la Tesi

DR. SANTIAGO IMPERIAL RODENAS

JULY 2019

INVESTIGATION OF BRANCHED AND LINEAR POLYMERS AS ORAL DELIVERY SYSTEMS OF ANTIMALARIAL DRUGS

Àvia, tu sempre havies volgut tenir un/a “doctor/a” a la familia. Ara en tindràs una…

TABLE OF CONTENTS

Malaria is an infectious disease that affects nearly half of the population in 90 countries around the world. In 2017 it was estimated that there were 219 million cases and 435,000 deaths disproportionately distributed worldwide. Indeed, 92 % of malaria cases and 93 % of malaria deaths occur in Africa, while the remaining of the cases are distributed among South East-Asia, Eastern Mediterranean, Western Pacific, and the Americas. Vast global efforts and large economic investments have been made to reduce, control and eliminate malaria, resulting in a great reduction of the incidence in the last two decades. Nevertheless, malaria remains a global public health issue. Actually, malaria in humans is caused by an intracellular protist which has an extremely complicated live cycle that occurs within two hosts, the human and the *Anopheles* vector. There are five parasite species of the genus *Plasmodium* capable to infect humans *P. ovale*, *P. malariae*, *P. knowlesi*, *P. vivax* and *P. falciparum*, the latter being responsible for the majority of the morbidity and mortality of this disease. Malaria is a treatable disease, however antimalarial drugs must cross at least three sequential membranes (EPM, PVM and PPM) in order to enter the intracellular parasite and reach appropriate therapeutic concentrations; reason why they required drug delivery systems (DDSs). In fact, nano-DDSs have shown to have a positive effect on disease treatment providing solutions to solubility, pharmacokinetics, target selectivity, and/or protection against degradation, resulting in a drug half-life increased. The aim of this thesis was to characterize different polymeric nanocarrier, branched or dendrimeric (DHP-bMPA and HDLDBC-bGMPA) and linear polyamidoamines (PAAs) (AGMA1, ISA1, ISA23 and ARGO7), as oral drug delivery systems. Results obtained performing *in vitro* experiments demonstrated that PAAs and dendrimers have low unspecific toxicity, no hemolitic activity, specific pRBCs targeting and drug encapsulation capacity. Furthermore, PAAs displayed slow degradation, affinity to parasite proteins, which could explain the preferential binding to pRBCs, and intake by macrophages, indicating PAAs potential to treat other intracellular parasitic disease like Leishmaniasis. Additionally, dendrimers that form spontaneous micellar carrier, and bind to merozoites, showed an intake by HUVEC cells in different location, which could be further investigated to treat as well other disease. On the other hand, encapsulated drugs with the two types of polymers showed optimal *in vivo* capacity to inhibit *Plasmodium* growth after i.v or oral administration. Moreover, when PAA-FITC where given to female mosquitoes' fluorescence was observed in the midgut and in the insect's tissues. In conclusion, the date showed in this thesis work presented the branched and the linear polymers investigated as a versatile platform for the encapsulation of orally administrated antimalarial drugs, for the direct administration of antimalarial to mosquitoes, and as potential carriers for the treatment of other parasitic diseases.

La malària és una malaltia infecciosa que afecta gairebé a la meitat de la població de 90 països d'arreu del món. El 2017 s'estima que va provocar 219 milions de casos i 435.000 morts, el 92% de casos i el 93% de morts es produïren a l'Àfrica. Els darrers anys s'han fet grans esforços globals i inversions econòmiques per reduir, controlar i eliminar la malària, cosa que ha comportat una gran reducció de la incidència en els últims 20 anys. No obstant això, aquesta malaltia continua sent un problema de salut pública global. En humans és causada per un protozou del gènere *Plasmodium* i concretament se'n coneixen cinc espècies diferents. Però la causant de més morbiditat i mortalitat és *P. falciparum*. La malaltia en si és tractable, però els fàrmacs antipalúdics han de creuar com a mínim tres barreres seqüencials per tal d'arribar al paràsit a una concentració suficientment elevada. Per això aquests principis actius requereixen sistemes d'administració de fàrmacs que han demostrat tenir efectes positius. L'objectiu d'aquesta tesi ha estat caracteritzar polímers ramificats (DHP-bMPA i HDLDBC-bGMPA) i lineals (AGMA1, ISA1, ISA23 i ARGO7) per l'administració oral d'antipalúdics. Els resultats obtinguts realitzant experiments *in vitro* i *in vivo* han demostrat que tots dos tipus de polímers tenen baixa toxicitat inespecífica, no tenen activitat hemolítica, tenen especificitat per pRBCs i bona capacitat d'encapsulació. Els PAAs han demostrat tenir una degradació lenta, afinitat per proteïnes del paràsit, i capacitat per entrar dins de macròfags, una propietat interessant per tractar altres malalties. A més a més els ramificats s'uneixen a merozoites i entren en macròfags. D'altra banda els medicaments encapsulats amb qualsevol dels dos tipus de polímers han mostrat una capacitat òptima *in vivo* per inhibir el creixement del *Plasmodiuim* després de l'administració i.v o oral. Per últim, PAAs-FITC administrats a mosquits femelles, s'han pogut observar a l'intestí i altres teixits. Per tant es pot concloure, que les dades recollides en aquesta tesi demostren que tant polímers ramificats com lineals són una plataforma versàtil per a l'encapsulació de medicaments antipalúdics per ser administrat via oral, per a l'administració directa a mosquits, i potencials nanocarriers pel tractament d'altres malalties parasitàries.

ACN	Acetonitrile
ACT	Artemisinin combination therapy
AFM	Atomic force microscopy
ARDS	Acute respiratory syndrome
ATR	Attenuated total reflectance
bis-GMPA	2,2'-bis(glycyloxymethyl)propionic acid
bis-MPA	2,2'-bis(hydroxymethyl)propionic acid
BC	Block copolymer
BSA	Bovine serum albumins
BS(r)	Blood stage ring
BS(l)	Blood stage lates
CB	Coupling buffer (5 mM EDTA, 50 mM Tris-HCl, pH 8.5)
CL	Cutaneous leishmaniasis
CLAG3	Cytoadherence-linked asexual gene 3
CMC	Critical micelle concentration
CNT	Carbon nanotubes
CQ	Chloroquine
COPOP	Cobalt-porphyrin-phospholipid
CSP	Circumsporozoite protein
CUAAC	Copper azide-alkyne cycloaddition
D	Day
DCL	Diffuse cutaneous leishmaniasis
DDS	Drug delivery system
DCM	Dichloromethane
DDT	Dichlorodiphenyl trichloroethane
DHA	Dihydroartemisinin
DHFR	Dihydrofolate reductase
DHP	Dendronixed hyperbranched polymer
DHPS	Dihydropteroate synthethase
DMF	Dimethylformamide
DNA	Deoxyribonucleic acid
DP	Dendronized polymer
DTT	1,4-Dithiothreitol
EE	Encapsulation efficiency
ELISA	Enzyme-linked immunosorbent assay
EMA	European Medicine Agency
EPM	Erythrocyte plasma membrane
ER	Endoplasmic reticulum
FACS	Fluorescent-assisted cell sorting
FBS	Foetal bovine serum
FITC	Fluorescein isothiocyanate
FDA	Food and Drug Administration
FTIR	Fourier transformed infrared
FV	Food vacuole
G	Generation
Gt	Gametocytes
GAG	Glycosamine glycan
GBP130	Glycophorin-binding protein 130
GIT	Gastro intestinal tract
GSH	Reduced glutathione
GSK	Glaxo Smith Kline

GSSG	Oxidazed glutathione
GUV	Giant unilamellar vesicles
G6PD	Glucose-6-phosphate dehydrogenase
HDLDBC	Hybrid dendritic-linear-dendritic block copolymer
His-TAG	Histidine tagged
HP	Hyperbranched polymer
HRP2	Histidine-rich protein 2
HSP	Heat shock proteins
HUVEC	Human umbilical vein endothelial cells
IC_{50}	Half maximal inhibitory concentration
IFAT	Immunofluorescence antibody test
iLP	Immuniliposome
IPTi	Intermittent preventive treatment in infants
IPTp	Intermittent preventive treatment in pregnancy
IRS	Indoor residual sprays
ITN	Insecticide-treated *bed* net
KAHRP	Knob associated histidine rich protein
LC-MS/MS	Liquid chromatography-tandem mass spectrometry
LCL	Localised cutaneous leishmaniasis
LLIN	Long-lasting infected net
LS	Liver stage
L-AmB	Liposomal amphotericin B
LP	Liposome
LUV	Large unilamelar vesicles
MALDI	Matrix-assisted laser desorption/ionization
MC	Maurer's clefts
MDA	Mass drug administration
MDGS	Millenium Development Goals
ML	Mucocutaneous leishmaniasis
MLV	Multilamellar vesicles
MPS	Mononuclear phagocytic system
MSP1	Merozoite surface protein 1
MTD	Maximum tolerated dose
MW	Molecular weight
NMR	Nuclear Magnetic Resonance
NNN	Novy-MacNeal-Nicolle medium
NP	Nanoparticle
NPP	New permeation pathways
O	Oocysts
OK	Ookinetes
PAA	Poly(amido-amines)
PABA	P-aminobenzoic acid
PAGE	SDS-polyacrylamide gel electrophoresis
PAMAM	Polyamidoamines dendrimers
PBS	Phosphate buffer saline
PBS-T	0.1 % Tween 20 in PBS
PCR	Polymerase chain reaction
PEG	Poly(ethyleneglycol)
PEO	Poly(ethylene oxide)
PfEMP1	*P. falciparum* erythrocyte membrane protein 1
PfPR	*P. falciparum* parasite rate
PHEM	240 mM pipes, 100 mM Hepes, 8 mM $MgCl_2$, 40 mM EGTA, pH 6.4
pLDH	Plasmodium lactate dehydrogenase

PLGA	Poly(lactide-co-glycolide acid)
PLL	Poly-L-lysine
PMMA	Poly(methyl methacrylate)
PMOXA-b-PDMS-b-PMOXA	Poly(2-methyl-2-oxazoline)-*block*-poly(dimethylsiloxane)-*block*-poly(2-methyl-2-oxazoline)
POCT	Point-of-care test
PPI	Poly(propylene imine)
PPLP4	Perforin-like protein 4 (PPLP4)
PPM	Parasite plasma membrane
PQ	Primaquine
pRBC	*Plasmodium* infected red blood cell
PSAC	Plasmodial surface anion channel
PTEX	Plasmodium translocon of exported proteins
PV	Parasitophorous vacuole
PVM	Parasitophorous vacuole membrane
Py17X	*P. yoelii yoelii 17X*
Py17XL	*P. yoelii yoelii 17X* lethal
Py17XNL	*P. yoelii yoelii 17X* non-lethal
QBC	Quantitative buffy-coat
QN	Quinacrine
RB	Reaction buffer (0.1 M sodium phosphate, 1 mM EDTA, pH 8.0)
RBC	Red blood cell
RDT	Raid diagnostic test
RER	Rough endoplasmic reticulum
RGD	Argine-glycine-aspartic acid
RHO	Rhodamine
RMP	Rodent malaria parasite
ROS	Reactive oxygen species
RPMI	Roswell Park Memorial Institute
RT	Room temperature
SDS	Sodium dodecyl sulfate
SEC	Size exclusion chromatography
SEM	Scanning electron microscopy
-SH	Sulfhydryl group
SMC	Seasonal malaria chemoprevention
SNAP	Spontaneous nanoliposome-antigen particleization
SP	Sulfadoxine - pyrimethamine
SUV	Small unilamellar vesicles
TBS	TBS-T without Tween
TBS-T	0.05 % Tween 20, 150 mM NaCl, 20 mM Tris-HCl, pH 7.5
TBTA	Tris[(1-benzyl-1H-1,2,3-triazol-4-yl)methyl]amine
TBVS	Transmission blocking vaccines
TEM	Transmission electron microscopy
THF	Tetrahydrofuran
TMS	Tetramethylsilane
TVN	Tubulovesicular network
UNICEF	United Nations International Children's Emergency Fund
VL	Visceral leishmaniasis
WHO	World Health Organization
4-AQs	4-Aminoquinolines
8-AQs	8-Aminoquinolines

INTRODUCTION

OBJECTIVES

RESULTS

DISCUSSION

CONCLUSIONS

REFERENCES

INTRODUCTION

1.1. EPIDEMIOLOGY

Malaria is an infectious disease that affects nearly half of the population in 90 countries around the world. In 2017 it was estimated that there were 219 million cases and 435,000 deaths disproportionately distributed worldwide. Indeed, 92 % of malaria cases and 93 % of malaria deaths occur in Africa, while the remainder of the cases are distributed among South East-Asia, Eastern Mediterranean, Western Pacific, and the Americas (World Health Organisation, 2018). About two thirds of deaths due to malaria involve children under five years old (Unicef, 2007), who are particularly susceptible to infection in areas with high malaria transmission due to frequent exposure and immature immunological protection (Wells, Alonso and Gutteridge, 2009; Tizifa *et al.*, 2018).

Plasmodium is a protists parasite of a genus which includes those causing malaria and is vectored by mosquitoes of the *Anopheles* genus. The female mosquito bites a human host between dusk and dawn every few days for egg development (Lardeux *et al.*, 2008). During the blood meal, saliva is injected containing anaesthetic, anti-coagulant and the parasite which develops in the human host (Paul and Brey, 2003).

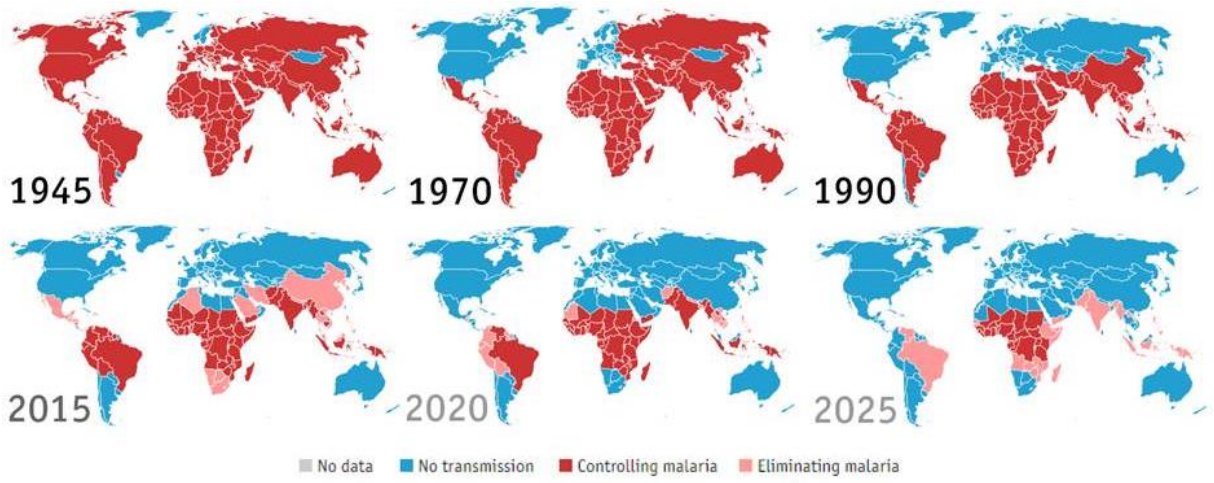

Figure 1. Global distribution of malaria between 1945 and 2025 (expected). In red, countries where malaria is under control, and in pink, countries where malaria is being eliminated. Figure adapted from The Economist: Oct 14th 2015 by S.C., J.F. and the Data Team.

Vast global efforts and large economic investments have been made worldwide to reduce, control and eliminate malaria, resulting in a great reduction of the incidence in the last 20 years (Figure 1) from 262 million cases and 839,000 deaths in 2000 (World Health Organization, 2015b) to the present 219 million cases and 435,000 deaths. Nevertheless, malaria remains a global public health issue (WHO, 2015).

Malaria is also known as “the epidemic of the poor”. The disease is largely determined by climate and ecological factors and not poverty *per se*. Nonetheless, the greatest impact of the disease is seen

amongst the poorest. The vicious cycle (Figure 2) between malaria and poverty was first described in 1957 by the Nobel prize of Medicine T.H. Weller who stated that "It has long been recognized that a malarious community is an impoverished community" (Gallup and Sachs, 1998), suggesting the two-sided causality between low-income countries and malaria (Teklehaimanot and Mejia, 2008). Poverty preserves the conditions where malaria thrives; for example, poor communities have little access to vector control or adequate drugs. Indeed, one of the main causes of death by malaria is the use of counterfeit drugs (Karunamoorthi, 2014). Additionally, malaria impedes economic growth and keeps communities in poverty (Sachs and Malaney, 2002) by reducing the income of the household. As shown in Figure 1, malaria was first eliminated in the richest countries of the African continent.

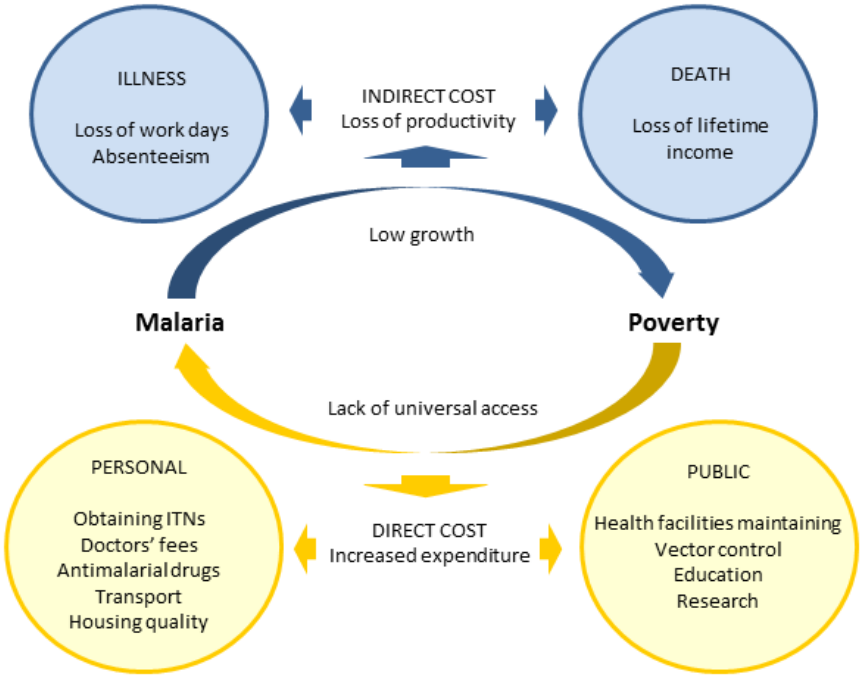

Figure 2. Vicious cycle between malaria and poverty and some of the direct and indirect factors linked to this cycle (Sachs and Malaney, 2002; Teklehaimanot and Mejia, 2008; Karunamoorthi, 2014).

1.2. PATHOPHYSIOLOGY

Malaria in humans is caused by five species of the intracellular protist *Plasmodium*, namely *P. ovale*, *P. malariae*, *P. knowlesi* (N. J. White, 2008), *P. vivax* and *P. falciparum*, the latter being responsible for the majority of the morbidity and mortality of this disease. Although there are many structural differences among *Plasmodium* species, they share many morphological features.

At present, *P. ovale* has a minor impact on public health and receives little attention in malaria research. Nonetheless, this species causes tertian malaria, and can induce relapses and severe symptoms such as acute respiratory distress syndrome (ARDS) and even death (Lau *et al.*, 2013). Malarial relapses due to *P. ovale* have yet to be confirmed, making further studies necessary to analyse malaria from all points of view. On the other hand, two sympatric species, *P. ovale curtis* and *P. ovale*

wallikeri, have been identified by molecular methods, both being common in sub-Saharan Africa, Oceania and Asia (Groger *et al.*, 2017).

The incidence of *P. malariae* malaria is significantly lower than that of *P. falciparum*, despite its wide distribution throughout the tropics and subtropics (Sutherland, 2016). The slow growth of this parasite enables it to survive in humans at low parasitemia for decades, and can cause nephrotic syndrome and anaemia (Langford *et al.*, 2015).

The most recently discovered parasite is *P. knowlesi*, which is a major cause of malaria in Malaysia (N. J. White, 2008). *P. knowlesi* has zoonotic transmission, a unique characteristic among *Plasmodium* spp. However, it is also able to infect humans by the bite of a mosquito infected by forest-dwelling macaques (World Health Organization, 2015b). Microscopically, trophozoites and schizonts are hard to differentiate from *P. malariae* and may be misdiagnosed (Barber *et al.*, 2017), leading to treatment failure.

The dominant human parasite species with the highest impact on public health are *P. falciparum* and *P. vivax* (World Health Organisation, 2017). *P. vivax* is the most widely distributed (World Health Organization, 2015b), being predominant outside Africa and having low endemicity in Africa (Howes *et al.*, 2016). *P. vivax* has the capacity to produce hypnozoites, a dormant intracellular liver stages, which are safe from immune attack during long mosquito-free cold seasons, which cause relapse weeks and even months after the initial infection, presenting the normal malaria symptoms of fever, chills, nausea, vomiting, and myalgia (Baird, 2004), with severe and fatal infection having been reported (Howes *et al.*, 2016).

The most prevalent malaria parasite in sub-saharan Africa is *P. falciparum*, accounting for 99.7 % of the cases in 2017 (World Health Organisation, 2018). This parasite can persist in the human host for long periods of time, causing asymptomatic cases characterized by a temperature less than 37.5 °C and the presence of the parasite in peripheral thick blood films (Gbalégba *et al.*, 2018). Patients carrying *P. falciparum* represent a potential reservoir for sustained transmission and are, therefore, an important challenge for the health system and for malaria elimination programmes (Ashley and White, 2014).

1.3. CLINICAL SYMPTOMS AND DIAGNOSIS

Malaria clinical symptoms appear after 7 or more days of incubation. The most common non-specific symptoms are acute fever and anaemia, and less commonly, headache, fatigue, chills, and sweating, resulting in massive misuse of antimalarial drugs. Malaria is preventable and curable, when diagnosed in time and treated. Otherwise it is associated with increased risk of severe disease and mortality, making effective diagnosis essential. Indeed, pregnant women and children, who are the two most vulnerable populations to suffer from severe malaria, do not show the classical symptoms, making correct diagnosis difficult (UNITAID, 2014).

The symptomatology of malaria is generally divided into uncomplicated malaria, characterized by the presence of the typical symptomatology and a positive parasitological test, and severe malaria, with the presence of potentially fatal symptoms such as impaired consciousness, multiple convulsions, severe anaemia, pulmonary oedema or shock (World Health Organization, 2015a). Organ failure and cerebral malaria are two typical symptoms of severe malaria caused by the accumulation of parasites in different organs or in brain capillaries leading to coma and eventually death (Carlson, 1993).

At present, the techniques routinely used for the diagnosis of malaria include microscopy (detection of the parasite and identification of the species) and rapid diagnostic tests (RDTs) (detection of antigen by immunochromatography). Microscopy detection was introduced about 100 years ago (Bailey *et al.*, 2013) while RDTs were implemented in the 1990s. Since then none of the new diagnostic tools such as serology, quantitative buffy-coat (QBC) concentration, or nucleic acid amplification techniques including polymerase chain reaction (PCR) and isothermal amplification (Krampa *et al.*, 2017) have been marketed or widely used.

Giemsa stain microscopy techniques are highly sensitive and specific and require highly skilled health workers and specific infrastructure. On the other hand, the two most commonly studied RDTs able to identify histidine-rich protein 2 (HRP2) and *Plasmodium* lactate dehydrogenase (pLDH), are specific, simple to perform, portable and disposable. Nonetheless, RDTs cannot replace microscopy since they are not quantitative and species differentiation is limited (Bell *et al.*, 2016). While both techniques are inexpensive, new and improved, highly sensitive techniques are essential since none of the current methods are able to detect submicroscopic densities (Hopkins *et al.*, 2007).

1.4. *PLASMODIUM FALCIPARUM*

Plasmodium falciparum is one of the two most relevant *Plasmodium* species. It is a member of the Apicomplexa family characterised by obligate intracellular single-celled parasites and the presence of an organelle call apicoplast as well as the apical complex. *Plasmodium* spp*.* and the apicomplexa *Toxoplasma gondii* have a number of unique mechanisms of host cell entry, division, motility and host cell manipulation thanks to the apicoplast (Seeber and Steinfelder, 2016).

1.4.1. Life cycle

The three main elements necessary for malaria infection are: a human host (or other vertebrate), a mosquito (invertebrate host) and a parasite.

In the human the cycle starts with a bite of a mosquito during which sporozoites are injected into the host dermis. Sporozoites are one of the two transmission stages of the cycle. Within 30 minutes the parasite enters the liver and invades hepatocytes, and thereafter replicates and produces thousands of new merozoites inside merosomes. Merosomes are between 12 and 18 µm in size, exit the liver intact and release around 100 – 200 merozoites (Baer *et al.*, 2007) into the blood stream, starting the erythrocytic cycle 5 to 10 days post infection. Merozoites infect red blood cells (RBCs), grow and divide from ring to trophozoite and then mature into schizonts. Schizonts contain new merozoites which infect healthy RBCs and perpetuate the asexual blood-stage cycle also known as the erythrocytic cycle. Depending on stress conditions, a small amount of these merozoites are committed to gametogenesis or sexual differentiation, producing gametocytes from stage I to V, the second transmission stage. These are then uptaken by the mosquito during a blood meal.

In the midgut of the mosquito, female and male gametocytes progress to macrogamete and microgamete, respectively. Fertilization of a macrogamete by a microgamete results in the formation of a zygote, which differentiates into a motile ookinete that moves through the midgut epithelium and forms an oocyst from which sporozoites are released and migrate to the salivary glands ready to infect

a new human host with the next bite (Figure 3) (Portugal, Drakesmith and Mota, 2011; Biamonte, Wanner and Le Roch, 2013).

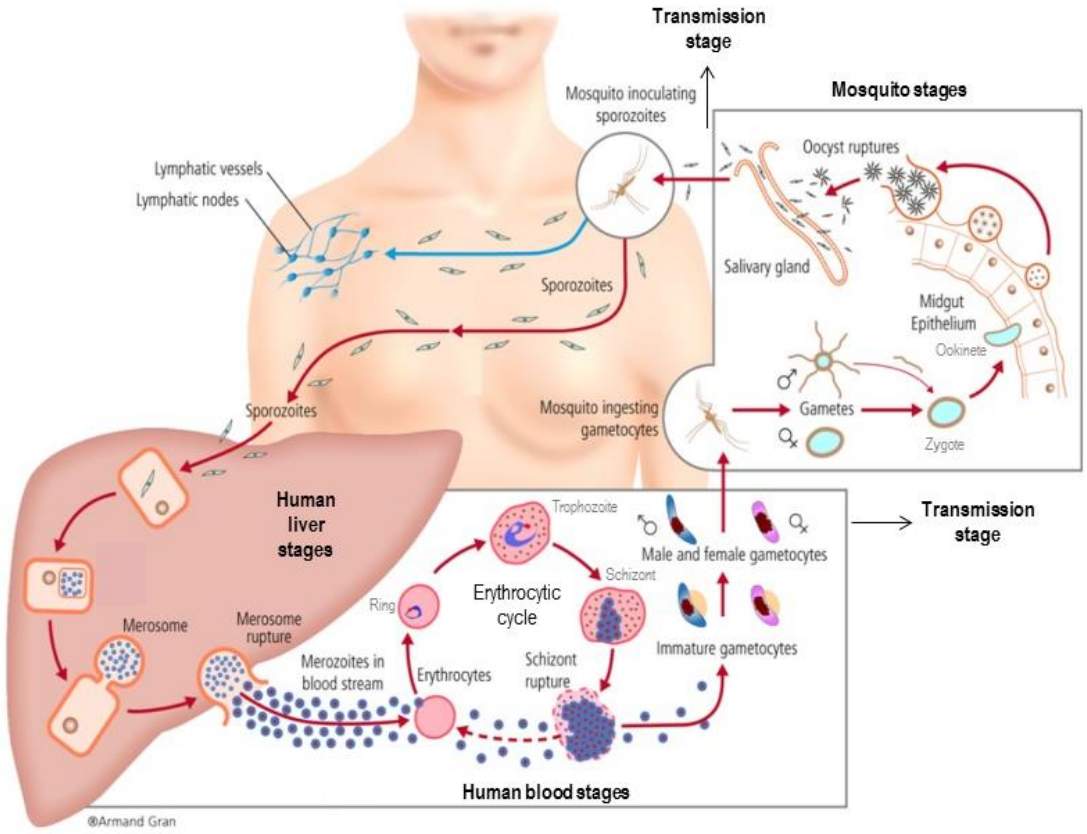

Figure 3. *P. falciparum* life cycle which takes place in two different hosts, the human and the mosquito. Asexual stages are present in the liver and in the blood stream and sexual stages are divided between the two hosts starting at the gametocyte stage in the human and evolving to sporozoites in the mosquito. Figure adapted from (García-Basteiro, Bassat and Alonso, 2012).

1.4.2. Erythrocytic stages (asexual proliferation)

During asexual proliferation malaria parasites invade and multiply inside RBCs. A complex 48 h development occurs following three successive morphological stages during which an average of 20 daughter merozoites are formed (Figure 4). Merozoites egress from *Plasmodium* infected red blood cells (pRBCs) reinvading healthy cells to preserve progression (Paul and Brey, 2003). Thereafter, clinical manifestations begin along with structural, biochemical and functional changes, mostly in the pRBC membrane.

Ring stage

pRBCs with ring stages (Figure 4 A)adopt the form of biconcave or cup shaped discs which circulate freely in the bloodstream and present mild modifications of adhesion and/or deformability (Buffet *et al.*, 2018). After penetrating fresh RBCs, merozoites form by invagination of the parasitophorous

vacuole (PV) and the parasitophorous vacuole membrane (PVM), which surrounds the parasite throughout its lifetime within the RBC (Maier *et al.*, 2009). A tubulovesicular network (TVN) is formed in the erythrocyte cytoplasm emerging from the PVM, including Maurer's clefts, confirming the transport of proteins outside the parasite plasma membrane (PPM) and PVM. The erythrocyte membrane is modified and small electron-dense protusions called knobs start to appear. The onset of pRBC modifications are a major task event in this stage confirmed by a peak in protein expression in late rings and early trophozoites (Marti *et al.*, 2004).

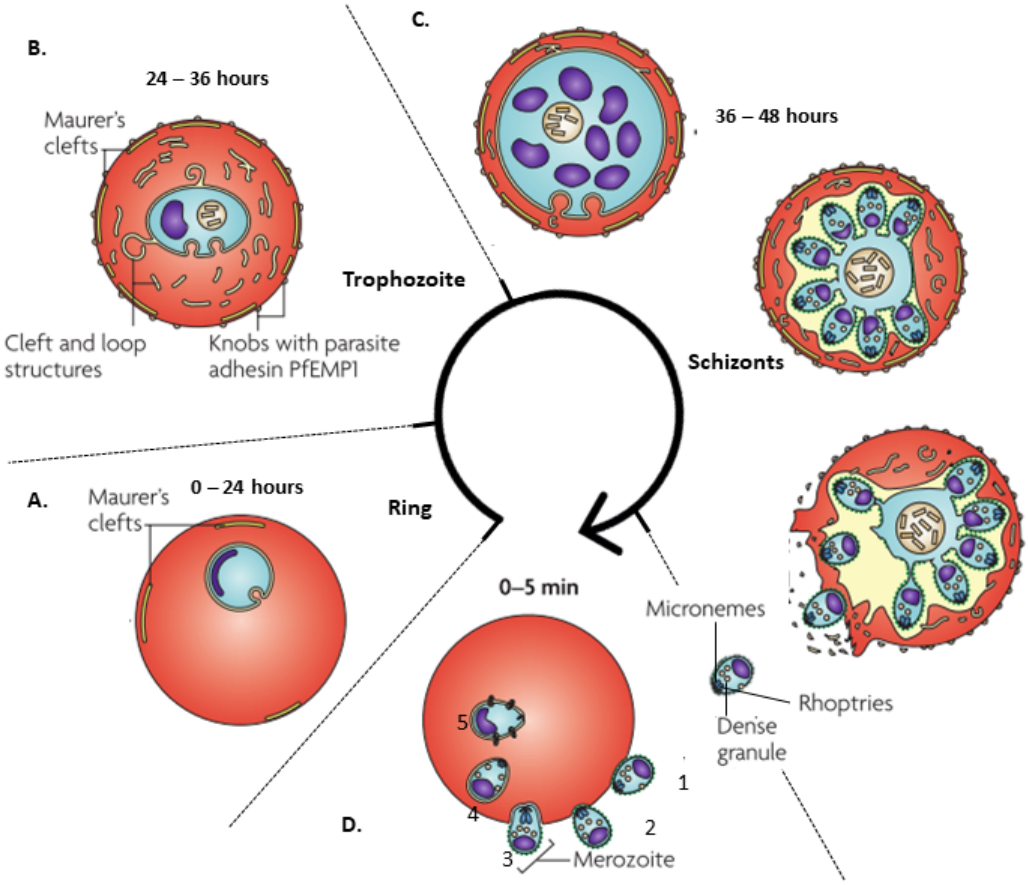

Figure 4. ***P. falciparum*** **erythrocytic life cycle** divided into four different stages, **(A) ring** (from 0 to 24 h), **(B) trophozoite** (from 24 to 36 h), **(C) schizonts** (from 36 to 48 h) and **(D) merozoites** (from 0 to 5 min). Figure adapted from (Maier *et al.*, 2009).

Trophozoite stage

Rings eventually change shape and grow rapidly to a more rounded form to become trophozoites (Figure 4 B) (Bannister *et al.*, 2000). Rings and trophozoites feed on the RBC and progressively modify the erythrocyte cytoplasm and membrane by exporting parasite proteins. Deformability and adhesion to endothelial cells, blood cells, platelets and other pRBCs, are gradually altered, reducing peripheral blood circulation and increasing sequestration in small vessels (Buffet *et al.*, 2018). Cytostomes are endocytic invaginations surrounded by PPM and PVM which fuse with the food vacuole (FV), and have two functions: ingest most of the pRBC cytosol and degrade approximately 80 % of the haemogoblin,

a key survival process in order to provide the growing parasite with sufficient space as well as amino acids. Nontoxic hemozoin crystal, the degradation product of haemoglobin, is formed from this stage onwards and can be easily observed by microscopy (Goodyer *et al.*, 1997; Bakar *et al.*, 2010).

Schizont stage

Trophozoites and schizonts (Figure 4 C) are considered mature cytoadherent stages without profound morphological changes; nevertheless, schizonts undergo repetitive nuclear divisions to become multinucleated. This endomitotic nuclear division occurs together with the preparation for merozoite formation, which involves the proliferation of rough endoplasmic reticulum (RER), the formation of free ribosomes and mitochondria, and the multiplication of plastids (Bannister *et al.*, 2000). Simultaneously, the internal cavity of the late trophozoite starts to disappear and FV moves to a central position allowing the parasite to grow and generate up to 32 daughter merozoites. Meorozoite elements start to assemble, beginning with the apical organelle. Finally, the Maurer's cleft collapses when there is clear merozoite segmentation (Grüring C1, Heiber A, Kruse F, Ungefehr J, Gilberger TW, 2011), a sign indicating the onset of active host dismantellation. In fact, there is a weakening and deconstruction of the host erythrocyte cytoskeleton by protein proteolysis and other proteases, resulting in the destruction of the RBC membrane. This systematic preparation takes place from 15 to 20 h before egression, even though egression is observed within a few seconds (Millholland *et al.*, 2011).

Merozoite stage

Merozoites are polarized cells which have the shape of a lemon and are around 1 µm in size. They are briefly extracellular and thus exposed to host antibodies. Each merozoite contains all the necessary elements to escape from the remnants of its host pRBC, find and attach to a new RBC, invade it and rapidly restart feeding (Bannister *et al.*, 2000). Relevant invasion proteins can be found in two locations, either on the surface or inside organelles. These organelles can be dense granules, rhoptries, or micronemes; the latter two being localized at the apical end (Cowman *et al.*, 2017).

The invasion process, which takes place from 0 to 5 minutes, involves the molecular interaction of numerous host receptors and parasite ligands and is divided into five different phases (Figure 4 C) (Maier *et al.*, 2009; Srinivasan *et al.*, 2011; Cowman *et al.*, 2017).

1. Primary attachment: random, reversible and weak initial contact involves micronemes and parasite receptor-RBC ligand interactions.
2. Reorientation and junction formation: once the RBC is recognised as being competent, the merozoite redirects itself to bring the apical end into close apposition with the RBC surface, triggering a tight high-affinity junction formation between the merozoite and the RBC. Then the rhoptry content is secreted into the RBC, facilitating invasion.
3. Invasion: the merozoite then moves through the tight junction as its actin-myosin motor and parasite surface proteins pull it into the RBC. In coordination with entry, the PV and its membrane form, incorporating lipids from the RBC membrane.
4. Membrane sealing (shedding of surface proteins): the surface coat is shed at the moving junction by a serine protease and upon reaching the posterior pole; the adhesive proteins at

the junction are proteolytically removed, facilitating resealing of the membrane (Cowman and Crabb, 2006).

5. Completion of invasion: remodelling of the host cell begins immediately after the parasite is inside.

1.4.3. Host red blood cells

Red blood cells are biconcave cells around 7 µm in size and have several remarkable characteristics. They do not contain nucleus or organelles for biosynthesis and are highly viscous internally, being therefore extremely elastic. Elasticity is determined by the intrinsic properties of the proteins and lipids (cholesterol and phospholipids) forming the membrane, and the 40 % of excess surface area compared to a sphere of the same volume. Moreover, RBCs can reversibly contract, allowing their passage through capillaries 3 to 5 µm across; however, this ability is lost as the cell ages. RBCs remain in the blood circulation for around 120 days (Mohandas and Gallagher, 2018; Schrier, 2018). The erythrocyte plasma membrane (EPM) is anchored to a 2-dimensional elastic network of skeletal spectrine-actin molecules and contains around 50 transmembrane proteins which have diverse functions. Some of these functions are transportation, adhesion and receptor signalling, as well as others not yet known. The plasma membrane is a key element for molecule transmembrane trafficking (anions, water, glucose, urea, among others), protein antigen exposure and cell structure definition (Mohandas and Gallagher, 2018).

In order to facilitate parasite survival, modifications of the host cell membrane and permeability start within 12 minutes post invasion (Proellocks *et al.*, 2016). This process takes place by the trafficking of hundreds of effector proteins which induce major changes in the structure, composition and function of the host cell. In addition, nutrients are taken up from blood plasma, and the immune system is evaded (Desai and Miller, 2015).

Parasite proteins are secreted beyond their own plasma membrane by vesicle-mediated selective transport. Proteins are transferred from the endoplasmic reticulum to various locations in the pRBC, assisted by the *Plasmodium* translocon of exported proteins (PTEX) located in the PVM (Figure 5). In fact, proteins need to be unfolded to transit PTEX, and are then folded again to reach their destination. This process is regulated by molecular chaperones such as heat shock proteins (HSPs). HSP70, which is associated with the co-chaperon HSP40 referred to as the DnaJ protein, and HSP90 facilitate the assembly of proteins into higher order complexes, the unfolding of protein structures and the translocation of proteins across membranes (Proellocks *et al.*, 2016). A number of proteins, known as exportome, have been identified and characterised and many follow this secretory path even though they have different destinations and functions (Maier *et al.*, 2009). For example, *P. falciparum* erythrocyte membrane protein 1 (PfEMP1) is inserted into the parasite plasma membrane, whereas glycophorin-binding protein 130 (GBP130) remains as a soluble protein in the cytoplasm (Koning-ward *et al.*, 2016).

Host cell membrane transformation

The main aim of host cell transformation is to establish a long lasting infection; this is achieved by parasite protein exportation and evasion of the immune system. pRBCs avoid the immune system with

two strategies: antigenic variation which allows the pRBCs to remain invisible to immune cells, and sequestration in microvessels, to escape spleen clearance. Sequestration is facilitated by cytoadhesion, increasing rigidity, and reorganization of the cytoskeleton membrane.

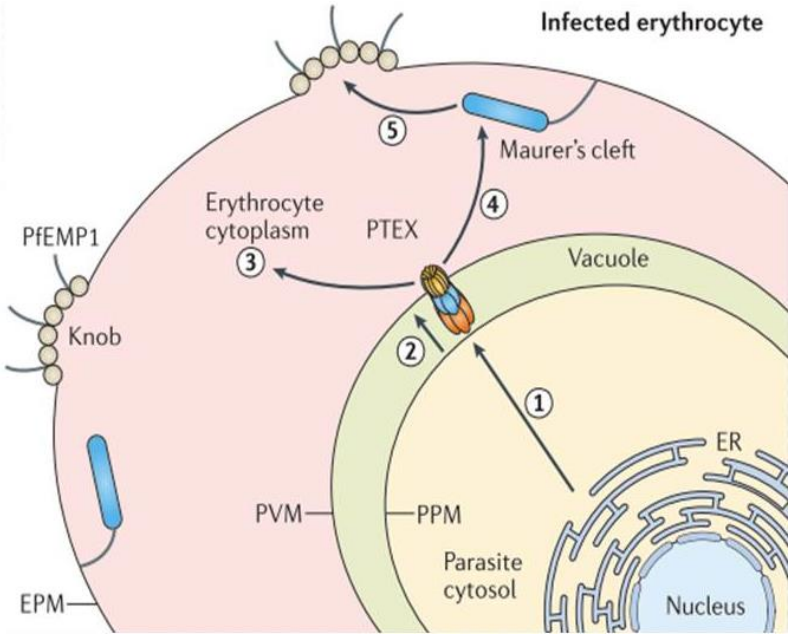

Figure 5. Schematic model of the five steps of parasite protein exportation into the erythrocyte cytoplasm. The endoplasmic reticulum (ER) recognises and processes export proteins which are trafficked across the parasite plasma membrane (PPM) (1). The *Plasmodium* translocon of exported proteins (PTEX) translocates them across the parasitophorous vacuole membrane (2) to three different final destinations: the erythrocyte cytoplasm (3), Maurer's clefts (4), and the erythrocyte plasma membrane (EPM) and membrane skeleton (5). Figure reproduced from (Koning-ward *et al.*, 2016).

Cytoadhesion is mediated by the presence of knob-like protrusions 20 h post-invasion, presenting a high concentration of the cytoadherence promoter PfEMP1 (Figure 5), which interacts with surface receptors of the endothelial cells (Smith *et al.*, 2014). PfEMP1 is a multiple-gene protein family encoded by hyper variable genes known as *var*, each of which represents a different antigenic form. Moreover, when the parasite is in the erythrocytic cycle, it is capable of changing its antigenic profile by switching expression between different *var* genes, thereby enabling evasion of the human immune system (Guizetti, Scherf and Biologie, 2013). During the merozoite stage, evasion is also essential, which occurs by antigenic proteins, and the most relevant is the merozoite surface protein 1 (MSP1). MSP1 plays an important role in the primary attachment for RBC invasion and it is highly polymorphic, which results in the production of immunologically distinct merozoites within a single infected individual. Consequently, recognition of the merozoites by antibodies become difficult and immune system attack is evaded (Belachew, 2018). Simultaneously, the presence of a large number of knobs in the erythrocyte plasma membrane, which develop by the assembly of knob-associated histidine rich protein (KAHRP) into a structure linked to the erythrocyte skeleton, leads the pRBC to adapt a more spherical shape and stiffness (Lavazec, 2017). In addition, the formation of actin filaments that connect Maurer's clefts to the erythrocyte membrane skeleton in the area of the knobs, promotes

reorganisation of the cytoskeleton, enhancing pRBCs adhesiveness, a key *in vivo* process for survival in the host (Gilson *et al.*, 2017).

Increased permeability

A number of transport systems are endogenous in RBCs. Indeed, for certain solutes such as K^+ ions, amino acids and lactate, there is more than one alternative transport pathway. Parasite infection up-regulates these transport pathways and induces the creation of new permeation pathways (NPPs) in the plasma membrane (Kirk, 2001). NPPs have properties can discriminate solutes by size and charge, having a preference for anions (Ginsburg and Stein, 2005; Desai, 2014). As a result, pRBC permeation is increased to anions, some organic cations, sugars, amino acids, purines, vitamins, and inorganic monovalent ions, a strategy used by the parasite to adapt to the ionic environment inside the erythrocyte. Another important role of NPPs is waste disposal of toxic substances such as lactic acid and oxidized glutathione (GSSG). Lactic acid is the end product of glucose metabolisation by glycolysis, which is increased 40 to 100 fold in pRBCs. After being exported to the RBC cytosol, part of the GSSG is transformed into reduced glutathione (GSH) which protects the parasite against oxidative stress (Kirk, 2001). Improved permeability appears around 20 h post invasion (Staines, Rae and Kirk, 2000).

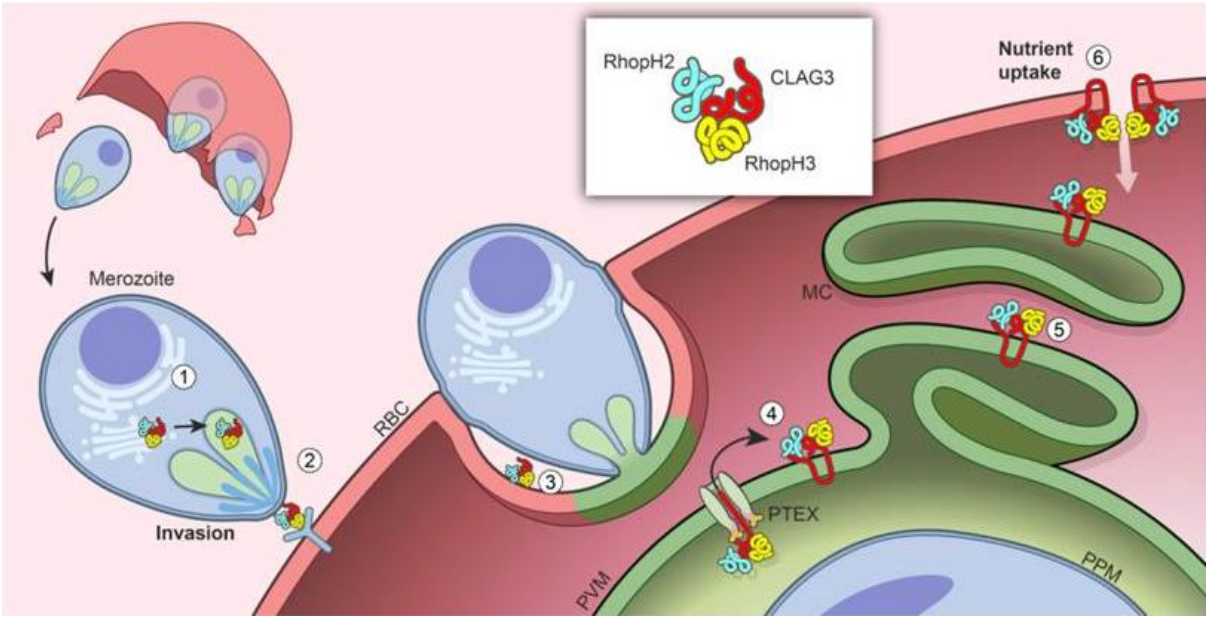

Figure 6. Trafficking model of the RhopH complex. Cotranslational assembly of the three-member RhopH (1). After merozoite egression, only RhopH3 contributes to invasion (2). The complex is then deposited in the PV (3), from where it is exported via PTEX (4) and trafficked via the Maurer's clefts (MC) (5) to the host RBC membrane. There, the complex determines nutrient uptake via PSAC (6). Figure reproduced from (Ito, Schureck and Desai, 2017).

Although knowledge of the different NPPs was previously provided by patch-clamp techniques (Desai, 2000), new techniques have contributed more in depth information on these pathways. To date only one molecular component, the cytoadherence-linked asexual gene 3 (CLAG3), has been implicated in the formation of a NPP (Koning-ward *et al.*, 2016), the plasmodial surface anion channel

(PSAC). Two rhoptry proteins, RhopH2 and RhopH3, are also involved in the formation of this channel and together with CLAG3 form the RhopH complex. This complex is synthesized in the schizont stage, located in merozoite rhoptries, and is delivered to healthy RBCs during invasion. The RhopH complex is then secreted into the PV and exported through PTEX to its final destination, that is the EPM, to form a new channel (Figure 6) (Ito, Schureck and Desai, 2017). There are around 1000 to 2000 copies of the PSAC voltage-dependent channel in each mature trophozoite, and they are implicated in the acquisition of parasite nutrients, thereby making PSAC essential for parasite survival (Chalapareddy and Desai, 2017).

More in depth characterisation of this specific channel for parasite survival, and likely others which remain to be found, would bring to light many molecules which could be targeted for therapeutic intervention against the malaria parasite.

1.4.4. Rodent models

Animal models are indispensable for malaria research. Nevertheless, the most adequate model has yet to be established. It has been suggested that humanized mice infected with *P. falciparum* and engineered to simulate humans at a cellular and molecular level could address the limitations of translating discoveries in non-human models to clinical applications (Pearson, Greiner and Shultz, 2008). However, this model is not ideal, and has a high rate of failure, low reproducibility of successful infection, and is expensive, due to the need for mice engrafted with human erythrocytes in the blood stream (Angulo-Barturen *et al.*, 2008; Arnold *et al.*, 2011).

A reliable, reproducible and affordable alternative are rodent malaria parasites (RMPs) which can provide relevant information on host defense and immunity mechanisms for all the stages of infection (Craig *et al.*, 2012). Four different species of RMPs which infect African rodents have been adapted to grow in the laboratory and used as *in vivo* malaria models: *P. yoelii, P. berghei, P. chabaudi and P. vinckei* (Carter and Diggs, 1977). In 2002 Carlton and colleagues (Carlton *et al.*, 2002) reported the genome sequence of *Plasmodium yoelii yoelii*, and since then further genomes have been described, demonstrating the high level of orthology (approximately 90 %) between RMP and human malarias in genome structure as well as in gene content, and thereby confirming the adequacy of the use and relevance of these models (Otto *et al.*, 2014).

Plasmodium yoelii yoelii 17X

Plasmodium yoelii is the preferred model to study the biology of liver stages and immunity (innate and acquired). *P. yoelii yoelii 17X* (*Py17X*) is considered an adequate model to study *P. falciparum in vivo* because of the similarity in symptoms, the presentation of cerebral malaria, pulmonary oedema, severe anaemia, liver injury and kidney pathology, due to sequestration by cytoadherence (Fu *et al.*, 2012). *Py17X* has two substrains, the non-lethal *Py17XNL* and the lethal *Py17XL*, which requires dietary p-aminobenzoic acid (PABA). PABA is used for the synthesis of the folate cofactor needed for both malaria parasite growth and host erythrocyte production (Kicska *et al.*, 2003; Chango and Abdennebi-Najar, 2011).

1.5. THE FIGHT AGAINST MALARIA

In 2000, world leaders identified malaria as a serious challenge for public health and one of the major impediments to global development, particularly in the poorest countries. This led to the proposal to significantly reduce malaria incidence and mortality by 2015, in concordance with the targets established in the millennium development goals (MDGs) (WHO and UNICEF, 2015). In 2015, major reductions were achieved in overall malaria incidence and mortality; but the goals were not entirely accomplished. Consequently, by the end of 2015, the World Health Assembly of the World Health Organization (WHO) adopted a new Global Technical Strategy for malaria 2016 – 2030 (GTS), providing post-MDG guidelines based on key lessons learned from the past. The WHO believes that every single country can become malaria free, and has therefore recommended tools, activities and strategies to achieve elimination. These global guidelines and policies are described in the new "Framework for Malaria Elimination" (World Health Organization, 2017a).

Over the past decades the control of malaria has largely relied on a small number of compounds of either drugs or insecticides. These active principles have been essential for many years, although, they are becoming obsoleted and losing efficacy, thereby underscoring the need for continuing research (Na-Bangchang and Karbwang, 2009). Resistance to both antimalarial drugs and insecticides is one of the most investigated challenges leading to delays in pre-elimination malaria phase (Healer *et al.*, 2017).

The WHO defines elimination as the 'reduction to zero incidences of indigenous cases of a specific malaria parasite species in a defined geographic area'. After elimination, continued measures are required to prevent re-establishment of transmission. On the other hand, eradication is defined as the 'permanent reduction to zero of the worldwide incidence of malaria infection caused by all species of human malaria parasites', and once achieved no measures are required.

Malaria eradication will not occur without a multifaceted approach, combining vaccines, treatment with insecticides and antimalarial drugs, along with case management, which includes adequate diagnosis and the availability of treatment (WHO and UNICEF, 2015). Another remarkable strategy in low to moderate transmission areas is mass drug administration (MDA). MDA aims to treat asymptomatic parasite carriers who silently transmit the parasite, by providing oral treatment to all members of the target community if possible, regardless of whether they are or not infected (Kaehler *et al.*, 2018). MDA was extensively used in the past, but the fear of accelerating resistance led to withholding this approach until the appearance of antimalarials capable of reducing the transmission stages, such as artemisinin-based combination therapies or primaquine. However, the limitations of the current diagnostic tools to detect asymptomatic patients contributed to the re-implementation of MDA (Newby *et al.*, 2015).

With malaria being included in the global agenda again, and with the acknowledgements of the importance of a multifaceted approach, 85 new products were in 2016 in the pipeline: 13 vector control products, 25 projects related to malaria vaccine and 47 new antimalarial medicines (Hemingway, Shretta, *et al.*, 2016).

1.5.1. Vector control

There are two main vector control interventions: insecticide-treated bed nets (ITNs) and indoor residual sprays (IRS), both of which seek to reduce physical contact between mosquitoes and humans. In 2000 started enormous efforts to achieve effective vector control coverage (Bhatt *et al.*, 2016), and then in 2012 WHO recommended full coverage of long-lasting insecticide-treated bed nets (LLINs), which provides effective insecticide protection for at least 3 years (Pulkki-Brännström *et al.*, 2012). These two interventions, LLINs and IRS, contributed to reducing the overall incidence of malaria by preventing 68 % and 13 % of cases, respectively, during the period between 2000 and 2015. Both preventive methods depend on the same type of insecticide chemical, pyrethroids, which were used for many years in monotherapy, facilitating the appearance of resistance first observed in Sudan in the 1970s (WHO, 2015). Recently, it has been proved the success of ivermectin as vector control administrated in humans as MDA. Ivermectin, a semi-synthetic derivate from the fermentation products of *Streptomyces avermectinius*, has an absorbation half-live ranging from 0.5 – 2.5 h and remains in the blood for approximately 6 days after a single dose and causes blood to become toxic for mosquitoes. Despite reducing mosquito survival, there is a knowledge gap on the expected clinical and public health impact of this drug (Chaccour *et al.*, 2013; Chaccour, Hammann and Rabinovich, 2017).

Aditionaly, dichlorodiphenyl trichloroethane (DDT), another renowned chemical widely used as an IRS, has a mechanism of action similar to that of pyrethroids. DDT was first deployed in the 1940s, but 30 years later it was recommended to discontinue its use following the demonstration of toxicity evidences and negative effects on the environment. Nowadays, the WHO only recommends the use of pyrethroids for LLINs and according to tight guidelines for the management of resistance which reduces treatment efficacy. Indeed, in certain areas of Africa some mosquito vectors are able to survive a concentration of 1000-fold higher than the one that kills susceptible mosquitoes, demonstrating the urgent need for the development of novel insecticides with different mechanisms of action. Alternatively, other minor vector control strategies, such as attacking immature mosquito stages and household improvements can be implemented, although these should always be put into effect in combination with LLINs and IRS in order to delay the appearance of resistance (Hemingway, Ranson, *et al.*, 2016; Huijben and Paaijmans, 2018).

1.5.2. Vaccines

Vaccines are among the most cost-effective tools for public health. The research community worldwide is pressed to find the perfect molecule or molecules that induce effective pathogen-specific immune response, which would protect against the infection. Current efforts are aimed at the 80 vaccine products in the preclinical development stage which are classified into different types depending on the target stage or vaccine components (Table 1). Vaccines can be formed by subunits or whole organisms, being the attenuated-sporozoite the most effective (Jadhav, Jadhav and Shah, 2012; Ouattara and Laurens, 2015; Coelho *et al.*, 2017).

Table 1. Most promising and advanced antimalarial vaccines divided according to the target stage and the component of the vaccine (Jadhav, Jadhav and Shah, 2012; Coelho *et al.*, 2017).

Name	Vaccine classification	Current status
Pre-erythrocytic vaccines		
RTS,S/AS01	Subunit	Phase IV
PfSPZ	Whole organism (radiation attenuation)	Phase II
GAP	Whole organism (genetic attenuation)	Phase I
CVac	Whole organism (chemical attenuation)	Phase I
Blood stage vaccines		
PfRH5	Subunit	Phase I
Chemical attenuated parasite	Whole organism	Preclinical
AMA1-RON2	Subunit	Preclinical
Transmission blocking vaccines		
Pfs25	Subunit	Phase I
Pfs230	Subunit	Phase I
Pfs47	Subunit	Preclinical
Multistage vaccines		
AMA1 MSP1 TRAP	Subunit	Phase II
P. vivax vaccines		
SPZ-Irrad	Whole organism (chemical attenuation)	Phase II

Early malaria vaccine research started in the 1930s. Nevertheless, it was not until 1987 that RTS,S, the most advanced vaccine to date, was created at the Glaxo Smith Kline (GSK) laboratories. The RTS,S/AS01 vaccine is composed of the repeat regions of the *P. falciparum* circumsporozoite protein fused to the hepatitis B virus surface antigen, and this is added to the proprietary AS01 adjuvant. Following a phase III trial conducted in 11 centres in 7 countries in sub-Saharan Africa, the vaccine showed 55.8 % protection in children aged 5 – 17 months and 31.1 % in infants aged 6 – 12 weeks, with three doses given. Efficacy varied by site with or without booster dose given 18 months later (Partnership, 2015; Coelho *et al.*, 2017). Despite these efforts, RTS,S only showed partial protection and 30 years later is still in phase IV, demonstrating the intricacy of the *P. falciparum* life cycle, and the complex nature of the parasite, with its antigenic variation poised to avoid the immune system. Used in combination with the tools currently available, a malaria vaccine with an efficacy of greater than 75 % would provide the extra necessary push to eliminate malaria (PATH Malaria Vaccine Initiative, 2018). The WHO in April 2019 published that this same year it would be performed the first large scale pilot project in three selected areas of three African countries, Ghana, Malawai and Kenya, with RTS,S/AS01, also known as Mosquirix. Per year 360,000 children across the three pilot countries will receive the vaccine from the health facilities where they normally attend.

Pre-erythrocytic vaccines: these vaccines aim to activate humoral and cellular immune response. They provide a certain level of protection by avoiding early invasion of the RBC, targeting liver cells infected by sporozoites and merosomes.

Blood stage vaccines: these vaccines do not prevent infection but rather disease and death by targeting merozoites. Actually, antigens expressed on the surface of merozoites and pRBCs are potential candidates if antigenic polymorphism is overcome.

Transmission blocking vaccines (TBVS): TBVS aim to block fertilization and stop reproduction by targeting gametocytes and/or ookinetes. There are few previous studies and clinical trials on TBVS, although these are now rapidly increasing.

Multistage vaccines: research on these types of vaccines which target different parasite stages may be of interest due to the nature of the infection and the complexity of the parasite.

1.5.3. Antimalarial drugs

Nevertheless, in the absence of a clinically effective vaccine against malaria and the increasing appearance of resistance to insecticides and classical drugs, antimalarial drugs are still the principal mainstay of malaria control and elimination resulting on an optimistic portfolio of new drugs. However, recently became clear that the ideal medicine is a combination of two or more components with different mechanisms of action and targets. Moreover, some of these new agents should be specially focused on protecting vulnerable populations, especially women in early pregnancy, and preventing relapses of *P. vivax* because of the impact on public health (Wells, Van Huijsduijnen and Van Voorhis, 2015).

Chemoprophylaxis

Drugs for chemoprotection should prevent infection in high risk groups which are: non-immune travelers to endemic areas and pregnant women and children living in endemic countries. The first group has not been previously exposed to the parasite, thus to avoid severe malaria, these individuals should start treatment before entering the country with atovaquone-proguanil, doxycycline, mefloquine, or primaquine (Table 2) (Ashley, Pyae Phyo and Woodrow, 2018). For the second high risk group the WHO recommends three different strategies (Table 2) (World Health Organization, 2015a):

a. Intermittent preventive treatment in pregnancy (IPTp): African women in their first or second pregnancy should receive sulfadoxine–pyrimethamine (SP) as part of antenatal care. Malaria during pregnancy is a risk for the women, the foetus and the newborn. If infection is by *P. vivax* chemoprophylaxis with chloroquine is performed.

b. Intermittent preventive treatment in infants (IPTi): African children living in areas with moderate-to-high malaria transmission should be treated with SP in order to reduce the mortality of children under 5 years of age, provided that SP is still effective in the corresponding area.

c. Seasonal malaria chemoprevention (SMC): sub-Sahel children less than 6 years old, living in highly seasonal malaria areas should receive amodiaquine plus SP.

Table 2. Summary of WHO recommendations for the prophylaxis and treatment of uncomplicated and severe malaria (World Health Organization, 2015a; Guo, 2016; Ashley, Pyae Phyo and Woodrow, 2018).

Chemoprophylaxis		
General indications	IPTp / IPTi	SMC
Atovaquone – proguanil Doxycycline Mefloquine Primaquine	Sulfadoxine – Pyrimethamine (SP)	Amodiaquine + SP
Uncomplicated malaria		
General indications	*P. vivax*, *P. malariae* & *P. ovale*	Pregnancy (1st semester)
ACTs Atovaquone – Proguanil Quinine	Chloroquine Primaquine	Quinine + Clindamycin Artesunate + Clindamycin
Severe Malaria		
General indication		
Artesunate	Artemether	Quinine / Quinidine

Treatment

The earlier and the more accurate the diagnosis of a suspected malaria infection, the better the prognosis, therefore a potential patient should be 'tested, treated with the appropriate antimalarial drugs and tracked' to avoid complications. In 2006, a large number of African countries adopted artemisinin in combination therapy (ACT) as the first line treatment, contributing to the reduction of malaria. In fact, WHO sets very specific guidelines for the treatment of uncomplicated malaria and severe malaria (Table 2) (World Health Organization, 2015a).

Uncomplicated malaria occurs when a patient presents symptoms and has a positive parasitological test, but with no features of severe malaria. Without treatment uncomplicated malaria can rapidly progress to severe malaria. On the other hand, severe malaria is life threatening, leading to the dysfunction of vital organs and rapid progression to death.

The majority of antimalarial drugs which are either currently commercialized or under development involve blood schizontocides, that target the asexual blood stages (Table 4) responsible of the symptomatology. Nevertheless, it has been shown that other stages, such as the transmission stages and liver dormant stages of *P. vivax* and *P. ovale* should be targeted in order to eliminate malaria (Wells, Alonso and Gutteridge, 2009).

Antimalarial drugs must cross at least three sequential membranes (EPM, PVM and PPM) in order to enter the intracellular parasite, reach appropriate therapeutic concentrations, achieve selective inhibition of one or more essential activities, and cause a rapid killing of the parasite. Drugs can cross the EPM by two different mechanisms: lipid-based diffusion and carrier-mediated uptake, being the carrier from the host RBCs or the parasite (Table 3). In contrast, drugs can cross the PVM thanks to a single large conductance ion channel present in high density in the PVM (Desai, 2012). An alternative transport across the PVM relates to its capacity to freely exchange large organic solutes. Up to now little is known about drug transport across the PPM (Basore *et al.*, 2015).

Table 3. Uptake mechanisms of small organic solutes such as nutrients and drugs across the EPM (Basore *et al.*, 2015).

Characteristics	Lipid-based diffusion	Carrier-mediated uptake
Restricted to uncharged chemicals	Yes	No
Saturable	No	Yes
Subjected to pharmacological inhibition	No	Yes
Sensitive to drug stereospecificity	No	Yes
Vary between cells	No	Yes
Allow movement of drug by mass action	Yes	Yes
Example	-	PSAC

Antimalarial drugs can be classified into different groups depending on their chemical class or function (Figure 8):

a. Amino alchohols (quinine, mefloquine, halofantrine and lumefantrine):

Quinine is an alkaloid from the bark of *Cinchona succirubra* (Rubiaceae) which had been the only malaria treatment for about 300 years. The quinoline moiety is responsible for the antimalarial properties against blood stages of all *Plasmodium* species inhibiting the formation of hemozoin and resulting in the parasite being poisoned by its own waste (Jones, Panda and Hall, 2015). Since 2006 quinine is no longer used as first line treatment, but it is used in the treatment of severe malaria in cases in which artemisinin is not available (Tse, Korsik and Todd, 2019).

Mefloquine was obtained as a result of trying to improve quinine with chemical synthesis strategies, acting in the parasite cytoplasm binding to the 80S ribosome unit, partially impeding protein synthesiss. It is a *P. falciparum* and *P. vivax* schizontocide, which also inhibits gametocytes and acts against oocysts. Mefloquine has a long half-life (21 days) and is an efficient prophylactic option. However, it can cause rare serious gastrointestinal and psychiatric side effects. It is normally used in combination with artesunate as ACT (Wong *et al.*, 2017).

Halofantrine was discovered at the same time as mefloquine, and its mechanisms of action seem to be similar to those of quinine, although it also acts against oocysts. It can be used for both prophylaxis and treatment, albeit with caution in patients with cardiovascular problems (Mbai, Rajamani and January, 2002).

Lumefantrine has a half-life of 1 to 6 days and is mainly used in uncomplicated or severe *P. falciparum* malaria and mainly in combination with artemether (Winstanley and Ward, 2006). Similar to chloroquine, lumefantrine increases free heme concentrations and reduces hemozoin formation. However, it is much less efficient, suggesting a different mechanism of action with a similar output. Lumefantrine also acts against oocysts and is also effective against *P. vivax* (Chen *et al.*, 2010; Lucca *et al.*, 2015).

b. Endoperoxides (artemisinin, artemether, artesunate and dihydroartemisinin):

Artemisinin, similarly to quinine, is a drug of plant origin extracted from *Artemisia annua*. The plant had been used by Chinese herbalists to cure many illnesses for hundreds of years. However, it was not until 1970 that artemisinin was properly identified as an active principle by Youyou Tu, who won a Nobel Prize in 2015 for her finding (Guo, 2016). Artemisinin and its derivates represent a new class of antimalarial agents. Artemisinin in particular is a potent antimalarial drug which is effective against nearly all sexual and asexual stages of the malaria

parasite, with a short half-life of around 1 hour. The method of action of artemisinin is not yet fully understood, but it has been suggested that it reduces GSH levels and increases toxic reactive oxygen species (ROS) to levels able to kill the parasite (Figure 7) (Kaphingst, Persky and Lachance, 2010; Kavishe, Koenderink and Alifrangis, 2017). Artemisinin derivates are used in combination therapy with other drugs having different methods of action and long half-lives to minimize avoid resistance evolution and increase efficacy (Kaphingst, Persky and Lachance, 2010).

Artemether is an oil-soluble derivate that metabolizes slowly to dihydroartemisinin (DHA), thus being less active than a direct treatment with DHA (Kaphingst, Persky and Lachance, 2010). It is used in combination with lumefantrine for uncomplicated malaria (Guo, 2016), and has a wide blood-stage specificity, reducing gametocyte load (World Health Organization, 2015a).

Artesunate is a water-soluble derivate which metabolizes to DHA within minutes. It can be used in monotherapy or in combination with amodiaquine, mefloquine or pyrimethamine-sulfadoxine. Other combinations are currently under study (Kaphingst, Persky and Lachance, 2010). Artesunate is active against all erythrocytic stages, is partially active against gametocyte stage V and is inactive against extra-erythrocytic forms, sporozoites, liver merosomes and merozoites (World Health Organization, 2015a).

Dihydroartemisinin (DHA) is the active metabolite, much more soluble in water than artemisinin, and thus more active. It is mostly used in combination with piperaquine since this drug is one of the few active agents against multidrug resistant *P. falciparum* in Southeast Asia. Nevertheless, this combination may soon lose efficacy due to the unanticipated appearance of clinical treatment failure in that area (Amaratunga *et al.*, 2016).

c. 4-Aminoquinolines (4-AQs) (chloroquine, piperaquine and amodiaquine):

Chloroquine (CQ) was considered the best and the most affordable option against malaria for decades, yet the appearance of *P. falciparum* resistance in the 1950s changed this situation. CQ accumulates in the digestive vacuole, after crossing the membrane as a neutral molecule, and then it becomes protonated due to the acidic intravacuolar pH. Once in the vacuole it is retained and binds to heme molecules inhibiting the formation of hemozoin (Figure 7) (Slater, 1993; Chinappi *et al.*, 2010). The absence of hemozoin formation in gametocytes stage IV and V accounts for the inactivity of CQ in mature gametocytes (Almela *et al.*, 2012). Moreover, CQ also interferes with the biosynthesis of nucleic acids (World Health Organization, 2015a). Nevertheless, CQ is still the first line treatment for uncomplicated malaria caused by *P. vivax*, *P. malariae* and *P. ovale*, despite not being active against hypnozoites (Ashley, Pyae Phyo and Woodrow, 2018).

Piperaquine is a CQ derivate which also accumulates in the food vacuole and inhibits heme detoxification. It was used as monotherapy in the 80s and 90s, but is now used in combination with DHA. Piperaquine inhibits immature gametocytes and is a good schizontocide with a long half-life of 4 to 6 hours (Kiboi *et al.*, 2009).

Amodiaquine metabolizes to its active metabolite desethylamodiaquine. Similar to CQ, amodiaquine accumulates in the food vacuole and interferes with heme detoxification (Ginsburg *et al.*, 1998). It is currently used in combination with artesunate thanks to its dual activity, inhibiting sexual stages and gametocyte maturation (Delves *et al.*, 2012).

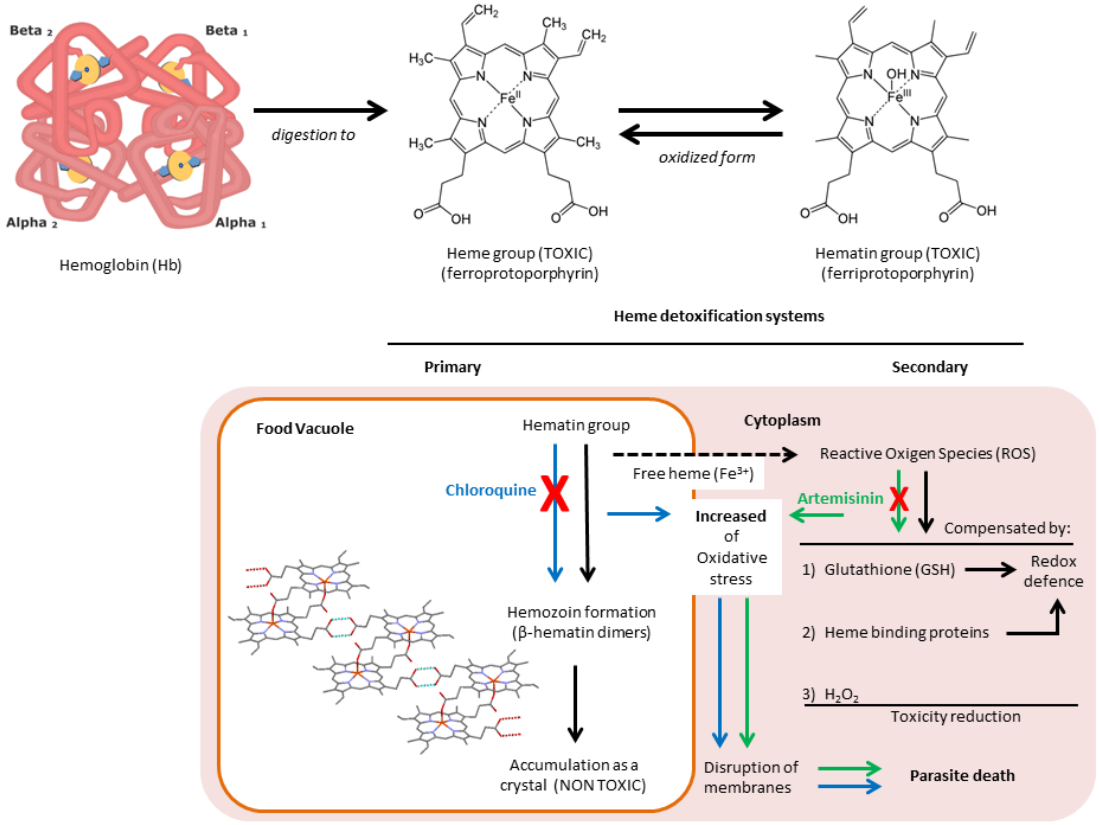

Figure 7. Haemoglobin digestion and haemoglobin-derivated heme detoxification systems used to reduce the toxicity of oxidative stress in the parasite. pRBCs digest almost all the haemoglobin present in the RBC. This hydrolysis releases heme groups which are lipophilic, and react with lipid bilayers of organelles and destabilize the cytoskeleton (Kumar and Bandyopadhyay, 2005). The hydrolysis also produces ROS which are toxic. There are two detoxification mechanisms: a primary system occurs in the food vacuole, where hematin groups resulting from the oxidation of heme groups are transformed into hemozoin and accumulate in a non-toxic crystal. The secondary system occurs in the cytoplasm, ROS are contained by three different methods: binding to GSH, proteins and/or to H_2O_2. Chloroquine blocks hemozoin formation (blue arrows), and artemisinin reduces the amount of GSH, increasing the amount of ROS (green arrows) (Moore *et al.*, 2006; Kumar *et al.*, 2007; Chinappi *et al.*, 2010; Kaphingst, Persky and Lachance, 2010).

d. 8-Aminoquinolines (8-AQs) (primaquine and tafenoquine):

Primaquine (PQ) is the first choice for transmission control strategies as it inhibits *P. falciparum* gametocytes, although the method of action is not yet fully understood. Additionally, PQ is active against relapse from *P. vivax* and *P. ovale* since it can kill hypnozoites. A 14-day regime makes compliance difficult wich had been improved by tafenoquine tratement (Kappe *et al.*, 2010). AQ is contraindicated in early pregnancy and for glucose-6-phosphate dehydrogenase (G6PD) deficient subjects because, in these individuals, the risk of hemolysis is increased (Deng *et al.*, 2018).

Tafenoquine is an analogue of PQ and it is a potent schizontocide against *P. vivax* and *P. falciparum*. It is also gametocytocidal (Kumar *et al.*, 2018) and is better than PQ against hepatic stages (Na-Bangchang and Karbwang, 2009). Tafenoquine seems to have the same effect as PQ in a single dose, although this has yet to be confirmed. Nonetheless, tafenoquine has the same disadvantages for G6PD deficient patients (Wells, Van Huijsduijnen and Van Voorhis, 2015).

Table 4. Main antimalarial drugs and their half-life, half maximal inhibitory concentration (IC_{50}) for non CQ-resistant *P. falciparum* strains, and stage of activity. BS(r): blood stages ring; BS(l): blood stage late; LS: liver stages; O: oocysts; OK: ookinetes, and Gt: gametocytes (Winstanley and Ward, 2006; Santos-Magalhães and Mosqueira, 2010; Delves *et al.*, 2012; World Health Organization, 2015a; Tse, Korsik and Todd, 2019).

Drug	Specific references	Half-life	IC_{50} (nM)	Stage of activity
Amodiaquine		4 – 10 d	21	BS(l), Gt
Artemether	(Sugiarto, Davis and Salman, 2017)	7 h	3	BS, LS
Artemisinin	(Vries and Dien, 1996; Kaphingst, Persky and Lachance, 2010; Kappe *et al.*, 2010)	2 – 5 h	15	BS(r), BS(l), Gt
Artesunate		1.5 – 2.5 h	6	BS(r), BS(l), LS
Atovaquone – Proguanil	(Winstanley and Ward, 2006)	2 – 3 d & 12 – 21 h	0.6 2000	BS(l), LS, OK
Chloroquine		7 – 12 d	31	BS(l)
Clindamycin	(Dahl and Rosenthal, 2007)	2 – 4 h	3	BS
Dihydroartemisinin		1 – 2.5 h	2	LS, O
Doxycycline	(Dahl and Rosenthal, 2007)	9 – 22 h	4000	BS
Halofantrine		1 – 2 d	23	BS(l), O
Lumefantrine		1 - 6 d	10	BS(l), O
Mefloquine	(Attlmayr *et al.*, 2006)	21 d	20	BS(l), O, Gt
Piperaquine		13 – 28 d	70	BS(l)
Primaquine	(Winstanley and Ward, 2006)	14 d	1000	LS, Gt
Quinine		3 – 26 h	138	BS(l)
Sulfadoxine – Pyrimethamine (SP)	(Attlmayr *et al.*, 2006; Kappe *et al.*, 2010)	4 – 11 d & 3 – 4 d	40600 1700	BS, O, OK
Quinacrine	(Gomes *et al.*, 2014)		100	BS, LS
Curcumin	(Reddy *et al.*, 2005)		5000	BS
Heparin	(Boyle *et al.*, 2010)		1900	BS

e. Antifolates (proguanil and pyrimethamine):

Proguanil has a half-life of 12 to 21 hours and it is used in combination with atovaquone despite its high cost (Na-Bangchang and Karbwang, 2009). Proguanil acts synergistically with atovaquone enhancing the ability of atovaquone to collapse the mitochondrial membrane potential at very low concentrations, whereas the metabolite cycloguanil act by inhibiting parasite dihydrofolate reductase (DHFR) (Boggild *et al.*, 2007).

Pyrimethamine has a long half-life of around 3 to 4 days and inhibits different parasitic stages including the hepatic, sexual, ookinetes and oocysts stages (Delves *et al.*, 2012). Pyrimethamine impedes the production of tetrahydrofolate, and thus, the biosynthesis of DNA and proteins because it is a competitive inhibitor of DHFR, a key enzyme in the biosynthesis of folate. In combination with sulfadoxine, an inhibitor of dihydropteroate synthase (DHPS), pyrimethamine produces a synergistic effect causing the death of the parasite (Sibley *et al.*, 2001). The mechanism behind this activity relates to the active transport system which human hosts have that allows the obtention of folic acid from the diet when DHFR is inhibited. In contrast, most microorganisms such as *Plasmodium* lack this capacity and must synthesize folate *de novo* but since DHFR is inhibited they end up dying because of a folate shortage (Foote and Cowman, 1994).

f. Antibiotics (doxycycline and clindamycin):

Doxycycline is poorly soluble and it is therefore not clear how it crosses membranes (Basore *et al.*, 2015), it is a slow-acting antimalarial which inhibits the synthesis of proteins,

and enhances the activity of other drugs such as quinine. It is used for the prophylaxis of pregnant women (Aditya *et al.*,2013).

Clindamycin is as well-known slow-acting antimalarial, and it is used in combination with quinine, a fast-acting drug. This combination has a regime of 7 days, and it is an alternative to artemisinin-based treatment for uncomplicated malaria in pregnant women (Ashley, Pyae Phyo and Woodrow, 2018). Its mechanism of action involves the inhibition of microbial protein synthesis by preferential binding to the 50S ribosomal subunit (World HealthOrganization, 2015a).

g. Others (atovaquone, sulfadoxine, quinacrine, curcumin and heparin):

Atovaquone is a hydroxynaphthoquinone with antimalarial activity against all *Plasmodium* species. It has a half-life of 2 to 3 days and is used in combination with proguanil. It acts by inhibiting the cytochrome electron transport system, resulting in the collapse of mitochondrial membrane potential (World Health Organization, 2015a).

Sulfadoxine (sulfonamides) has a long half-life of 4 to 11 days and inhibits DHPS, a key enzyme in the biosynthesis of folates. Sulfadoxine is mainly active against late asexual stages and is always used with pyrimethamine (Sibley *et al.*, 2001).

Quinacrine (QN) (also known as mepacrine or atabrine), a deriviate of Methylene Blue, is no longer used in clinical practice because of the high probability of undesirable side effects. As other antimalarial drugs, QN inhibits the formation of the hemozoin crystal by binding heme groups (Auparakkitanon *et al.*, 2003). QN has the unique characteristic of being fluorescent with an excitation maximum at 436 nm and emission maximum at 525 nm according to the Sigma Product information for quinacrine dihidrochloride.

Curcumin, a hydrophobic Indian specie extracted from *Curcuma longa*, is a potent biological compound with several interesting characteristics including anti-tumorigenic, anti-oxidant, anti-inflammatory and anti-microbial activity (Araújo and Leon, 2001). Despite curcumins' poor absorption and rapid metabolism resulting in low bioavailability, in 2005 it was reported to have antimalarial activity in *in vivo* models reducing parasitemia up to 80 % and curing almost 30 % of mice with an unknown mechanism of action (Reddy *et al.*, 2005). Therefore, if bioavailability is improved or it is used in combination plus its low cost, curcumin can be a potential interesting treatment (Anand *et al.*, 2007).

Heparin belongs to the family of glyocosamine glycans (GAGs); it inhibits antithrombin III and factor Xa, resulting in anticoagulant activity (Hirsh and Fuster, 2001). Heparin has a high average negative charge and is able to interact with many types of proteins. It also has other biological activities, such as antimalarial activity. Indeed, heparin was previously used for the treatment of severe malaria, but it was abandoned because of its strong anticoagulant action leading to adverse effects such as intracranial bleeding (Munir *et al.*, 1980; Rampengan, 1991). As an antimalarial drug heparin has specific binding affinity for pRBCs versus RBCs, and it has been suggested that the antimalarial activity *per se* is achieved by inhibition of merozoite invasion (Marchisio, Longo and Ferruti, 1973; Kulane *et al.*, 1992), and induction of proteolytic cleavage of the major surface protein circumsporozoite protein (CSP) (Valle-Delgado, Urbán and Fernàndez-Busquets, 2013). Moreover, heparin disrupts rosette formation, cell – cell adhesion formed via the parasite protein PfEMP1 (Albrecht *et al.*, 2011), which is a causative factor of severe malaria (Skidmore *et al.*, 2008). Additionally, the parasite must have been exposed to heparin in the blood during its long coevolutionary history with humans and yet parasite resistance has not been described to date (Marchisio, Longo and Ferruti, 1973).

Oral bioavailability, depends on drug absorption across the intestinal epithelium, which is strongly influenced by drug solubility and permeability, whereas volume distribution of antimalarial drugs may be large, plasma concentrations may be low because of low target cell specificity, which requires multiple dosages and thereby increases possible undesirable side effects and also hinders compliance (Urbán and Fernàndez-Busquets, 2014). Non-specific targeting which decreases efficacy can be counteracted by formulating novel antimalarial drugs, but its high cost makes the development of new delivery systems a more cost effective decision (Murambiwa *et al.*, 2011). Targeted delivery systems with increased bioavailability and selectivity, allow a local lethal high dose of the drug to the malaria parasite while maintaining a low intake of the total amount, avoiding side effects (Urbán and Fernàndez-Busquets, 2014).

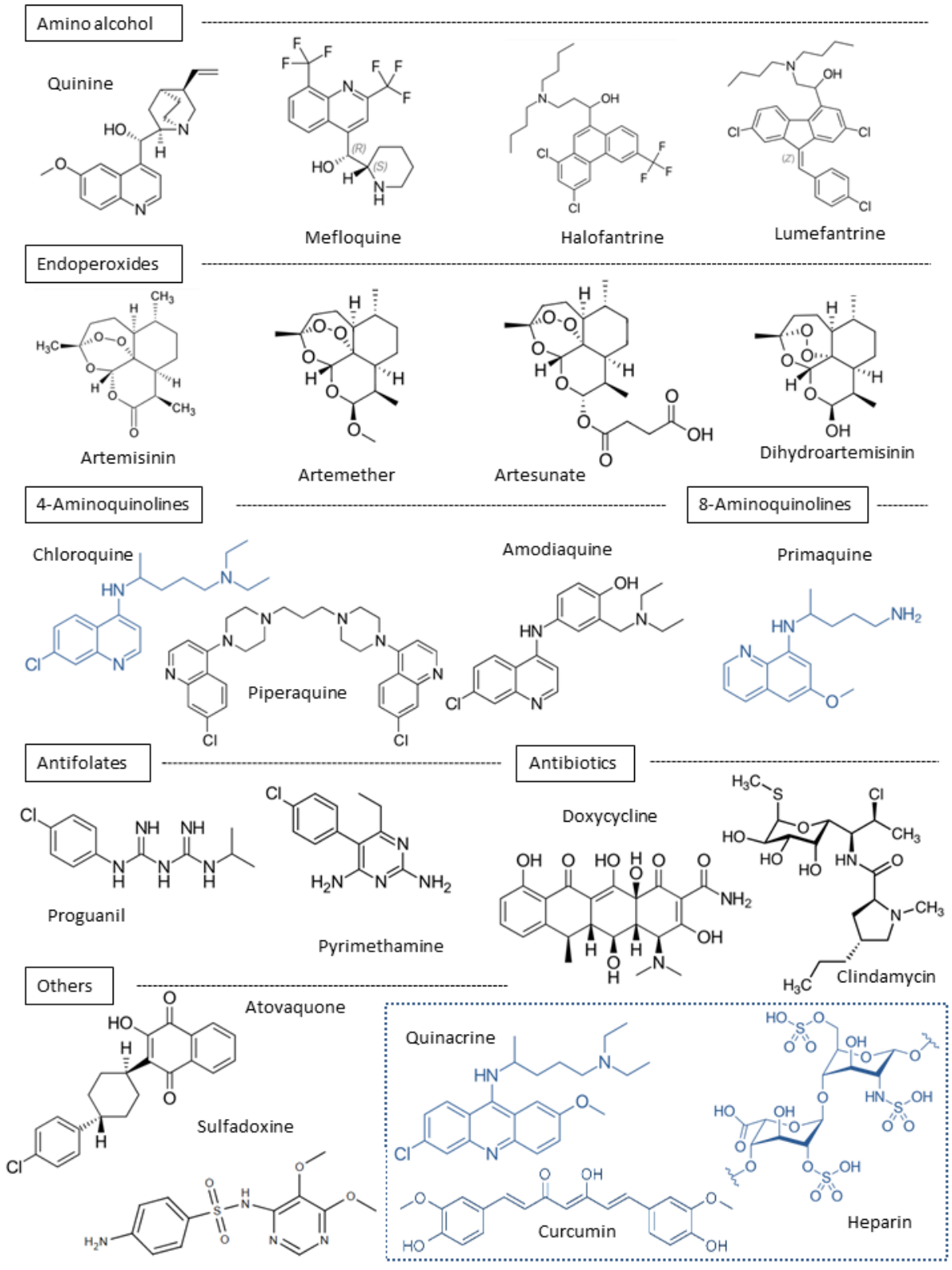

Figure 8. Chemical structure of the main antimalarials described by the WHO or of interest in this research. Molecules shown in blue have been used in this thesis. Figure adapted from (Na-Bangchang and Karbwang, 2009; Delves *et al.*, 2012; World HealthOrganization, 2015a).

2.1. INTRODUCTION TO NANOTECHNOLOGY

Nanotechnology allows the manipulation of materials of nanoscale size and can be applied in a vast variety of disciplines, such as cosmetics, in the field of energy, bioengineering, defence and security and in medicine and drugs. For many years nanotechnology has been used in oncology to overcome drug toxicity, physiological barriers and/or cellular mechanisms , thereby helping the drug to reach tumoral tissue and improving drug distribution, decreasing metabolism and drug clearance and resulting in an increased half-life in the target tissue (Morales-Orue, Chicas-Sett and Lara, 2019).

The application of nanotechnology in the health sector is known as nanomedicine. Although nanotechnology is a young science, it is gaining increasing importance. Since the 1990s, nanotechnology had been investigated in order to improve different fields of medicine such as disease diagnosis and treatment (Krukemeyer, Krenn and Huebner, 2015). Nanomedicine takes advantage of the properties and characteristics of nanomaterials to optimise existing methods for preventing, controlling and curing diseases at a molecular level (Kim, Rutka and Chan, 2010), by improving classical drugs with drug delivery nanosystems, such as nanospheres or nanocapsules, or by participating in the formulation of new drugs, which is, however, a much more expensive strategy.

The properties of the nanomaterials or nanoparticles (NPs) which range in size between 1 to 100 nm, differ from those of larger objects. Microparticle properties are comparable to the original material, but the behaviour of nanoparticles is novel and changeable compared to the original material, due to the large surface volume relationship which they provide, and to changes in their optical, electrical and magnetic properties (Panneerselvam and Choi, 2014).

Many consider nanotechnology to be too futuristic, not suitable for commercialization and expensive. Nonetheless, it is being successfully applied to personalize treatment in some diseases such as cancer in economically rich countries (Mvango *et al.*, 2018). Many nanocarriers made of a wide variety of materials, including carbon nanotubes, metal particles, dendrimers, polymer particles, and shapes, like spheres, cubes, rods, plates or stars and conjugated to several target molecules have been explored (Figure 9). This technology is therefore fully available today and can offer important benefits to developing countries, providing inexpensive and innovative biomedical solutions to many diseases, among which malaria (Kumar, 2009; Najer *et al.*, 2018).

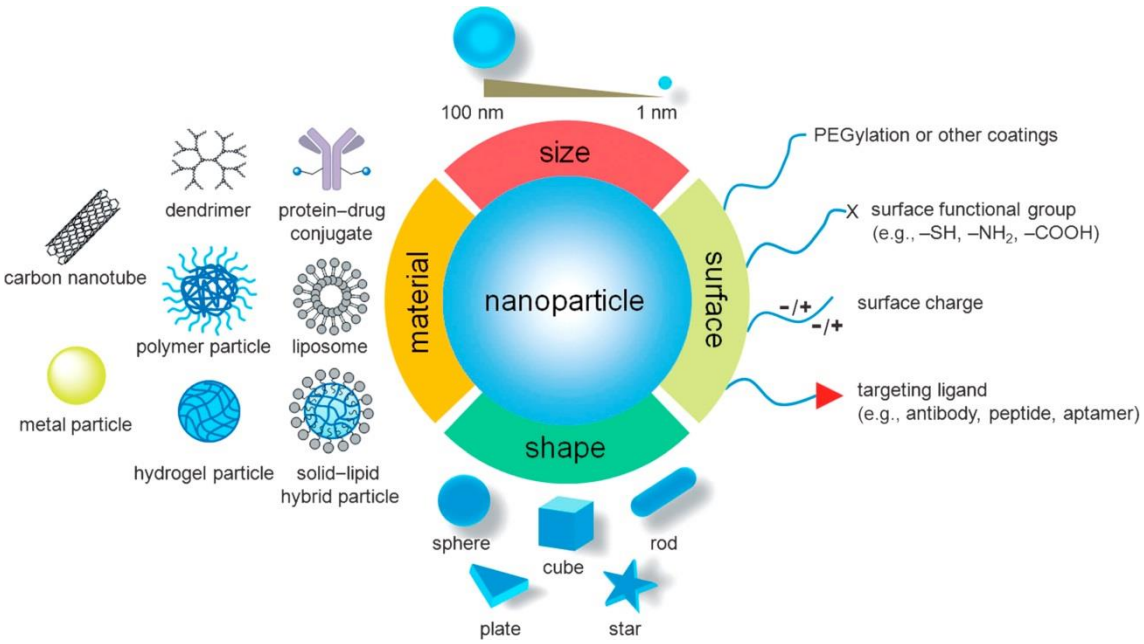

Figure 9. Schematic representation of the alternatives for nanoparticle formation. Figure reproduced from (Sun *et al.*, 2014).

2.1.1. Nanotechnology in the fight against malaria

Diagnosis

As mentioned in Chapter I, it is essential to diagnose malaria in the early stage, and up to now only three highly sensitive techniques are widely used: microscopic analysis, immunology and polymerase chain reaction (PCR-based) techniques, all of which are based on technologies half a century old (Ragavan *et al.*, 2018). Nevertheless, they have several limitations such as low speed of analysis, the need for skilled operators, poor detection threshold and inability to simultaneously detect multiple strains of infectious agents. Nanotechnology can contribute to changing this situation and finally contributing to obtaining low-cost, user-friendly and robust systems to achieve accurate identification of the parasite, correct measurement of disease severity and thereby indicate the most adequate treatment to be implemented (Hauck *et al.*, 2010).

Up to now, nanodiagnostic research includes: nanoparticle-based, nanodevice-based or point-of-care test (POCT) platforms. Nanoparticle-based platforms using metallic and magnetic NPs are the most successfully applied; for example, gold nanoparticles have been used to immobilize antibodies and for signal enhancement, and magnetic nanoparticles have been used as hemozoin detectors. Nonetheless, nanoparticle-based platforms are still far from meeting the real demands in the clinical setting. Alternatively, nanodevices can overcome certain limitations such as the difficulty in detecting co-infections or low parasitemias. Lab-on-a-chip is an integrated platform that could potentially contribute to the development of low-cost portable devices using a low amount of sample (≤ 100 µL). These new tools will contribute to obtaining optimal nanotechnology-based POCTs, which must be portable and allow *in situ* results, which are indispensable features for malaria detection and control (Taylor *et al.*, 2014; Krampa *et al.*, 2017; Wang *et al.*, 2017).

Vaccine formulations

Despite the availability of a recombinant malaria vaccine candidate, RTS'S/AS01, which showed partial protection in young children, there remains an urgent need for a more efficient malaria vaccine. RTS'S already involve the use of nanotechnology techniques in that the adjuvant system, A0S1, consists of a liquid suspension of liposomes with two immunostimulant components (Malaria Vaccine Initiative, 2009). Nevertheless, nanotechnology could contribute even more. Recently, a new technology has been proposed using the self-assembly properties of certain nanomaterials to build simple stable nanoparticle vaccines as adjuvants applying the knowledge that the greater the number of antigens expressed in a vaccine, the higher the possibility of parasite recognition in each phase of the life cycle. Therefore, this newly proposed system, known as spontaneous nanoliposome-antigen particleization (SNAP), allows the assembly of a variety of antigens modified with histidine-tags (his-tags) which spontaneously bind to liposomes containing cobalt-porphyrin-phospholipid (CoPoP). This opens the door not only for a more efficient vaccine, but also for transmission blocking vaccines. The SNAP approach safely induces durable antibody responses in orders of magnitude greater than other adjuvants (Figure 10) (Huang *et al.*, 2018; Oakes and Jewell, 2018).

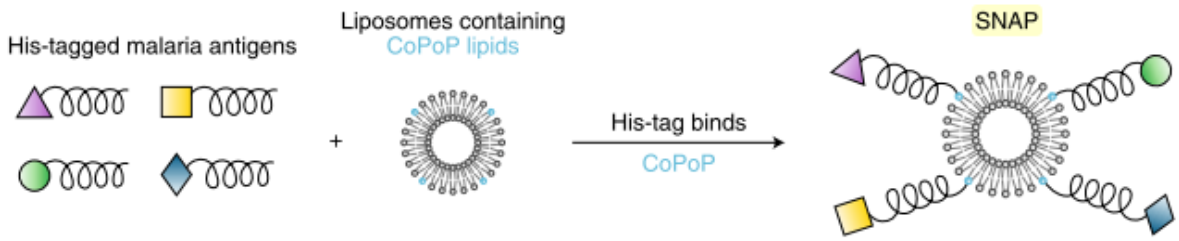

Figure 10. Spontaneous nanoliposome-antigen particleization approach. Malaria peptides (purple triangle, yellow square, green circle and blue diamond) representing potential antigens expressed during different stages of the parasite lifecycle, are modified with a his-tag and incubated with liposomes containing CoPoP (light blue small circle) which undergoes SNAP. Figure reproduced from (Oakes and Jewell, 2018).

Treatment

The drug discovery process is extremely challenging, expensive, lengthy and with a reduced output of novel drugs due to the high risk of failure (Shaw, 2017). However, the costs and time can be reduced by developing improved drugs through nanotechnology. Drug delivery systems (DDSs) are innovative strategies the ultimate goal of which is to develop clinically improved formulations for treating diseases in patients (Urbán and Fernàndez-Busquets, 2014).

Nano-DDSs have shown to have a positive effect on disease treatment providing solutions to solubility, pharmacokinetics, target selectivity, and/or protection against degradation, resulting in an increase in drug half-life. The fact that the drug remains longer in the bloodstream increases the time for interaction with the pRBCs membrane and parasite membrane, allowing a reduction in drug dose, frequency and treatment duration (Santos-Magalhães and Mosqueira, 2010; Kundu *et al.*, 2015). Eventually these would also reduce the possibility of the appearance of resistance and side effects (Thakkar and Brijesh, 2016).

Furthermore, nanotechnology can improve the pharmacokinetic profile of drugs and their therapeutic outcome by targeting antimalarials specifically to their site of action. In addition, many antimalarial compounds are charged, and hence, require transportation into the parasite (Murambiwa *et al.*, 2011). Likewise, nanotechnology is a useful tool to restore the use of older toxic drugs by modifying their biodistribution and reducing toxicity (Urbán *et al.*, 2011). Another important issue is the route of administration; a single oral dose would be the ideal choice for clinically uncomplicated malaria, whereas parental therapy is advocated in severe and complicated malaria (Aditya *et al.*, 2013).

2.2. ANTIMALARIAL DRUG DELIVERY SYSTEMS

Up to now, the main carriers evaluated for antimalarial drug delivery have been liposomes, solid lipid nanoparticles, polymeric nanoparticles, cyclodextrins and dendrimers (Figure 11) (Aditya et al., 2013). They are formed by biocompatible and biodegradable synthetic, semi-synthetic or natural polymers or lipids and can encapsulate, entrap, adsorb, or chemically attach hydrophilic or/and lipophilic active therapeutic molecules in different locations, depending on the material used (Dennis, Peoples and Johnson, 2015). Although new active therapeutic molecules should be studied, it is more cost-effective to improve already existing drugs with DDSs which can even enable the encapsulation of various antimalarial compounds in a single particle (Thakkar and Brijesh, 2016). The release of the active principle can be triggered upon a change in pH, temperature, redox potential or the concentration of specific enzymes. Indeed, the parasite cytosol and its reducing environment could easily initiate drug release, and the consequent drug activity (Najer *et al.*, 2018).

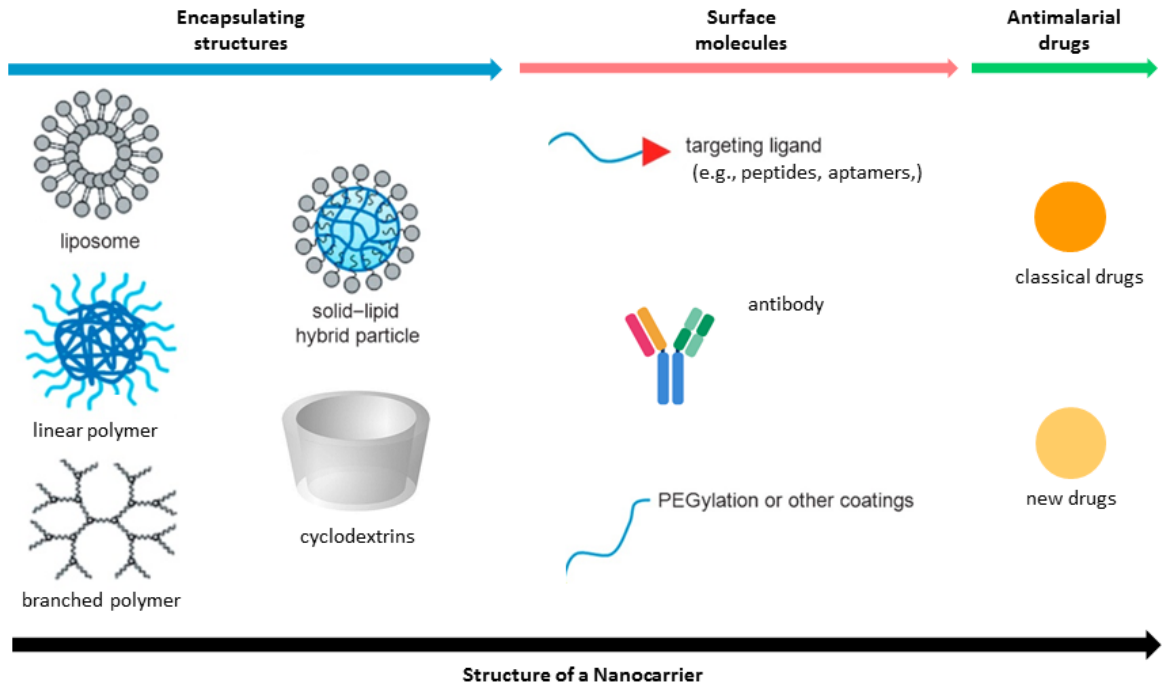

Figure 11. Components of nanocarriers. DDSs against malaria can be formed by either two or three components: a encapsulating structure itself, optional surface molecules, and the therapeutic agent (Urbán *et al.*, 2011; Aditya *et al.*, 2013; Sun *et al.*, 2014; Urbán and Fernàndez-Busquets, 2014; Dennis, Peoples and Johnson, 2015; Thakkar and Brijesh, 2016).

One of the main challenges of DDS is the release, at the most adequate time, of the drug agent inside the target cell, in a safe and reproducible manner to avoid exposure to sensitive adjacent healthy cells or tissues (Urbán and Fernàndez-Busquets, 2014). This can be achieved by either passive targeting, where there is a natural selection and accumulation of certain carriers in a particular targeted cell, or active targeting, when the uptake is facilitated by surface-functionalization (Urbán *et al.*, 2011).

2.3. LIPID-BASED NANOCARRIERS

Lipid-based nanocarriers are one of the most promising approaches as antimalarial DDS, and liposomes (LPs) in particular have been the most studied to date, being biodegradable and nontoxic (Gregoriadis, 1988). LPs mimic the structure of biological cells. They are spherical assemblies of natural or synthetic amphiphilic phospholipids with cholesterol (Figure 12 A). These structures are classified according to their structure size and lamellarity (Figure 12 B), and have the capacity to entrap both hydrophilic and hydrophobic drugs in the aqueous core or in the bilayer membrane respectively, and can thereby deliver both drugs simultaneously (Aditya *et al.*, 2013; Li *et al.*, 2019). LP size, structure and chemical composition can be easily controlled during the formation process. Nevertheless, the efficacy of drug encapsulation, release rate and final size is determined by the composition and content of the bilayer (Mvango *et al.*, 2018).

The surface of liposomes can be functionalized with several cell specific recognition ligands, which facilitate membrane fusion and compensates for the lack of endocytic capacity in RBCs. Liposomes conjugated with specific antibodies are known as immunoliposomes (iLPs). Furthermore, iLPs have shown to modify their pharmacokinetics by increasing the interaction with RBCs as a result of reducing liver uptake (Singhal and Gupta, 1986). As mentioned previously, in the past heparin was used to treat several cerebral malaria (Munir *et al.*, 1980). However, its use was abandoned because of its strong anticoagulation activity. Heparin loses anticoagulant activity when covalently immobilized on a substrate, thereby making it a potential targeting molecule since it demonstrates antimalarial activity and specific targeting of pRBCs (Marques *et al.*, 2014; Fernàndez-Busquets, 2016). LPs can also be decorated with the hydrophilic polyethyleneglycol-ylated (PEGylated) phospholipid lengthening the LP time in circulation (Couvreur and Vauthier, 2006).

Previous studies by our group demonstrated that iLPs studded with monoclonal antibodies raised against the erythrocyte surface protein glycophorin A were capable of targeting 100 % RBCs and pRBCs, at a low concentration of 0.5 µM of total lipids in the culture, with > 95 % of added liposomes retained on cell surfaces. Moreover, after exposing early stages of *P. falciparum* in *in vitro* cultures to iLPs loaded with 50 nM CQ for 15 min, growth was completely arrested, while 200 nM of the free drug showed no effect. *In vivo* results were also remarkable; iLPs cleared the pathogen at a CQ dose of 0.5 mg/kg, while free CQ did so at 1.75 mg/kg (Moles*et al.*, 2015).

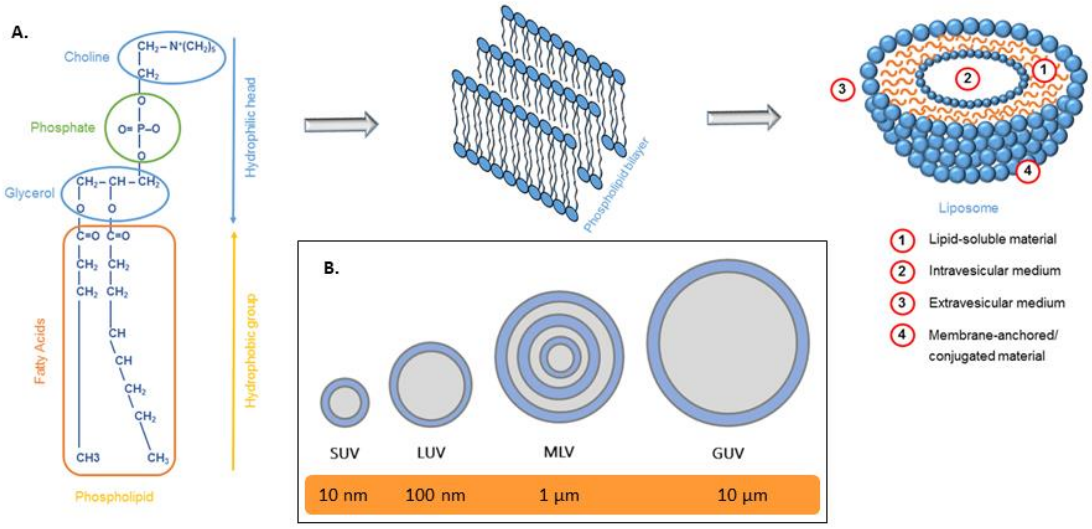

Figure 12. (A) Schematic illustration of the LP self-assembly process which starts with phospholipid molecules, which form a bilayer membrane, and converts into liposomes. **(B) LP classification** according to the size and number of lipid bilayers. Small unilamellar vesicles (SUV) around 10 nm; large unilamelar vesicles (LUV) around 100 nm; multilamellar vesicles (MLV) around 1 µm; and giant unilamellar vesicles (GUV) around 10 µm. Figure adapted from (Nogueira *et al.*, 2015).

Alternatively, liposomes positively charged and electrostatically functionalized with heparin, at a non-anticoagulant concentration, showed better antimalarial activity compared to iLPs. A 3-fold improvement was observed, demonstrating the dual capacity of heparin as a targeting molecule and as an antimalarial drug. Nevertheless, is would be interesting to study the use of heparin fragments for future nanovectors to further reduce anticoagulant activity (Marques *et al.*, 2014).

Liposomes bearing cell-specific recognition ligands on their surfaces have been widely considered as drug carriers in therapy due to their non-toxic and biodegradable character (Gregoriadis, 1988). Nevertheless, liposome-based administration has not yet progressed towards a working therapeutic strategy for malaria, probably because there is still a lack of sufficient specific markers towards *Plasmodium*-infected RBCs. Additionally, liposomes have other limitations such as: a relatively short plasma half-life, deficient in long term stability, they require temperature controlled storage, are expensive when used with antibodies, and are not suitable for oral administration (Table 5) (Nogueira *et al.*, 2015; Teixeira, Carbone and Souto, 2017). Although in general terms LPs has a low to moderate loading drug capacity, Moles *et al.* achieved large encapsulations > 90 % for weak basic drugs, like CQ or PQ, using the pH gradient loading method in liposomes containing neutral saturated phospholipids (Moles *et al.*, 2015). Conversely, polymer-based nanocarriers can overcome some of these drawbacks.

Table 5. Comparison of the characteristics of liposomes and polymeric nanoparticles. Table adapted from (Date, Joshi and Patravale, 2007).

Characteristics	Liposomes	Polymeric NPs
Parental delivery	Possible	Possible
Oral delivery	Not possible	Possible
Ability to deliver hydrophobic and hydrophilic drugs	Yes	Yes
Physical stability	+	+++
Biological stability	+	+++
Biocompatibility	+++	++
Ease of sterilization	+	++
Drug targeting	++	++
Drug loading	Low to moderate	Moderate
Ease of commercialization	+	+
Ability to deliver biotechnological therapeutics	++	++

2.4. POLYMER-BASED NANOCARRIERS

Polymer-based carriers are the second most investigated nanocarriers as DDSs. They are solid colloidal particles with a size between 1 and 1000 nm, and conserve many of the characteristics of LPs, including being biodegradable and biocompatible, possibility of parental delivery, ability to deliver hydrophobic and hydrophilic drugs and capacity to be functionalized; moreover, they have certain advantages over LPs (Table 5) (Date, Joshiand Patravale, 2007). The polymeric nature of these particles makes them more stable in biological fluids and under harsh preparation conditions; it also helps to have a shorter processing time, and the storage conditions are less restricted than for lipid based particles (Santos-Magalhães and Mosqueira, 2010). Drug loading into nanoparticles can be achieved by two strategies. The first approach involves the drug being added during the formation of the nanoparticle, and in the second approach the drug is added after particle formation (Kumari, Yadav and Yadav, 2010). The result of both strategies is that the drug is either entrapped, adsorbed or covalently attached to the polymer. Then once the nanocarrier reaches the targeted cell, the drug is released by desorption, diffusion through the polymeric matrix or erosion of the particle (Lockman *et al.*, 2002).

Like LPs, polymer-based NPs can be rapidly cleared by the mononuclear phagocytic system (MPS) in the liver and by splenic filtration after intravenous (iv) injection. Nevertheless, polymer-based nanocarriers can be easily formulated for oral delivery, the first choice for clinically uncomplicated malaria (Date, Joshi and Patravale, 2007).

Oral administration is the most accepted form of drug administration because of patient convenience and compliance, cost-effectiveness, and avoidance of risk of infection and pain compared to parenteral route (Raza *et al.*, 2019). Nevertheless, many native drugs are not suitably absorbed through the oral route due to several factors such as poor solubility, poor stability in the gastric environment, low drug penetration and/or absorption, and metabolic degradation. Bioavailability is also reduced when the drug is exposed to physicochemical barriers found throughout the whole gastrointestinal tract (GIT) before reaching the blood stream (Figure 13 A and B). The gut lumen is lined with a single layer of intestinal epithelium mainly made up of enterocytes but also containing a few

macrophages. Both cell types are in charge of protecting against unknown particles and microorganisms present in the intestinal lumen, and cells selectively filter into circulation. The intestinal epithelium can be crossed by different mechanisms: paracellular transport (between enterocytes), and transcellular transport (across enterocytes), which can be passive or mediated by receptors, carriers, or macrophages (Figure 13 C). The GIT is lined with viscoelastic mucus which makes penetration of the barrier difficult and has a pH ranging from 1 to 7 (Ensign, Cone and Hanes, 2012; Dilnawaz, 2017). Moreover, the GIT contains other proteins and cell types, such as the major drug efflux transporter, P-glycoproteins, and M cells, which are believed to be less protected by the mucus, thus they are common delivery targets for nanocarriers (Date, Hanes and Ensign, 2016).

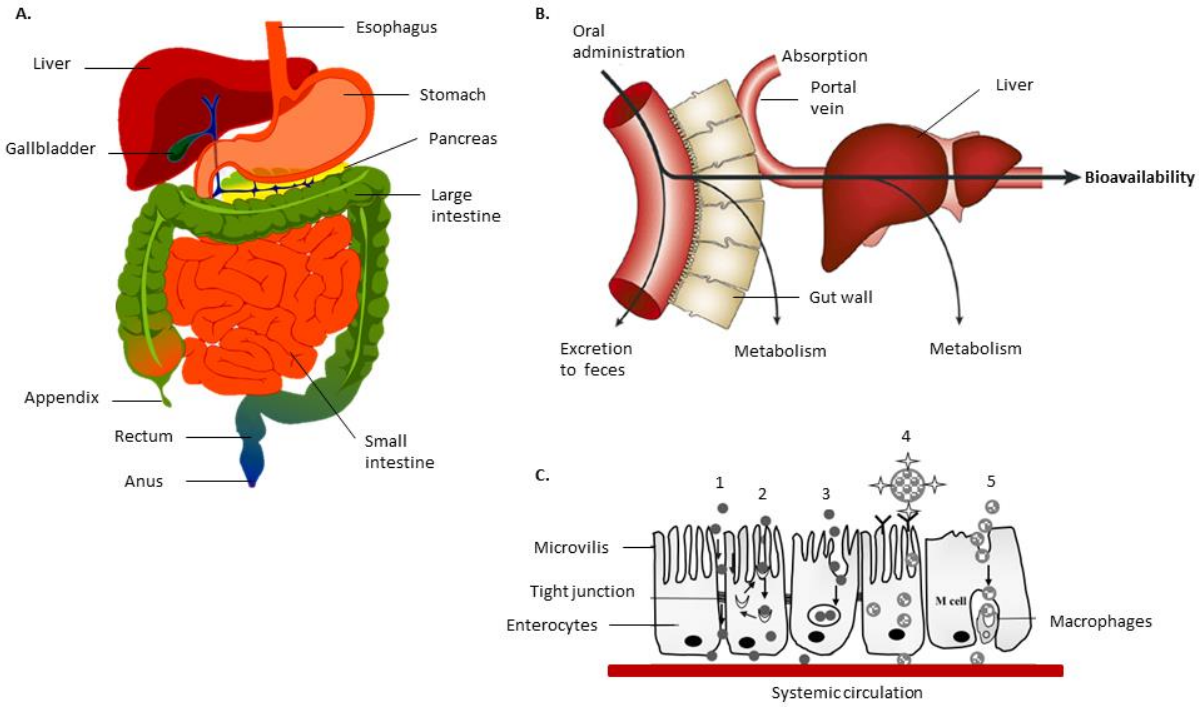

Figure 13. (A) Organs forming the gastrointestinal tract. (B) Oral bioavailability is defined as the fraction of an orally administered drug that reaches the systemic circulation after absorption, excretion, and small intestine and hepatic metabolism. **(C) Transport types across the intestinal epithelium:** paracellular transport (1), carrier-mediated transport (2), transcellular passive transport (3), receptor-mediated nanoparticulate transport (4), and macrophage-mediated nanoparticulate transport (5). Figures adapted from the PNG Library and (Dilnawaz,2017).

Polymer-based nanoparticles are promising tools to address many of the challenges associated with oral formulation. Actually, drug-polymer nanoparticles administered orally show greater stability and protection against proteolytic enzymes than administration of the free drug, as the encapsulating polymer protects against the harsh gastric environment. When nanoparticles adhere to the mucus, the retention time is increased and immediate clearance avoided, resulting in a higher drug payload across the GIT (Dilnawaz, 2017). Transport across epithelium partially depends on nanoparticle size, whereas drug release depends on polymer used. Moreover, surface charge and hydrophilicity have an impact on transport. Particles with an overall a total positive charge interact better with the mucus, whereas highly hydrophilic nanocarriers are poorly absorbed (Alonso, 2004; Kumari, Yadav and Yadav, 2010;

Raza *et al.*, 2019). Polymeric nanoparticles, such as LPs, can be engrafted with ligands like PEG to increase retention or with chitosan, which has bioadhesive properties (Plapied *et al.*, 2011).

2.4.1. Linear polymers

Linear polymers are giant molecules formed by polymerization of covalently bound monomers resulting in polydisperse linear structures.

Poly(amido-amine)s

Poly(amido-amine)s (PAAs) are a unique family of synthetic polymers obtained by Michael-type stepwise polyaddition of *prim*- or *sec*-amines to bisacrylamides at room temperature with no added catalysts. High monomer concentrations and a relatively low reaction temperature in water produce the best outcomes. Actually, the resulting polymers have number- and weight-average molecular masses usually ranging between 5,000 – 40,000 and 10,000 – 70,000 Da respectively, with a polydispersity index of 1.5 – 2.0 depending on the purification method used. They are amphoteric linear polymers carrying in the same monomer tert-amino and amino groups regularly arranged along the main chain, and acid functions as side substituents, usually carboxyl groups. Thus, their average excess charge depends on pH (Urbán, Ranucci and Fernàndez-Busquets, 2015). This family of polymers exhibits a combination of properties which makes them a potential tool in the field of biomedicine as polymer therapeutics (term used to describe a polymer behaving as the bioactive or as the inert carrier) (Liechty *et al.*, 2010). Additionally, PAAs are biocompatible and biodegradable in aqueous media, including physiological fluids, they are environmentally friendly, simple synthesize and they are easy to scale up (Ferruti, Marchisio and Duncan, 2002; Manfredi *et al.*, 2007; Ferruti, 2013). All these characteristics are relevant for malaria chemotherapy given the current need for MDA, in contrast to individual intravenous injection of liposomal formulations (Urbán and Fernàndez-Busquets, 2014).

PAAs have been used as gene delivery vehicles (Griffiths *et al.*, 2013), and they can be highly functionalized, for example with heparin with which they form stable complexes (Ferruti, 2013). Actually, PAA resins were used in the past to neutralize the anticoagulanet activity of heparin in solution (Ferruti, Marchisio and Duncan, 2002). In general, the toxicity of PAAs increased with their average positive charge. Indeed, strong cationic PAAs are therefore highly basic, toxic and with a high hemolysis activity. However, amphoteric PAAs can be safely administered parentally without the risk of long term accumulation and displaying minimum cytotoxicity or hemolysis at a pH of 7.4. This can be done because they contain carboxyl groups that can switch from a prevailingly cationic to a prevailingly anionic state in a relatively small pH interval (Ferruti *et al.*, 2000). Additionally, their degradation seems to be purely hydrolytic compare to other polymers and is strongly influenced by pH, but does not seem to be affected by the presence of lysosomal enzymes at pH 5.5 (Ranucci E, Spagnoli G, Ferruti P, Sgouras D, 1991).

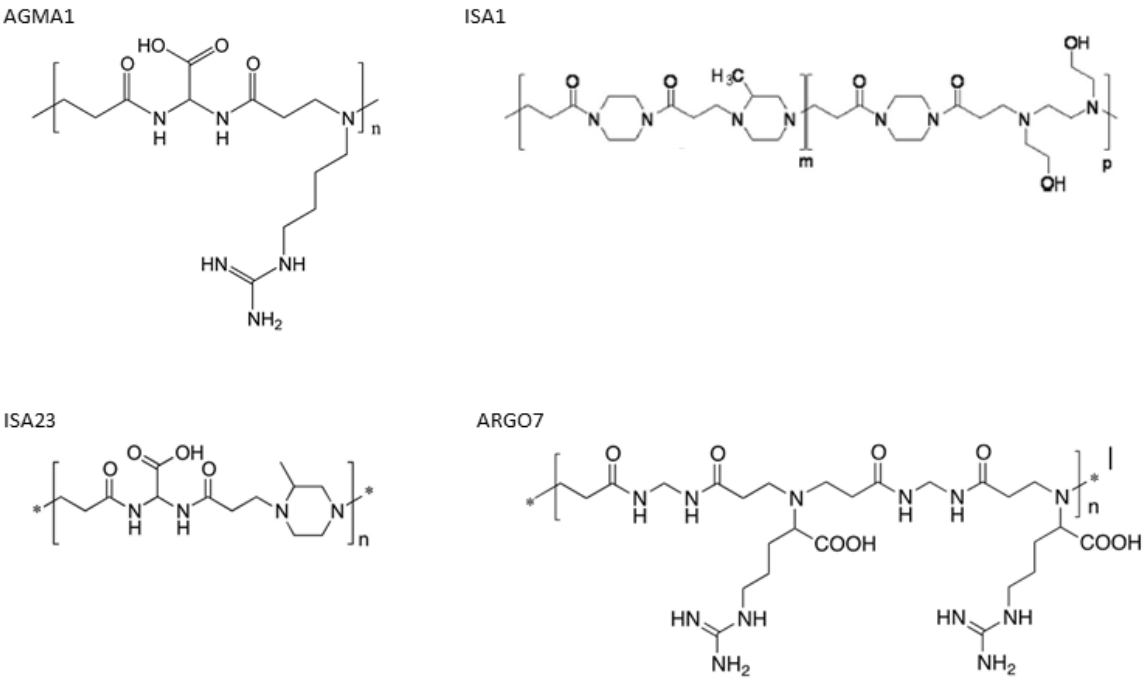

Figure 14. Chemical structure of a monomer of the amphoteric poly(amido-amines) AGMA1, ISA1, ISA23 (Urbán *et al.*, 2014) and ARGO7.

When PAAs are smaller than 70 nm of diameter they can be permeable to pRBCs, being a feature that is shared with peptides and proteins. AGMA1, ISA1 and ISA23 (Figure 14) fulfill this requirement, adopting a globular conformation that has been demonstrated by atomic force microscopy (Urbán *et al.*, 2014). Nonetheless, ARGO7 is a new PAA and remains to be investigated as an antimalarial (Figure 14).

a. AGMA1 is an amphoteric polymer which disproved the theory of prevailingly cationic polymers being toxic. Each unit contains three ionizable groups: a strong acid, a medium-strength base, and a strong base, resulting in excess positive charges of 0.55 up to a pH of 10.5. Despite being prevailingly cationic, AGMA1 proved nontoxicity and nonhemolytic activity *in vitro*, between pH 4.0 to 7.4 (Franchini *et al.*, 2006). The absence of hemolytic properties is not related to a lack of membrane interaction, but rather to a deficiency in inducing damage in the membrane. Unexpectedly, when AGMA1 is injected into the blood stream it behaves like an anionic polymer since it is not toxic, therefore, Ferruti *et al*. hypothesised that AGMA1 is able to be localised on the blood cell membranes without destabilizing them, consequently AGMA1 escapes from the clearance process (Ferruti *et al.*, 2007). In addition, AGMA1 had been described as a transfection promoter capable of forming stable complexes with DNA (Richardson *et al.*, 2001). Previous studies showed that AGMA1 has antimalarial activity *in vitro* in a concentration and size dependent manner. It has also been shown to have a sufficient loading capacity for CQ and PQ, and preferential targeting to pRBCs, as well as significant interaction with RBCs. *In vivo*, AGMA1 showed a concentration peak at 1.5 h after injection and was not detectable 3 h later (Urbán *et al.*, 2014). This more rapid disappearance from the blood stream compared to other PAAs, can be explained by its strong structural resemblance

to the tripeptide arginine-glycine-aspartic acid (RGD) which is known to play a role in the binding of extracellular proteins to cell surface integrins as AGMA1 does (Franchini *et al.*, 2006).

b. ISA1 is a weakly cationic polymer with excess positive charges of 0.55 per unit at a pH of 7.4, due to the presence of a single ionization group, a *tert*-amine. Actually, the antiviral activity of ISA1 is directly related to its positive charge (Ferruti, 2013). In a study by Urbán *et al*., ISA1 showed a highly specific selectivity towards pRBCs and a low capacity to incorporate a substantial amount of the antimalarial drugs, CQ and PQ (Urbán *et al.*, 2014).

c. ISA23 is the only amphoteric polymer of the four presented here, with a negative excess charge of 0.38 per unit at pH 7.4. At this pH, the single strong carboxyl group is protonated, and the two basic tertriary amine groups are weakly protonated, making ISA23 nontoxic, nonhaemolytic and circulates for a long time in bloodstream when injected in mice (Richardson, Ferruti and Duncan, 2009). Furthermore, after being internalized in cells by pinocytosis, ISA23 promotes the intracellular trafficking of DNA and proteins (Richardson *et al.*, 2001). Similar to AGMA1, ISA23 has a high loading capacity for CQ and PQ, demonstrating a certain antimalarial activity in a concentration and size dependent manner, and having high specificity towards pRBCs *in vitro*. *In vivo* ISA23 persisted in the blood up to 72 h after showing a peak concentration 1.5 h post-injection (Urbán *et al.*, 2014).

d. ARGO7 is a relevant example of a novel branch of PAAs named poly(amido-amine acid)s (PAACs), obtained by the polyaddition of natural α-amino acids and glycines to bis(acrylamide)s. Although ARGO7 is a PAAC, it maintains amphoteric properties; it has a folded structure and has been shown to be endowed with cell permeation ability and minimal cytotoxicity (Manfredi *et al.*, 2017). ARGO7 requires several months for the synthesis of a high molecular weight product, in contrast to the 7 days required to synthesis AGMA1, ISA1 and Isa23. This amphoteric prevailingly cationic polymer has a positive excess charge of 0.25, and it is rich in arginine, sharing some of the unique biological properties of polyarginine cell permeating peptides (Ferruti *et al.*,2014).

2.4.2. Branched polymers

Branched polymers or dendritic polymers are macromolecules containing a large number of repetitive units arranged in a branched structure, which adopts a globular configuration packed more loosely than linear polymers. Moreover, branched polymers are much more complex than linear polymers and have great potential as multifunctional nano-scale devices, such as gene delivery systems and DDS, since their architecture and size can be highly controlled (Liu and Fréchet, 1999).

Classical dendrimers, made with a single type of monomers, have an accurately defined chemical structure, and are synthesized under well-controlled conditions. This leads to monodisperse compounds formed by three different parts: the central core, the branches and the terminal groups. These groups are present at the outer surface of the macromolecule and provide areas which can be modifiable to functionalize the structure (Figure 15 C) (Bugno, Hsu and Hong, 2015). The increasing

number of repetitive branching units determines the generation (G) of the dendrimer (Liu and Fréchet, 1999).

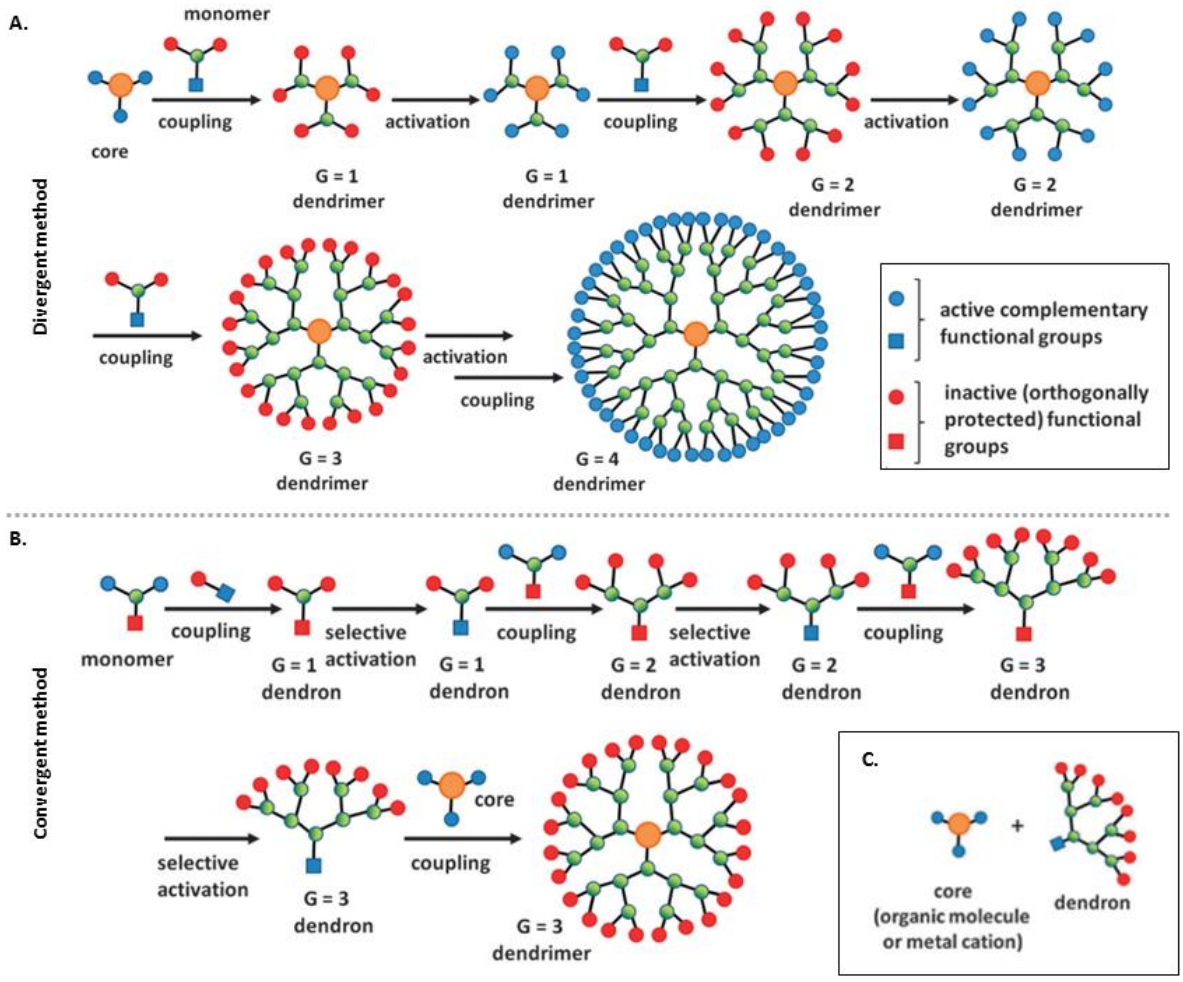

Figure 15. (A) Synthesis of dendrimers according to the divergent method for a fourth generation dendrimer with a repetitive cycle of coupling and activation. **(B) Synthesis of dendrimers according to the convergent method** for a third generation dendrimer with a repetitive cycle of coupling and selective activation. **(C) Parts of a dendrimer:** the core and the dendron, a single branch of a dendrimer made by branches in green and terminal functional groups in red. Figure adapted from (Sowinska and Urbanczyk-Lipkowska, 2014).

The primary methods for the synthesis of dendrimers can be classified into two complementary approaches which are drastically different from those of classical polymers, and involve time and experience: divergent and convergent. Divergent synthesis utilizes a polyfunctional core which, through successive activation and condensation reactions, the dendrimer grows radially from the core to the surface (Figure 15 A), sometimes resulting in higher generation dendrimers with defects (Tomalia, 1985). Conversely, convergent synthesis, enables dendrimers to be synthesized radially from the surface to the focal point (Figure 15 B), where dendrimer defects can be minimised (Hawker and Fréchet, 1990). Over time more effective methods have been developed with fewer reaction steps and shorter reaction times. Thus, new types of dendrimers have been designed, containing different building blocks, the so-called block dendrimers. Some of these block dendrimers are known as “Janus

dendrimers" which possess at least two different types of terminal functionalities that are positioned in separate parts of the dendrimer surface combining several properties in one molecule. Nonetheless, despite improvements in the synthesis techniques, high-generation dendrimers (>G5) without defects are still hard to produce, due to steric issues (Sowinska and Urbanczyk-Lipkowska, 2014).

Some of the branched polymers most frequently investigated have shown an ease of functionalization through amino-based chemistry and are commercially available. These are polyamidoamines (PAMAM), poly(propylene imine) (PPI), and poly-L-lysine (PLL) dendrimers. PAMAM dendrimers produced by the divergent method are extremely monodisperse for earlier generation (1 – 5 G). PAMAM do not show toxicity for low generation dendrimers; however, toxicity increases with each generation, due to the increase of the positive charges. In fact, they are the dendrimers most commonly used as drug delivery systems due to their hydrophilicity, biocompatibility, and non-immunogenicity (Pearson *et al.*, 2012).

In contrast, PPI, a cationic dendrimer also widely used with terminal amino groups, showed toxicity, although PPI toxicity does not follow the PAMAM toxicity pattern (Kesharwani, Jain and Jain, 2014). Indeed, PPI toxicity is reduced with the synthesis of a fluorinated-PPI. Fluorinated-PPI shows a high transfection efficacy similar to Lipofectamine 2000, and low cytotoxicity *in vitro*. Thus, when fluorinated, PPI can be used in gene therapy to treat various diseases (Liu *et al.*, 2014). The cationic dendrimer PLL is mostly often used as a gene carrier, and differs from PAMAM and PPI in that PLL is mostly asymmetric and extremely flexible; however, it is an indicated molecule to be used as drug carrier (Roberts *et al.*, 2009).

The external layer of branched polymers can be easily conjugated to drugs and targeting moieties, and the internal layers are suitable for encapsulation of drug molecules, which improve drug efficacy, reducing drug toxicity and controlling drug mechanisms (Twibanire and Grindley, 2014). Up to now, only two dendritic structures have been studied for the treatment of malaria (Mhlwatika and Aderibigbe, 2018): a block copolymer explained later on, and a 4G glycodendrimer PLL. This PLL had polyethylenegycol (PEG-100) as a core for the delivery of chloroquine phosphate with or without peripheral D-galactose, which showed a sustained drug release behaviour *in vitro* as well as *in vivo* with reduced cytotoxicity when coated with galactose (Agrawal, Gupta and Jain, 2007).

Dendritic polymers can be classified in subgroups, depending on their shape, structure, branching, solubility, chirality and attachment:

Hyperbranched polymers (HPs)

Hyperbranched polymers have a high branching density per unit, with a random structure compared to perfectly branched polymers. Actually, HPs have gained attention in the past years because of their greater availability and ease of scale-up compared to classical dendrimers. HPs can be obtained with a polymerization reaction of a single step, which however, limits the accuracy of the resulting compound, leading to a certain polydipersion (Gao and Yan, 2004). HPs possess many properties attributed to their analogues, such as: globular shape, flexible chains and a high amount of

multifunctional groups, to control and adjust properties. Therefore they are a suitable alternative to perfect dendrimers as building blocks for dendritic nanocarriers systems (Voit and Lederer, 2009).

Dendronized polymers (DPs)

Dendronized polymers are a type of polymers produced by the combination of linear and dendritic molecules as side pendent moieties. DPs can be obtained by direct polymerization of dendritic macromonomers or by attaching dendrons to a linear polymeric core (Figure 16 A) (Gao and Yan, 2004). These hybrid macromolecules have properties of both parental structures and enable the designing of well-defined amphiphilic dendronized polymers, which can bring about supremolecular aggregates in an aqueous phase (Calderón *et al.*, 2007).

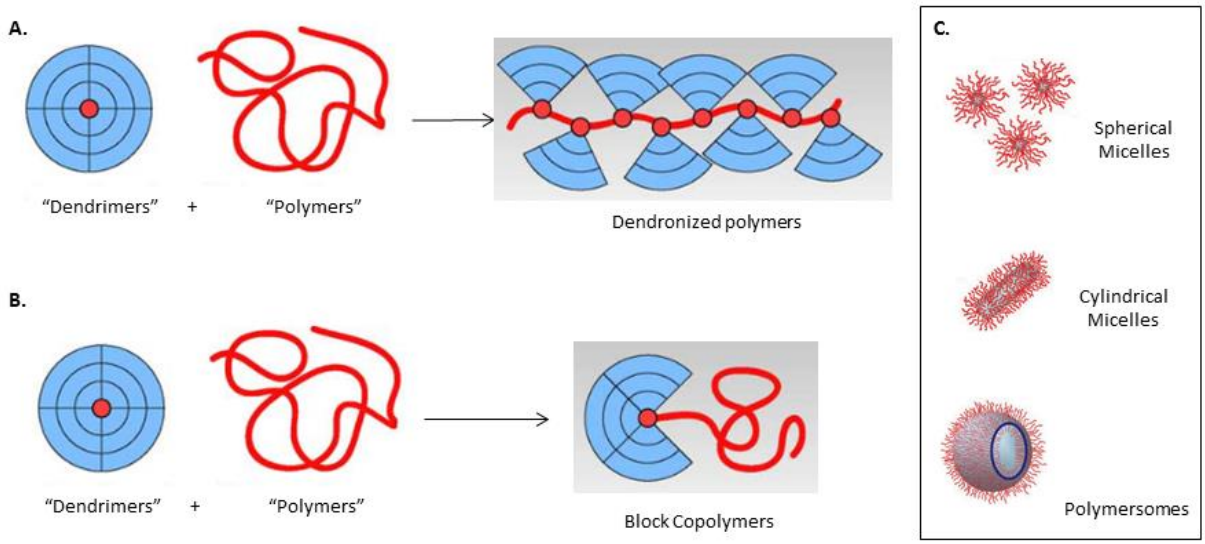

Figure 16. (A) Synthesis of dendronized polymers with a third generation dendrimer and a linear polymer (Frauenrath, 2005). **(B) Synthesis of block copolymers** with a third generation dendrimer and a linear polymer (Frauenrath, 2005). **(C) Morphologies adopted** by self-assembly block copolymers in water (Blanazs, Armes and Ryan, 2009).

With the aim of obtaining the properties of dendrimers and hyperbranched polymers in a single structure, Wu *et al.* introduced low generation dendrimers into a hyperbranched polymeric backbone to yield dendronized hyperbarnched polymers (DHPs). The synthesis of DHPs is much easier than that of high generation dendrimers, leading to structures with fewer defects compared to normal HPs (Wu *et al.*, 2015).

Block copolymers (BCs)

Block copolymers contain two different monomers grouped in distinct blocks along a polymer chain with various architectures, from linear to branch, among others (Figure 16 B). They have a versatile composition that can be precisely controlled with the advances in polymer synthesis (Feng *et al.*, 2017).

Amphiphilic block copolymers have the ability to self-assemble in solution forming vesicles. These vesicles can adopt different morphologies: spherical micelles, cylindrical micelles and polymersomes (Figure 16 C), and they exhibit superior mechanical and physical properties compareed to lipid-based vesicles (Blanazs, Armes and Ryan, 2009). Besides, these vesicles contain a hydrophobic interior, which can entrap drugs, surrounded by a hydrophilic shell, often composed of poly(ethylene oxide) (PEO). PEO can form hydrogen bonds with the aqueous surrounding and form a tight shell, which provides many advantages: resistance against protein adsorption and cellular adhesion, protection of the drug from hydrolysis and enzymatic degradation, and prevention against reticuloendothelial system recognition, thereby increasing the circulation time in blood (Feng *et al.*, 2017).

As an antimalarial nanotechnology strategy to block invasion and increase exposure of merozoites to the host immune system, Najer *et al*. used a polymersome composed by amphiphilic copolymers combined with heparin, to mimic RBC membranes (Najer *et al.*,2014). Following the same strategy, a recent study by the same group used larger polymersomes of around 7 µm, known as heparin giant unilamellar vesicles (GUVs). These vesicles mimic the RBC membrane, and they are formed with electroformation techniques and the same two copolymers as those previously mentioned: poly(2-methyl-2-oxazoline)-*block*-poly(dimethylsiloxane)-*block*-poly(2-methyl-2-oxazoline) (PMOXA-b-PDMS -b-PMOXA), and PDMS-b-heparin. This micro strategy was also able to bind to the parasite ligand *Pf*MSP1. Furthermore, merozoites interacted and deformed this large-sized RBC membrane mimic, interrupting the life cycle of the parasite and exposing the merozoite to the host immune system (Najer *et al.*, 2016).

A type of block copolymer is the hybrid dendritic-linear-dendritic block copolymers (HDLDBCs). These polymers have been exploited for different applications such as gene therapy and drug delivery due to their precise molecular structure, globular shape, high functionality of the dendrimer segment, and the combination of variant linear and dendritic segments (Wang *et al.*, 2008). Previous studies by our group have investigated the use of two different HDLDBCs based on the triblock copolymer Pluronic® F127 coupled at both ends with a glycine-terminated dendron of two generations, G1 and G3, derived from 2,2'-bis(hydroxymethyl)propionic acid (bis-MPA), as a nanocarrier for CQ and PQ. Both macrostructures were detected inside pRBCs, and the dendritic polymer with G3 dendron loaded with CQ and PQ showed a 3- and 4-fold better IC_{50} down to 4.0 and 1.1 µm, respectively compared to the free drug (Movellan *et al.*, 2014). Despite these positive results, the resulting drug-loaded carriers were above the 70 nm described as the upper limit for the entry of nanoparticles into pRBCs through the NPPs (Goodyer *et al.*, 1997), suggesting that these structures could be improved with better synthesis.

3.1. EPIDEMIOLOGY

Leishmaniasis is a neglected disease endemic in large areas of the tropics, subtropics and the Mediterranean basin. In fact, the disease is basically a zoonosis, therefore humans, which get infected by the bite of a sandfly, are only incidental hosts in the life cycle (Grimaldi and Tesh, 1993). It is present in 97 countries worldwide, putting at risk more than 350 million people. By 2018, WHO reported that Leishmaniasis was responsible for around 1 million new cases, concentrated mostly in 18 countries, however, only a small fraction of those new cases eventually developed symptoms which are a spectrum of clinical manifestations, like visceral leishmaniasis (VL) or cutaneous leishmaniasis (CL) (Figure 17), that includes three clinical manifestations (WHO, 2019), explained later on. In the South of Europe, where the main reservoir are dogs, there is a high prevalence of asymptomatic humans infected by *L. infantum*, suggesting a latent public health issue. Asymptomatic cases are apparently infected healthy individuals (Michel *et al.*, 2011) who will not develop clinical disease, unless they suffer from immunosuppression or coinfections (Georgiadou, Makaritsis and Dalekos, 2015).

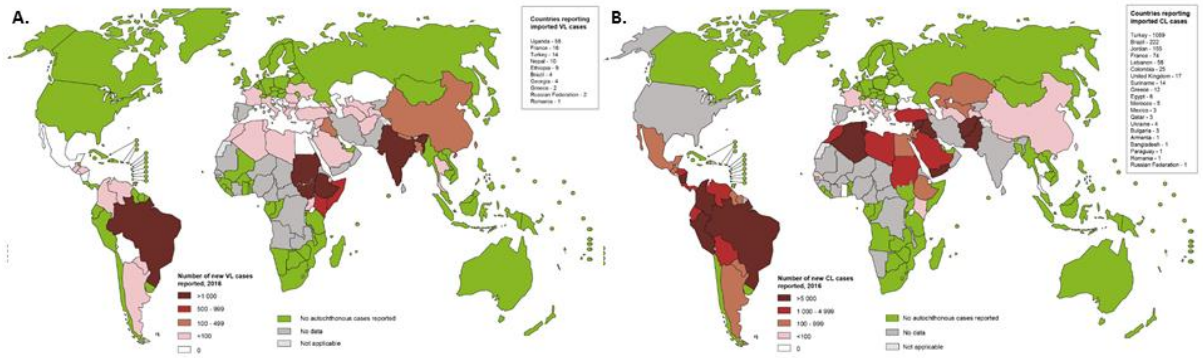

Figure 17. Global Lesihmaniasis distribution for **(A) visceral leihsmaniasis** and **(B) cutaneous lesishmaniasis.** Figure adapted from (WHO, 2019).

Leishmaniasis is caused by flagellated protozoans of the genus *Leishmania* vectored by sandflies. From the 800 existing phlebotomine sandflies, only 98 species of the genera *Phlebotomus* and *Lutzomyia* have been proven or suspected to transmit human leishmaniasis. As for *Plasmodium*, only female sandflies attack mammals to take blood meals for the correct development of the eggs (Maroli *et al.*, 2013). A deep understanding of relationship between sandflies and *Leishmania* is crucial for strategy development, disease control and prediction of transmission patterns (Akhoundi *et al.*, 2016).

3.2. PATHOPHYSIOLOGY

Leishmania parasites belong to the Trypanosomatidae family, which consists of three dixenous genera (life cycle occurs either in vertebrates or in plants and invertebrates), which are *Trypanosoma, Phytomonas, and Leishmania*. And eleven monoxenous genera (life cycle occurs only in invertebrates),

which are *Leptomonas, Crithidia, Blastocrithidia, Sergeia, Wallacemonas, Blechomonas, Jaenimonas, Angomonas, Strigomonas, and Kentomonas*. Moreover, *Leishmania* parasites also belongs to the subfamily Leishmaniinae formed by *Leishmania* and *Crithidia*, and to the genus *Leishmania*. Actually, up to date, 53 species of *Leishmania* had been reported (Akhoundi *et al.*, 2016), and more than 20 species are known to be pathogenic for humans causing different clinical manifestations: visceral leishmaniasis, localize or diffuse cutaneous leishmaniasis or mucocutaneous leishmaniasis. Leishmaniasis manifestations can be divided depending on the localization of cases: Old World (Africa, Asia, and Europe) and New World (the Americas and Oceania), and depending on the causing agent determined by the localization of cases (Table 6) (Maroli *et al.*, 2013).

Table 6. Classification of *Leishmania* spp. depending on the clinical disease they cause and their location. The Old world includes Africa, Asia and Europe, and the New world the Americas and Oceania (Maroli *et al.*, 2013; Akhoundi *et al.*, 2016).

Clinical disease	Old World	New World
Visceral leishmaniasis (VL)	*L. donovani, L. infantum*	*L.infantum (L. chagasi synosym)*
Localised cutaneous leishmaniasis (LCL)	*L. tropica, L. major and L. aethiopica*	*L. mexicana complex (L. mexicana, L. amazonensis, L. pifanoi, L. garnhami, and L. venezuelensis) or the subgenus Viannia (L. braziliensis, L. guyanensis, L. panamensis, L. naiffi, L. shawi, L. lainsoni, and L. peruviana).*
Diffuse cutaneous leishmaniasis (DCL)	*L. aethiopica*	*L. amazonensis*
Mucocutaneous leishmaniasis (ML)		*L. braziliensis (Viannia subgenus), L. guyanen-sis, L. panamensis, and L. amazonensis*

Leishmania parasites need phlebotomine sand flies to complete their life cycle and to propagate. In fact, *Leishmania* spp. are transmitted in the Old World, by 42 species of sandflies belonging to the *Phlebotomus* genus, whereas in the New World by 56 species from the *Lutzomyia* genus. Sandflies are normally more active during night time hours (Georgiadou, Makaritsis and Dalekos, 2015).

Precisely *L. infantum* is the causing agent of VL in children and immunosuppressed adults in the Mediterranean area (North Africa and Europe), Asia and Brazil. However, dogs in these areas are the main victims suffering from zoonotic VL (Michel *et al.*, 2011).

3.2.1. *Leishmania* spp. life cycle

Leishmania spp. are obligated intracellular protozoa, with a life cycle involving the mammalian host (humans and dogs) and the vector host (sandflies) and it takes between 53 to 100 days to complete. In fact, humans are the main vertebrate host, while dogs are the main reservoirs. When a sandfly bites its host, regurgitate *Leishmania* promastigotes into the skin, which parasite cells from the MPS, which comprise monocytes, macrophages, and dendritic cells. Majority of the infected cells are macrophages, and the parasite avoid their killing activity. Phagocytic cells that contain lysosomes in their cytosol,

internalize promastigotes, the transient form in humans, forming a phagosome that fuses to internal lysosomes forming phagolysosomes. The inner part of a phagolysosoma is hydrolytic, nevertheless, promastigotes are completely adapted to this condition and transform to amastigotes, which get surrounded by a parasitophorous vacuole. This process takes place between 3 to 5 days, then amastigotes divide within phagolysosomes over a period of 4 to 6 days, until eventually, host cell lysis freeing parasites which infect new macrophages, either locally or in distant tissues after dissemination. This part of the cycle, from promastigote to amastigote, can occurs in both humans and dogs being an anthroponotic or zoonotic cycle respectively. Afterwards, when a sandfly blood feed on an infected host, macrophages infected with amastigotes are taken, these move to the midgut where they rapidly differentiate back into promastigotes. Then, they divide and migrate to proboscis completing the life cycle (Figure 18) (Moradin and Descoteaux, 2012; Esch and Petersen, 2013; Shaw and Carter, 2014; Torres-Guerrero *et al.*, 2017).

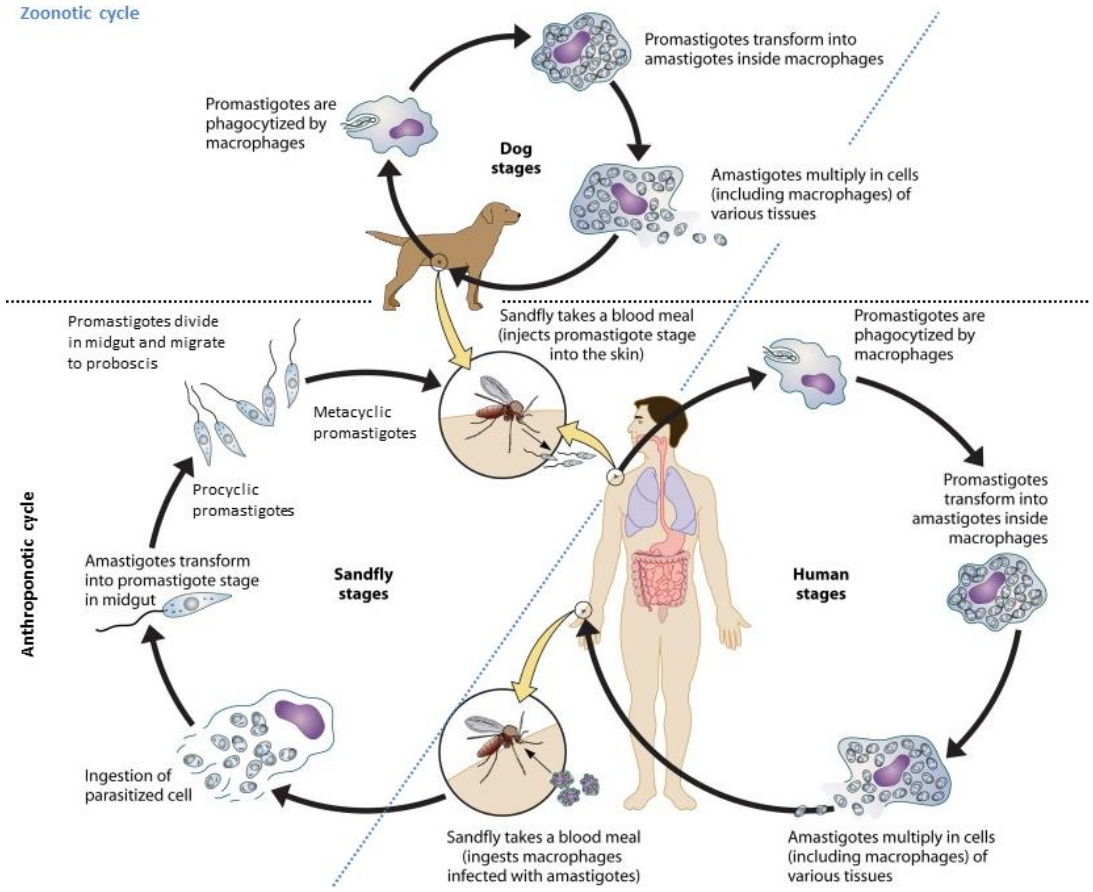

Figure 18. *Leishmania* spp. life cycle which takes place in two different hosts, the human host and the sandfly host. Figure adapted from (Esch and Petersen, 2013).

Amastigotes are responsible for the maintenance and propagation of leishmaniasis and are the virulent form responsible for the different clinical symptoms in humans, thus the perfect target for vaccine development (Selvapandiyan, Dey and Gannavaram, 2014).

Amastigote stage

Amastigotes are obligated intracellular parasites that measure from 2.5 to 3.5 µm (Figure 19 B) found in macrophages, thus highly adapted to the low pH of the phagolysosome conditions to favour their survival (Besteiro *et al.*, 2007). They are non-flagellated and non-motile forms with a large nucleus and a rod-like organelle called the kinetoplast, that is made up of tightly concatenated extranuclear DNA (Torres-Guerrero *et al.*, 2017). Actually, kinetoplast DNA had been used as a detection tool of *Leishmania* spp. in clinical samples (Ghodratollah *et al.*, 2015).

Promastigote stage

Promastigotes are extracellular, motile, flagellated forms found in sandflies, and they can be divided in two stages. Procyclic stages, which are longer in cell body length and have a remnant flagellum. These stages are located in the insect's midgut and they are multiplicative stages, nonetheless they are not mammalian infected forms. Conversely, metacyclic stages, with a longer flagellum, are located in the thoracic midgut and proboscis, and they do not divide but infect mammalian cells, and survive in it since they are resistance to the complement of host cells (Figure 19 B) (Selvapandiyan, Dey and Gannavaram, 2014).

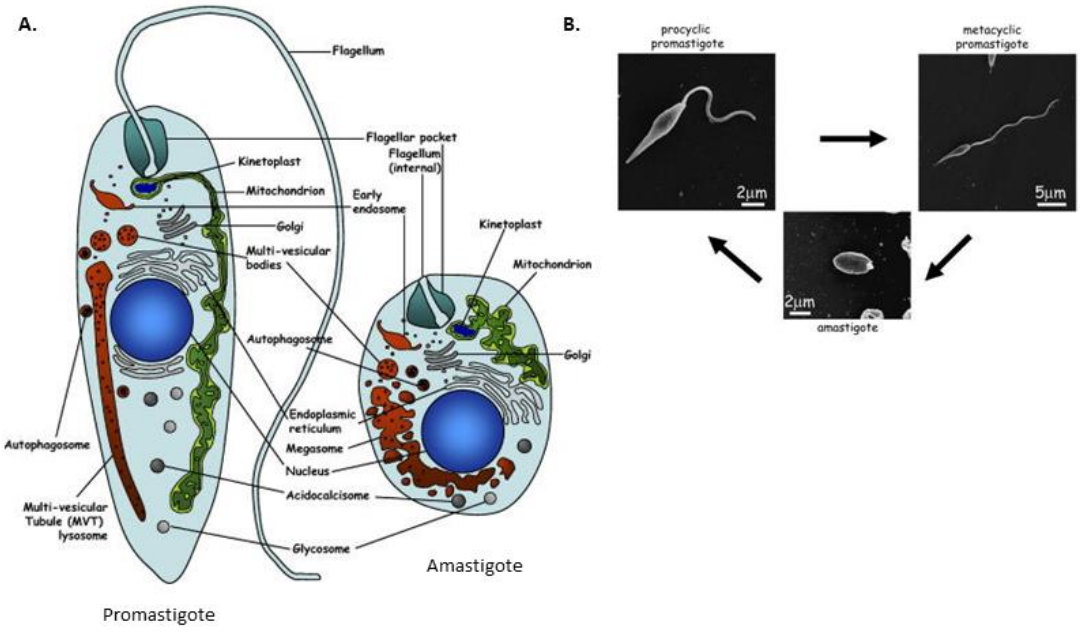

Figure 19. (A) Promastigote and amastigote schematic representation of the main intracellular organelles. **(B) Scanning electron microscope images** of the main life cycle stages (Besteiro *et al.*, 2007).

3.3. CLINICAL SYMPTOMS AND DIAGNOSTIC

Clinical features have different degrees of severity that depends on *Leishmania* spp., host immune system, and cell type invaded. Even though clinical symptoms include a broad range of manifestations, they can be classified into two main forms, visceral leishmaniasis, and cutaneous leishmaniasis, and

this one can be subdivided into three groups localised, diffuse and mucocutaneous leishmaniasis (Grimaldi and Tesh, 1993).

3.3.1. Visceral leishmaniasis (VL)

VL, also known as kala-azar, is the most severe form of leishmaniasis. And, as mentioned earlier, is caused by two different species depending on the localization of the case. In India, Nepal, Sudan, South Sudan, and Ethiopia VL is caused by *Leishmania donovani*, presenting an anthroponotic cycle, where humans are the reservoir. In the Mediterranean area, VL is caused by *Leishmania infantum*, presenting a zoonotic cycle where dogs are the main reservoir (WHO, 2010). However particularly rare, it had been reported other ways to transmit this disease, via intravenous drug use, blood transfusion, organ transplantation, congenital infection and laboratory accidents (Georgiadou, Makaritsis and Dalekos, 2015).

In VL there is a primary infection of phagocytic cells, then amastigotes spread through blood circulation infecting the mononuclear phagocyte system (also known as the reticulo endothelial system) of liver, spleen, bone marrow, lymph nodes and intestine. This causes fever, pallor, anaemia, weakness, anorexia, hepatomegaly, splenomegaly and lymphadenopathy (Steverding, 2017; Torres-Guerrero *et al.*, 2017). Symptoms appear 3 to 8 month post infection and can result in death if not treated (WHO, 2010). There is a relatively high rate of coinfection with HIV in Southern Europe reactivating the subclinical infection to symptomatic infection with similar symptoms than VL, but plus diarrhoea. In this coinfections, relapses occur in a higher frequency and diagnostic is normally delayed due to a focus on HIV diagnose and treatment (Lauletta *et al.*, 2018).

3.3.2. Localised cutaneous leishmaniasis (LCL)

LCL, the most common clinical presentation, is characterized by an infection of macrophages resident in the skin. At the sandfly bite, or on exposed parts of the body, the infection causes small erythemas that normally develop to a single papular or nodular skin lesions, which ulcerates and self-heals within few months leaving permanent scars (Bennis *et al.*, 2018).

3.3.3. Diffuse cutaneous leishmaniasis (DCL)

In DCL, as for LCL, first there is an infection of macrophages resident in the skin, and then, there is a development of multiple, slow progressing nodules which involve the entire body. Although these nodules do not ulcerate, they do not self-cure. Dissemination is due to the anergic character of lesions, meaning that there is a lack of cellular immune response to parasite antigens allowing the parasite to disseminate (Steverding, 2017; Torres-Guerrero *et al.*, 2017).

3.3.4. Mucocutaneous leishmaniasis (MCL)

MCL, also known as espundia, only occurs in South America and arise from a small percentage of cutaneous cases. In MCL first appears a skin lesion that heals, and several months to several years after, the disease spread attacking mucous membranes of the nose, mouse, and throat, causing ulceration of these tissues, and destruction of the nasal septum, lips, and palate, resulting in facial disfiguration. These lesions almost never heal spontaneously (WHO, 2010; Steverding, 2017).

Early diagnosis, to prevent disabilities and death, should be based on clinical features and supported by laboratory testing. The diagnostic of suspected leishmaniasis can be approached by three ways: clinical, parasitological and serological. The most common technique, with the highest specificity, is the direct observation of amastigotes via microscopy in materials from suspected lesions obtained by biopsies, scraping or smears. Frequently, bone narrow and spleen aspiration are performed for diagnostic, with sensitivity of 70 % and 96 % respectively. However, splenic aspiration is associated with a high risk of haemorrhages and bowel perforation (Zijlstra *et al.*, 1992). Moreover, the culture of these samples, preferably with Novy-MacNeal-Nicolle medium (NNN), allows the observation of promastigotes, facilitating characterization and identification of species. Molecular parasitological diagnosis is done by PCR and is particularly useful in cases with low parasite load like in MCL (WHO, 2010; de Vries, Reedijk and Schallig, 2015; Georgiadou, Makaritsis and Dalekos, 2015).

Serological tests, for VL and CL, are mainly based on immunofluorescence antibody test (IFAT), enzyme-linked immunosorbent assay (ELISA), western blot, lateral flow assay, and direct agglutination test. For VL, IFAT, ELISA, and western blot had shown good accuracy. Nevertheless, these techniques require equipment that is poorly adapted to the field setting. On the other hand, for CL, serological tests have low sensibility and variable specificity due to the poor humoral response provoked by the infection. Serological tests can give false positives since specific antibodies remain detectable up to several years after being cured (de Vries, Reedijk and Schallig, 2015; van Griensven and Diro, 2019).

3.4. TREATMENT

LCL is a self-healing disease, nevertheless, the rest required treatment to avoid relapses and/or fatal consequences. In fact, treatment is commonly given for persistent (more than 6 months), disseminated or large lesions. Alternatively, it is also given for lesions located on joints or on the face. Treatment can be given, locally or systemically, depending on the type and extension of lesions (de Vries, Reedijk and Schallig, 2015). First line VL treatment is a single dose of liposomal amphotericin B (L-AmB), which has the highest therapeutic efficacy, and the most favorable safety profile, nonetheless, it is expensive (Bern *et al.*, 2006). In contrast, the first line CL treatment is parental pentavalent antimony in two different forms, sodium stibogluconate, and meglumine antimoniate. These two drugs can have serious, normally reversible, side effects, and resistances started to appear in India and Nepal. Actually, these treatments for MCL showed variable efficacy (Table 7) (Reithinger *et al.*, 2007; WHO, 2010; Ramalho *et al.*, 2018).

There are alternative treatments for both diseases, which include miltefosine, paromomycin, amphotericin B and pentamidine isethionate (Table 7). Although the amount of current drugs is still small, expensive and majority of them causes serious side effects. Additionally, leishmaniasis

treatment is challenging and long, with low efficacy, resulting in low adherence. In fact, in some endemic areas drugs may be in limited supply, particularly in the more rural areas where leishmaniasis normally occurs. Furthermore, there is no vaccine yet (Shaw and Carter, 2014; Sundar and Chakravarty, 2015).

Table 7. First line and alternative treatment of leishmaniasis depending on the clinical disease. Treatment for cutaneous leihsmaniasis includes LCL, DLC and MCL (Reithinger *et al.*, 2007; WHO, 2010; van Griensven and Diro, 2019).

Clinical disease	First line treatment	Alternative treatment
Visceral leishmaniasis (VL)	Liposomal Amphotericin B (L-AmB)	Pentavalent antimony Miltefosine Paromomycin
Cutaneous leishmaniasis (CL)	Pentavalent antimony	Amphotericin B Pentamidine isetionate Miltefosine

In some cases, it might be required supportive treatment before therapy to increase healing rates. For example, rehydration, nutritional supplementation, blood transfusion to correct anemia and treatment of concomitant infections with appropriate antibiotics (Georgiadou, Makaritsis and Dalekos, 2015).

3.5. NANOMEDICINE TO FIGHT LEISHMANIASIS

The causing agent of leishmaniasis is an intracellular parasite, like *Plasmodium*, thus conventional formulations have difficulties to reach this type of parasites prompting the usage of high dose causing increased toxicity. Once again, nanotechnology strategies, such as biocompatible lipid and polymeric nanoparticles, can be interesting approaches for DDSs to treat leishmaniasis. These biomaterials protect the active principle against physical, chemical, and/or enzymatic degradation, help to improve pharmacokinetics, and enhance bioavailability. Consequently, a lower dose can be used and systemic toxicity reduced (Gutiérrez *et al.*, 2015).

One advantage, of leishmaniasis over malaria, is that macrophages are highly phagocytic, facilitating the entrance of drug-loaded nanoparticles. AmB is currently the most antileishmanial agent, thus the majority of efforts in nanothechnology have been focus on loading this drug in different NPs. Three commercialized examples of lipid-based NPs are unilamellar liposomes, lipid complex, and colloidal cholesterol suspension. However, the liposome formulation is the one with the highest plasma half-life, lowest toxicity and the highest efficacy against both clinical forms. Actually, L-AmB is the only nanomedicine approved for parental VL treatment, whereas for CL, L-AmB is not a widespread treatment, due to its high cost and undefined optimum dosing regimen, as a result of a great uptake by the liver (Yardley and Croft, 2000).

Other strategies are being under study, like polymer, metal and carbon-based nanoparticles. Different research groups had been working on poly(lactide-co-glycolide acid) (PLGA) NPs to encapsulate AmB. The drug-loaded NP was more efficient, less cytotoxic and hemotoxic, than the free drug. Nevertheless, so far no systemic administration of PLGA NPs have been approved for clinical use

(Van de Ven *et al.*, 2012; Palma *et al.*, 2018). On the other hand, Gherbawy *et al.* proofed that silver NP had antibacterial activity by the production of large amounts of ROS, which have the ability to kill *Leishmania* parasites (Gherbawy *et al.*, 2013). Moreover, carbon compounds are gaining interest due to their mechanical, thermal and optical properties. For instances, it was studied carbon nanotubes (CNT) covalently attached to AmB, administrated intraperitoneally and orally to hamsters, and they both showed good antileishmania activity and stability. The advantage of this formulation is that is much more economical than L-AmB (Prajapati *et al.*, 2011, 2012). With this respect, as for malaria, the oral route is recommended for both VL and CL, due to the ease of administration and high patient compliance (Sousa-Batista and Rossi-Bergmann, 2018).

Even though liposome alternatives and macrophage targeted delivery systems are gaining interest since they have great potential reducing the duration of the treatment, and frequency of administration, no products had reached the market place yet showing a gap to be filled with further research in nanotechnology (Bruni *et al.*, 2017).

OBJECTIVES

The main objective of this thesis is to contribute new strategies for the oral administration of antimalarial drugs, based on biocompatible, biodegradable, environmentally friendly, and inexpensive polymer drug carriers, which specifically target and deliver the active principle to *Plasmodium*-infected cells. Such strategies would result in low overall doses, but sufficiently high locally, in order to be lethal for the parasite, thus reducing the risk of drug resistance and undesirable side effects.

The specific objectives are:

1. Unspecific toxicity evaluation of different polymer-based nanocarriers.

2. Characterization of the nanocarriers in terms of targeting towards pRBCs, merozoites or other cells (e.g. HUVEC and macrophages), antimalarial activity *per se*, and drug loading capacity.

3. Investigation of the targeting mechanism of polymer-based nanocarriers towards pRBCs.

4. Analysis of the antimalarial activity of drugs encapsulated in polymer-based nanocarriers, *in vitro* in *Plasmodium falciparum* 3D7 cultures, and *in vivo* after intravenous or oral administration to *Plasmodium yoelii*-infected mice.

5. Explore the possible targeting of polymer-based nanocarriers towards *Plasmodium* mosquito stages.

RESULTS

ARTICLE 1

Micelles carriers based on dendritic macromolecules containing bis-MPA and glycine for antimalarial drug delivery

Elisabet Martí Coma-Cros*, Alexandre Lancelot*, María San Anselmo, Livia Neves Borgheti-Cardoso, Juan José Valle-Delgado, José Luis Serrano, Xavier Fernàndez-Busquets, and Teresa Sierra

** These authors contributed equally*

Biomater Sci. 2019 Feb 11; doi: 10.1039/c8bm01600c

ARTICLE 2

Polyamidoamine nanoparticles for the oral administration of antimalarial drugs

Elisabet Martí Coma-Cros, Arnau Biosca, Joana Marques, Laura Carol, Patricia Urbán, Diana Berenguer, Maria Cristina Riera, Michael Delves, Robert E. Sinden, Juan José Valle-Delgado, Lefteris Spanos, Inga Siden-Kiamos, Paula Pérez, Krijn Paaijmans, Matthias Rottmann, Amedea Manfredi, Paolo Ferruti, Elisabetta Ranucci, and Xavier Fernàndez-Busquets

Pharmaceutics 2018, 10, 225; doi:10.3390/pharmaceutics10040225

MICELLES CARRIERS BASED ON DENDRITIC MACROMOLECULES CONTAINING BIS-MPA AND GLYCINE FOR ANTIMALARIAL DRUG DELIVERY

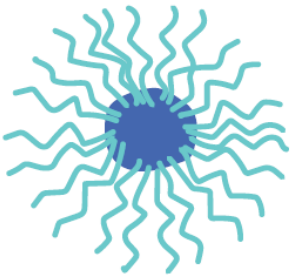

Article 1: Short summary

Current antimalarial drugs are in free form in the bold circulation, have little or non-specificity for their main target *Plasmodium* infected red blood cells (pRBCs), and high cellular unspecificity, demanding for low drug concentration to minimize undesirable side effects, and the risk of sublethal doses, contrarily high doses favour the appearance of resistant pathogen strains. Therefore, antimalarial drugs required delivery approaches such us drug delivery systems (DDSs) to achieve the intake of total dose sufficiently low to be innocuous for the patient but locally high enough to be lethal for malaria parasites.

Biomaterials for antimalarial drug transport need to be investigated in order to attain these objectives. Dendrimers in precise, stand out as valuable candidates due to their inherent features for building nanostructures with controlled size and morphology, and their surface can be functionalized. In this work we have explored the potential ability of two cationic dendritic macromolecules as nanocarriers to deliver antimalarial drugs targeting specifically pRBCs. These particles after drug encapsulation have a size smaller than 30 nm, to facilitate their entry into pRBCs, and are a new hybrid dendritic-linear-dendritic block copolymer based on Pluronic® F127 and amino terminated 2,2'-bis(glycyloxymethyl)propionic acid dendrons with a poly(ester amide) skeleton (**HDLDBC-bGMPA**), and an amino terminated dendronized hyperbranched polymer with a polyester skeleton derived from 2,2'-bis(hydroxymethyl)propionic acid (**DHP-bMPA**), which provided self-assembled and unimolecular micelles respectively.

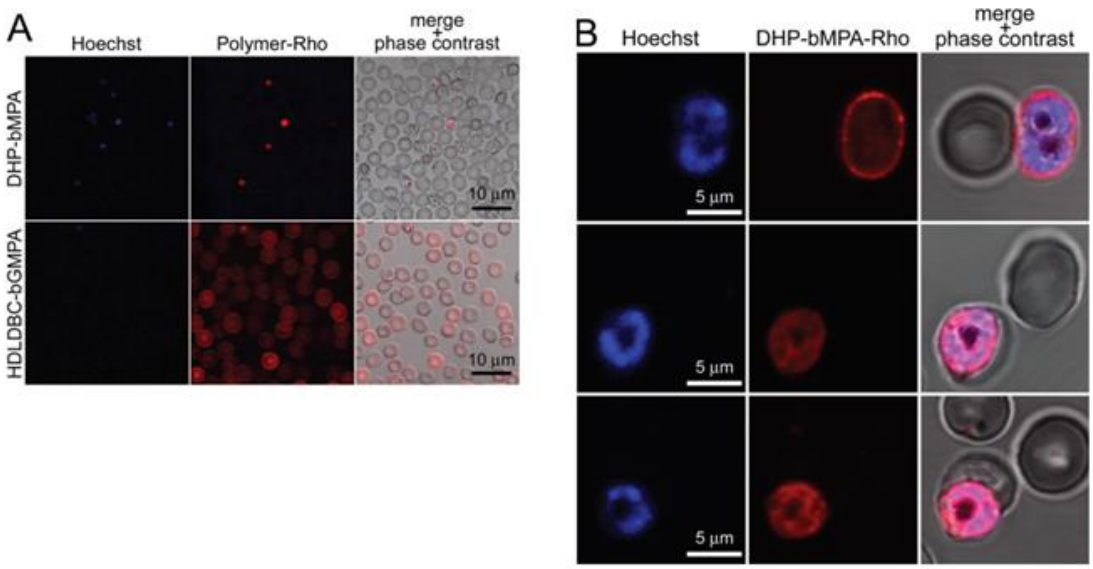

Figure 20. Fluorescence microscopy cell targeting analysis of rhodamine-labeled DHP-bMPA and HDLDBC-bGMPA to non-fixed RBCs and pRBCs. **(A) Conventional fluorescence microscopy** cell targeting of both polymers. **(B) Confocal fluorescence microscopy** cellular and subcellular targeting of DHP-bMPA-Rho.

Both branched polymers interacted with merozoites, nevertheless they showed different targeting properties towards RBCs and HUVEC. Whereas HDLDBC-bGMPA was incorporated by all RBCs, it had a cytosolic localization in HUVEC cells. Conversely, DHP-bMPA showed clear targeting specificity, mainly for parasite late forms, and nuclear localization in HUVEC cells; these results suggest specific binding of DHP-bMPA to *Plasmodium* falciparum exported antigens present in late forms. Moreover, both structures could load chloroquine, primaquine and quinacrine with encapsulation efficiencies between 31 % and 60 %, being HDLDBC-bGMPA capable to load a larger amount. However, the antimalarial activity of those was not improved *in vitro* compared to the drug free form. Conversely, intravenously HDLDBC-bGMPA *in vivo* improved survival (3 out of 5 mice lived ≥ 20 days) when compared to the untreated control group, which typically died at day 6, but it did not improve when compared to the free CQ group. This improvement could be related to the fact that HDLDBC-bGMPA targets all RBCs. Post encapsulation TEM, AFM and DLS analysis discarded possible alteration in size and shape of the dendritic molecules. Thus, modifications of the polymer architecture or chemistry might contribute to improving antimalarial activity in the encapsulated forms. As well, a small size rise, up to 50 to 100 nm, would contribute to a reduction of the blood clearance rates probably improving the overall antimalarial activity.

Biomaterials Science

PAPER

View Article Online
View Journal

Cite this: DOI: 10.1039/c8bm01600c

Micelle carriers based on dendritic macromolecules containing bis-MPA and glycine for antimalarial drug delivery†

Elisabet Martí Coma-Cros,‡[a,b,c] Alexandre Lancelot,‡[d] María San Anselmo,[d] Livia Neves Borgheti-Cardoso,[a,b,c] Juan José Valle-Delgado,[e] José Luis Serrano,*[d,f] Xavier Fernàndez-Busquets*[a,b,c] and Teresa Sierra*[f]

Biomaterials for antimalarial drug transport still need to be investigated in order to attain nanocarriers that can tackle essential issues related to malaria treatment, *e.g.* complying with size requirements and targeting specificity for their entry into *Plasmodium*-infected red blood cells (pRBCs), and limiting premature drug elimination or drug resistance evolution. Two types of dendritic macromolecule that can form vehicles suitable for antimalarial drug transport are herein explored. A new hybrid dendritic-linear-dendritic block copolymer based on Pluronic® F127 and amino terminated 2,2′-bis(glycyloxymethyl)propionic acid dendrons with a poly(ester amide) skeleton (HDLDBC-bGMPA) and an amino terminated dendronized hyperbranched polymer with a polyester skeleton derived from 2,2′-bis(hydroxymethyl)propionic acid (DHP-bMPA) have provided self-assembled and unimolecular micelles. Both types of micelle carrier are biocompatible and exhibit appropriate sizes to enter into pRBCs. Targeting studies have revealed different behaviors for each nanocarrier that may open new perspectives for antimalarial therapeutic approaches. Whereas DHP-bMPA exhibits a clear targeting specificity for pRBCs, HDLDBC-bGMPA is incorporated by all erythrocytes. It has also been observed that DHP-bMPA and HDLDBC-bGMPA incorporate into human umbilical vein endothelial cells with different subcellular localization, *i.e.* cytosolic and nuclear, respectively. Drug loading capacity and encapsulation efficiencies for the antimalarial compounds chloroquine, primaquine and quinacrine ranging from 30% to 60% have been determined for both carriers. The resulting drug-loaded nanocarriers have been tested for their capacity to inhibit *Plasmodium* growth in *in vitro* and *in vivo* assays.

Received 10th December 2018,
Accepted 25th January 2019
DOI: 10.1039/c8bm01600c
rsc.li/biomaterials-science

Introduction

According to the latest estimates, around 219 million cases of malaria occurred globally in 2017 and the disease led to 435 000 deaths.[1] People living in the poorest countries are the most vulnerable, with approximately 90% of deaths in Africa, of which 70% are children under 5 years of age. Although increased prevention and control measures have led to a reduction in malaria mortality rates by more than 42% globally since 2000, an estimated 3.4 billion people are still at risk of being infected and developing disease. Despite the undeniable importance of malaria elimination on the global research agenda, current vaccines in development do not offer prospects of complete protection[2] and the available front-line drugs are rapidly losing efficacy, with resistance already evolved to the first-line drug artemisinin.[3] As a result, since 2014 the malaria incidence and mortality decline have stalled. Thus, alternative strategies[4] working through radically new mechanisms are urgently needed. Antimalarial drugs can potentially target a suite of pathogen life stages inside two different hosts: humans and the insect vector. Infection starts when a parasitized female *Anopheles* mosquito, while taking a blood meal, inoculates sporozoites of the malaria parasite, the

[a]*Nanomalaria Group, Institute for Bioengineering of Catalonia (IBEC), The Barcelona Institute of Science and Technology, Baldiri Reixac 10-12, ES-08028 Barcelona, Spain. E-mail: xfernandez_busquets@ub.edu*
[b]*Barcelona Institute for Global Health (ISGlobal, Hospital Clínic-Universitat de Barcelona), Rosselló 149-153, ES-08036 Barcelona, Spain*
[c]*Nanoscience and Nanotechnology Institute (IN2UB), University of Barcelona, Martí i Franquès 1, ES-08028 Barcelona, Spain*
[d]*Instituto de Nanociencia de Aragón (INA), Química Orgánica, Facultad de Ciencias, Universidad de Zaragoza, Spain. E-mail: joseluis@unizar.es*
[e]*Department of Bioproducts and Biosystems, School of Chemical Engineering, Aalto University, PO Box 16300, FI-00076 Aalto, Finland*
[f]*Instituto de Ciencia de Materiales de Aragón (ICMA), Facultad de Ciencias, Universidad de Zaragoza-CSIC, Spain. E-mail: tsierra@unizar.es*
†Electronic supplementary information (ESI) available. See DOI: 10.1039/c8bm01600c
‡These authors contributed equally.

protist *Plasmodium* spp. In the liver, sporozoites develop into merozoites,[5] which enter the circulation, invade red blood cells (RBCs)[6] and replicate asexually through ring, trophozoite and schizont stages to produce daughter cells that invade new RBCs to perpetuate the blood-stage cycle. Some parasites eventually differentiate into sexual stages, female or male gametocytes that are ingested by a mosquito from peripheral blood. Following fertilization in the insect's midgut, the zygote differentiates into an ookinete that moves through the midgut epithelium and forms an oocyst, which releases sporozoites. The malaria transmission cycle is restarted when sporozoites migrate to the salivary glands and are injected into a human with the mosquito's next bite.

Most chemotherapeutic approaches against malaria are targeted at the asexual, blood-stage parasites that are responsible for all symptoms and pathologies of the disease.[7] Currently administered antimalarial drugs are in free form in the blood circulation and have poor specificity for *Plasmodium*-infected RBCs (pRBCs). This incurs the risk of having to deliver large overall doses over an extended period of time to compensate for drug removal through spleen and liver clearance and kidney filtration. However, patient non-compliance and low concentration thresholds to ward off potential side effects often end up in sublethal local drug amounts reaching infected cells, which in turn stimulate resistance evolution. Because malaria pathophysiology is so complex and the disease is so widespread, it is generally accepted that to achieve eradication a combination of weapons will be needed.[8] These include the improvement of existing approaches and the development of new ones,[9] with drug therapy remaining the mainstay of treatment and prevention,[10] and nanotechnology being able to provide innovative useful tools.[11] The objective of delivering drugs exclusively to a selected site with minimal exposure for sensitive adjacent healthy cells or tissues is the holy grail of the fast-developing nanomedicine field.[12] Encapsulation of drugs in targeted nanovectors is a rapidly growing area with a clear applicability to infectious disease treatment,[13] and pharmaceutical nanotechnology has been identified as a potentially essential asset to the future fight against malaria.[14,15]

In the search for suitable nanocarriers for the treatment of infectious diseases, dendrimers stand out as valuable candidates due to their inherent features for building nanostructures with controlled size, morphology and surface functionalization.[16] In a previous work we had explored different amphiphilic cationic dendritic derivatives based on 2,2′-bis(hydroxymethyl)propionic acid (bis-MPA)[17] as nanocarriers for the targeted delivery of antimalarial drugs.[18] These dendritic derivatives consisted of Janus dendrimers[19] or hybrid dendritic-linear-dendritic block copolymers (HDLDBC),[20] and both self-assembled into micelles with glycine groups at the surface. Although some of these structures exhibited specific pRBC targeting and *in vitro* antimalarial activity, they had an excessive unspecific toxicity, a very large size after antimalarial drug loading (>150 nm), and their *in vivo* tests had been preliminary.

Here we build on our previous work to explore new specifically targeted delivery systems for antimalarial drugs of a size after drug encapsulation (<30 nm) sufficiently small to facilitate their entry into pRBCs.[21] Accordingly, two types of cationic dendritic derivative are proposed, which mainly differ in the way they form the nanocarrier, either self-assembled micelles or unimolecular micelles. As for the former, and on the basis of the promising results shown by the previously reported Pluronic® F127 HDLDBC derivative that contained polyester dendrons,[18] we have herein conjugated Pluronic® F127 with poly(ester amide) dendrons to generate a new micelle-forming self-assembling amphiphilic cationic HDLDBC (Fig. 1A). The combination of the hydrolytic degradability of ester linkages and the stability and H-bond-forming ability of amide groups has proven very interesting for the design of synthetic polymers for biomedical applications.[22,23] Accordingly, a poly(ester amide) dendron conjugated at both ends of Pluronic® F127 has been herein envisaged as a possibility to modulate the size and stability of self-assembled micelles given the additional H-bonding interactions due to amide groups. The dendron employed derives from the monomer 2,2′-bis(glycyloxymethyl)propionic acid (bis-GMPA), which was recently described by us as one of the few examples of poly(ester amide) dendritic structures reported in the literature, which showed high potential for biomedical applications due to the biocompatibility, degradability and positive results in drug and gene delivery of its dendritic derivatives.[24] As for the achievement of a unimolecular micelle carrier, we have

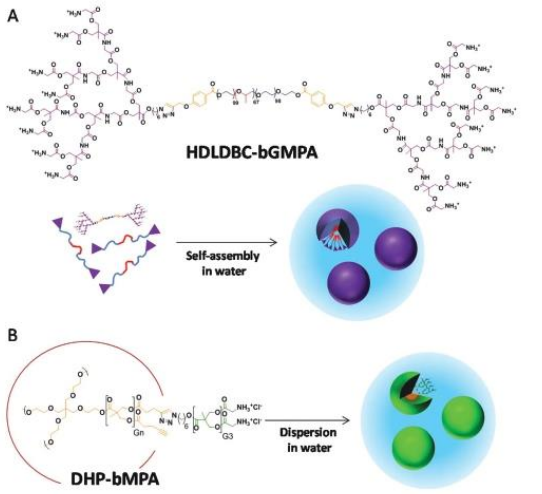

Fig. 1 Chemical structure and cartoon representation of (A) micelle formation by HDLDBC-bGMPA, a hybrid dendritic-linear-dendritic block copolymer composed by Pluronic F127 and dendrons derived from 2,2′-bis(glycyloxymethyl)propionic acid (bis-GMPA), and (B) DHP-bMPA, dendronized hyperbranched polymers derived from 2,2′-bis(hydroxymethyl) propionic acid (bis-MPA) hyperbranched polymers and bis-MPA dendrons functionalized with glycine groups.

selected dendronized hyperbranched polymers (DHPs), also called pseudo-dendrimers, based on a hyperbranched polymer of bis-MPA, conjugated at its periphery with bis-MPA dendrons with exposed glycine moieties (Fig. 1B). We demonstrated that these DHP-bMPA derivatives could deliver DNA into mesenchymal cells.[25] However, their potential as drug carriers remains to be explored. In this respect, these polymers showed appropriate biocompatibility and degradability that make them interesting to be investigated as carriers for antimalarial drug delivery.

Both types of structure have been investigated for their targeting towards pRBCs, and the drug loading capacity and encapsulation efficiencies of the carriers have been tested with the antimalarial compounds chloroquine (CQ), primaquine (PQ) and quinacrine (QN). The resulting nanocarriers have been assayed for their capacity to inhibit *Plasmodium* growth in *in vitro* and *in vivo* assays.

Materials and methods

Reagents

Unless otherwise indicated, all reagents were purchased from Sigma-Aldrich® or Acros™, and used always without further purification. Dichloromethane (DCM) and tetrahydrofuran (THF) were dried using solvent purification systems.

Synthesis and characterization of the dendritic derivatives

Globular DHP-bMPA dendronized hyperbranched polymers as well as DHP-bMPA-Rho, a DHP containing covalently linked rhodamine B fluorophore, were synthesized as previously reported by us.[25] HDLDBC-bGMPA was prepared by copper azide–alkyne cycloaddition (CuAAC) coupling of the *t*-Boc protected bis-GMPA dendron and the Pluronic® F127 bis(alkyne) derivative as depicted in Fig. 2A.

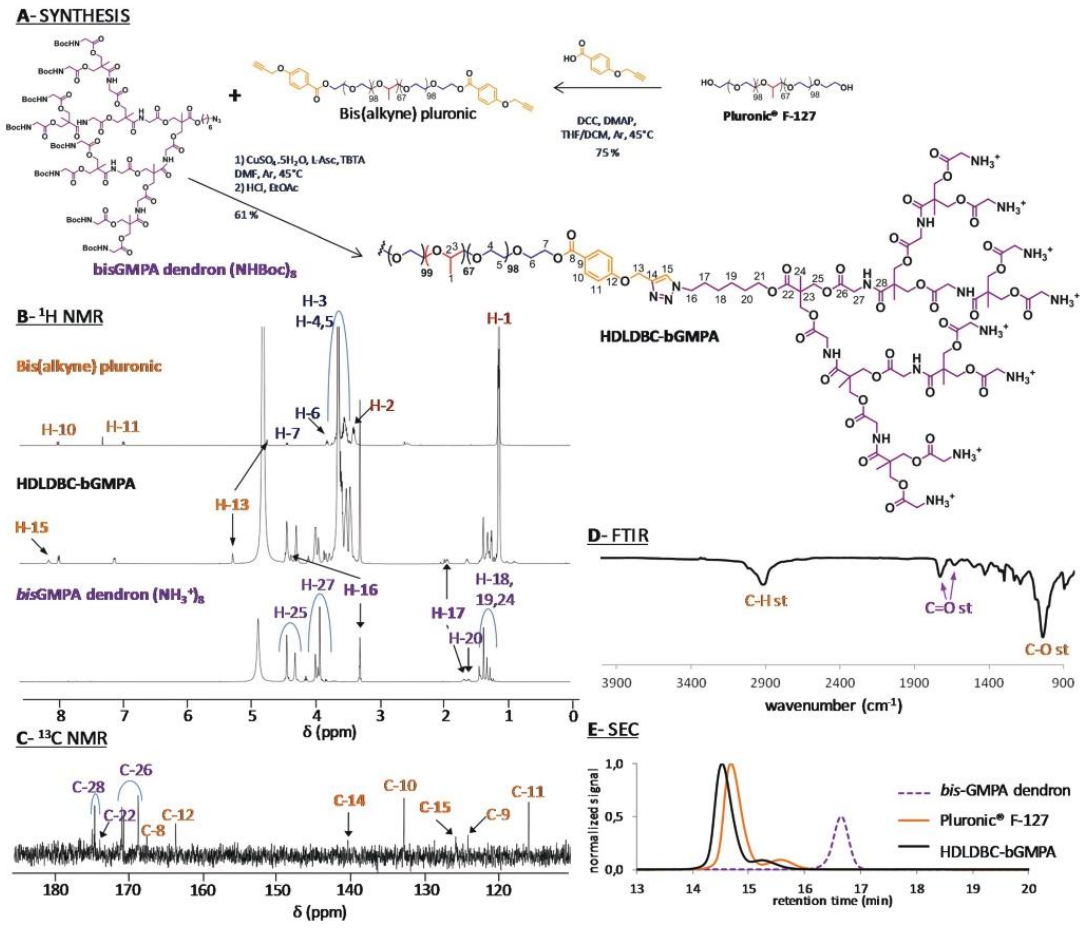

Fig. 2 Synthesis of HDLDBC-bGMPA (A) and chemical characterization by ^{1}H NMR (B), ^{13}C NMR (C), FTIR (D) and SEC (E). ^{1}H NMR spectra with signal relative integration, the ^{1}H–^{1}H COSY NMR spectra and full ^{13}C NMR spectra of HDLDBC-bGMPA are gathered in the ESI.†

Synthetic procedure and analytical data of *t*-Boc protected HDLDBC-bGMPA. Alkyne functionalized Pluronic® F127 (1.00 g, 7.74×10^{-2} mmol, 1.00 eq.) and bis-GMPA dendron $(NHBoc)_8$ (514 mg, 2.01×10^{-1} mmol, 2.60 eq.) were dissolved into 8 mL of dimethylformamide (DMF) in a Schlenk flask and 3 vacuum–argon cycles were made to remove the air. The reaction mixture was stirred under argon atmosphere at 45 °C. $CuSO_4 \cdot 5H_2O$ (18.2 mg, 6.19×10^{-2} mmol, 0.80 eq.), L-ascorbate (24.1 mg, 1.24×10^{-1} mmol, 1.60 eq.) and tris[(1-benzyl-1*H*-1,2,3-triazol-4-yl)methyl]amine (TBTA, 32.8 mg, 6.19×10^{-2} mmol, 0.80 eq.) were dissolved into DMF (4 mL) in a second Schlenk flask and exposed to 3 vacuum–argon cycles. The copper solution was stirred under argon atmosphere at 45 °C for 15 min and was added through a cannula to the previous azide–alkyne reaction. The resulting mixture was stirred under argon atmosphere at 45 °C for 2 days. Then, hot brine (100 mL) was added to the reaction mixture and the product was extracted with dichloromethane (3 × 100 mL). The organic phases were collected, washed with hot brine (2 × 100 mL), dried over anhydrous $MgSO_4$ and the solvent was evaporated under reduced pressure to obtain a yellow solid. The crude product was precipitated into cold diethyl ether, recovered by filtration and washed with cold diethyl ether to yield a white powder. Finally, the product was dialyzed (cellulose membrane, 1000 Da cut-off, Spectra/Por®) against methanol for 24 h to obtain a light yellow solid (855 mg, 61%). ^{1}H NMR (400 MHz, $CDCl_3$) δ (ppm): 1.11 (m, 201H), 1.26 (m, 42H), 1.41 (m, 152H), 1.62 (m, 4H), 1.94 (m, 4H), 3.38 (m, 67H), 3.44–3.74 (m, ~1000H), 3.81 (t, J = 4.8 Hz, 4H), 3.88 (m, 32H), 3.94 (m, 8H), 3.88 (m, 16H), 4.11 (t, J = 6.4 Hz, 4H), 4.18–4.35 (m, 60H), 4.43 (t, J = 4.8 Hz, 4H) 5.29 (s, 4H), 5.35 (bs), 7.02 (d, J = 8.8 Hz, 4H), 7.17 (bs), 7.82 (s, 2H), 8.00 (d, J = 8.0 Hz, 4H). FTIR (ν_{max}/cm^{-1}): 3360 (N–H st), 2883 (C–H st), 1755 (C═O st ester), 1718 (C═O st carbamate), 1670 (C═O st amide), 1533 (N–H δ), 1468 (CH_2, –CH_3 δ), 1101 (C–O–C st). SEC (ref PMMA): 2 populations; M_w 19 745 g mol^{-1}; $Đ$: 1.08.

Cleavage of *t*-Boc protecting groups and analytical data of HDLDBC-bGMPA. *t*-Boc protected HDLDBC-bGMPA (653 mg, 3.62×10^{-2} mmol, 1.00 eq.) was dissolved into ethyl acetate (3 mL), and a saturated solution of $HCl_{(g)}$ (7 mL) in ethyl acetate was carefully added to it. The reaction was stirred at room temperature for 45 min until a white gel appeared. The mixture was diluted with ethyl acetate (40 mL) and was stirred for an additional 30 min. Then, it was stirred under vacuum to remove the hydrochloric acid and the solvent was evaporated under reduced pressure. The gel was washed first with pure ethyl acetate and subsequently with pure methanol. In each case, the solution was stirred for 15 min under vacuum in order to remove the residual hydrochloric acid traces and then, the solvent was evaporated under reduced pressure to obtain a solid (615 mg, quantitative). ^{1}H NMR (500 MHz, CD_3OD) δ (ppm): 1.14 (m, 201H), 1.27 (s, 6H), 1.32 (s, 20H), 1.39 (s, 24H), 1.64 (m, 4H), 1.95 (m, 4H), 3.47 (m, 67H), 3.51–3.73 (m, ~1000H), 3.84 (t, J = 4.8 Hz, 4H), 3.96 (s, 8H), 4.00 (s, 16H), 4.03 (s, 32H), 4.12 (t, J = 6.0 Hz, 4H), 4.31 (m, 24H), 4.45 (m, 40H) 5.30 (s, 4H), 7.38 (d, J = 8.8 Hz, 4H), 8.23 (d, J = 8.8 Hz, 4H), 8.19 (s, 2H). ^{13}C NMR (125 MHz, CD_3OD) δ (ppm): 17.4–18.3, 26.3, 26.9, 29.3, 31.1, 41.5, 42.2, 47.3, 51.3, 62.6–76.8, 115.9, 124.2, 125.8, 132.8, 140.4, 163.7, 167.6, 168.8, 170.8–171.2, 174.0, 174.7–175.0. FTIR (ν_{max}/cm^{-1}): 3600–3300 (bs N–H$^+$), 2885 (C–H st), 1751 (C═O st ester), 1663 (C═O st amide and N–H$^+$ δ), 1545 (N–H δ), 1468 (CH_2–, CH_3 δ), 1099 (C–O–C st).

Characterization techniques. ^{1}H and ^{13}C Nuclear Magnetic Resonance (NMR) experiments were performed using a Bruker AV-400 (^{1}H: 400 MHz, ^{13}C: 100 MHz) or a Bruker AV-500 (^{1}H: 500 MHz, ^{13}C: 125 MHz) spectrometer (Bruker Corporation, Billerica, MA, USA), employing as solvents deuterated chloroform ($CDCl_3$), deuterated methanol (CD_3OD) or deuterated dimethyl sulfoxide ($(CD_3)_2SO$). The chemical shifts are inidcated in ppm relative to tetramethylsilane (TMS) and the coupling constant in Hz; the solvent residual peak was used as internal standard for spectrum calibration. Fourier transformed infrared (FTIR) spectroscopy was performed using a Bruker Vertex 70 spectrophotometer in ATR (attenuated total reflectance) mode and recorded between 4000 and 800 cm^{-1}. Size exclusion chromatography (SEC) was performed with a Walter e2695 Alliance employing two in series HR4 and HR1 Styragel columns (500 and 10^4 Å of pore size, respectively) and a Waters 2424 evaporation light scattering detector with a sample concentration of 1 mg mL^{-1} in THF (HPLC grade) with a flow rate of 1 mL min^{-1} at 35 °C; poly(methyl methacrylate), PMMA, was used as standard for calibration.

Self-assembly of HDLDBC-bGMPA

HDLDBC-bGMPA was mixed with the corresponding amount of distilled water and cooled down to 4 °C for 30 min until complete dissolution. Then, the solution was slowly heated to room temperature to trigger the formation of the water soluble nanocarriers. The critical micelle concentration (CMC) was determined using the Nile Red technique.[26] Briefly, 2 mL of distilled water solutions of HDLDBC-bGMPA with concentrations ranging from 0.1 to 5 mg mL^{-1} were prepared at 25 °C. Nile Red was dissolved in ethanol at a concentration of 0.25 mM and 10 μL of this solution was added to each sample. The mixtures were then stirred at room temperature for 1 h in the dark with an orbital shaker. The fluorescence emission spectrum of each solution was recorded with a PerkinElmer LS 55 fluorimeter after excitation at λ_{ex} = 550 nm.

Preparation of carrier-antimalarial drug conjugates and drug release assays

The antimalarial compounds CQ, PQ and QN were encapsulated within the corresponding carrier (DHP-bMPA or HDLDBC-bGMPA) following the oil-in-water procedure previously employed by us for CQ and PQ.[18] Briefly, each dendritic derivative and the corresponding drug were dissolved into a mixture of DCM and distilled water (1 : 1) at feeding ratios of $w_{DHP} : w_{drug}$ = 1 : 0.5 and $w_{HDLDBC} : w_{drug}$ = 1 : 1. The samples were vigorously stirred at room temperature employing an orbital shaker under ventilation until complete evaporation of DCM (around 2 h). Non-encapsulated drug was removed by

dialysis (regenerated cellulose membrane, MW 1000 Da cut off, Spectra/Por®) against distilled water (200 mL) at 4 °C for 16 h. The amount of encapsulated drug was indirectly determined: the quantity of drug present in the dialysis water was measured by UV-VIS spectrometry (Varian Cary50 Probe UV-visible spectrophotometer) at the wavelengths of $\lambda_{A(CQ)}$ = 345 nm for CQ, $\lambda_{A(PQ)}$ = 259 nm for PQ and $\lambda_{A(QN)}$ = 280 nm for QN and was subtracted from the initially incorporated drug. The samples were freeze-dried with a Telstar Cryodos 50 freeze-dryer in order to increase their stability over long storage periods.

The release of CQ encapsulated within HDLDBC-bGMPA and DHP-bMPA was studied by dialysis against phosphate buffered saline (PBS). 2 mL of the dendrimer/drug conjugates were dialyzed against 200 mL of PBS (regenerated cellulose dialysis membrane, MW 1000 Da cut-off, Spectra/Por®) under stirring at 37 °C. For CQ determination, aliquots (2 mL) were withdrawn at different times from the waters of dialysis up to 72 h (specifically at 0, 2, 4, 6, 24, 48, and 72 h). An identical procedure was performed with a control solution of free CQ at the same concentration as in the conjugate preparation.

Fluorescent labeling of HDLDBC-bGMPA

HDLDBC-bGMPA nanocarriers were labeled by encapsulating a low water soluble modified rhodamine B ($Rho(C17)_2$) red fluorophore previously reported by us,[27] and the oil-in-water procedure was employed to encapsulate the fluorophore within the nanocarrier. The selected feeding ratio in this case was (1 : 0.15) ($w_{HDLDBC} : w_{Rho}$). The release profile of $Rho(C17)_2$ from the dendrimer/$Rho(C17)_2$ conjugates was studied by dialysis similarly as the drug release procedure described above. In this case, 2 mL of the HDLDBC-bGMPA/$Rho(C17)_2$ conjugate containing 0.15 mg mL^{-1} of encapsulated $Rho(C17)_2$ were dialyzed (regenerated cellulose membrane, MW 2000 Da cut off, Spectra/Por®) against distilled water (200 mL) at 37 °C. At different times up to 72 h, 2 mL aliquots were withdrawn from where the quantity of $Rho(C17)_2$ was determined by measuring fluorescence intensity (λ_{ex} = 540 nm, λ_{em} = 580 nm).

Transmission electron microscopy (TEM) and atomic force microscopy (AFM) analysis

TEM images were obtained with a FEI TECNAI T20 electron microscope (FEI Company, Eindhoven, The Netherlands) with 200 kV beam power, using holey carbon film 300 mesh coppered grids (Agar Scientific Ltd). A droplet of an aqueous solution of the sample at a concentration of 1 mg mL^{-1} was deposited on the grid and let to adsorb for 30 s, removing the excess aqueous solution by blotting with filter paper. A droplet of a 3% w/v aqueous solution of phosphotungstic acid used as negative stain was deposited on the grid and left for 10 s before removing the excess staining solution by blotting with filter paper. The grid was dried for at least 24 h under atmospheric pressure at room temperature. The average size of the different nanocarriers was obtained by analysing ≥100 structures in ≥4 TEM images.

For AFM analyses, 10 μL of 1 μg mL^{-1} or 10 ng mL^{-1} dendrimer solution in double deionised water (ddH_2O; MilliQ system, Millipore) were deposited on cleaved mica substrates and, after an adsorption time of about 5 min, 40 μL ddH_2O were added. High-resolution images were obtained with a MultiMode 8 atomic force microscope equipped with a NanoScope V controller (Bruker Corporation) operating in ScanAsyst mode in liquid, using ScanAsyst-Fluid + probes (Bruker Corporation).

Plasmodium falciparum cell culture and parasite growth inhibition assay

P. falciparum 3D7 was grown *in vitro* in human RBCs of blood group type B prepared as described elsewhere[28] using previously established conditions.[29] Briefly, parasites (thawed from glycerol stocks) were cultured at 37 °C in T25 flasks (SPL Life Sciences) containing RBCs in Roswell Park Memorial Institute (RPMI) complete medium (supplemented with 5 g L^{-1} Albumax II and 2 mM glutamine) under a gas mixture of 92% N_2, 5% CO_2, and 3% O_2. Synchronized ring stage cultures were obtained by 5% sorbitol lysis and synchronized late stage cultures were obtained using 70% Percoll® (GE Healthcare) purification to enrich in late trophozoites and early schizonts;[30] the medium was changed every 2 days maintaining 3% hematocrit. For culture maintenance, parasitemias were kept below 5% late forms by dilution with fresh RBCs. The human blood used in this work was commercially obtained from the *Banc de Sang i Teixits* (http://www.bancsang.net). Blood was not specifically collected for this research; the purchased units had been discarded for transfusion, usually because of an excess of blood relative to anticoagulant solution. Prior to their use, blood units underwent the analytical checks specified in the current legislation. Before being delivered to us, unit data were anonymized and irreversibly dissociated, and any identification tag or label had been removed in order to guarantee the non-identification of the blood donor. No blood data were or will be supplied, in accordance with the current *Ley Orgánica de Protección de Datos* and *Ley de Investigación Biomédica*. The blood samples will not be used for studies other than those made explicit in this research. Experiments were approved by the Ethics Committee of the *Hospital Clínic de Barcelona*.

To isolate *P. falciparum* merozoites, a 3D7 strain culture was tightly synchronized (sorbitol lysis on day 1, 70% Percoll® followed after 2 h by sorbitol on day 4, sorbitol on day 6), and after a further 40 h a final 70% Percoll® treatment was done. Purified late stages were cultured in 10 mL of complete RPMI without adding fresh RBCs, and when the majority of parasites were segmented schizonts, E-64 protease inhibitor was added to a final concentration of 10 μM. Between 6 to 10 h later, the culture was centrifuged at 730*g* for 8 min and the pelleted cells were taken up in 20 mL of PBS. The suspension was passed sequentially through a 18G needle and a 1.2 μm filter (Sartorius Stedim® Minisart) blocked for 30 min with PBS/1% BSA. Merozoites in PBS were collected in a 50 mL Falcon tube previously blocked for 1 h with PBS/1% BSA, and finally centri-

fuged at 2200*g* for 10 min. The supernatant was removed leaving about 200 μL of a merozoite suspension in PBS, which was immediately used for targeting analysis.

For growth inhibition assays, *P. falciparum* 3D7 cultures were adjusted to 3% hematocrit and 1.5% parasitemia with more than 90% of parasites at ring stage after sorbitol synchronization. 75 μL of these *Plasmodium* cultures were plated in 96-well plates and incubated for 40 h at 37 °C in the presence of free drugs and dendrimer–drug conjugates (added in a volume of 75 μL). After addition of 0.5 μM Syto-11 (Thermo Fisher Scientific, Inc.), parasitemia was determined by flow cytometry as previously described.[28]

Cytotoxicity and hemolysis assays

Human umbilical vein endothelial cells (HUVEC, ATCC) were cultured in Medium 199 (M199, LabClinics) supplemented with 10% heat-inactivated foetal bovine serum (FBS, PAA Laboratories, Germany), 1% each penicillin/streptomycin (Biological Industries), and 10 mM glutamine (complete M199). 5000 cells per well were plated in 96-well plates (Thermo Fisher Scientific Inc.) and after 24 h at 37 °C in 5% CO_2 atmosphere the medium was substituted by dilutions of the dendrimers in 100 μL of culture medium without FBS, and incubation was resumed for 48 h. 10 μL of 4-[3-(4-iodophenyl)-2-(4-nitrophenyl)-2H-5-tetrazolio]-1,3-benzene disulfonate labeling reagent (WST-1, Roche Diagnostics GmbH) was added to each well, and the plate was incubated in the same conditions for a further 3 h. After thoroughly mixing for 1 min on a shaker, the absorbance of the samples was measured at 440 nm using a Benchmark Plus microplate reader (Bio-Rad Laboratories Inc.). WST-1 in the absence of cells was used as blank and samples were prepared in triplicate for each experiment, including positive (10% bleach) and negative (PBS) controls.

For hemolysis assays, human blood collected in citrate-phosphate-dextrose buffer was washed as described previously.[28] After the last washing step RBCs were diluted in PBS to yield a solution with 6% hematrocrit. 100 μL of RBCs from this suspension and 100 μL of a dendrimer sample were added to a 96-well plate. Each assay was performed in triplicate, including positive (1% Triton X-100) and negative (PBS) controls. After incubating for 3 h at 37 °C in 90% N_2, 5% CO_2, and 5% O_2, samples were collected in eppendorf tubes, spun at 16 000*g* for 5 min, and the supernatant absorbance was finally measured at 541 nm.

Cell targeting analysis

400 μL of desynchronized living *P. falciparum* 3D7 cultures were stained for 30 min with 4 μg mL^{-1} of the DNA dye Hoechst 33342. HUVEC (1.5×10^4 cells per cm^2) were treated equally but for the use of complete M199 as culture medium, and nuclei staining done at day 3 after plating (10 μg Hoechst 33342 per mL). After 3 washes with complete RPMI or M199, respectively, *Plasmodium* cultures and HUVEC were incubated in the presence of 0.15 mg mL^{-1} dendrimer conjugated to rhodamine, for 90 min in the corresponding medium at 37 °C with gentle stirring. Purified merozoites were incubated for 10 min at room temperature (RT) in the simultaneous presence of Hoechst 33342 and rhodamine-labeled dendrimers. After washing with incomplete medium, nonfixed samples were placed in a 8-well LabTek chamber slide system (Lab-Tek®II, catalog number 155409) and the fluorescence of Hoechst 33342, FITC and rhodamine ($\lambda_{ex/em}$: 350/461, 488/520 and 553/627 nm, respectively) was observed with an IX51 inverted fluorescence microscope (Olympus). Confocal fluorescence microscopy analysis was done with a Leica TCS SP5 laser scanning confocal microscope equipped with a DMI6000 inverted microscope, blue diode (405 nm), Argon (458/476/488/496/514 nm), diode pumped solid state (561 nm) and Helium–Neon (594/633 nm) lasers and PLAN APO 63× oil (NA 1.4) immersion objective lens. For flow cytometry analysis, *Plasmodium* cultures were diluted in PBS to a final concentration of 1–10 × 10^6 cells per mL, and samples were analyzed using a LSRFortessa™ flow cytometer instrument (BD Biosciences) set up with the 5 lasers, 20 parameters standard configuration. The single-cell population was selected on a forward-side scatter scattergram. Rhodamine was excited using a yellow-green laser (561 nm), and its fluorescence collected through a 582/15 nm filter. Hoechst 33342 was excited with a violet laser (405 nm), and its fluorescence collected using a 450/40 nm filter.

Determination of the maximum tolerated dose (MTD) in mice

Seven week-old inbred BALB/cAnR mouse females (18–20 g, Janvier Laboratories) were maintained under standard environmental conditions (20–24 °C and 12 h/12 h light/dark cycle) with *ad libitum* access to food and water. To ensure administration and minimize injection stress, the animals were anesthetized with isoflurane (4% for induction and 2.5% for maintenance) in an oxygen stream, while a 250 μL bolus was administered intravenously. To reduce the number of animals used, an adaptation of OECD 425 Test Guideline was followed, which consisted of a single ordered dose progression. The first mouse received the dose initially planned for antimalarial activity assays (see below), and the dose for the next animal was either increased or decreased by a factor of 3.2 depending on whether the first animal survived or died, respectively. Each mouse was injected and evaluated for at least 48 h before the next animal was treated. All animals were observed for toxic signs during 14 days after dose injection. Following this protocol, three different concentrations of the dendrimers (11.7, 37.5 and 120 mg kg^{-1}) were evaluated, prepared in PBS from a 50 mg mL^{-1} stock solution of dendrimers in sterile ddH_2O. In the presence of toxic effects including, among others, >20% reduction in animal weight, aggressive and unexpected animal behavior or the presence of blood in faeces, animals were immediately anesthetized using a 100 mg kg^{-1} Ketolar plus 5 mg kg^{-1} Midazolan mixture and sacrificed by cervical dislocation. Dendrimer MTD was therefore defined upon completion of the assay as the highest dosage exhibiting an absence of the aforesaid toxicity signs. The animal care and use protocols followed adhered to the specific national and

international guidelines specified in the Spanish Royal Decree 53/2013, which is based on the European regulation 2010/63/UE. The studies reported here were performed under protocols reviewed and approved by the Ethical Committee on Clinical Research from the Hospital Clínic de Barcelona (Reg. HCB/2014/0910).

Antimalarial activity assay *in vivo* and dot-blot assays

The *in vivo* antimalarial activity of free CQ and of dendrimer-CQ conjugates was analyzed in a 4-day blood suppressive test as previously described.[31] Briefly, BALB/c mice were inoculated intraperitoneally with 2×10^6 RBCs from *Plasmodium yoelii yoelii* 17XL (PyL) MRA-267-infected mice. Treatment started 4 h later (day 0) with a single dose of 1.9 mg CQ per kg per day administered intravenously as diphosphate–drug or dendrimer–drug, followed by identical dose administration for the next 3 days. Tested compounds were prepared in PBS and the control groups received PBS. Parasitemia was monitored daily by microscopic examination of Giemsa-stained thin blood smears using the Plasmoscore 1.3 software (Burnet Institute, Melbourne, Australia). When all surviving animals had completely cleared *Plasmodium* infection they were re-infected (on day 69) with *P. yoelii yoelii* 17XL (PyL) MRA-267 as above and left untreated. Survival was monitored until day 90, when blood samples (400 μL) were collected on 10 μL of 10% EDTA, centrifuged for 5 min (470*g*), and the obtained plasma supernatants were stored at −20 °C. 3 μL of *P. yoelii yoelii* 17XL (PyL) MRA-267 extracts[32] containing 1.5 μg protein were applied and allowed to dry on a nitrocellulose membrane (0.45 μm, Bio-Rad, catalog number 1620145). Non-specific sites were blocked with 5% BSA in TBS-T (0.05% Tween 20, 150 mM NaCl, 20 mM Tris-HCl, pH 7.5) for 1 h at RT. Then the membrane was first incubated (30 min, RT) with the plasma supernatants dissolved in TBS-T (1 : 5000 dilution), washed (TBS-T, 3 × 5 min), and then treated with a secondary goat anti-mouse antibody conjugated to horseradish peroxidase (Millipore) in TBS-T (1 : 10 000 dilution; 30 min, RT), followed by 3 × 5 min washes with TBS-T and one wash with TBS (TBS-T without Tween). Finally the membrane was incubated with ECL Prime Western Blotting Detection Reagent (Luminol, Amersham) for 30–60 s and scanned (ImageQuant LAS4000, GE Healthcare).

Statistical analysis

Data are presented as the mean ± standard error of at least three independent experiments, and the corresponding standard errors in histograms and graphs are represented by error bars. Percentages of viability were obtained using non-treated cells as control of survival and IC_{50} values were calculated by nonlinear regression with an inhibitory dose–response model using GraphPad Prism5 software. Concentrations were transformed using natural log for linear regression. Regression models were adjusted for replicates and assay data.

Results and discussion

Preparation and characterization of the nanocarriers

Synthesis and characterization of HDLDBC-bGMPA. HDLDBC-bGMPA was synthesized for the first time for this study by CuAAC of the bis(alkyne) derivative of Pluronic® F127 and two *t*-Boc protected amino-terminated bis-GMPA dendrons (Fig. 2A and ESI†). The *t*-Boc-protected bis-GMPA dendron of 3rd generation with an azide group at the focal point and eight terminal amino groups was synthesized as previously described by us.[24] The synthesis of the alkyne functionalized Pluronic® was carried out by esterification of Pluronic® F127 with 4-(prop-2-ynyloxy)benzoic acid as we reported previously.[18] The CuAAC reaction was performed in DMF at 45 °C under argon atmosphere during 2 days. The Cu(I) catalytic species was formed "*in situ*" by reduction of Cu(II) salt with (L)-ascorbate while TBTA was added to increase its stability. An excess of dendron (1.3 mole of dendron per 1.0 mole of alkyne group) was used to obtain a complete functionalization of the linear polymer. The *t*-Boc protecting groups were removed from the dendrons in acidic conditions with HCl in ethyl acetate and the final product was obtained with a moderate yield of 61%.

The correct grafting of the two bis-GMPA dendrons at the extremities of Pluronic® F-127 was first controlled by ^{1}H (Fig. 2B) and ^{13}C (Fig. 2C) NMR experiments (see Fig. S1.1, S1.2 and S1.3† for ^{1}H–^{1}H COSY and full ^{1}H and ^{13}C NMR spectra). The appearance of a peak at 8.19 ppm (H-15) in the ^{1}H NMR spectrum and two peaks at 125.8 (C-15) and 140.4 ppm (C-14) in the ^{13}C NMR spectrum confirmed the formation of the triazole rings. Additionally, three other signals were shifted downfield in the ^{1}H NMR spectra of the final HDLDBC when compared with the spectra of its two precursors. Thus, the signal corresponding to the methylene protons in the α-position of the triazole rings belonging to the linear polymeric part (H-13) was shifted from 4.72 to 5.30 ppm. The signals corresponding to the methylene protons in the α- and β-positions of the triazole rings belonging to the dendritic part (H-16 and H-17) were shifted from 3.20 and 1.65 to 4.45 and 1.95 ppm, respectively. Moreover, the relative integrations of the signals corresponding to the dendrons and linear polymer corroborated the grafting of two dendrons at the terminal position of the Pluronic® F-127 (Table S1.1†).

The characteristic bands of the bis-GMPA dendrons and Pluronic® F-127 could be observed in the FTIR spectrum, (Fig. 2D). First, the presence of the poly(ether) Pluronic® F-127 was asserted by the intense band at 1101 cm^{-1} (C–O bond vibration stretching) and the two intense bands at 2881 and 1344 cm^{-1} (C–H bond vibrations). Second, the presence of the poly(ester amide) bis-GMPA dendrons was confirmed by the two bands at 1755 and 1664 cm^{-1} corresponding to C=O bond vibration stretching of ester and amide groups, respectively.

SEC was performed with the *t*-Boc-protected precursor of HDLDBC-bGMPA due to its low solubility in the elution solvent employed for chromatography, *i.e.* THF (Fig. 2E). Two

peaks were observed in the chromatograms of both, the commercial Pluronic® F-127 and the HDLDBC, showing the polydispersity of these compounds. The correct functionalization of Pluronic® was nevertheless asserted as both peaks corresponding to it showed lower retention time than the two peaks corresponding to the starting Pluronic® F-127. Additionally, no peak corresponding to residual free bis-GMPA dendron could be observed. In summary, all experimental data obtained during the characterization of HDLDBC-bGMPA confirmed the correct insertion of two bis-GMPA dendrons at each extremity of the linear polymer and the absence of unreacted free linear polymer or dendron.

Structural studies. The ability of HDLDBC-bGMPA to self-assemble in water forming micellar nanocarriers was confirmed by CMC determination using the Nile Red method (Fig. 3A). The fluorescence intensity of this solvatochromic fluorophore increases drastically when it migrates into and is retained within the lipophilic part of aggregates formed by the self-assembly of amphiphilic molecules.[26] Thus, a CMC of 1.0 mg mL^{-1} for HDLDBC-bGMPA was determined, which was consistent with the formation of micelles in which the lipophilic core of the central linear Pluronic® block copolymer is surrounded by hydrophilic ammonium terminated dendrons. Rounded structures were observed in AFM and negatively stained TEM images of HDLDBC-bGMPA. The average diameter calculated from TEM micrographs was 13 ± 3 nm, consistent with the height of the structures determined in water by AFM (Fig. 3B and C), and with the average in number value measured by DLS, 26 ± 6 nm (Fig. S2.1.A†).

The morphology of two globular dendronized hyperbranched polymers, DHP-bMPA, was also analyzed by TEM and AFM (Fig. 3D–F). The two generations tested (n = 3 and n = 4 in Fig. 1B) appeared as rounded objects, with average diameters calculated from TEM images of 9.8 ± 2.7 nm and 13.5 ± 3.5 nm, respectively. These dimensions are consistent with the expected formation by these dendronized hyperbranched polymers of unimolecular micelles well dispersed in aqueous solution.[33,34] DLS measurements of DHP-bMPA (n = 4) gave a diameter of 11 ± 2 nm (Fig. S S2.1.B†). As for HDLDBC-bGMPA carriers, the size of DHP-bMPA unimolecular micelles results *a priori* appropriate to enter into pRBCs.[21]

Unspecific toxicity and hemolysis assays. None of the dendritic derivatives was cytotoxic or hemolytic up to a concentration of 0.15 mg mL^{-1} (Fig. 3G and H), which is 10 times higher than the highest amount to be used later for *in vitro* growth inhibition assays, and 8 times higher than the daily dose to be used later for *in vivo* assays.

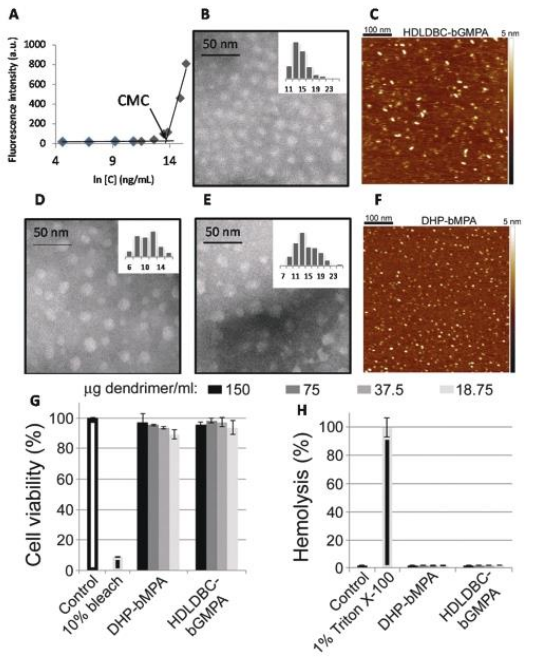

Fig. 3 Characterization of nanocarriers. Nile Red fluorescence intensity as a function of HDLDBC-bGMPA concentration (A), TEM image (B) and AFM image in water on mica surface (C) of HDLDBC-bGMPA, TEM images of DHP-bMPA (n = 3 and n = 4 in Fig. 1B; D and E, respectively), and AFM image of DHP-bMPA (n = 4 in Fig. 1B) in water on mica surface (F). Cytotoxicity (G) and hemolysis assay (H) of the largest DHP-bMPA (n = 4 in Fig. 1B) and HDLDBC-bGMPA.

In vitro targeting analysis

Rhodamine labeling of the nanocarriers. In order to explore the targeting behavior of the nanocarriers towards pRBCs, DHP-bMPA-Rho (Fig. 4A), a DHP-bMPA covalently labeled with an average of seven rhodamine B moieties per macromolecule, was prepared as previously described.[25] HDLDBC-bGMPA nanocarriers were labeled by encapsulating a lipophilic modified rhodamine B ($Rho(C17)_2$) red fluorophore, using the oil-in-water procedure as previously reported by us.[27] In order to check the stability of this labeling, $Rho(C17)_2$ release from the HDLDBC-bGMPA/$Rho(C17)_2$ conjugates was studied by dialysis. Unmodified water-soluble rhodamine B fluorophore was encapsulated within HDLDBC-bGMPA micelles following the same protocol, to be used as a control. The resulting release profiles showed that whereas 50% of the encapsulated rhodamine B is released during the first 2 h, $Rho(C17)_2$ is kept encapsulated throughout the 72 h of the experiment (Fig. 4B).

Erythrocyte targeting analysis. Fluorescence microscopy analysis of non-fixed samples (Fig. 5A) showed that whereas HDLDBC-bGMPA was incorporated by all RBCs, DHP-bMPA exhibited at the same concentration a clear targeting specificity for pRBCs. Higher-resolution confocal fluorescence microscopy images of DHP-bMPA-containing samples revealed that the polymer fluorescence was associated to the pRBC plasma membrane and to intraerythrocytic parasites (Fig. 5B). In the latter case fluorescence was not detected in the RBC cytosol and was circumscribed by the plasma membrane of *Plasmodium*. These observations suggested a specific binding of DHP-bMPA to *Plasmodium falciparum* antigens.

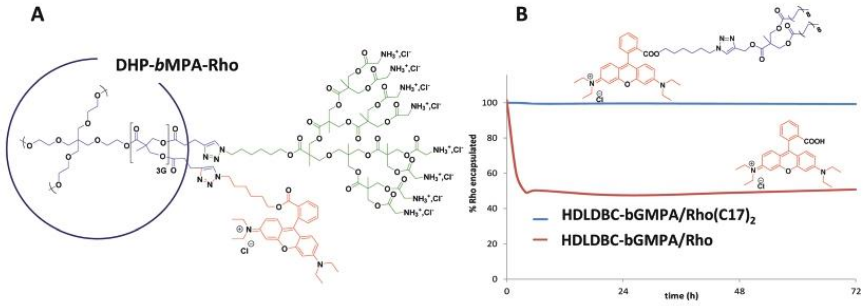

Fig. 4 Rhodamine labeling of the nanocarriers. Chemical structure of the covalently labeled DHP-bMPA-Rho derivative (A), and release profile of the fluorescent rhodamine labels, $Rho(C17)_2$ and Rho, from the nanocarrier HDLDBC-bGMPA (B).

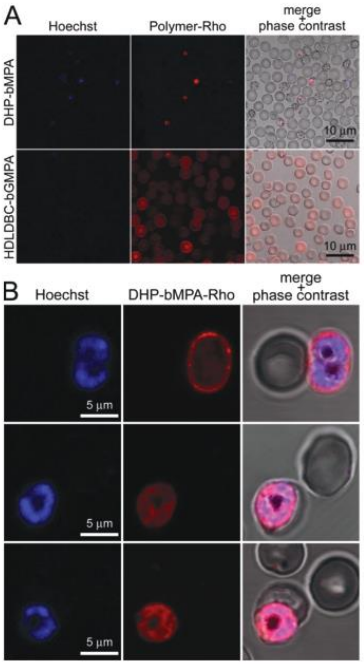

Fig. 5 Fluorescence microscopy cell targeting analysis of rhodamine-labeled DHP-bMPA and HDLDBC-bGMPA to non-fixed RBCs and pRBCs. (A) Conventional fluorescence microscopy cell targeting of both polymers. (B) Confocal fluorescence microscopy cellular and subcellular targeting of DHP-bMPA-Rho.

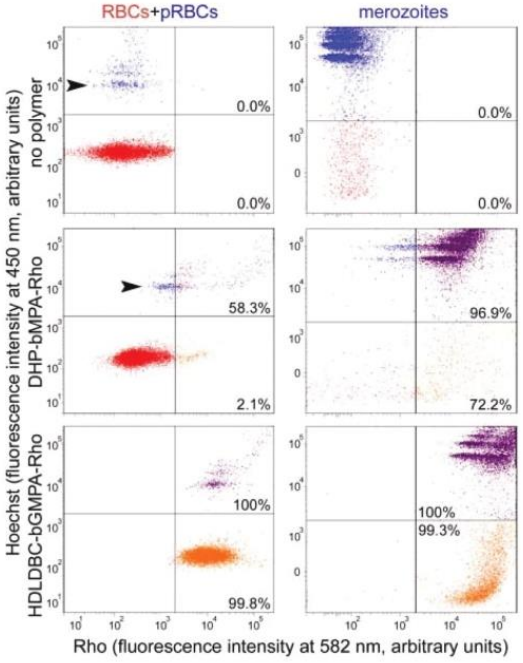

Fig. 6 Flow cytometry analysis of the targeting of rhodamine-labeled DHP-bMPA and HDLDBC-bGMPA to RBCs, pRBCs and merozoites (the latter two represented in blue, upper left areas; their DNA is stained by Hoechst 33342). pRBCs and merozoites positive for rhodamine are shown in purple (upper right areas) whereas orange (lower right areas) indicates cells or cell debris (the latter only in merozoite samples) lacking DNA that are associated to the polymers. Percentages indicate the fraction of rhodamine-positive counts relative to the total number of recorded cells or particles in each sample. Arrowheads indicate ring stages.

The differential RBC targeting of DHP-bMPA and HDLDBC-bGMPA was confirmed by flow cytometry assays (Fig. 6); whereas HDLDBC-bGMPA associated with *P. falciparum* merozoites and with both parasitized and non-parasitized erythrocytes, DHP-bMPA interacted only with merozoites and with pRBCs. HDLDBC-bGMPA interaction with both RBCs and pRBCs does not invalidate it as a potential carrier of antimalarial drugs in targeted delivery strategies. As we have shown before, delivering antimalarial compounds to non-infected erythrocytes might represent an interesting therapeutic approach whereby *Plasmodium* would encounter a hostile environment since the very first moment after RBC inva-

sion.[35,36] This scenario resulted in a significantly improved efficacy of drugs encapsulated inside liposomes targeted to both pRBCs and to non-parasitized red blood cells.[35,37]

The modest binding of DHP-bMPA to early ring forms, where the parasite has not significantly modified the erythrocyte membrane, suggests that this polymer might interact predominantly with exported *Plasmodium* antigens, which are scarce in rings and completely absent from non-parasitized RBCs.

Endothelial cell targeting analysis. Other cell types besides RBCs will be exposed to targeted polymers used as drug carriers in the blood stream, mainly leukocytes and blood vessel endothelium. Of these, leukocytes are in numbers several orders of magnitude below those of RBCs, but endothelial cells are sufficiently abundant to compete with pRBCs for nanocarrier intake. We have shown above that, at the polymer concentrations used in this work, endothelial cells do not experience significant cytotoxic effects. However, they might contribute to the clearance from the blood of a significant amount of polymers, thus reducing the efficacy of nanovector preparations. When endothelial cell uptake of the polymers was analyzed by fluorescence microscopy, it was observed that both DHP-bMPA and HDLDBC-bGMPA were incorporated by HUVEC cells. However, whereas HDLDBC-bGMPA had a cytosolic localization, the subcellular targeting of DHP-bMPA was found to be exclusively nuclear (Fig. 7). This result offers interesting perspectives for the use of this type of polymers in the targeting to cell types other than erythrocytes and to different subcellular locations. Nevertheless, the observed interaction of both polymers with the endothelial lining has to be taken into account in future pharmacokinetic studies regarding potential applications as drug carriers against the blood stages of malaria.

In vitro antimalarial activity of drug-loaded nanocarriers

Drug encapsulation. CQ, PQ and QN were encapsulated within DHP-bMPA and HDLDBC-bGMPA nanocarriers. Except where otherwise indicated, the DHP-bMPA structure used hereafter in this work will be $n = 4$. The encapsulation was performed following the oil-in-water method at feeding ratios of 1 : 0.5 (w_{DHP}/w_{drug}) and 1 : 1 (w_{HDLDBC}/w_{drug}), respectively. This procedure allowed to encapsulate all three antimalarial drugs in DHP-bMPA nanocarriers with drug loading contents around 20% in weight and good encapsulation efficiencies, ranging from 37% to 60% (Table 1). A smaller DHP-bMPA ($n = 3$ in Fig. 1B) was also used to encapsulate all three antimalarials, obtaining similar drug contents and loading efficiencies (Table S2.1†). As for the HDLDBC-bGMPA carrier, higher loading capacities, between 30% and 48% in weight, and rather good encapsulation efficiencies, ranging from 31% to 48%, were attained.

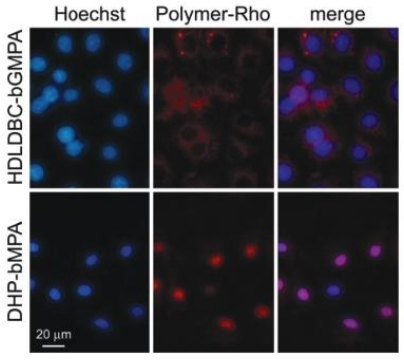

Fig. 7 Fluorescence microscopy cell targeting analysis of rhodamine-labeled DHP-bMPA and HDLDBC-bGMPA to HUVEC cells.

Table 1 Encapsulation of CQ, PQ and QN in HDLDBC-bGMPA and DHP-bMPA nanocarriers and average diameters of the carrier/drug systems determined by TEM

	Drug	mg drug/mg carrier	EE[a] (%)	Average diameter (nm)
HDLDBC-bGMPA	Empty			13 ± 3
	CQ	0.307	31	17 ± 3
	PQ	0.408	41	11 ± 2
	QN	0.475	48	14 ± 6
DHP-bMPA	Empty			13.5 ± 3.5
	CQ	0.246	60	20 ± 7
	PQ	0.214	60	19 ± 8
	QN	0.229	37	12 ± 3

[a] Encapsulation efficiency (EE, %) represents the fraction of encapsulated drug relative to the quantity used to perform the encapsulation.

All the aqueous solutions obtained after the encapsulation procedure were freeze-dried in order to enhance stability during storage of the carrier/drug systems. The effective encapsulation of drugs was asserted by comparing the absorption spectra of the drugs in water with those of the re-dissolved carrier/drug freeze-dried conjugates (Fig. S2.3 and S2.4†). In all cases, the differences observed reflect interactions between nanocarriers and drugs.

TEM images of drug-containing nanocarriers showed in all cases homogeneous dispersions of rounded objects (Fig. 8), the diameters of which were similar to those of empty nanocarriers, and always ≤20 nm (Table 1). This small size should favor their entry in pRBCs, since *Plasmodium* induces new permeation pathways that confer to the host cell an increased permeability to a wide range of particles up to diameters of 50–70 nm.[21] Whereas the unimolecular micelles formed by DHP-bMPA in water (Fig. 8A) had an average diameter around 13.5 nm, DHP-bMPA/drug systems had an average diameter between 12 and 20 nm. Likewise, the loading of antimalarial drugs within HDLDBC-bGMPA nanocarriers resulted in structures with average sizes ranging from 11 to 17 nm (Fig. 8B), whereas the empty nanocarrier had an average size around 13 nm. AFM observation of both CQ-loaded carriers confirmed the formation of these rounded objects (Fig. 8).

***In vitro* antimalarial activity assays.** When the corresponding formulations of HDLDBC-bGMPA and DHP-bMPA

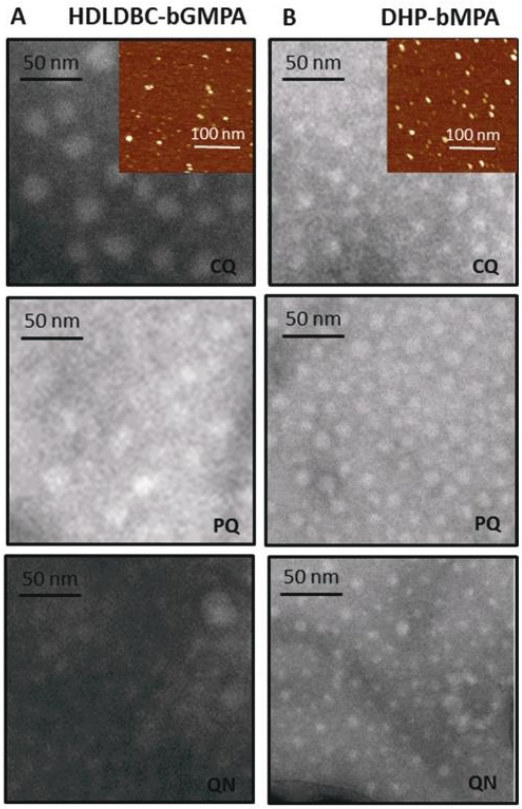

Fig. 8 Negatively stained TEM images of the drug-loaded nanocarriers HDLDBC-bGMPA (A) and DHP-bMPA (B). Insets show AFM images of the corresponding CQ-loaded nanocarriers.

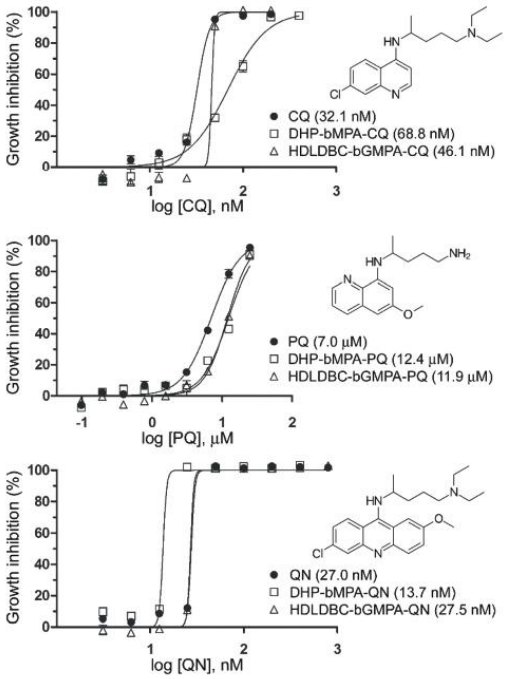

Fig. 9 Growth inhibition assays of *P. falciparum in vitro* cultures treated with CQ, PQ and QN, either free or encapsulated in HDLDBC-bGMPA and DHP-bMPA. In parentheses are indicated the corresponding IC_{50} values.

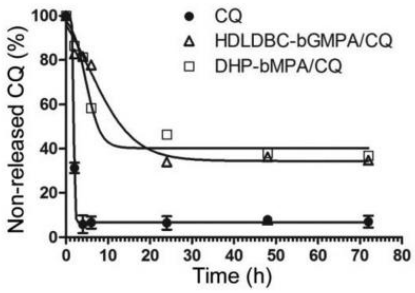

Fig. 10 Release profiles of CQ from the dendrimers DHP-bMPA and HDLDBC-bGMPA at 37 °C.

conjugated with CQ, PQ and QN were tested in growth inhibition assays of *P. falciparum in vitro* cultures, the encapsulated drugs had IC_{50} values comparable to those of the free compounds (Fig. 9), indicating an adequate release of the drugs from the polymers. However, the good targeting of the nanostructures towards pRBCs offered prospects for a better performance of the encapsulated drugs, suggesting that part of the nanoparticle-conjugated compounds might not be adequately released. To explore this possibility, the release dynamics against PBS of CQ encapsulated within HDLDBC-bGMPA and DHP-bMPA was analyzed during three days (Fig. 10). As already described for other dendritic derivatives,[18] CQ was progressively released from both nanocarriers in a process that reached completion in about 24 h; after this time, about 35% of CQ remained stably encapsulated. Modifications of the polymer architecture or chemistry to endow it with more porosity or less affinity for the drugs might contribute to an improved drug release profile.

In vivo antimalarial activity of CQ-loaded nanocarriers

MTD assays indicated that DHP-bMPA and HDLDBC-bGMPA could be safely administered to mice without evident signs of animal distress up to respective doses of at least 37.5 and 120 mg kg^{-1}. For the evaluation of the formulations in an *in vivo* model of malaria, we selected CQ because, being the *in vitro* performance of its encapsulated form *vs.* the free compound similar to that of PQ and QN, this drug had been suc-

cessfully tested in our group as part of different polymeric and liposomal encapsulations.[18,35,38] When polymer-CQ conjugates were administered intravenously (1.9 mg CQ per kg per day for 4 consecutive days) to mice infected with the lethal murine malaria parasite *P. yoelii yoelii* 17XL (PyL) MRA-267, DHP-bMPA-CQ did not improve survival significantly, but animals treated with HDLDBC-bGMPA-CQ survived much longer (3 out of 5 mice lived ≥20 days) than untreated controls, which typically died at day 6 (Fig. 11A and C). One mouse treated with HDLDBC-bGMPA-CQ was actually cured and, when re-infected at day 69 and left untreated, it recovered completely without showing any symptoms of malaria or developing parasitemia above the detection level of microscopy examination. The detection in the plasma of this cured animal of antibodies against *P. yoelii* antigens (Fig. 11B) was consistent with the development of immunity against the disease. Free CQ-treated controls which were administered the same drug concentration were cured in 4 out of 5 animals, which became also resistant to re-infection. Although HDLDBC-bGMPA-encapsulated CQ did not improve the efficacy of such a good drug as CQ, the strategy presented here can be adapted to the targeted drug delivery of other antimalarials, already existing or yet to be discovered.

In vivo, HDLDBC-bGMPA-CQ worked better than DHP-bMPA-CQ, possibly because the former targets all RBCs. The loading of antimalarial drugs into non-parasitized red blood cells has been described as an efficient approach to significantly reduce parasite survival,[35,36] as long as neither nanocarriers nor drugs affect the natural role of erythrocytes as O_2 and CO_2 transporters. Both dendrimeric structures studied in this work lack significant *in vitro* cytotoxicity and hemolytic activity, suggesting that they will not interfere with the red blood cell physiology. HDLDBC-bGMPA then holds promise for the development of innovative antimalarial prophylactic strategies at the cell level whereby *Plasmodium* would be exposed to drugs since the very first moment after invading a host cell.

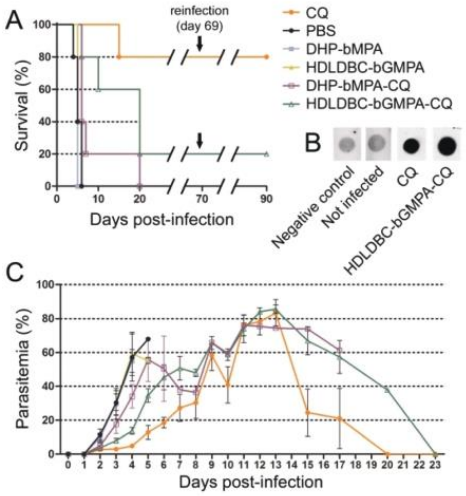

Fig. 11 Four-day blood suppressive antimalarial activity assay of free CQ and of carrier-CQ conjugates. (A) Kaplan–Meier plot of the survival of *P. yoelii yoelii* 17XL (PyL) MRA-267-infected mice treated with 1.9 mg CQ per kg per day for 4 consecutive days, administered intravenously as diphosphate–drug or dendrimer–drug. When all surviving animals had completely cleared *Plasmodium* infection they were re-infected (on day 69) with *P. yoelii* and left untreated. (B) Dot blot for the detection at day 90 in the plasma of surviving animals of antibodies against *P. yoelii*. The negative control was processed substituting PBS for plasma. (C) Parasitemia counts of the different mouse groups until animal death or parasite clearance.

The modest *in vivo* efficacy of the encapsulated formulations relative to the free drug is, in part, likely resulting from renal and splenic clearance of the nanoparticles, in addition to their endothelial cell uptake. Nanoparticles must be larger than 20 nm in diameter to avoid filtration by the kidney,[39] and smaller than 100 nm to avoid a specific sequestration by sinusoids in spleen and fenestra of liver, which are approximately 150–200 nm in diameter.[40] Therefore, systemically administered nanoparticles should have diameters from 20 to 100 nm,[41] and overall, literature suggests that nanoparticles in the 50–100 nm size range display the lowest blood clearance rates.[42] Since the average diameter of the dendrimeric nanoparticles used here is just below 20 nm, increasing their size to *ca.* 50 nm might provide an improved pharmacokinetics and better *in vivo* performance.

In addition, upon intravenous administration of nanoparticles, these are coated by a variety of serum proteins which are recognized by the scavenger receptor on macrophage cell surfaces and internalized, leading to a significant loss of nanoparticles from the circulation.[43] The serum proteins binding on the nanoparticles are also termed "opsonins", and the macrophages contributing the major loss of injected dose are also known as the reticuloendothelial system or mononuclear phagocyte system. Reducing protein binding is the key point for developing a long-circulation nanoparticle formulation. To minimize opsonization, the most commonly used strategy is to conjugate onto the surface of the nanoparticles the polyethylene glycol polymer[44] or polyoxazolines,[45] both hydrophilic polymers that provide good steric hindrance for preventing protein binding.

Finally, in addition to expanding blood residence time and reducing unspecific interactions with non-target cells and tissues, a faster targeting dynamics can be conferred to the nanoparticles by coating them with molecules binding pRBCs with certain degree of specificity, as it has been described for heparin.[46,47] Here we have shown that although DHP-bMPA exhibited a remarkable preferential binding to pRBCs *vs.* RBCs, about 40% of pRBCs interacted with this polymer similarly as a fraction of the non-infected erythrocyte population did (Fig. 6). The functionalization of DHP-bMPA-Rho with up to 15% heparin-FITC (w/w) did not affect the targeting specificity of the polymer towards pRBCs (Fig. S3.1†), and it actually favored specific interactions with pRBCs *vs.* RBCs (data not shown). The known activity of

heparin as targeting element of liposomes[47] suggests that its presence on the nanocarrier increased the number of polymers bound to each pRBC. Last but not least, since heparin has antimalarial activity, this result indicates that it can be a constituent of pRBC-targeted multicomponent nanoparticles carrying different types of antimalarial agents.

Conclusions

To eradicate malaria, there is an urgent need for the combination of different strategies working together, because it is unlikely for a single approach to be capable of success. It is important to emphasize the importance of implementing in advance efficient methods of antimalarial drug encapsulation and targeted delivery in order to make a good use of future therapeutic compounds. This should result in a more rational administration regime that could contribute to expand the time during which drugs can be used before resistance evolves. In addition, such strategy might widen the number of chemicals that reach the clinic if eventual unspecific toxicities can be reduced through a targeted delivery approach. The resulting lower overall doses should not trigger pernicious side-effects in the patient while keeping high local doses on the parasite in order to quickly eliminate all the cells of the pathogen, thus reducing the evolution of resistances. Here, we have described micellar carriers based on dendritic macromolecules containing bis-MPA and glycine that hold promise for the development of future antimalarial nanomedicines targeted to both *Plasmodium*-infected and non-infected erythrocytes.

Authors contributions

The manuscript was written through the contributions of all authors. All authors have given approval to the final version of the manuscript.

Conflicts of interest

There are no conflicts to declare.

Acknowledgements

This research was supported by grants BIO2014-52872-R, CTQ2015-70174-P, MAT2015-66208-C3-1-P (Ministerio de Ciencia, Innovación y Universidades, Spain, including FEDER funds), 2014-SGR-938 (Generalitat de Catalunya, Spain), and (Gobierno de Aragón-FSE). ISGlobal and IBEC are members of the CERCA Programme, Generalitat de Catalunya. A. L. thanks the Ministerio de Ciencia, Innovación y Universidades for his grant (FPU12/05210). L. N. B.-C. is supported by the European Commission under Horizon 2020's Marie Skłodowska-Curie Actions COFUND scheme (Grant Agreement no. 712754) and by the MINECO's Severo Ochoa programme (Grant SEV-2014-0425 (2015–2019)). The authors would like to acknowledge the use of the Servicios Científico Técnicos of CEQMA (Universidad de Zaragoza-CSIC) and of the LMA (INA-Universidad de Zaragoza). The authors acknowledge support of the publication fee by the CSIC Open Access Publication Support Initiative through its Unit of Information Resources for Research (URICI).

Notes and references

1 World Health Organization, World Malaria Report 2018. http://www.who.int/malaria/publications/world-malaria-report-2018/report/en/, 2018.
2 V. S. Moorthy, R. D. Newman, P. Duclos, J. M. Okwo-Bele and P. G. Smith, *Lancet Infect. Dis.*, 2013, **13**, 280–282.
3 A. Mbengue, S. Bhattacharjee, T. Pandharkar, H. Liu, G. Estiu, R. V. Stahelin, S. S. Rizk, D. L. Njimoh, Y. Ryan, K. Chotivanich, C. Nguon, M. Ghorbal, J. J. Lopez-Rubio, M. Pfrender, S. Emrich, N. Mohandas, A. M. Dondorp, O. Wiest and K. Haldar, *Nature*, 2015, **520**, 683–687.
4 P. L. Alonso and M. Tanner, *Nat. Med.*, 2013, **19**, 150–155.
5 M. Prudêncio, A. Rodriguez and M. M. Mota, *Nat. Rev. Microbiol.*, 2006, **4**, 849–856.
6 A. F. Cowman and B. S. Crabb, *Cell*, 2006, **124**, 755–766.
7 K. S. Griffith, L. S. Lewis, S. Mali and M. E. Parise, *J. Am. Med. Assoc.*, 2007, **297**, 2264–2277.
8 R. G. Feachem, A. A. Phillips, G. A. Targett and R. W. Snow, *Lancet*, 2010, **376**, 1517–1521.
9 P. L. Alonso, *Int. Microbiol.*, 2006, **9**, 83–93.
10 J. P. Daily and J. Clin, *Pharmacol.*, 2006, **46**, 1487–1497.
11 European Science Fundation: ESF Forward Look on Nanomedicine 2005. http://www.nanopharmaceuticals.org/files/nanomedicine.pdf, 2005.
12 M. Saltzman and T. Desai, *Ann. Biomed. Eng.*, 2006, **34**, 270–275.
13 P. Urbán, J. J. Valle-Delgado, E. Moles, J. Marqués, C. Díez and X. Fernàndez-Busquets, *Curr. Drug Targets*, 2012, **13**, 1158–1172.
14 N. Kuntworbe, N. Martini, J. Shaw and R. Al-Kassas, *Drug Dev. Res.*, 2012, **73**, 167–184.
15 P. Urbán and X. Fernàndez-Busquets, *Curr. Med. Chem.*, 2014, **21**, 605–629.
16 M. Selin, L. Peltonen and L. M. J. Bimbo, *J. Drug Delivery Sci. Technol.*, 2016, **34**, 10–20; H. Yang, *Nanomedicine*, 2016, **12**, 309; A. M. Caminade and C. O. Turrin, *J. Mater. Chem. B*, 2014, **2**, 4055–4066; P. Kesharwani, K. Jain and N. K. Jain, *Prog. Polym. Sci.*, 2014, **39**, 268–307.
17 S. García-Gallego, A. M. Nyström and M. Malkoch, *Prog. Polym. Sci.*, 2015, **48**, 85–110.
18 J. Movellan, P. Urbán, E. Moles, J. M. De la Fuente, T. Sierra, J. L. Serrano and X. Fernàndez-Busquets, *Biomaterials*, 2014, **35**, 7940–7950.

19 R. D. Sikwal, R. S. Kalhapure and T. Govender, *Eur. J. Pharm. Sci.*, 2017, **97**, 113–134.
20 B. S. Bolu, R. Sanyal and A. Sanyal, *Molecules*, 2018, **23**, 1570–1595.
21 I. D. Goodyer, B. Pouvelle, T. G. Schneider, D. P. Trelka and T. F. Taraschi, *Mol. Biochem. Parasitol.*, 1997, **87**, 13.
22 A. Fonseca, M. A. Gil and P. M. Simões, *Prog. Polym. Sci.*, 2014, **39**, 1291–1311.
23 M. Winnacker and B. Rieger, *Polym. Chem.*, 2016, **7**, 7039–7046.
24 A. Lancelot, R. González-Pastor, R. Clavería-Gimeno, P. Romero, O. Abián, P. Martín-Duque, J. L. Serrano and T. Sierra, *J. Mater. Chem. B*, 2018, **6**, 3956–3968.
25 A. Lancelot, R. González-Pastor, A. Concellón, T. Sierra, P. Martín-Duque and J. L. Serrano, *Bioconjugate Chem.*, 2017, **28**, 1135–1150.
26 M. C. A. Stuart, J. C. van de Pas and J. B. F. N. Engberts, *J. Phys. Org. Chem.*, 2005, **18**, 929–934.
27 I. Jiménez-Pardo, R. González-Pastor, A. Lancelot, R. Clavería-Gimeno, A. Velázquez-Campoy, O. Abián, M. B. Ros and T. Sierra, *Macromol. Biosci.*, 2015, **15**, 1381–1391.
28 P. Urbán, J. Estelrich, A. Cortés and X. Fernàndez-Busquets, *J. Controlled Release*, 2011, **151**, 202–211.
29 S. L. Cranmer, C. Magowan, J. Liang, R. L. Coppel and B. M. Cooke, *Trans. R. Soc. Trop. Med. Hyg.*, 1997, **91**, 363–365.
30 C. Lambros and J. P. Vanderberg, *J. Parasitol.*, 1979, **65**, 418–420.
31 D. A. Fidock, P. J. Rosenthal, S. L. Croft, R. Brun and S. Nwaka, *Nat. Rev. Drug Discovery*, 2004, **3**, 509–520.
32 J. Marques, E. Vilanova, P. A. S. Mourão and X. Fernàndez-Busquets, *Sci. Rep.*, 2016, **6**, 24368.
33 G. R. Newkome, C. N. Moorefield, G. R. Baker, M. J. Saunders and S. H. Grossman, *Angew. Chem., Int. Ed. Engl.*, 1991, **30**, 1178–1180.
34 X. Fan, Z. Lia and X. J. Loh, *Polym. Chem.*, 2016, **7**, 5898–5919.
35 E. Moles, P. Urbán, M. B. Jiménez-Díaz, S. Viera-Morilla, I. Angulo-Barturen, M. A. Busquets and X. Fernàndez-Busquets, *J. Controlled Release*, 2015, **210**, 217–229.
36 E. Moles and X. Fernàndez-Busquets, *Future Med. Chem.*, 2015, **7**, 837–840.
37 E. Moles, S. Galiano, A. Gomes, M. Quiliano, C. Teixeira, I. Aldana, P. Gomes and X. Fernàndez-Busquets, *Biomaterials*, 2017, **145**, 178–191.
38 P. Urbán, J. J. Valle-Delgado, N. Mauro, J. Marques, A. Manfredi, M. Rottmann, E. Ranucci, P. Ferruti and X. Fernàndez-Busquets, *J. Controlled Release*, 2014, **177**, 84–95.
39 D. Venturoli and B. Rippe, *Am. J. Physiol.: Renal Physiol.*, 2005, **288**, F605–F613.
40 X. Duan and Y. Li, *Small*, 2012, **9**, 1521–1532.
41 M. E. Davis, Z. Chen and D. M. Shin, *Nat. Rev. Drug Discovery*, 2008, **7**, 771–782.
42 F. Alexis, E. Pridgen, L. K. Molnar and O. C. Farokhzad, *Mol. Pharm.*, 2008, **5**, 505–515.
43 M. C. Woodle, M. S. Newman and J. A. Cohen, *J. Drug Targeting*, 1994, **2**, 397–403.
44 S. D. Li and L. Huang, *Mol. Pharm.*, 2008, **5**, 496–504.
45 R. B. Restani, J. Conde, R. F. Pires, P. Martins, A. R. Fernandes, P. V. Baptista, V. D. B. Bonifácio and A. Aguiar-Ricardo, *Macromol. Biosci.*, 2015, **15**, 1045–1051.
46 X. Fernàndez-Busquets, *Future Med. Chem.*, 2013, **5**, 737–739.
47 J. Marques, E. Moles, P. Urbán, P. Prohens, M. A. Busquets, C. Sevrin, C. Grandfils and X. Fernàndez-Busquets, *Nanomedicine*, 2014, **10**, 1719–1728.

Article 1: Supplementary information

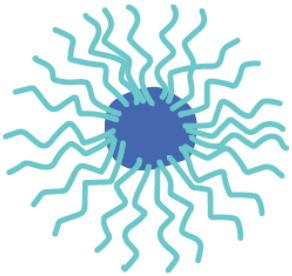

Electronic Supplementary Material (ESI) for Biomaterials Science.

Micelle carriers based on dendritic macromolecules containing bis-MPA and glycine for antimalarial drug delivery

Elisabet Martí Coma-Cros[a,b,c,1], Alexandre Lancelot[d,1], María San Anselmo[d], Livia Neves Borgheti-Cardoso[a,b,c], Juan José Valle-Delgado[f], José Luis Serrano[d,*], Xavier Fernàndez-Busquets[a,b,c,*], Teresa Sierra[e,*].

Supplementary Information

S1. Synthesis and chemical characterization of HDLDBC-bGMPA, bGMPA(NH_3^+)$_8$-Pluronic® F127-bGMPA(NH_3^+)$_8$.

S2. Self-assembly of nanocarriers in water and antimalarial drug encapsulation.

S3. Targeting experiments.

S1. Synthesis and chemical characterization of HDLDBC-bGMPA, bisGMPA(NH_3^+)$_8$-Pluronic® F127- bisGMPA(NH_3^+)$_8$

Synthesis of bisGMPA(NHBoc)$_8$- Pluronic® F127- bisGMPA(NHBoc)$_8$

Alkyne functionalized Pluronic® F127 (1.00 g, 7.74×10^{-2} mmol, 1.00 eq.) and t-Boc *bis*-GMPA dendron (514 mg, 2.01×10^{-1} mmol, 2.60 eq.) were dissolved into 8 mL of dimethylformamide (DMF) in a Schlenk flask and 3 vacuum-argon cycles were made to remove the air. The reaction mixture was stirred under argon atmosphere at 45 °C. $CuSO_4{\cdot}5H_2O$ (18.2 mg, 6.19×10^{-2} mmol, 0.80 eq), (*L*)-ascorbate (24.1 mg, 1.24×10^{-1}mmol, 1.60 eq.) and TBTA (32.8 mg, 6.19×10^{-2} mmol, 0.80 eq.) were dissolved into DMF (4 mL) in a second Schlenk flask and exposed to 3 vacuum-argon cycles. The copper solution was stirred under argon atmosphere at 45 °C for 15 min and was added through a cannula to the previous azide-alkyne reaction mixture. The resulting mixture was stirred under argon atmosphere at 45 °C for 2 days. Then, hot brine (100 mL) was added to the reaction mixture and the product was extracted with dichloromethane (3 × 100 mL). The organic phases were collected, washed with hot brine (2 × 100 mL), dried over anhydrous $MgSO_4$ and the solvent was evaporated under reduced pressure to obtain a yellow solid. The crude product was precipitated into cold diethyl ether, recovered by filtration and washed with cold diethyl ether to yield a white powder. Finally, the product was dialyzed (cellulose membrane, 1000 Da cut-off, Spectra/Por®) against methanol for 24 hours to obtain a light yellow solid (855 mg, 61%).

^{1}H (400 MHz, $CDCl_3$) δ (ppm): 1.11 (m, 201H), 1.26 (m, 42H), 1.41 (m, 152H), 1.62 (m, 4H), 1.94 (m, 4H), 3.38 (m, 67H), 3.44-3.74 (m, ~1000H), 3.81 (t, 4H, J = 4.8 Hz), 3.88 (m, 32H), 3.94 (m, 8H), 3.88 (m, 16H), 4.11 (t, J = 6.4 Hz, 4H), 4.18-4.35 (m, 60H), 4.43 (t, J = 4.8 Hz, 4H) 5.29 (s, 4H), 5.35 (bs), 7.02 (d, J = 8.8 Hz, 4H), 7.17 (bs), 7.82 (s, 2H), 8.00 (d, J = 8.0 Hz, 4H). FTIR (ν_{max}/cm^{-1}): 3360 (N-H st), 2883 (C-H st), 1755 (C=O st ester), 1718 (C=O st carbamate), 1670 (C=O st amide), 1533 (N-H δ), 1468 (CH_2, -CH_3 δ), 1101 (C-O-C st).

SEC (ref PMMA): 2 populations; Mw 19745 g.mol^{-1}; Đ: 1.08.

Synthesis ofHDLDBC-BGMPA, bisGMPA(NH_3^+)$_8$-Pluronic® F127- bisGMPA(NH_3^+)$_8$

*Bis*GMPA(NHBoc)$_8$-Pluronic® F127-*bis*GMPA(NHBoc)$_8$ (653 mg, 3.62×10^{-2} mmol, 1.00 eq.) was dissolved into ethyl acetate (3 mL), and a saturated solution of $HCl_{(g)}$ (7 mL) in ethyl acetate was carefully added to it. The reaction mixture was stirred at room temperature for 45 min until a white gel appeared. The reaction mixture was diluted with ethyl acetate (40 mL) and was stirred for an additional 30 min. Then, it was stirred under vacuum to remove the hydrochloric acid and the solvent was evaporated under reduced pressure. The gel was washed firstly with pure ethyl acetate and subsequently with pure methanol. In each case, the solution was stirred for 15 min under vacuum in order to remove the residual hydrochloric acid traces and then, the solvent was evaporated under reduced pressure to obtain a solid.

^{1}H (500 MHz, CD_3OD) δ (ppm): 1.14 (m, 201H), 1.27 (s, 6H), 1.32 (s, 20H), 1.39 (s, 24H), 1.64 (m, 4H), 1.95 (m, 4H), 3.47 (m, 67H), 3.51-3.73 (m, ~1000H), 3.84 (t, J = 4.8 Hz, 4H), 3.96 (s, 8H), 4.00 (s, 16H), 4.03 (s, 32H), 4.12 (t, J = 6.0 Hz, 4H), 4.31 (m, 24H), 4.45 (m, 40H) 5.30 (s, 4H), 7.38 (d, J = 8.8 Hz, 4H), 8.23 (d, J = 8.8 Hz, 4H), 8.19 (s, 2H).

^{13}C NMR (125 MHz, CD_3OD) δ (ppm): 17.4-18.3, 26.3, 26.9, 29.3, 31.1, 41.5, 42.2, 47.3, 51.3, 62.6-76.8, 115.9, 124.2, 125.8, 132.8, 140.4, 163.7, 167.6, 168.8, 170.8-171.2, 174.0, 174.7-175.0.

FTIR (ν_{max}/cm^{-1}): 3600-3300 (bs N-H^+), 2885 (C-H st), 1751 (C=O st ester), 1663 (C=O st amide and N-H^+ δ), 1545 (N-H δ), 1468 (CH_2-, CH_3 δ), 1099 (C-O-C st).

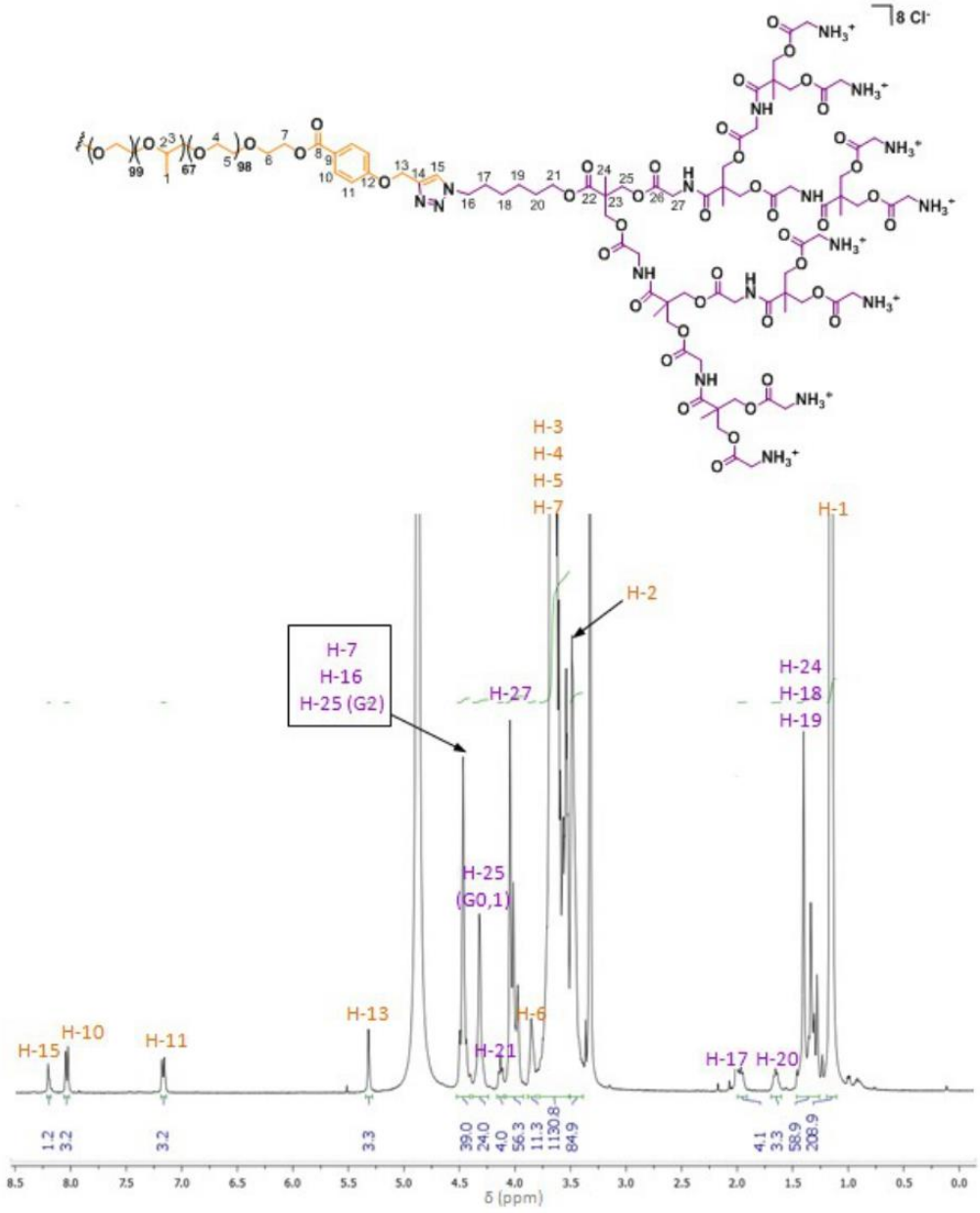

Fig. S1.1. ^{1}H NMR spectrum of $(NH_3^+)_8$-HDLDBC-$(NH_3^+)_8$ with signals relative integration recorded at 400 MHz in CD_3OD.

Table S1.1. Theoretical and measured signal integrations of ^{1}H NMR signals.

δ (ppm)	proton	theoretical signal integration	measured signal integration
1.14	H-1	201	208.9
1.27-1.39	H-18,19,24	50	58.9
1.64	H-20	4	3.3
1.95	H-17	4	4.1
3.47	H-2	67	84.9
3.51-3.73	H-3,4,5	~1000H	1131.8
3.84	H-6	4	undetermined[1]
3.96-4.03	H-27	56	56.3
4.12	H-21	4	4
4.31	H-25(G0,1)	24	24.0[2]
4.45	H-7,16,25(G2)	40	39.0
5.30	H-13	4	3.3
7.38	H-11	4	3.3
8.23	H-10	4	3.2
8.19	H-15	2	1.2

[1]Due to the overlapping of the signals at 3.51-3.73 and 3.84 ppm, the relative integration of this signal could not be determined experimentally. [2]Relative integration signal used as reference.

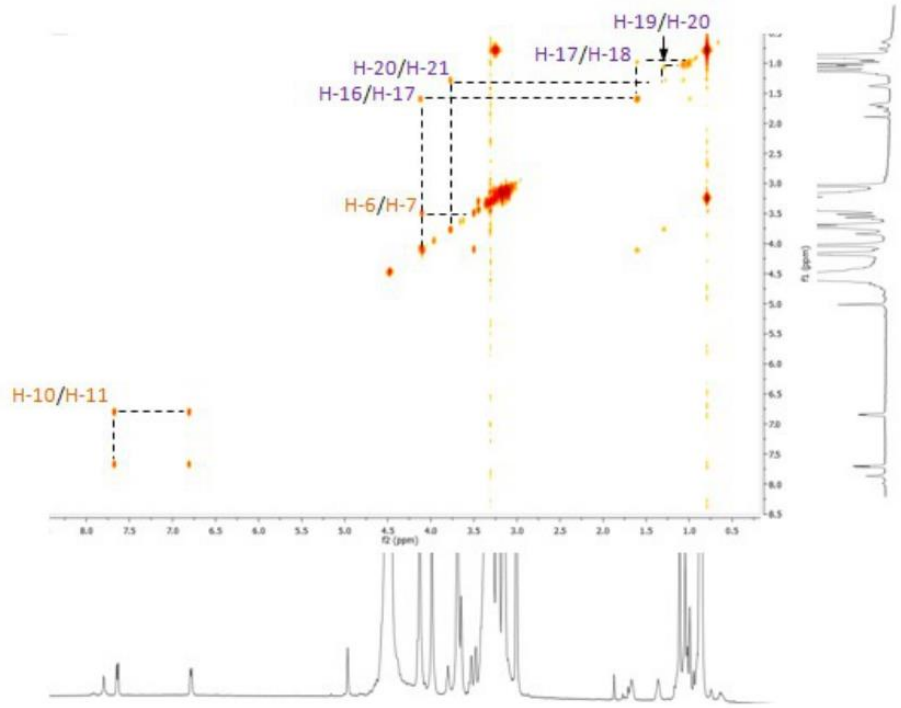

Fig. S1.2. ^{1}H-^{1}H COSY spectrum of bisGMPA(NH_3^+)$_8$-Pluronic® F127-bisGMPA(NH_3^+)$_8$ (HDLDBC-bGMPA) recorded at 500 MHz in CD_3OD.

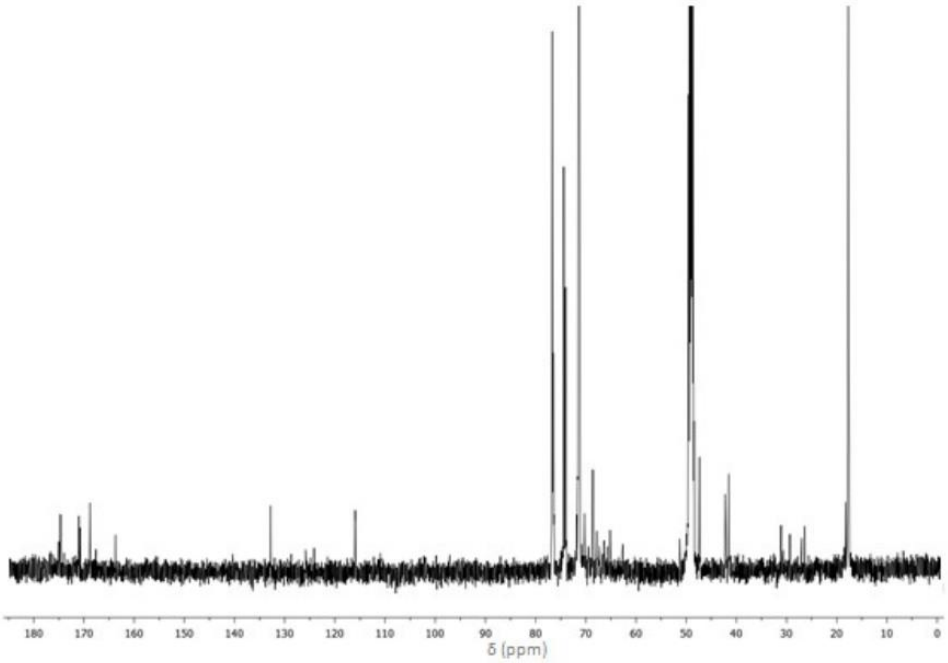

Fig. S1.3. ^{13}C NMR spectrum of bisGMPA(NH_3^+)$_8$-Pluronic® F127-bisGMPA(NH_3^+)$_8$ (HDLDBC-bGMPA) recorded at 125 MHz in CD_3OD.

A. HDLDBC-bGMPA

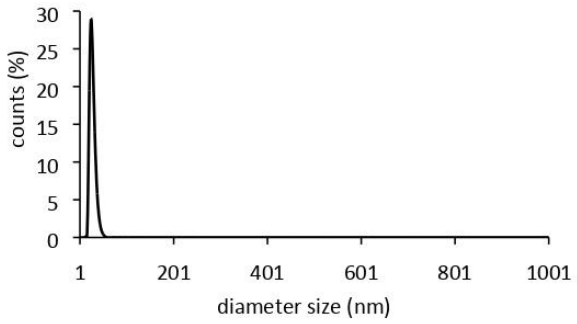

B.DHP-bMPA (n=4)

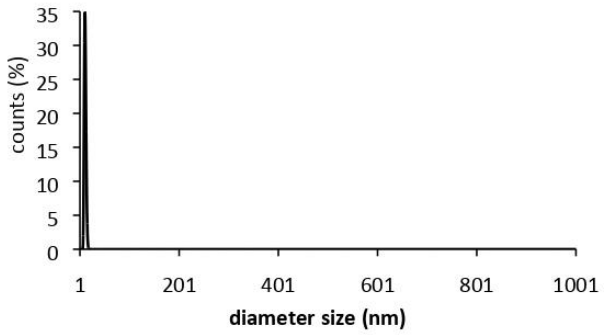

C.

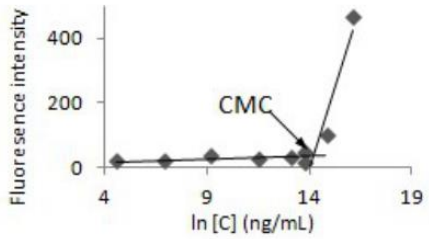

Fig. S2.1. A. DLS curve of HDLDBC-bGMPA and B. DLS curve of DHP-bMPA (n =4). DLS measurements were performed with a Malvern Instruments Nano ZS at 1mg/mL at 25°C ; results are given as size distribution in number. C. CMC determination for naked Pluronic® F-127 at 25 °C according to the Nile Red fluorescence determination.

Table S2.1. Drug loading within the smallest DHP-bMPA (n=3 in Fig. 1B)

drug	mg drug/mg carrier	EE[1] (%)
CQ	0.318	65
PQ	0.127	26
QN	0.233	46

[1]EE refers to encapsulation efficiency.

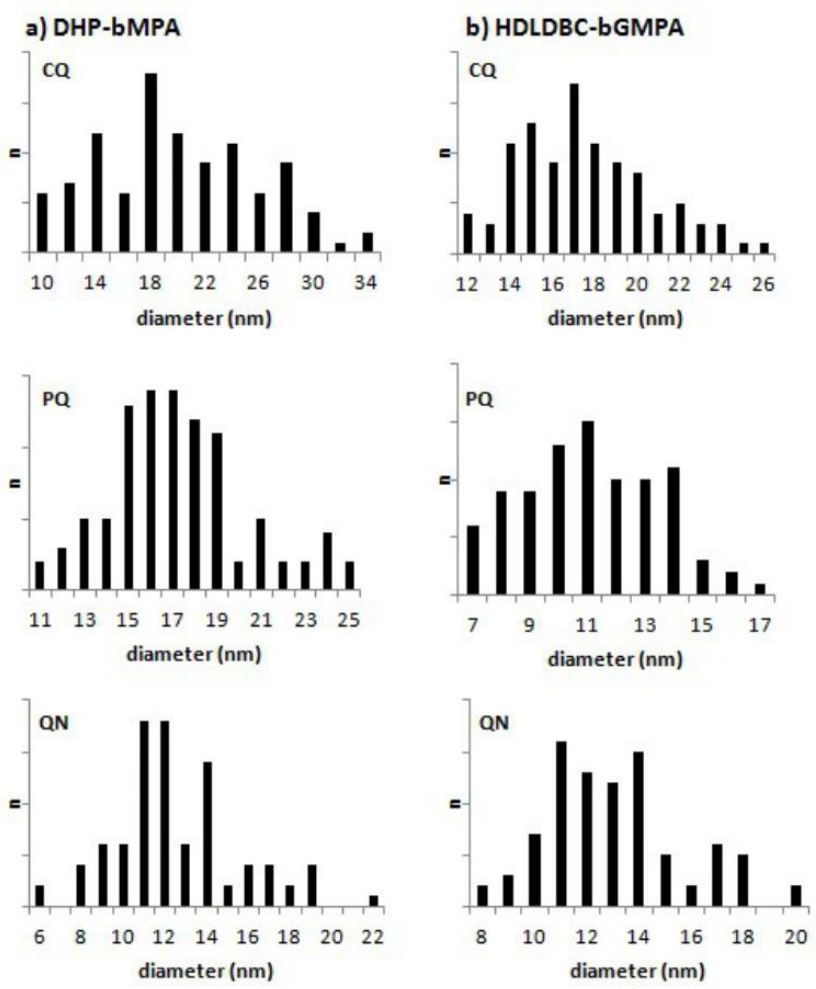

Fig. S2.2. Size distribution histograms of DHP-bMPA- and HDLDBC-bGMPA-drug conjugates.

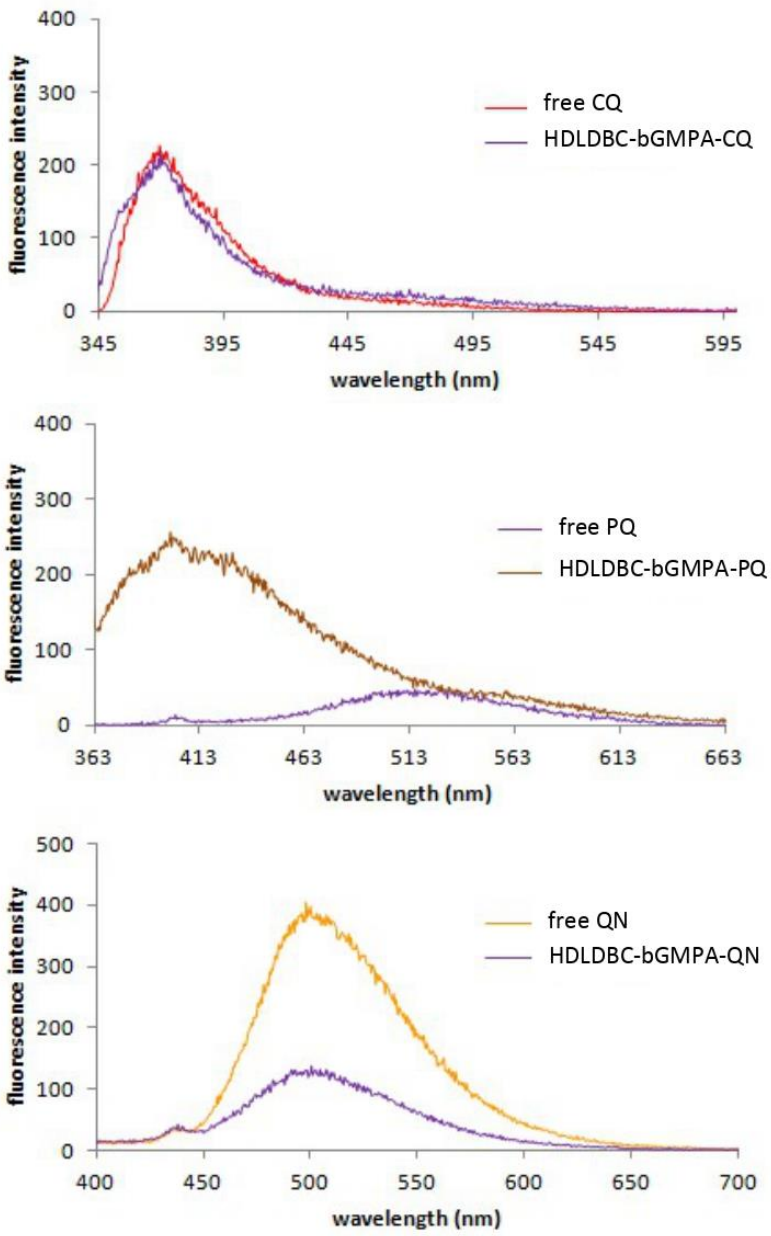

Fig. S2.3. Fluorescence spectra in water of equal concentrations of antimalarial drugs either free or in HDLDBC-bGMPA conjugates.

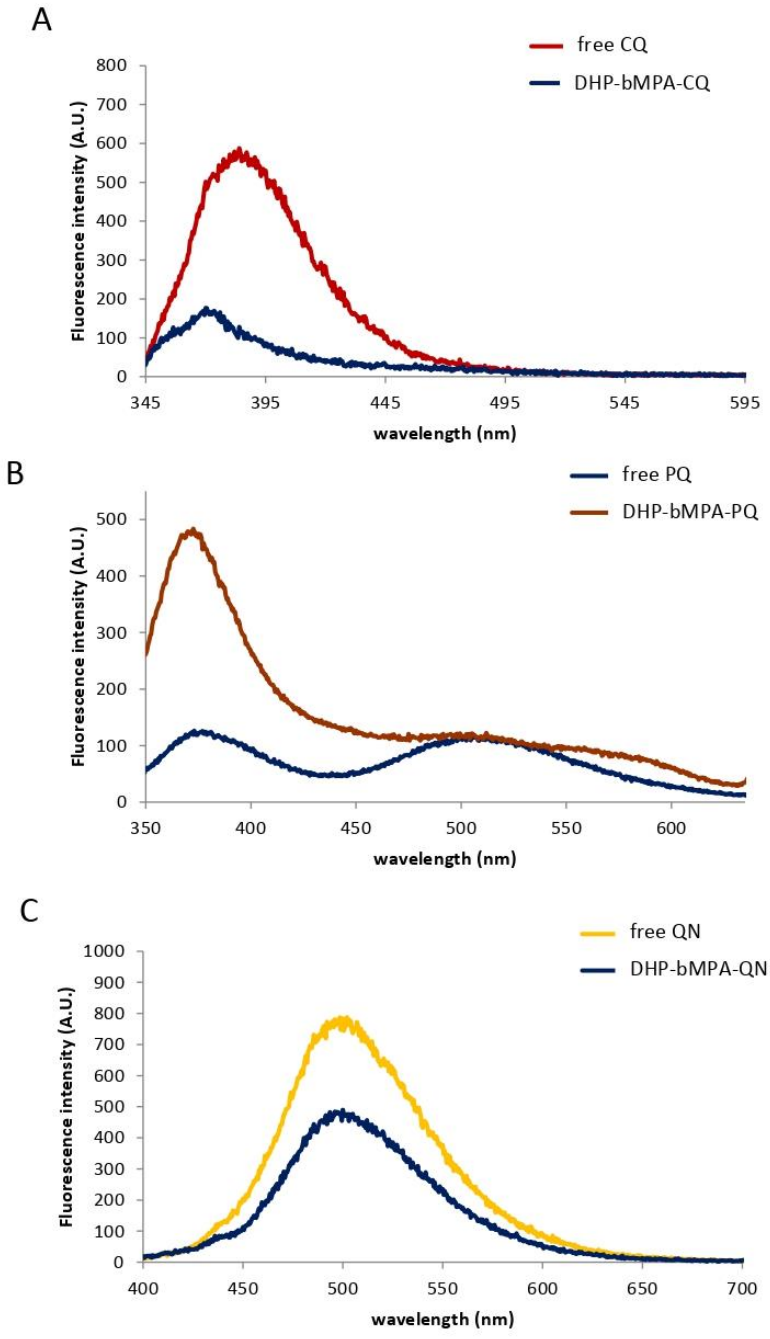

Fig. S2.4. Fluorescence spectra in water of equal concentrations of antimalarial drugs either free or in DHP-bMPA conjugates.

Complexation of DHP-bRho with heparin-FITC

In order to study the possible benefits of the conjugation of heparin to the polymers for their pRBC targeting specificity[1], DHP-bMPA-Rho was complexed to heparin-FITC through electrostatic interactions between the positive charges of the ammonium groups of the dendrimer and the negatively charged sulfate groups of heparin. The formation of the complexes between heparin and DHP-bMPA-Rho was studied by UV/Vis spectroscopy with the Methylene Blue competition assay. Free Methylene Blue absorbance (λ_{max} = 665 nm) shifts when complexed to heparin (λ_{max} = 565 nm). For this assay, samples containing heparin (10 µg/mL) and Methylene Blue 50 µM were dissolved in 10 mM TRIS·HCl, pH 7.4, and placed in a 96-well culture plate. They were gently rotationally stirred at room temperature for 15 min to allow Methylene Blue to fully complex heparin. Then, the DHPs were added to the samples at different (w_{DHP}/w_{Hep}) ratios and the final volume of the samples was adjusted to 150 µL. They were newly stirred for another 30 min. UV/Vis spectra were recorded between 400 and 800 nm with an EPOCH UV/Vis spectrophotometer. The maximum A_{665}/A_{565} ratio was calculated to determine the w_{DHP}/w_{Hep} ratio at which 100% of Methylene Blue is displaced. This ratio corresponds to the ratio at which the maximum DHP/heparin association is achieved. The experiments were made in triplicate.

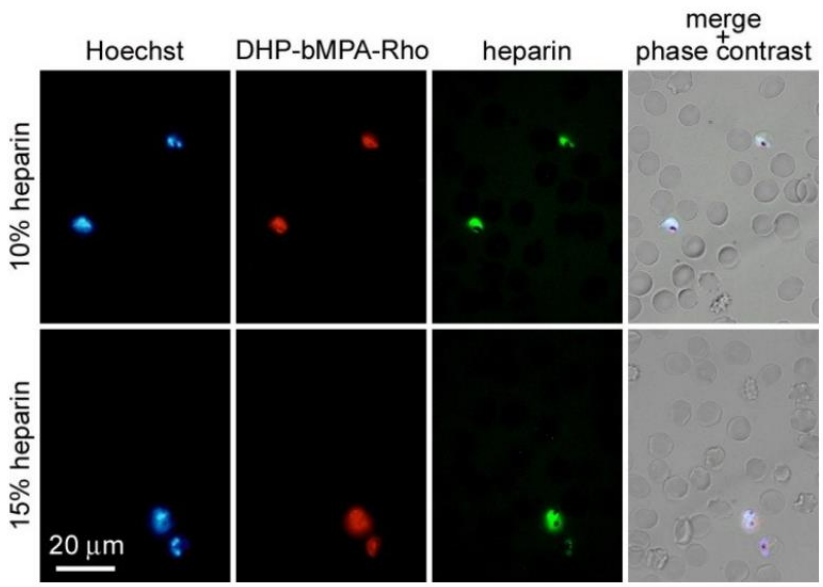

Fig. S3.1. Fluorescence microscopy cell targeting analysis to RBCs and pRBCs of rhodamine-labeled DHP-bMPA coated with FITC-labeled heparin.

[1] Marques J., Moles E., Urbán P., Prohens P., Busquets M.A., Sevrin C., Grandfils C., Fernàndez-Busquets X. Application of heparin as a dual agent with antimalarial and liposome targeting activities towards *Plasmodium*-infected red blood cells. *Nanomedicine* 2014 ;10:1719-1728.

POLYAMIDOAMINE NANOPARTICLES FOR THE ORAL ADMINISTRATION OF ANTIMALARIAL DRUGS

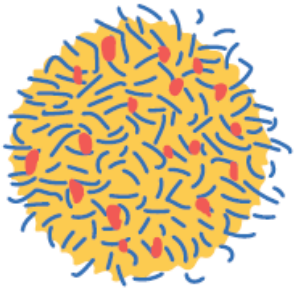

Article 2: Short summary

Despite huge efforts to fight malaria, in 2017 this infectious disease caused by the protist *Plasmodium spp.* registered 219 million cases and claimed the lives of 435,000 people, mainly young African children in developing regions. The number of malaria-related deaths had been reduced significantly, however, not enough. Malaria pathophysiology is so complex and the disease is still so widespread. Thus it is generally accepted that to achieve eradication a combination of tools and strategies to target different parasite stages will be needed. In fact, there is a demand for oral formulations to target the asexual *Plasmodium* stages in the peripheral bloodstream for the current strategies for mass drug administration (MDA). Moreover, recommendations for future interventions stress the importance of also targeting transmission stages of the parasite, the stage transferred between humans and mosquitoes.

Drug therapy still remains the mainstay of treatment and prevention. And oral administration should be the chosen route when possible, since it is patient-friendly, painless, easy for self-administration, cheaper than parental route and does not required keeping the cold chain. In fact, MDA requires oral administration and aims to target the parasite reservoir in treating asymptomatic parasite carriers who silently transmit the parasite. The strategy is to treat all members of a targeted community, whether infected or not.

Therefore, nanotechnology can provide innovative useful strategies contributing to find new antimalarial drugs or substantially improve old ones, increasing their oral bioavailability and stability, which can be used in MDA and other startegies to fight malaria.

Encapsulation of drugs in targeted nanovectors is a rapidly growing area with clear applicability to infectious disease treatment, and pharmaceutical nanotechnology has been identified as a potentially essential tool in the future fight against malaria. With the advent of nanoscience, renewed hopes have appeared of finally obtaining the long sought-after *magic bullet* against malaria in the form of a nanovector for the targeted delivery of antimalarial compounds exclusively to *Plasmodium*-infected red blood cells (pRBCs), increasing drug efficacy and minimizing the induction of resistance to newly developed therapeutic agents.

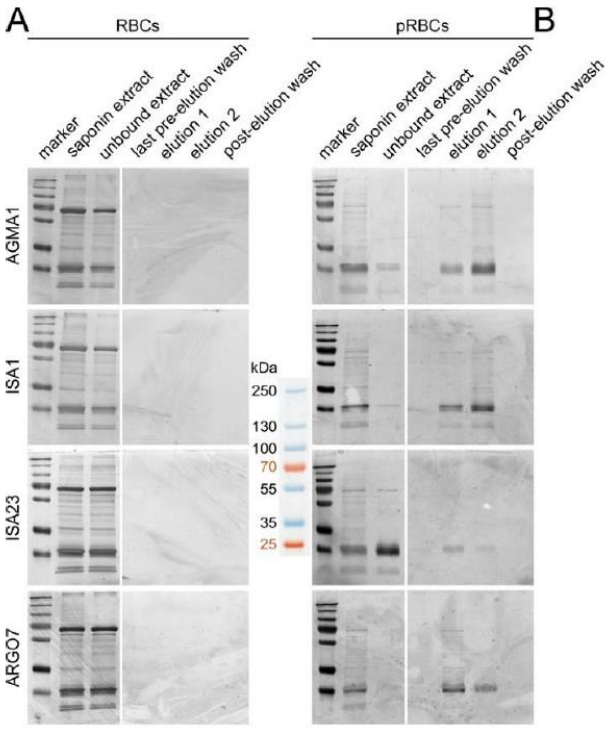

Figure 21. Silver-stained SDS-PAGE of pRBC saponin extracts run through four affinity chromatography columns where AGMA1, ISA1, ISA23 or ARGO7 had been immobilized. (**A**) **A RBC extract** was first loaded, and after the corresponding washing-elution-washing steps (**B**) **a pRBC extract** was loaded in the same column. The approximate masses (kDa) of the seven bands from the molecular weight marker are indicated in the space between the gels.

We have engineered polyamidoamine (PAA)-derived nanovectors which degrade during GIT transit, and combine into a single chemical structure drug encapsulating capacity, antimalarial activity, low unspecific toxicity, specific pRBC targeting, optimal *in vivo* activity, and affordable synthesis cost. Our recent data suggest that the antiparasitic mechanism of PAAs consists of a coating of *Plasmodium* that has the effect of blocking the erythrocyte invasion of egressed parasites. The ensuing prolonged exposure of *Plasmodium* to the immune system might be applied to the design of new malaria prophylactic approaches where PAAs could play a dual role as carriers of antimalarial drugs and as boosters of immunity. In addition to binding egressed merozoites, PAA-based nanoparticles are capable of penetrating late-stage pRBCs and of adsorbing on intracellular merozoites of both human and murine malaria. Affinity chromatography assays indicate that the specific targeting of PAAs to pRBCs results from the presence of adhesive proteins exported by the parasite to parasitized erythrocyte membranes. The mechanism of pRBC entry by PAAs has not been elucidated yet but it seems to be related to the known increased permeability of parasitized cells to small nanostructures. Preliminary experiments where fluorescently labelled PAAs were administered to living *Anopheles atroparvus* and *Anopheles gambiae* mosquitoes revealed the presence of the polymers in the circulatory fluids of the insect, thus opening new possibilities for the application of PAAs to malaria therapeutics.

pharmaceutics

MDPI

Article

Polyamidoamine Nanoparticles for the Oral Administration of Antimalarial Drugs

Elisabet Martí Coma-Cros [1,2], Arnau Biosca [1,2], Joana Marques [1,2], Laura Carol [1,2], Patricia Urbán [1,2], Diana Berenguer [3], Maria Cristina Riera [3], Michael Delves [4], Robert E. Sinden [4], Juan José Valle-Delgado [5], Lefteris Spanos [6], Inga Siden-Kiamos [6], Paula Pérez [1,2], Krijn Paaijmans [1], Matthias Rottmann [7,8], Amedea Manfredi [9], Paolo Ferruti [9], Elisabetta Ranucci [9] and Xavier Fernàndez-Busquets [1,2,*]

1 Barcelona Institute for Global Health (ISGlobal, Hospital Clínic-Universitat de Barcelona), Rosselló 149-153, ES-08036 Barcelona, Spain; elisabet.marti@isglobal.org (E.M.C.-C.); abiosca@ibecbarcelona.eu (A.B.); joana.a.marques@gmail.com (J.M.); lauracarol.20@gmail.com (L.C.); urban.patricia@gmail.com (P.U.); paupga20@gmail.com (P.P.); krijn.paaijmans@asu.edu (K.P.)

2 Nanomalaria Group, Institute for Bioengineering of Catalonia (IBEC), The Barcelona Institute of Science and Technology, Baldiri Reixac 10-12, ES-08028 Barcelona, Spain

3 Laboratori de Parasitologia, Departament de Microbiologia i Parasitologia Sanitàries, Facultat de Farmàcia, Universitat de Barcelona, Av. Joan XXIII s/n, ES-08028 Barcelona, Spain; berenguer.diana@gmail.com (D.B.); mcriera@ub.edu (M.C.R.)

4 Department of Life Sciences, Imperial College, South Kensington, London SW7 2AZ, UK; michael.delves@lshtm.ac.uk (M.D.); r.sinden@imperial.ac.uk (R.E.S.)

5 Department of Bioproducts and Biosystems, School of Chemical Engineering, Aalto University, P.O. Box 16300, FI-00076 Aalto, Finland; juanjose.valledelgado@aalto.fi

6 Institute of Molecular Biology and Biotechnology, FORTH, N. Plastira 100, 700 13 Heraklion, Greece; spanos@imbb.forth.gr (L.S.); inga@imbb.forth.gr (I.S.-K.)

7 Swiss Tropical and Public Health Institute, Socinstrasse 57, CH-4051 Basel, Switzerland; matthias.rottmann@swisstph.ch

8 Universität Basel, Petersplatz 1, CH-4003 Basel, Switzerland

9 Dipartimento di Chimica, Università degli Studi di Milano, via Golgi 19, IT-20133 Milano, Italy; amedea.manfredi@unimi.it (A.M.); paolo.ferruti@unimi.it (P.F.); elisabetta.ranucci@unimi.it (E.R.)

* Correspondence: xfernandez_busquets@ub.edu; Tel.: +34-93-227-5400 (ext. 4581)

Received: 19 October 2018; Accepted: 6 November 2018; Published: 10 November 2018

Abstract: Current strategies for the mass administration of antimalarial drugs demand oral formulations to target the asexual *Plasmodium* stages in the peripheral bloodstream, whereas recommendations for future interventions stress the importance of also targeting the transmission stages of the parasite as it passes between humans and mosquitoes. Orally administered polyamidoamine (PAA) nanoparticles conjugated to chloroquine reached the blood circulation and cured *Plasmodium yoelii*-infected mice, slightly improving the activity of the free drug and inducing in the animals immunity against malaria. Liquid chromatography with tandem mass spectrometry analysis of affinity chromatography-purified PAA ligands suggested a high adhesiveness of PAAs to *Plasmodium falciparum* proteins, which might be the mechanism responsible for the preferential binding of PAAs to *Plasmodium*-infected erythrocytes vs. non-infected red blood cells. The weak antimalarial activity of some PAAs was found to operate through inhibition of parasite invasion, whereas the observed polymer intake by macrophages indicated a potential of PAAs for the treatment of certain coinfections such as *Plasmodium* and *Leishmania*. When fluorescein-labeled PAAs were fed to females of the malaria mosquito vectors *Anopheles atroparvus* and *Anopheles gambiae*, persistent fluorescence was observed in the midgut and in other insect's tissues. These results present PAAs as a versatile platform for the encapsulation of orally administered antimalarial drugs and for direct administration of antimalarials to mosquitoes, targeting mosquito stages of *Plasmodium*.

Keywords: *Anopheles*; antimalarial drugs; malaria; mosquitoes; nanomedicine; nanotechnology; *Plasmodium*; polymers; polyamidoamines; targeted drug delivery

1. Introduction

Oral administration of antimalarial drugs is the best route in terms of patient compliance: it makes people feel less sick and reduces medical cost because of its ease of administration [1]. Currently used antimalarials, however, are not easily dissolved in aqueous solvents or show poor membrane permeability, which, in addition to their sensitivity to degradation, makes their oral delivery challenging [2]. To overcome this obstacle, incorporating polymers in the formulation is a strategy that has been used to give drugs increased solubility and membrane-trespassing capacity, and to protect labile compounds from digestive enzymes and extreme pH variations [3]. Polymeric nanocarriers are generally stable during gastrointestinal tract (GIT) transit [4], and given the versatility associated with their constituent materials (natural, semisynthetic or synthetic) as well as the variety of methods by which they are processed (e.g., spray-drying, emulsion techniques, precipitation, solvent extraction/evaporation), they can be used for the delivery of a wide range of cargoes [3]. Furthermore, advances in polymer chemistry enable exquisite control over the nanoarchitecture and biophysical properties of polymeric nanocarriers, which facilitates controlled or triggered drug delivery [5]. Polycations, in particular, are especially adept at oral administration because of their capacity to promote drug absorption by a variety of mechanisms, among which an increased GIT retention due to their mucoadhesive properties [6]. The systemic exposure to orally delivered polycations is low compared to the parenteral route, and therefore better tolerance is expected. Certain polycations such as polyamidoamine (PAA) polymers have the capacity to increase the epithelial permeability to conjugated drugs and biomacromolecules [6], mainly by potentiating paracellular transport although some systems may boost transcytotic passage as well. Also, anionic PAA polymers have been described as more efficiently transported across the intestinal epithelium, primarily through the paracellular route [7]. However, despite numerous studies on oral PAA bioavailability [6–10], it remains unexplored to what extent this administration method provides the necessary plasma drug concentrations for the pharmaceutical development of oral antimalarial formulations targeting *Plasmodium* parasites inside red blood cells (RBCs).

The PAA structures AGMA1 and ISA23, with respective isoelectric points of 10.0 and 5.5, had been explored for the encapsulation and targeted delivery of the antimalarial drugs chloroquine (CQ) and primaquine [11]. Fluorescence-assisted cell sorting, confocal fluorescence microscopy, and transmission electron microscopy results indicated that AGMA1 and ISA23 polymers with hydrodynamic radii around 7 nm had specific targeting to *Plasmodium*-infected RBCs (pRBCs) vs. non-infected erythrocytes, and to intraerythrocytic *Plasmodium falciparum* and *Plasmodium yoelii* merozoites, whereas AGMA1 itself exhibited a mild antimalarial activity. Mice inoculated with a lethal strain of the murine malaria species *P. yoelii* were freed of parasites after intraperitoneal administration of PAA-encapsulated CQ, whereas the same amount of free drug was unable to cure the animals.

Notwithstanding these promising results, several questions remained open, among them which is the mechanism behind the specificity of binding of PAAs to pRBCs, and whether PAAs could be applied to the current need of mass drug administration for non-complicated malaria by oral delivery [1]. With these two main objectives, previous synthetic protocols [11] have been adapted to obtain larger PAA structures that will take longer to degrade in the aggressive GIT environment. We present the characterization of these new polymers in terms of structure, cellular and subcellular targeting, and antimalarial activity after CQ encapsulation, both in in vitro growth inhibition assays of the human malaria parasite *P. falciparum* and in in vivo experiments where *P. yoelii*-infected mice have been orally administered CQ-loaded PAAs. We also communicate the preliminary results of a radically new approach to malaria control and elimination, where PAAs were orally fed to the malaria mosquito

vectors *Anopheles atroparvus* and *Anopheles gambiae* in preparation for future strategies that will target *Plasmodium* stages in the insect [12].

2. Materials and Methods

2.1. Polyamidoamine (PAA) Synthesis and Characterization

Unless otherwise indicated, all reagents were purchased from Sigma-Aldrich (St. Louis, MO, USA). Linear ISA23 [13], ISA1 [14], AGMA1 [15] and ARGO7 [16] were synthesized by stepwise Michael-type addition of *prim*- or *sec*-amines to bisacrylamides, as previously described [11], extending the reaction time to 14 days. Previously reported methods were followed for fluorescein isothiocyanate (FITC) labeling of the polymers [11,15] and for their loading with CQ [11]. FITC-labeled PAAs were obtained by reaction of FITC with PAAs bearing limited amounts of NH_2 pendants, which were synthesized as previously reported for AGMA1 [15]. Therefore, fluorescein is bound to PAAs through a urethan function, which has proved to be extremely stable in physiological conditions [17]. The conjugation of PAAs with FITC was finally confirmed by NMR. To assess the encapsulated CQ content just before in vitro and in vivo analyses, PAAs were hydrolyzed overnight with 0.1 M NaOH, pH was neutralized with 5 M HCl to solubilize the precipitated drug, and CQ was determined by measuring $A_{340\ nm}$; a calibration curve was prepared with known concentrations of CQ diphosphate identically processed. The incorporation of sulfhydryl groups in PAAs was done using standard amino-functional pyridyl disulfide chemistry [18,19], which is described in detail in the Supplementary Materials for the three PAAs later used for in vivo assays. The nanoparticle size was assessed by nanoparticle tracking analysis, using a NanoSight LM10 (Malvern Instruments Ltd., Malvern, UK). The experiments were performed in phosphate-buffered saline (PBS) at 25 °C at a concentration of 10 mg/mL, except for ARGO7 which was dissolved at 2.5 mg/mL. For scanning electron microscopy (SEM) analysis, PAAs were dissolved in isopropanol at 5 µg/mL. Fifteen microliters of this PAA solution were placed on a Si sheet (MicroChemicals, Ulm, Germany) previously cleaned, first with acetone, then with ethanol, and finally with isopropanol. Samples were allowed to dry for 48 h at room temperature (RT, ca. 20 °C) and imaged with a Nova NanoSEM™ 230 scanning electron microscope (FEI Company, Eindhoven, The Netherlands). For atomic force microscopy (AFM) analysis, 10 µL of 1 mg/mL polymer solutions in double-deionized water (ddH_2O; MilliQ system, Millipore, Burlington, MA, USA) were deposited on cleaved mica substrates and, after an adsorption time of about 5 min, 40–60 µL of ddH_2O were added. High-resolution images were obtained with a MultiMode 8 atomic force microscope equipped with a NanoScope V controller (Bruker Corporation, Billerica, MA, USA) operating in ScanAsyst mode in liquid. ScanAsyst-Fluid+ probes (Bruker Corporation) were used in the experiments.

2.2. Matrix-Assisted Laser Desorption/Ionization Tandem Time-of-Flight (MALDI TOF/TOF) Analysis

PAA samples (1 mg/mL) were incubated for the times indicated in simulated fasted-state gastric fluid (80 µM Na-taurocholate, 34.2 mM NaCl, adjusted with HCl to pH 1.6). MALDI mass spectra were recorded using a 4800 Plus MALDI TOF/TOF (ABSciex, Framingham, MA, USA) instrument equipped with Nd:YAG solid state laser (355 nm, 200 Hz frequency, 3–7 ns pulse). Analyses were performed in both positive linear and reflector mode. Solutions of the samples (1 µL) were mixed with 1 µL of a saturated matrix solution of 2,5-dihydroxybenzoic acid in acetonitrile; 1 µL of this mixture was spotted on the sample plate and left to dry before the analysis.

2.3. Plasmodium falciparum Cell Culture and Parasite Growth Inhibition, Hemolysis and Unspecific Cytotoxicity Assays

P. falciparum 3D7 in vitro cultures were prepared as described elsewhere [20,21]. Parasites were grown at 37 °C in T25 flasks (SPL Life Sciences, Gyeonggi-do, Korea) containing human RBCs of blood group type B in a Roswell Park Memorial Institute (RPMI) medium supplemented with 5 g/L Albumax II and 2 mM glutamine (complete RPMI), following previously established conditions [22].

Two hundred microliters of these *Plasmodium* cultures were plated in 96-well plates and incubated for 48 h at 37 °C in the presence of free drugs and PAA-drug conjugates dissolved in RPMI. Parasitemia was determined by microscopic counting of blood smears or by flow cytometry as previously described [20].

The human blood used in this work was from voluntary donors and commercially obtained from the *Banc de Sang i Teixits* (www.bancsang.net). Blood was not collected specifically for this research; the purchased units had been discarded for transfusion, usually because of an excess of blood relative to anticoagulant solution. Prior to their use, blood units underwent the analytical checks specified in the current legislation. Before being delivered to us, unit data were anonymized and irreversibly dissociated, and any identification tag or label had been removed in order to guarantee the non-identification of the blood donor. No blood data were or will be supplied, in accordance with the current *Ley Orgánica de Protección de Datos* and *Ley de Investigación Biomédica*. The blood samples will not be used for studies other than those made explicit in this research.

Merozoite invasion inhibition assays were performed as previously described [23], in 150 µL of culture treated with PAAs dissolved in RPMI. The following equations were used to assess invasion and maturation rates:

$$\text{Invasion} = \frac{\text{rings day } n}{(\text{trophozoites} + \text{schizonts}) \text{ day } n-1} \quad (1)$$

$$\text{Maturation} = \frac{(\text{trophozoites} + \text{schizonts}) \text{ day } n}{\text{rings day } n-1} \quad (2)$$

Hemolysis and unspecific cytotoxicity assays were done as described elsewhere [20]. For AGMA1, cytotoxicity assays were done in Phenol Red-free medium.

2.4. Cell Targeting Analysis

Living *P. falciparum* 3D7 cultures were stained for 30 min with 4 µg/mL of the DNA dye Hoechst 33342 (λex/em: 350/461 nm). After three washes with complete or incomplete RPMI the cells were incubated with gentle stirring in the presence of 0.25 mg/mL PAA-FITC for 90 min in complete or incomplete RPMI at 37 °C. After washing with PBS, nonfixed samples were placed in an eight-well chamber slide system (Lab-Tek®II, catalog number 155409). Confocal fluorescence microscopy analysis was done with a TCS SP5 laser scanning confocal microscope (Leica, Vienna, Austria) equipped with a DMI6000 inverted microscope, blue diode (405 nm), Argon (458/476/488/496/514 nm), diode pumped solid state (561 nm) and HeNe (594/633 nm) lasers and PLAN APO 63× oil (NA 1.4) immersion objective lens. For flow cytometry analysis, pRBCs were diluted in PBS to a final concentration of $1-10 \times 10^6$ cells/mL, and samples were analyzed using a LSRFortessa™ flow cytometer instrument (BD Biosciences, San Jose, CA, USA) set up with the five-laser, 20-parameter standard configuration, as previously described [11].

A macrophage cell line of mouse tumor origin (RAW 264.7) was grown in RPMI medium supplemented with 10% fetal calf serum, 100 µg/mL streptomycin, and 100 U/mL penicillin (complete medium) at 37 °C in an atmosphere containing 5% CO_2. Macrophages (300 µL, 5×10^4 cells/mL) were cultured in an eight-well Lab-Tek chamber slide system. After 24 h those cells that did not adhere were washed out; 48 h later, the culture was washed three times with PBS, and macrophages were treated in RPMI with 300 µL of PAA-FITC at 0.5 mg/mL. Samples were incubated for 90 min in the same conditions before washing PAAs with RPMI and staining plasma membranes with 5 µg/mL WGA-rhodamine (10 min, RT). Wells were then washed with RPMI and refilled with 300 µL complete medium before proceeding to observation of the fluorescence of FITC and rhodamine (respective λex/λem: 488/520 and 553/627 nm) with an IX51 inverted fluorescence microscope (Olympus, Tokyo, Japan). Confocal fluorescence microscopy images of [PAA-FITC]-treated macrophages were obtained as described above for RBCs, including Hoechst 33342 staining of nuclei.

2.5. Generation of Polyclonal Antibodies against PAAs

Immunization of rabbits was done in the facilities of the Animal Experimentation Services from the Faculty of Pharmacy at the University of Barcelona (UB) following standard protocols. The animal study was approved by the UB Animal Research Committee and the Government of Catalonia, and conducted in accordance with the Guide for the Care and Use of Laboratory Animals published by the U.S. National Institutes of Health [24]. PAAs were coupled to the carrier protein ovoalbumin and injected to two NZW rabbit females (Minimal Disease Level quality), following this immunization calendar: day 0, preimmune blood collection (reference for antibody production induced by the antigen injection) and primary immunization (intradermal injections at six to eight sites per rabbit of an aggregated amount of 250 µg PAA in a total volume of 1 mL Freund's complete adjuvant); boosters were administered every 21 days, with the same amount of antigen emulsified in Freund's incomplete adjuvant. Antibody titer was determined by enzyme-linked immunosorbent assay (ELISA, see below) of partial bleedings between immunizations, at days 52, 73, and 93, when the animals were euthanized and exsanguinated.

Serum antibodies to PAAs were assayed using an internal standard operating procedure. Briefly, flat-bottom 96-well ELISA plates (Nunc®) were coated at 4 °C overnight with 100 ng/well of antigen conjugated to bovine serum albumin (BSA) diluted in 15 mM Na_2CO_3, 35 mM $NaHCO_3$, pH 9.6. Plates were washed with 0.1% Tween 20 in PBS (PBS-T) and then blocked with 5% skimmed milk in PBS (2 h, RT). After the plates were washed again, the test serum was diluted in 0.1% BSA, 0.05% Tween 20 in PBS, added to antigen-coated wells in triplicate, and incubated for 2 h at RT. A duplicate control dilution series of a non-hyperimmune rabbit antiserum, obtained at day zero, was also included in each plate. After extensive washing, the plates were incubated for 2 h with peroxidase-labeled goat anti-rabbit IgG (Bio-Rad, Hercules, CA, USA) diluted in the same buffer. Bound antibodies were measured by adding the substrate solution (SIGMA*FAST*™ OPD, o-phenylenediamine dihydrochloride) and determining $A_{450\ nm}$ with a Multilabel Victor3 plate reader (Perkin Elmer, Turku, Finland). A 4 Parameter Logistic (4PL) nonlinear regression model was used in all ELISA assays for the antibody titer calculation. Sera were finally stored at −20 °C until use.

Polyclonal antibodies against PAAs present in the rabbit serum (15 mg total Ig/mL) were tested in a dot blot assay. Briefly, 3 µL of 3 mg PAA/mL dilutions in ddH_2O were applied and allowed to dry on a nitrocellulose membrane (0.45 µm, Bio-Rad, catalog number 1620145). As a positive control, 3 µL of a 1:25,000 serum dilution were spotted on the same membrane. Non-specific sites were blocked with 5% BSA in TBS-T (0.05% Tween 20, 150 mM NaCl, 20 mM Tris-HCl, pH 7.5) for 1 h at RT. Then the membrane was first incubated (30 min, RT) with rabbit plasma containing the polyclonal antibodies dissolved in TBS-T at 0.15 mg total Ig/mL (1:100 dilution), washed (TBS-T, 3× 5 min), and then treated with a secondary goat anti-rabbit antibody conjugated to horseradish peroxidase (AB6721, Abcam, Cambridge, UK) in TBS-T at 1 µg/mL (30 min, RT), followed by three 5-min washes with TBS-T and one wash with TBS (TBS-T without Tween 20). Finally, the membrane was incubated with ECL Prime Western Blotting Detection Reagent (Luminol, Amersham, UK) for 30–60 s and scanned (ImageQuant LAS4000, GE Healthcare, Chicago, IL, USA).

2.6. Affinity Chromatography

Half a milliliter of SulfoLink Coupling Resin, activated with iodoacetyl groups (Thermo Fisher Scientific, Waltham, MA, USA), was added to a snap cap spin column (Thermo Scientific Pierce, Waltham, MA, USA) to achieve a final column volume of 0.25 mL. For the covalent immobilization of PAAs functionalized with sulfhydryl groups (PAA-SH) on the sulfhydryl-reacting columns, these were equilibrated with coupling buffer (CB: 5 mM EDTA, 50 mM Tris-HCl, pH 8.5) and loaded with 0.5 mL of 20 mg/mL PAA-SH in CB. After gentle mixing (RT, 15 min) the columns were placed upright, and after 30 min at RT they were centrifuged (1 min, 1000 g) and washed with CB. Coupling efficacy was assessed by determining the amount of free sulfhydryl groups in the samples before and after passing through the column. Briefly, a calibration curve was prepared with dithiothreitol dissolved in 130 µL of reaction

buffer (RB: 0.1 M sodium phosphate, 1 mM EDTA, pH 8.0), to which 2.5 µL of a 4 mg/mL Ellman's reagent solution in RB were added. After 15 min incubation at RT, $A_{412\,nm}$ was determined. Then 5 mg/mL solutions of each PAA-SH in RB were processed in the same way. Unoccupied binding sites were blocked by adding 2 column volumes of quenching buffer (50 mM L-Cys-HCl in CB), followed by gentle mixing, upright incubation, centrifugation, and washing as above. Two milligrams of protein in 0.5 mL of fresh saponin extracts [25] of RBCs or pRBCs synchronized with 70% Percoll (GE Healthcare) at *Plasmodium* late stages were loaded onto each column. After mixing, upright incubation (1 h) and centrifugation as above, columns were washed with 3 to 10 column volumes of PBS. Bound proteins were eluted with a pre-warmed (55 °C) elution buffer (1× Laemmli sample buffer, supplemented with 355 mM 2-mercaptoethanol). For SDS-polyacrylamide gel electrophoresis (PAGE) analysis, samples were heated at 90 °C for 5 min in an elution buffer, and electrophoresed in 1 mm-thick 12.5% SDS-polyacrylamide gels (Mini Protean II System, Bio-Rad), which were silver-stained as previously described [26]. For the identification of PAA-binding pRBC proteins (see below), a second gel was fixed with acetic acid:ethanol:ddH_2O (1:4:5) and stained with colloidal Coomassie Blue in 20% methanol.

2.7. Liquid Chromatography-Tandem Mass Spectrometry (LC-MS/MS)

Colloidal Coomassie Blue-stained gel bands were digested separately and tryptic digests were pooled to be analyzed by LC-MS/MS in a single injection. For manual in-gel digestion of proteins with trypsin, excised SDS-PAGE bands were washed sequentially with 25 mM NH_4HCO_3 and acetonitrile (ACN), reduced in 20 mM DTT (60 min, 56 °C), alkylated in 50 mM iodoacetamide (30 min, 30 °C, protected from light), and digested with 1.2 µg of porcine trypsin (sequencing grade modified Trypsin Gold, Promega, Madison, WI, USA) for 16 h at 37 °C. The resulting peptides were extracted from the gel matrix with 10% formic acid (FA) and ACN, and the extracts from each lane were pooled and dried in a SpeedVac concentrator.

Mass spectrometry was performed in a NanoAcquity HPLC system (Waters, Milford, MA, USA) coupled to an OrbitrapVelos mass spectrometer (Thermo Scientific). Dried extracts were taken up in 1% FA and an aliquot was injected into the liquid chromatography system equipped with a reverse-phase C18 column (75 µm internal diameter, 25 cm length, 1.7 µm particle NanoAcquity BEH column, Waters), with a mobile phase 1–40% B gradient in 60 min followed by a 40–60% B gradient in 10 min (A: 0.1% FA in water; B: 0.1% FA in ACN) and a flow rate of 250 nL/min. Eluted peptides were ionized in an emitter needle (PicoTipTM, New Objective, Zurich, Switzerland) with an applied spray voltage of 2 KV. A 300–1700 m/z range of peptide masses was analyzed in data dependent mode where a full scan was acquired with a resolution of 60,000 full width at half maximum at 400 m/z. Within this range, the 15 most abundant peptides ($\geq$500 counts) were selected from each scan and fragmented in the linear ion trap using collision-induced dissociation (38% normalized collision energy) with He as the collision gas. The scan time settings were: Full MS: 250 ms (1 microscan) and MSn: 120 ms. Generated raw data files were collected with Thermo Xcalibur (v. 2.2).

A database was created by merging all human protein entries present in the Swiss Prot database with all entries for *Plasmodium* present in the Uniprot database (January 2016). A small database with common laboratory protein contaminants was also added and .raw data files obtained in the LC-MS/MS analyses were used to search with a SequestHT search engine using Thermo Proteome Discover (v. 1.4.1.14) against the aforementioned database. Both target and a decoy database were searched to obtain a false discovery rate (FDR), and thus estimate the number of incorrect peptide-spectrum matches that exceeded a given threshold, applying preestablished search parameters (enzyme: trypsin; missed cleavage: 5; fixed modifications: carbamidomethyl of cysteine; variable modifications: oxidation of methionine; peptide tolerance: 10 ppm and 0.6 Da for MS and MS/MS spectra, respectively). To improve the sensitivity of the database search, the semi-supervised learning machine Percolator was used in order to discriminate correct from incorrect peptide spectrum matches. Percolator assigns a q-value to each spectrum, which is defined as the minimal FDR at which the

identification is deemed correct (0.01, strict; 0.05, relaxed). These q values are estimated using the distribution of scores from decoy database search.

2.8. Transmission Electron Microscopy (TEM) of Cell Sections

pRBC cultures were treated with 0.5 mg PAA/mL at 37 °C for 90 min, when cryosections were prepared as described [11]. Collected cryosections were incubated at RT on drops of 2% gelatin in 0.1 M PHEM buffer [27] for 30 min at 37 °C, followed by (all solutions in 0.1 M PHEM buffer) 20 mM glycine for 15 min, 10% fetal bovine serum (FBS) for 10 min, and 1% FBS for 5 min. Then they were incubated for 1 h in the presence of rabbit ISA23 antiserum diluted 1:500 in 0.1 M PHEM buffer supplemented with 1% FBS. After three washes on drops of 0.2% FBS in 0.1 M PHEM buffer for 10 min, sections were incubated for 20 min with anti-rabbit IgG coupled to 12-nm colloidal gold particles (Jackson ImmunoResearch, West Grove, PA, USA) using a 1:30 dilution in 0.1 M PHEM buffer supplemented with 1% FBS. This was followed by three washes with drops of 0.1 M PHEM buffer for 10 min, a 5-min fixation in 1% glutaraldehyde, 0.1 M PHEM buffer, and 10 1-min washes with ddH_2O. The observations were done in a Tecnai Spirit electron microscope (FEI Company, Hillsboro, OR, USA) with a CCD SIS Megaview III camera. Controls included omission of polymer, omission of anti-PAA antibody, and staining of non-infected RBCs.

2.9. Determination of PAA-FITC Presence in Blood and Toxicity Assays in Mice

Inbred BALB/cAnNHsd female, 6–8-week-old mice (BALB/c; Harlan Laboratories, Indianapolis, IN, USA) were dosed orally with 100 mg/kg PAA-FITC dissolved in PBS. Then 15-µL blood samples were collected in Microvette® tubes (Sarstedt) using the cross-sectional cut method, before dosing (t_0) and at 1, 6, and 24 h post-administration. Blood samples were centrifuged for 5 min (4000 g) and stored at −20 °C; 10 µL of the supernatant were diluted 10 times with PBS and used to measure FITC fluorescence in a Spectramax Gemini XS microplate fluorimeter (Molecular Devices, LLC, Sunnyvale, CA, USA; λex/em: 485/530 nm). For in vivo toxicity assays, polymer solutions were prepared in PBS and each sample was injected intraperitoneally in three BALB/c mice; PBS was administered to control animals. Mice were individually monitored for eight days following a drug dosage regime as in the in vivo antimalarial assays performed in this work (see below). In the presence of toxic effects including, among others, >20% reduction in animal weight, aggressive and unexpected animal behavior or the presence of blood in feces, animals were immediately anesthetized using a 100 mg/kg Ketolar plus 5 mg/kg Midazolan mixture and sacrificed by cervical dislocation. Polymer maximum tolerated dose (MTD) was therefore defined upon completion of the assay as the highest dosage exhibiting an absence of the aforesaid toxicity signs. All experiments involving mice were performed in accordance with the corresponding relevant guidelines and regulations. The studies reported here were performed under protocols reviewed and approved by the Ethical Committee on Clinical Research from the *Hospital Clínic de Barcelona* (Reg. HCB/2014/0910; date of approval 14 October 2014). The animal care and use protocols followed adhered to the specific national and international guidelines specified in the Spanish Royal Decree 53/2013, which is based on the European regulation 2010/63/UE.

2.10. Antimalarial Activity Assay In Vivo

The in vivo antimalarial activity of free CQ and of PAA-CQ conjugates was analyzed in a four-day blood suppressive test as previously described [28]. Briefly, BALB/c mice were inoculated intraperitoneally with 2×10^6 RBCs from *P. yoelii yoelii* 17XL (PyL) MRA-267-infected mice. Treatment started 2 to 4 h later (day 0) with a single dose of 5 mg CQ kg^{-1} day^{-1} administered as diphosphate-drug or PAA-drug by oral administration followed by identical dose administration for the next three days. Tested compounds were prepared in PBS and the control groups received PBS. Parasitemia was monitored daily by microscopic examination of Giemsa-stained thin blood smears. When all surviving animals had completely cleared *Plasmodium* infection they were re-infected (on

day 35) with *P. yoelii* as above and left untreated. A group of animals infected and left untreated was always used as a control of a correct parasite inoculation. Survival was monitored until day 62.

2.11. PAA Administration to Mosquitoes

Wild *Anopheles atroparvus* mosquitoes (ca. 1000 individuals) were collected from a pig farm in the Ebre delta, in collaboration with the *Consorci de Serveis Agroambientals de les comarques del Baix Ebre i Montsià*. Females were arm-fed to produce the next generation of mosquitoes. Newly hatched female mosquitoes (F1 generation) were starved for 48 h prior to feeding them (day 0) with ISA1-FITC nanoparticles (0.125 mg/mL) incorporated in their sugar meal (0.1 mg glucose/mL), in a cage protected from light. Sugar-fed females were separated from non-fed mosquitoes and used in the experiment (continuously kept in the dark, and with access to sugar water without the labeled polymer). At different times, females were anesthetized with ether and immobilized live on a microscope slide with Vaseline and Parafilm® for confocal fluorescence microscopy examination (λex/em: 495/519 nm).

Six to eight female *Anopheles gambiae* mosquitoes were tested for each PAA-FITC. The mosquitoes were removed to cups and allowed to feed for two days on 10% sucrose provided in a filter mounted on a 1-mL syringe. On day 3 the sucrose was replaced with PAA-FITC at a concentration of 0.25 mg/mL diluted in 10% sucrose. A control was included where the mosquitoes continued to feed on sucrose. After another three or five days, mosquitoes were dissected and midguts and salivary glands were fixed in 4% formaldehyde. The dissected organs were viewed under a Zeiss Axioskop 2 Plus microscope fitted with an Axiovert CCD camera (Zeiss, Oberkochen, Germany).

2.12. Statistical Analysis

Data are presented as the mean ± standard error of at least three independent experiments, and the corresponding standard errors in histograms are represented by error bars. Percentages of viability were obtained using non-treated cells as control of survival and IC_{50} values were calculated by nonlinear regression with an inhibitory dose-response model using GraphPad Prism5 software. Concentrations were transformed using natural log for linear regression. Regression models were adjusted for replicates and assay data.

3. Results

3.1. Characterization of PAAs and Stability Analysis in GIT Conditions

Following synthesis, PAAs were size fractionated to have a range of molecular masses from 5 to 100 kDa, well above the maximum size previously evaluated for intraperitoneal administration (<25 kDa, [11]). AFM images taken in water on mica surfaces revealed homogeneous dispersions of particles up to 5 nm in height (Figure 1A). To evaluate their possible degradation during GIT transit, the polymers were incubated for different times in simulated fasted-state gastric fluid and subjected to MALDI TOF/TOF analysis, which permitted identification of molecules up to a molecular mass of ca. 7 kDa. Although large polymers escaped detection, this strategy allowed us to follow the degradation process over time. MALDI chromatograms exhibited regularly spaced peaks (Figure 1C), whose masses differed by discrete units that corresponded to multiples of the mass of the main building block of the respective polymers (e.g., 329 Da for ARGO7; Figure 1B). Hydrolytic degradation was evident after 6 h of incubation (Figure 1D) and reached its maximum at around 19 h (Figure 1E).

The four PAAs, initially synthesized as relatively homogeneously sized preparations, acquired when dissolved in PBS a higher size and polydispersity according to nanoparticle tracking analysis (Figure S1), with estimated hydrodynamic diameters between 50 and 400 nm. In the high ionic strength of PBS, the repulsive forces between the polymer charged groups are screened, thus promoting macromolecular associations. Scanning electron microscopy analysis of the polymers dissolved in isopropanol (an aggregation-promoting solvent) revealed branched structures reaching lengths of several microns (Figure 2). PAAs have relatively large hydrodynamic volumes if compared with

vinyl polymers of similar mass, indicating a tendency to assume an extended chain conformation in solution [29].

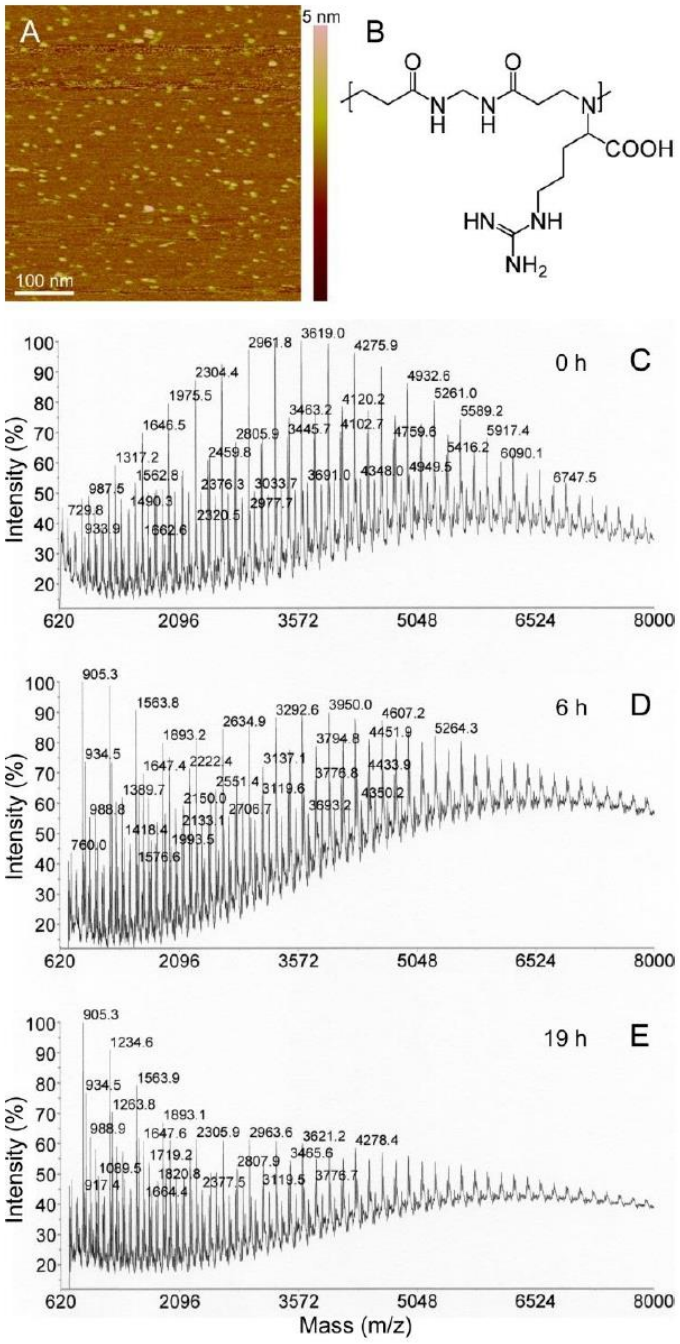

Figure 1. Analysis of PAA stability in GIT conditions. (**A**) AFM image in water of AGMA1. (**B**) Chemical structure of the ARGO7 repeating unit. (**C**–**E**) MALDI TOF/TOF analysis of the degradation of ARGO7 in simulated fasted-state gastric fluid.

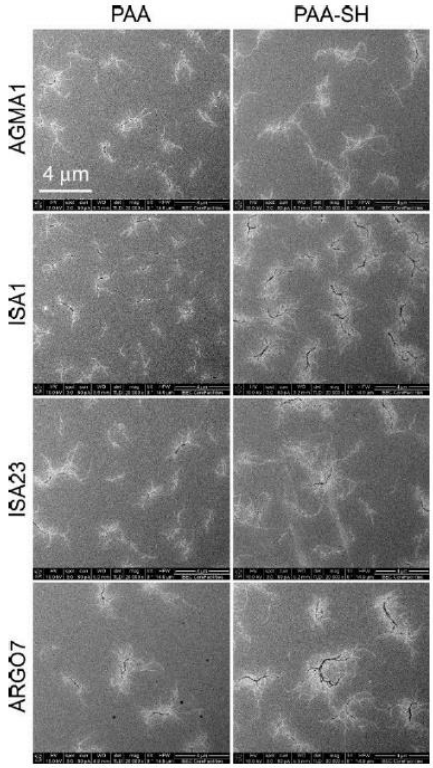

Figure 2. SEM analysis of PAAs, before (PAA) and after the introduction of sulfhydryl groups (PAA-SH).

3.2. Cell Targeting of PAAs

As already reported for smaller polymers [11], in flow cytometry analyses PAAs did not exhibit a clear affinity for pRBCs vs. the uninfected RBCs present in the same culture (Figure S2). In complete medium little binding was observed to either cell, but in incomplete medium, PAA-cell interactions increased with both RBCs and, especially, with late-stage pRBCs (characterized by a stronger Hoechst signal due to the presence of several parasite daughter cells and therefore a larger DNA content). The differences in cell targeting observed by flow cytometry between complete and incomplete RPMI could be related to a screening effect of the proteins present in complete medium, which might prevent polymer interactions with cell membranes. Indeed, a high level of protein binding has been reported with the serum substitute Albumax used in complete RPMI [30]. This observation must be taken into account when designing in vivo experiments due to the high protein concentration found in plasma.

Confocal fluorescence microscopy examination of [PAA-FITC]-treated late-stage *P. falciparum* cultures indicated that the polymers accumulated inside the parasitophorous vacuole where the parasite is contained (Figure S3). The absence of fluorescence in the RBC cytosol of parasitized cells was consistent with the lack of FITC signal in RBCs, although according to flow cytometry data in incomplete RPMI, non-parasitized RBCs significantly interacted with some PAAs, especially with AGMA1 and ISA23 (Figure S2). Polyclonal antibodies generated against ISA23 (Figure S4) were used to investigate potential entry routes of PAAs into pRBCs. Although the antibody signal was not abundant, it could be occasionally observed associated with the plasma membrane and in intracellular areas not enclosed by a membrane (Figure S5). These observations reinforced the hypothesis that PAAs traverse the pRBC lipid bilayer through a diffusion mechanism, as previously suggested from preliminary data obtained based on the indirect detection of PAA-FITC using anti-fluorescein antibodies [11].

When PAAs were incubated in the presence of macrophages in incomplete RPMI, only ISA23 was significantly taken up by the cells according to fluorescence microscopy analysis (Figure 3A). This result is consistent with the observation that ISA23 showed in the same buffer the highest interaction of all four PAAs with non-infected RBCs. Taken together, these experimental evidences indicate that ISA23 has a strong affinity for lipid bilayers, as it can be observed in confocal fluorescence microscopy images of [ISA23-FITC]-treated macrophage cultures where, in addition to cell membranes, also vesicular extracellular structures were shown to interact with the polymer (Figure 3B). Previous data showed that ISA23 had a remarkably high blood residence time [15], with about 25% of the polymer still present in the circulation 24 h after its intraperitoneal administration to mice [11]. This suggested that despite the incorporation of ISA23 into macrophages, the overall polymer concentration in blood will not be significantly affected by this cell intake.

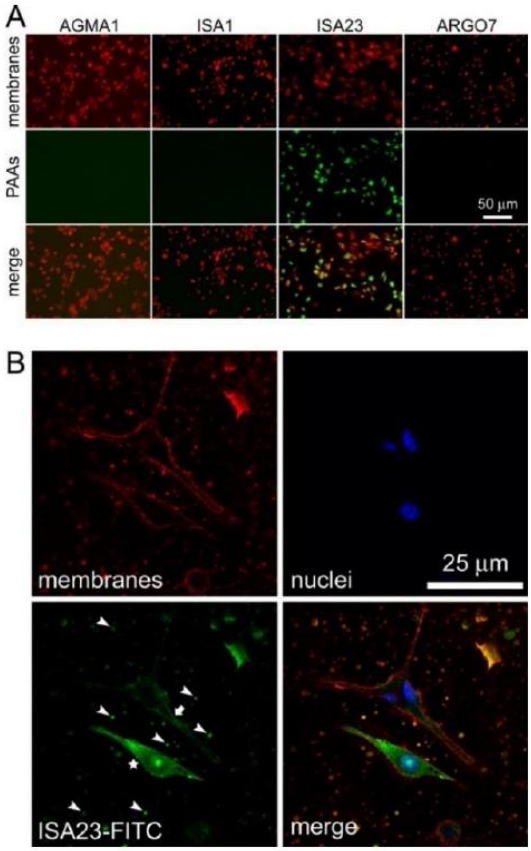

Figure 3. Fluorescence microscopy analysis of PAA-FITC uptake by macrophages. (**A**) Conventional fluorescence microscopy of all PAA samples. (**B**) Confocal fluorescence microscopy of the ISA23-FITC sample. Two macrophages are shown, one with intense intracellular FITC labeling (star) and another with plasma membrane labeling (arrow). Arrowheads point at some of the abundant vesicular structures present in the culture that have also incorporated the polymer.

3.3. Affinity Chromatography Analysis of PAA-Binding pRBC Proteins

To investigate the molecular mechanism responsible for the preferential entry of PAAs into pRBCs vs. RBCs, an affinity chromatography approach was chosen. The four PAAs were functionalized with sulfhydryl groups that would be used to crosslink the polymers to SulfoLink columns (see Figure 2 for a SEM control of polymer structures after the incorporation of sulfhydryl groups). Coupling efficacy

of PAAs to columns was found to range from 50% to 90%. According to silver-stained SDS-PAGE gels, no proteins could be detected to bind PAA-columns upon loading of uninfected RBC saponin extracts (Figure 4A). However, after loading the same columns with equal total amounts of identically prepared pRBC saponin extracts, several bands corresponding to proteins eluted from the affinity columns could be observed in the silver-stained gels of all four PAAs (Figure 4B). From a Coomassie Blue gel run in parallel with higher sample amounts loaded, the lanes from the separating gel were excised and analyzed by LC-MS/MS, where a total of 507 proteins were identified, 365 human and 142 from the *P. falciparum* 3D7 strain used. Many *Plasmodium* proteins were found to bind more than one PAA (see Table S1 for a list of *Plasmodium* proteins binding two, three, or all four PAAs), and over one-quarter (37 out of 142) interacted with the four polymers, which strongly validated the specificity of the identified PAA-protein interactions. Although the identified sequences belonged to a wide variety of families, it was remarkable the detection of several proteins involved in cell adhesion or present in the cell membrane, such as glycophorin-binding protein, erythrocyte membrane protein 3, mature parasite-infected erythrocyte surface antigen, ring-exported protein 1, surface protein P113, and high molecular weight rhoptry protein 3. We also noted the presence of several heat-shock proteins. This result strongly suggested the presence in pRBC saponin extracts of adhesive proteins interacting both with PAAs (hence the binding to affinity columns) and with RBC components (hence the presence of human RBC proteins in the fractions eluting from the columns loaded with pRBC extracts). This scenario might also explain the increased uninfected RBC targeting of some PAAs in the presence of pRBCs (Figure S2), if pRBC-secreted proteins associate with uninfected erythrocytes in the culture, e.g., through the extracellular vesicle trafficking that has been described between pRBCs [31].

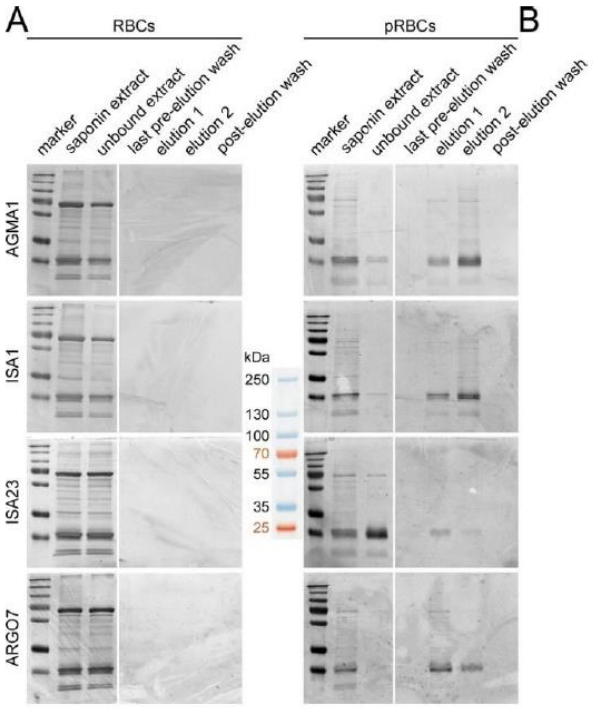

Figure 4. Silver-stained SDS-PAGE of pRBC saponin extracts run through four affinity chromatography columns where AGMA1, ISA1, ISA23 or ARGO7 had been immobilized. (**A**) A RBC extract was first loaded, and after the corresponding washing-elution-washing steps (**B**) a pRBC extract was loaded in the same column. The approximate masses (kDa) of the seven bands from the molecular weight marker are indicated in the space between the gels.

In agreement with this hypothesis, we observed in immunoTEM preparations of *Plasmodium* intraerythrocytic stages numerous events of what appeared to be the budding from pRBC membranes of small vesicles below 50 nm in diameter (Figure 5). These structures, also abundantly detected in the extracellular space, seemed to be formed from protrusions of the outer bilayer leaflet of the plasma membrane, although from the static TEM images it could not be discerned whether they were leaving or entering the erythrocyte. Larger lipid bilayer-enclosed vesicles just under 500 nm in diameter that were detected in the close vicinity of the pRBC plasma membrane (both inside and outside the cell) were also observed to contain and/or be associated with the smaller vesicles. This vesicular traffic was less abundant in uninfected RBC control samples, although a detailed quantitative analysis would be required to confirm this qualitative observation.

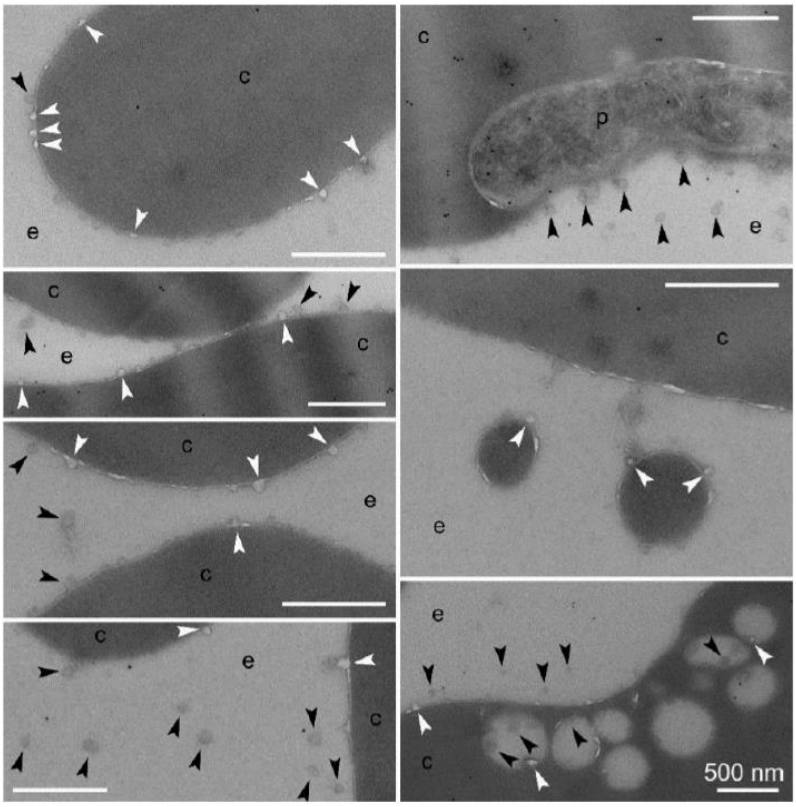

Figure 5. ImmunoTEM analysis of vesicular entities in *P. falciparum* in vitro cultures—e, extracellular area; c, RBC cytosol; p, *Plasmodium*. White arrowheads indicate structures in the process of budding from or merging with RBCs; black arrowheads point at vesicles not fused to RBC membranes. Size bars represent 500 nm.

None of the polymers was hemolytic or cytotoxic up to 1 mg/mL (Figure S6). MTD assays in mice confirmed the significant toxicity already observed for smaller ISA1 polymers at 50 mg/kg [11], whereas the other structures were well tolerated up to 200 mg/kg. This result was in agreement with previous data reporting higher toxicity for positively charged PAA dendrimers vs. their anionic counterparts after oral administration to mice [9], which led us to discard ISA1 for the preparation of in vivo tests in mice.

3.4. In Vitro Plasmodium Growth Inhibition Assays

CQ loaded into AGMA1, ISA23 and ARGO7 polymers reached drug payloads of 14.2%, 32.6% and 35.6% respectively; these drug contents were confirmed just before performing in vitro and in vivo assays (15.9%, 32.1% and 36.0% respectively). AFM images taken in water did not reveal significant changes in the globular structure of the polymeric nanoparticles induced by the incorporation of drug (Figure S7). SEM images after isopropanol treatment indicated that CQ loading resulted in more compact aggregated polymer structures (Figure S8), especially for those PAAs carrying more drug, which might be due to a template effect induced on the polymer by the cargo. As already described for smaller PAA structures [11], encapsulation did not improve the in vitro activity of CQ (Figure S9). Previous data reporting a modest in vitro antimalarial activity of some PAAs (particularly AGMA1) [11] led us to explore the suspected antiparasitic mechanism in more detail. Based on the known antimalarial activity of certain polymers like heparin, operating through inhibition of the RBC invasion by the parasite [32–36], we performed an invasion inhibition assay (Figure 6). Whereas the maturation rate of intraerythrocytic *P. falciparum* in the presence of polymers was not significantly affected up to 1 mg PAA/mL, the invasion rate in the presence of AGMA1 was clearly reduced in a dose-dependent manner, indicating that most likely the antimalarial activity mechanism of this polymer is based, as for heparin, on invasion inhibition.

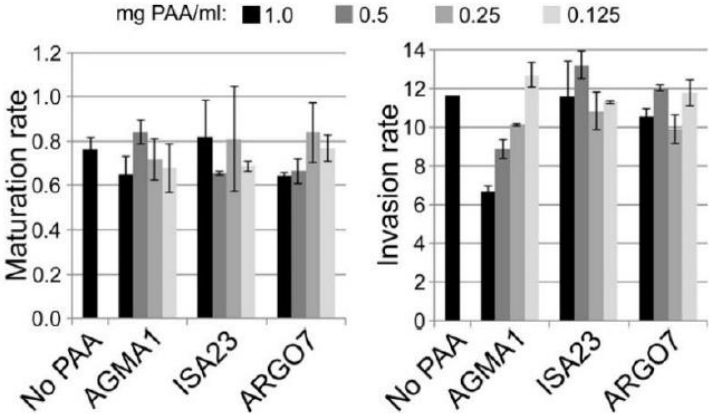

Figure 6. In vitro determination in the presence of PAAs of *P. falciparum* maturation and invasion rates.

3.5. Oral Administration to Mice

Upon oral administration to mice of PAA-FITC, fluorescence could be detected in the circulation 24 h later (Figure S10A), although we could not rule out artifacts due to potential cleavage of the PAA-FITC bond during GIT transit. However, the presence in plasma of orally administered ISA23 could be determined in dot blot assays using ISA23 antiserum (Figure S10B), indicating that at least this polymer is able to enter the blood circulation when fed to mice.

When administered orally at 5 mg CQ kg^{-1} day^{-1}, PAA encapsulation only slightly improved the activity compared to the free drug (Figure 7A), with three mice cured out of five (3/5) for ISA23-CQ, two out of four for ARGO7-CQ, and two out of five for both AGMA1-CQ and free CQ. When these nine surviving animals were re-infected with *P. yoelii* and left untreated, all of them recovered completely, without presenting symptoms of the disease and with parasitemia levels below microscopy detection thresholds (Figure 7B). Control naïve infected animals left untreated developed malaria, showing high levels of parasitemia (Figure S11). This result indicated that the animals had developed immunity against *Plasmodium*, a result in agreement with previous reports of immune protection induced in malaria-infected mice that had been administered curative drug doses [23].

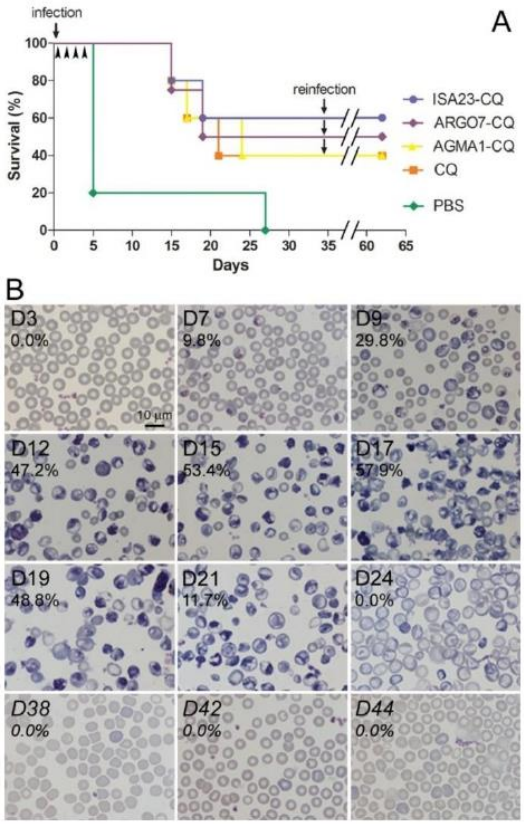

Figure 7. In vivo antimalarial activity assays. (**A**) Kaplan–Meier plot for the in vivo assay of the effect on *P. yoelii*-infected mice (n = 5 animals/sample except for ARGO7-CQ, where one of the infections was not successful) of CQ administered orally at 5 mg kg^{-1} day^{-1}, either as a free drug or polymer-conjugated. (**B**) Microscopic images of blood smears prepared on different days (D0 was the day of the first infection, and reinfection was on day 35), used to determine parasitemias in a *P. yoelii*-infected mouse treated with AGMA1-CQ.

3.6. Oral Administration to Mosquitoes

With the aim of exploring radically new antimalarial strategies we decided to investigate if PAAs could be used in future innovative approaches against malaria involving the direct administration to mosquitoes of nanocarriers capable of encapsulating antiplasmodial drugs. To obtain additional preliminary data on the potential effect of PAAs on mosquito viability, we decided to use for this assay ISA1, which had shown the highest in vivo toxicity in mice. When *A. atroparvus* mosquitoes were fed ISA1-FITC incorporated in their sugar meal, the polymer fluorescence could be detected one day after ingestion in the insect gut (Figure 8A) and three days post-feeding in body tissues outside of the gut, including a location in the thorax, near the head, in the vicinity of the salivary glands (Figure 8B). ISA1-FITC seemed to diffuse through the midgut and circulate via the hemolymph and was detected up to six days after its ingestion, being the thorax region where fluorescence lasted longer. In a similar feeding assay done with *A. gambiae*, dissection of the mosquito organs revealed the presence of AGMA1-FITC, ARGO7-FITC and ISA23-FITC in the midgut but not in the salivary glands (Figures S12 and S13). No significant effect on mosquito life span was observed for any of the PAAs.

Preliminary targeting assays of PAA-FITC to mosquito stages of *Plasmodium* (*P. falciparum* gametocytes and *Plasmodium berghei* ookinetes, oocysts and sporozoites) did not reveal PAAs binding directly to any of these parasite forms (Figures S14–S17).

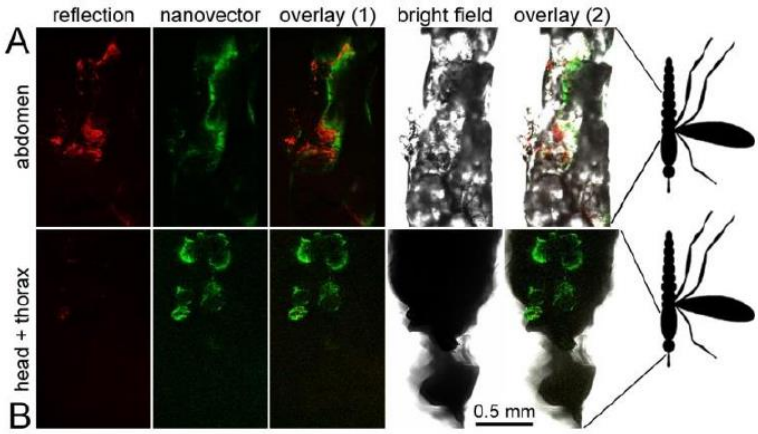

Figure 8. Direct delivery of PAAs to *Anopheles*. Newly hatched *A. atroparvus* were fed fluorescein-labeled ISA1 incorporated in their sugar meal. Confocal fluorescence microscopy indicated the presence of fluorescein signal (**A**) in the midgut (first day post-feeding) and (**B**) in a region of the thorax consistent with salivary gland location (three days post-feeding). In red is shown the reflection of excitation light on the cuticle of the insect.

4. Discussion

The four PAAs assayed here interact with proteins belonging to the chaperone and glycophorin-binding families. Chaperones are required in a multitude of biological systems for the correct folding of proteins; in particular Hsp70 and Hsp90 facilitate the assembly of proteins into higher order complexes and their translocation across membranes [37]. The key role of chaperones in the cell suggests that part of the modest antimalarial activity of some PAAs might be based on their binding to intracellular components. Such a scenario is consistent with the finding that AGMA1, whose antimalarial activity is highest [11], is also the PAA associating with a larger number of *Plasmodium* proteins (Table S1). The binding of PAAs to parasite ligands is unlikely to be based on unspecific electrostatic interactions, because ISA1 and AGMA1, whose cationic character is similar (both have an average of 0.55 positive charges per unit at pH 7.4), share only about 55% of the identified affinity chromatography purified proteins. A significant portion of AGMA1 did show hepatic localization after intravenous injection in mice [15], which presents this polymer as an interesting candidate for therapies targeting the dormant liver stages (hypnozoites) of some *Plasmodium* species.

The first glycophorin-binding protein identified in *Plasmodium* was GBP130 [38], which has been shown to play a role in decreasing the membrane rigidity of pRBCs, a process involved in protein trafficking. Being glycophorin a receptor for the malaria parasite during its adhesion to red blood cells [39], the finding that PAAs associate with the parasite-encoded glycophorin-binding protein can open new therapeutic avenues based on blocking *Plasmodium*–red blood cell interactions. Invasion inhibition assays showed that AGMA1, at non-toxic concentrations that do not affect the maturation of intraerythrocytic *P. falciparum*, does reduce invasion rates in a dose-dependent manner. Among other proteins identified to bind several PAAs are the surface protein P113 and the high molecular weight rhoptry protein 2. The coupling of PAAs to these ligands might mask essential interactions of *Plasmodium* with the RBC membrane, blocking or significantly slowing down invasion. The resulting increased exposure of the parasite to the immune system might partially contribute to the protection against malaria infection observed in [PAA-CQ]-treated mice. This knowledge could be applied to the design of new antimalarial approaches where PAAs might play a dual role as carriers of drugs and as vaccination adjuvants. Regarding potential future clinical applications, it is relevant that this effect is obtained following oral intake, since this is the preferred form of administration of treatments for non-complicated malaria.

Contrary to intact erythrocytes, which lack endocytosis of large macromolecules, pRBCs develop mechanisms that confer an increased permeability to particles up to 70 nm across [40,41], which might permit the entry of PAAs below that size. This limitation leaves a narrow margin for the design of orally administered antimalarial nanocarriers, which must be synthesized with a sufficiently large size to reach the GIT without significant degradation whereas once in the blood circulation they need not be larger than a few dozen nm. PAAs, however, could be more readily adaptable to the treatment of other blood-infecting pathogens whose host cell is not the erythrocyte. The prevailingly anionic polymer ISA23 exhibited the clearest interaction with cell membranes from both RBCs and macrophages, being massively endocytosed by the latter. Such capacity presents this polymer as an interesting candidate for the coencapsulation, oral administration, and targeted delivery of drugs to treat common coinfections of pathogens parasitizing these two cell types, such as *Plasmodium* and the macrophage-infecting *Leishmania*.

The modest amelioration in the antimalarial activity of orally administered CQ provided by encapsulation in PAA polymers could be significantly improved in different ways. An increased specificity of delivery can be obtained upon functionalization of the nanocarriers with targeting molecules, e.g., antibodies against either pRBCs [20] or both parasitized and non-parasitized erythrocytes [25], or glycosaminoglycans such as heparin, which has shown specific pRBC binding [42,43]. On the other hand, coating of the nanovessels with polyethylene glycol (PEG) is a standard method used to reduce immune clearance and thereby increase circulation times allowing the carriers to reach their target site [44]. Nevertheless, this last strategy has to be more thoroughly explored because PEGylation of anionic PAA dendrimers has been described to lead to a significant decrease in intestinal cell uptake [7]. The proof-of-concept approach researched here using CQ can be extrapolated to other drugs being less efficient, more toxic, or still undiscovered. The finding that PAA encapsulation did slightly improve the exceptionally good performance of CQ as antimalarial opens perspectives for the successful application of these polymers to future orally administered therapeutic and/or prophylactic strategies.

A largely unexplored avenue in antimalarial drug development is targeting the parasite stages in the insect vector itself [45]. Preliminary data following feeding of PAA-FITC to *A. atroparvus* and *A. gambiae* indicate that the ingested polymers are not immediately excreted and have a long residence time in the midgut of both species, and in the case of *A. atroparvus* other locations in the vicinity of the salivary glands seem likely. Mosquito-dwelling parasite stages could be efficiently reached by specifically targeted nanovectors (e.g., tagged with heparin, which has been shown to bind *Plasmodium* ookinetes [43]) encapsulating the corresponding drugs. Although more studies are required, including a characterization of the longevity of nanocarriers inside the mosquito, our results suggest that encapsulated antimalarial drugs could be directly dispensed to *Anopheles* from fixed-volume containers where the drug does not become diluted with time as when it is in the blood circulation. This strategy not contemplating administration to humans would significantly reduce clinical trials and treatment development costs, thus allowing for faster transferability.

Supplementary Materials: The following are available online at http://www.mdpi.com/1999-4923/10/4/225/s1, Figure S1: Nanoparticle tracking analysis of PAAs, Figure S2: Flow cytometry analysis of the interaction of PAAs-FITC with RBCs and pRBCs in complete and incomplete RPMI, Figure S3: Confocal fluorescence microscopy targeting study of PAAs to *P. falciparum*-containing pRBCs, Figure S4: Generation of rabbit polyclonal antibodies against ISA23, Figure S5: ImmunoTEM analysis of the subcellular localization of ISA23 in *P. falciparum* ring stages, Figure S6: PAA cytotoxicity and hemolysis assays, Figure S7: AFM images on mica of PAAs and of PAA–CQ complexes, Figure S8: SEM analysis of PAAs, Figure S9: Growth inhibition assay of the effect of PAA-encapsulated CQ on in vitro *P. falciparum* cultures, Figure S10: Detection in blood of orally administered PAAs, Figure S11: Microscopic images of blood smears prepared on days 3 and 5 post-infection from control *P. yoelii*-infected naïve mice left untreated, Figures S12 and S13: Direct delivery of PAAs to *Anopheles gambiae*, Figure S14: Targeting assay of PAA-FITC to *P. falciparum* gametocytes, Figure S15: Targeting assay of PAA-FITC to *P. berghei* ookinetes, Figure S16, Targeting assay of PAA-FITC to *P. berghei* oocysts, Figure S17: Targeting assay of PAA-FITC to *P. berghei* sporozoites, Table S1: PAA-binding proteins from the *P. falciparum* 3D7 strain identified in affinity chromatography columns.

Author Contributions: Conceptualization, P.F., E.R. and X.F.-B.; methodology, E.M.C.-C. and P.U.; validation, E.M.C.-C.; formal analysis, E.M.C.-C. and X.F.-B.; investigation, E.M.C.-C., A.B., J.M., L.C., P.U., D.B., J.J.V.-D., L.S., P.P. and A.M.; resources, M.C.R., M.D., R.E.S., J.J.V.-D., I.S.-K., K.P., M.R., E.R. and X.F.-B.; data curation, E.M.C.-C.; writing—original draft preparation, E.M.C.-C.; writing—review and editing, E.M.C.-C. and X.F.-B.; visualization, E.M.C.-C.; supervision, E.M.C.-C., M.C.R., M.D., R.E.S., I.S.-K., K.P., M.R., E.R. and X.F.-B.; project administration, X.F.-B.; funding acquisition, P.F., E.R. and X.F.-B.

Funding: This research was funded by (i) *Fondazione Cariplo*, Italy, grant number 2013-0584, (ii) *Ministerio de Economía, Industria y Competitividad*, Spain (which included FEDER funds), grant number BIO2014-52872-R, (iii) ERA-NET Cofund EURONANOMED, grant number 2017-178 (NANOpheles), and (iv) *Generalitat de Catalunya*, Spain, grant number 2014-SGR-938.

Acknowledgments: ISGlobal and IBEC are members of the CERCA Programme, *Generalitat de Catalunya.*

Conflicts of Interest: The authors declare no conflict of interest. The funders had no role in the design of the study; in the collection, analyses, or interpretation of data; in the writing of the manuscript, or in the decision to publish the results.

References

1. World Health Organization. *Guidelines for the Treatment of Malaria*, 3rd ed.; World Health Organization: Geneva, Switzerland, 2015; Available online: http://apps.who.int/iris/bitstream/10665/162441/1/9789241549127_eng.pdf (accessed on 13 July 2018).
2. Bergström, C.A.S.; Holm, R.; Jørgensen, S.A.; Andersson, S.B.E.; Artursson, P.; Beato, S.; Borde, A.; Box, K.; Brewster, M.; Dressman, J.; et al. Early pharmaceutical profiling to predict oral drug absorption: Current status and unmet needs. *Eur. J. Pharm. Sci.* **2014**, *57* (Suppl. C), 173–199. [CrossRef] [PubMed]
3. Plapied, L.; Duhem, N.; des Rieux, A.; Preat, V. Fate of polymeric nanocarriers for oral drug delivery. *Curr. Opin. Colloid Interface Sci.* **2011**, *16*, 228–237. [CrossRef]
4. Ryan, K.B.; Maher, S.; Brayden, D.J.; O'Driscoll, C.M. Nanostructures overcoming the intestinal barrier: Drug delivery strategies. In *Nanostructured Biomaterials for Overcoming Biological Barriers*, 1st ed.; Alonso, M.J., Csaba, N.S., Eds.; The Royal Society of Chemistry: Cambridge, UK, 2012; pp. 63–90. ISBN 978-1-84973-363-2.
5. Raemdonck, K.; Braeckmans, K.; Demeester, J.; De Smedt, S.C. Merging the best of both worlds: Hybrid lipid-enveloped matrix nanocomposites in drug delivery. *Chem. Soc. Rev.* **2014**, *43*, 444–472. [CrossRef] [PubMed]
6. Schulz, J.D.; Gauthier, M.A.; Leroux, J.C. Improving oral drug bioavailability with polycations? *Eur. J. Pharm. Biopharm.* **2015**, *97 Pt B*, 427–437. [CrossRef]
7. Sweet, D.M.; Kolhatkar, R.B.; Ray, A.; Swaan, P.; Ghandehari, H. Transepithelial transport of PEGylated anionic poly(amidoamine) dendrimers: Implications for oral drug delivery. *J. Control. Release* **2009**, *138*, 78–85. [CrossRef] [PubMed]
8. Yellepeddi, V.K.; Ghandehari, H. Poly(amido amine) dendrimers in oral delivery. *Tissue Barriers* **2016**, *4*, e1173773. [CrossRef] [PubMed]
9. Thiagarajan, G.; Greish, K.; Ghandehari, H. Charge affects the oral toxicity of poly(amido amine) dendrimers. *Eur. J. Pharm. Biopharm.* **2013**, *84*, 330–334. [CrossRef] [PubMed]
10. Huang, X.; Wu, Z.; Gao, W.; Chen, Q.; Yu, B. Polyamidoamine dendrimers as potential drug carriers for enhanced aqueous solubility and oral bioavailability of silybin. *Drug Dev. Ind. Pharm.* **2011**, *37*, 419–427. [CrossRef] [PubMed]
11. Urbán, P.; Valle-Delgado, J.J.; Mauro, N.; Marques, J.; Manfredi, A.; Rottmann, M.; Ranucci, E.; Ferruti, P.; Fernàndez-Busquets, X. Use of poly(amidoamine) drug conjugates for the delivery of antimalarials to *Plasmodium*. *J. Control. Release* **2014**, *177*, 84–95. [CrossRef] [PubMed]
12. Urbán, P.; Ranucci, E.; Fernàndez-Busquets, X. Polyamidoamine nanoparticles as nanocarriers for the drug delivery to malaria parasite stages in the mosquito vector. *Nanomedicine* **2015**, *10*, 3401–3414. [CrossRef] [PubMed]
13. Ranucci, E.; Ferruti, P.; Lattanzio, E.; Manfredi, A.; Rossi, M.; Mussini, P.R.; Chiellini, F.; Bartoli, C. Acid-base properties of poly(amidoamine)s. *J. Polym. Sci. A Polym. Chem.* **2009**, *47*, 6977–6991. [CrossRef]
14. Lavignac, N.; Nicholls, J.L.; Ferruti, P.; Duncan, R. Poly(amidoamine) conjugates containing doxorubicin bound via an acid-sensitive linker. *Macromol. Biosci.* **2009**, *9*, 480–487. [CrossRef] [PubMed]

15. Ferruti, P.; Franchini, J.; Bencini, M.; Ranucci, E.; Zara, G.P.; Serpe, L.; Primo, L.; Cavalli, R. Prevailingly cationic agmatine-based amphoteric polyamidoamine as a nontoxic, nonhemolytic, and "stealthlike" DNA complexing agent and transfection promoter. *Biomacromolecules* **2007**, *8*, 1498–1504. [CrossRef] [PubMed]
16. Ferruti, P.; Mauro, N.; Falciola, L.; Pifferi, V.; Bartoli, C.; Gazzarri, M.; Chiellini, F.; Ranucci, E. Amphoteric, prevailingly cationic L-arginine polymers of poly(amidoamino acid) structure: Synthesis, acid/base properties and preliminary cytocompatibility and cell-permeating characterizations. *Macromol. Biosci.* **2014**, *14*, 390–400. [CrossRef] [PubMed]
17. Ranucci, E.; Spagnoli, G.; Latini, R.; Bernasconi, R.; Ferruti, P. On the suitability of urethane bonds between the carrier and the drug moiety in poly(ethyleneglycol)-based oligomeric prodrugs. *J. Biomater. Sci. Polym. Ed.* **1994**, *6*, 133–139. [CrossRef] [PubMed]
18. Donghi, D.; Maggioni, D.; D'Alfonso, G.; Amigoni, F.; Ranucci, E.; Ferruti, P.; Manfredi, A.; Fenili, F.; Bisazza, A.; Cavalli, R. Tricarbonyl-rhenium complexes of a thiol-functionalized amphoteric poly(amidoamine). *Biomacromolecules* **2009**, *10*, 3273–3282. [CrossRef] [PubMed]
19. Ferruti, P.; Ranucci, E.; Trotta, F.; Gianasi, E.; Evagorou, E.G.; Wasil, M.; Wilson, G.; Duncan, R. Synthesis, characterisation and antitumour activity of platinum(II) complexes of novel functionalised poly(amido amine)s. *Macromol. Chem. Phys.* **1999**, *200*, 1644–1654. [CrossRef]
20. Urbán, P.; Estelrich, J.; Cortés, A.; Fernàndez-Busquets, X. A nanovector with complete discrimination for targeted delivery to *Plasmodium falciparum*-infected versus non-infected red blood cells in vitro. *J. Control. Release* **2011**, *151*, 202–211. [CrossRef] [PubMed]
21. Cranmer, S.L.; Magowan, C.; Liang, J.; Coppel, R.L.; Cooke, B.M. An alternative to serum for cultivation of *Plasmodium falciparum* in vitro. *Trans. R. Soc. Trop. Med. Hyg.* **1997**, *91*, 363–365. [CrossRef]
22. Lambros, C.; Vanderberg, J.P. Synchronization of *Plasmodium falciparum* erythrocytic stages in culture. *J. Parasitol.* **1979**, *65*, 418–420. [CrossRef] [PubMed]
23. Marques, J.; Vilanova, E.; Mourão, P.A.S.; Fernàndez-Busquets, X. Marine organism sulfated polysaccharides exhibiting significant antimalarial activity and inhibition of red blood cell invasion by *Plasmodium*. *Sci. Rep.* **2016**, *6*, 24368. [CrossRef] [PubMed]
24. National Research Council (US). *Guide for the Care and Use of Laboratory Animals*, 8th ed.; The National Academies Press: Washington, DC, USA, 2011; ISBN 978-0-309-15400-0.
25. Moles, E.; Urbán, P.; Jiménez-Díaz, M.B.; Viera-Morilla, S.; Angulo-Barturen, I.; Busquets, M.A.; Fernàndez-Busquets, X. Immunoliposome-mediated drug delivery to *Plasmodium*-infected and non-infected red blood cells as a dual therapeutic/prophylactic antimalarial strategy. *J. Control. Release* **2015**, *210*, 217–229. [CrossRef] [PubMed]
26. Switzer, R.C., III; Merril, C.R.; Shifrin, S. A highly sensitive silver stain for detecting proteins and peptides in polyacrylamide gels. *Anal. Biochem.* **1979**, *98*, 231–237. [CrossRef]
27. Schliwa, M.; van Blerkom, J. Structural interaction of cytoskeletal components. *J. Cell Biol.* **1981**, *90*, 222–235. [CrossRef] [PubMed]
28. Fidock, D.A.; Rosenthal, P.J.; Croft, S.L.; Brun, R.; Nwaka, S. Antimalarial drug discovery: Efficacy models for compound screening. *Nat. Rev. Drug Discov.* **2004**, *3*, 509–520. [CrossRef] [PubMed]
29. Ferruti, P.; Marchisio, M.A.; Duncan, R. Polyamidoamines: Biomedical applications. *Macromol. Rapid Commun.* **2002**, *23*, 332–355. [CrossRef]
30. Ofulla, A.O.; Orago, A.S.; Githure, J.I.; Burans, J.P.; Aleman, G.M.; Johnson, A.J.; Martin, S.K. Determination of fifty percent inhibitory concentrations (IC50) of antimalarial drugs against *Plasmodium falciparum* parasites in a serum-free medium. *Am. J. Trop. Med. Hyg.* **1994**, *51*, 214–218. [CrossRef] [PubMed]
31. Regev-Rudzki, N.; Wilson, D.; Carvalho, T.; Sisquella, X.; Coleman, B.; Rug, M.; Bursac, D.; Angrisano, F.; Gee, M.; Hill, A.; et al. Cell-cell communication between malaria-infected red blood cells via exosome-like vesicles. *Cell* **2013**, *153*, 1120–1133. [CrossRef] [PubMed]
32. Xiao, L.; Yang, C.; Patterson, P.S.; Udhayakumar, V.; Lal, A.A. Sulfated polyanions inhibit invasion of erythrocytes by plasmodial merozoites and cytoadherence of endothelial cells to parasitized erythrocytes. *Infect. Immun.* **1996**, *64*, 1373–1378. [PubMed]
33. Najer, A.; Wu, D.; Bieri, A.; Brand, F.; Palivan, C.G.; Beck, H.P.; Meier, W. Nanomimics of host cell membranes block invasion and expose invasive malaria parasites. *ACS Nano* **2014**, *8*, 12560–12571. [CrossRef] [PubMed]

34. Bastos, M.F.; Albrecht, L.; Kozlowski, E.O.; Lopes, S.C.P.; Blanco, Y.C.; Carlos, B.C.; Castiñeiras, C.; Vicente, C.P.; Werneck, C.C.; Wunderlich, G.; et al. Fucosylated chondroitin sulfate inhibits *Plasmodium falciparum* cytoadhesion and merozoite invasion. *Antimicrob. Agents Chemother.* **2014**, *58*, 1862–1871. [CrossRef] [PubMed]
35. Kulane, A.; Ekre, H.P.; Perlmann, P.; Rombo, L.; Wahlgren, M.; Wahlin, B. Effect of different fractions of heparin on *Plasmodium falciparum* merozoite invasion of red blood cells in vitro. *Am. J. Trop. Med. Hyg.* **1992**, *46*, 589–594. [CrossRef] [PubMed]
36. Boyle, M.J.; Richards, J.S.; Gilson, P.R.; Chai, W.; Beeson, J.G. Interactions with heparin-like molecules during erythrocyte invasion by *Plasmodium falciparum* merozoites. *Blood* **2010**, *115*, 4559–4568. [CrossRef] [PubMed]
37. Saibil, H. Chaperone machines for protein folding, unfolding and disaggregation. *Nat. Rev. Mol. Cell Biol.* **2013**, *14*, 630–642. [CrossRef] [PubMed]
38. Lyon, J.A.; Thomas, A.W.; Hall, T.; Chulay, J.D. Specificities of antibodies that inhibit merozoite dispersal from malaria-infected erythrocytes. *Mol. Biochem. Parasitol.* **1989**, *36*, 77–85. [CrossRef]
39. Pasvol, G. Receptors on red cells for *Plasmodium falciparum* and their interaction with merozoites. *Philos. Trans. R. Soc. Lond. B Biol. Sci.* **1984**, *307*, 189. [CrossRef] [PubMed]
40. Kirk, K. Membrane transport in the malaria-infected erythrocyte. *Physiol. Rev.* **2001**, *81*, 495–537. [CrossRef] [PubMed]
41. Goodyer, I.D.; Pouvelle, B.; Schneider, T.G.; Trelka, D.P.; Taraschi, T.F. Characterization of macromolecular transport pathways in malaria-infected erythrocytes. *Mol. Biochem. Parasitol.* **1997**, *87*, 13–28. [CrossRef]
42. Marques, J.; Moles, E.; Urbán, P.; Prohens, R.; Busquets, M.A.; Sevrin, C.; Grandfils, C.; Fernàndez-Busquets, X. Application of heparin as a dual agent with antimalarial and liposome targeting activities towards *Plasmodium*-infected red blood cells. *Nanomed. Nanotechnol. Biol. Med.* **2014**, *10*, 1719–1728. [CrossRef] [PubMed]
43. Marques, J.; Valle-Delgado, J.J.; Urbán, P.; Baró, E.; Prohens, R.; Mayor, A.; Cisteró, P.; Delves, M.; Sinden, R.E.; Grandfils, C.; et al. Adaptation of targeted nanocarriers to changing requirements in antimalarial drug delivery. *Nanomed. Nanotechnol. Biol. Med.* **2017**, *13*, 515–525. [CrossRef] [PubMed]
44. Gulati, N.M.; Stewart, P.L.; Steinmetz, N.F. Bioinspired shielding strategies for nanoparticle drug delivery applications. *Mol. Pharm.* **2018**, *15*, 2900–2909. [CrossRef] [PubMed]
45. Paaijmans, K.; Fernàndez-Busquets, X. Antimalarial drug delivery to the mosquito: An option worth exploring? *Future Microbiol.* **2014**, *9*, 579–582. [CrossRef] [PubMed]

Article 2: Supplementary information

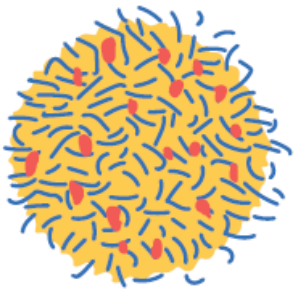

pharmaceutics

MDPI

Supplementary Materials: Polyamidoamine Nanoparticles for the Oral Administration of Antimalarial Drugs

Elisabet Martí Coma-Cros, Arnau Biosca, Joana Marques, Laura Carol, Patricia Urbán, Diana Berenguer, Maria Cristina Riera, Michael Delves, Robert E. Sinden, Juan José Valle-Delgado, Lefteris Spanos, Inga Siden-Kiamos, Paula Pérez, Krijn Paaijmans, Matthias Rottmann, Amedea Manfredi, Paolo Ferruti, Elisabetta Ranucci and Xavier Fernàndez-Busquets

Supplementary Methods

1. Reagents

4-Aminobutylguanidine sulfate (97%), lithium hydroxide monohydrate (99%), 2-methylpiperazine (98%), *N,N'*-methylenebisacrylamide (96%), cystamine hydrochloride (96%), 2-mercaptoethanol (99%) and calcium chloride (97%) were purchased from Sigma-Aldrich and used as received. 2,2-bis(acrylamido)acetic acid (94%) was synthesized as previously described [1].

2. Instruments

^{1}H and ^{13}C NMR spectra were run on a Bruker Advance 400 spectrometer operating at 400.132 (^{1}H) and 100.623 (^{13}C) MHz. Size exclusion chromatography traces were obtained with a Knauer Pump 1000 equipped with a Knauer Autosampler 3800, TSKgel G4000 PW and G3000 PW TosoHaas columns connected in series, Light Scattering Viscotek 270 Dual Detector, UV detector Waters model 486, operating at 230 nm, and a refractive index detector Waters model 2410. The mobile phase was Tris-HCl buffer, pH 8.0 (0.05 M with 0.2 M sodium chloride). The flow rate was 1 mL/min and sample concentration 1% *w*/*v*.

3. Synthesis of PAAs

3.1. ISA1

Bis(acryloyl)piperazine (1.00 g, 5.15 mmol), *N,N'*-bis(hydroxyethyl)ethylenediamine (0.27 g, 2.575 mmol) and 2-methylpiperazine (0.395 g, 2.575 mmol) were dissolved in distilled water (2.0 mL) under nitrogen atmosphere and the reaction mixture was maintained at room temperature for 80 h. After this time, the product was isolated by diluting with water (3 mL), acidifying with a few drops of 12 M hydrochloric acid down to pH 4 and finally ultrafiltering through a membrane with a nominal molecular weight cutoff of 5000 Da. The retained portion was recovered by freeze-drying. Yield: 0.95 g.

1H NMR (D_2O): d = 1.08 (d, C**H**$_3$-CH); 2.46 (m, C**H**); 2.53 (m, C**H**$_2$-CON); 2.7 (m, C**H**$_2$-CH$_2$-CON); 3.50-3.55 (C**H**$_2$-NCO); 3.61 (C**H**$_2$-O); 3.63-3.65 (*t*-amine C**H**$_2$-N).

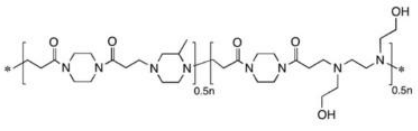

ISA1

3.2. ISA23

2,2-bis(acrylamido acetic) acid (1.00 g, 5.03 mmol) and lithium hydroxide monohydrate (0.21 g, 5.03 mmol) were dissolved in distilled water (2.0 mL) under nitrogen atmosphere, and piperazine

(0.433 g, 5.03 mmol) was then added to the obtained solution. The reaction mixture was maintained under nitrogen atmosphere at room temperature, and occasionally stirred, for 72 h. After this time, the product was isolated as described for ISA1. Yield: 1.01 g.

NMR spectral data as in [2].

ISA23 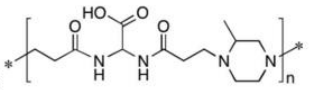

3.3. AGMA1

2,2-bis(acrylamido acetic) acid (1.00 g, 5.03 mmol) and lithium hydroxide monohydrate (0.21 g, 5.03 mmol) were dissolved in distilled water (2.5 mL) under nitrogen atmosphere. Agmatine sulfate (1.18 g, 5.03 mmol) and lithium hydroxide monohydrate (0.21 g, 5.03 mmol) were then added to this solution. The reaction mixture was maintained under nitrogen atmosphere at room temperature, and occasionally stirred, for 72 h. After this time, the product was isolated as described for ISA1. Yield: 1.5 g.

NMR spectral data as in [3].

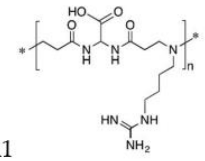

AGMA1

3.4. ARGO7

N,N'-methylenebisacrylamide (1.00 g, 6.22 mmol) was dispersed in water (4 mL), and L-arginine (1.095 g, 6.225 mmol) and calcium chloride were added under vigorous stirring under nitrogen atmosphere. The reaction mixture was then heated to 50 °C under stirring for 2 days. It gradually became homogeneous and was kept under nitrogen atmosphere for a further 3 weeks. The terminal double bonds in the resultant product, if any, were saturated by adding morpholine (54.48 mg, 0.622 mmol) and incubating at room temperature for a further 2 h. After this time, the product was isolated as described for ISA1. Yield: 1.00 g.

NMR spectral data as in [4].

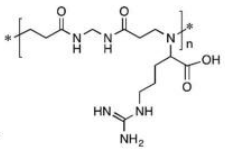

ARGO7

4. Incorporation of thiol units into PAAs

4.1. ARGO7-SH

L-Arginine (6.190 g, 35 mmol) and calcium chloride (0.401 g, 3.5 mmol) were added to a suspension of *N,N'*-methylenebisacrylamide (8.030 g, 50 mmol) in water (18 mL) under vigorous stirring. The reaction mixture was then heated to 50 °C until dissolution and kept under nitrogen atmosphere with gentle stirring for 1 day. After this time, the reaction mixture was cooled down to room temperature and cystamine dihydrochloride (1.759 g, 7.5 mmol) and lithium hydroxide monohydrate (0.636 g, 15 mmol) were added. The reaction mixture was kept at room temperature for 3 months and then water (40 mL) and excess mercaptoethanol (8.0 mL) were added to the hydrogel formed. Dissolution occurred after 6 days, when the solution obtained was diluted with water (100 mL), acidified to pH 4.5 with 37% hydrochloric acid and finally ultrafiltered through a membrane

with nominal molecular weight cutoff of 3000 Da. The product was recovered in 55% yield by freeze-drying the retained fraction. $\bar{M}n$ = 6700, PDI = 1.48.

^{1}H NMR (D_2O): δ (ppm) = 1.58–1.95 (br, CHC$\underline{H}_2$C$\underline{H}_2$); 2.65-2.80 (m, NHCOC$\underline{H}_2$); 2.90-2.92 (m, C$\underline{H}_2$S); 3.17-3.30 (m, CH$_2$C$\underline{H}_2$NH); 3.35-3.53 (m, NCOCH$_2$C$\underline{H}_2$N and NC$\underline{H}_2$CH$_2$S); 3.70-3.76 (m, NC$\underline{H}$COOH); 4.54-4.56 (br s,NHC$\underline{H}_2$NH).

^{13}C NMR (D_2O): δ (ppm) = 19.1 (C$\underline{H}_2$S); 24.4 (CHCH$_2$C$\underline{H}_2$); 25.5 (CHC$\underline{H}_2$CH$_2$); 30.5 (NHCOC$\underline{H}_2$); 40.8 (CH$_2$C$\underline{H}_2$NH); 44.3 (NHCH$_2$NH); 44.7 (NCH$_2$C$\underline{H}_2$); 55.2 (NC$\underline{H}_2$CH$_2$S); 66.6 (C$\underline{H}$COOH); 156.8 (H$_2$NC=NH); 172.8 (NHCO); 174.1 (COOH).

AGMA1-SH and ISA23-SH were prepared as reported for ARGO7-SH, by performing the reactions at room temperature for 14 days and using the reagent amounts indicated below.

4.2. AGMA1-SH

4-aminobutylguanidine (agmatine) sulfate (3.244 g, 14.0 mmol); 2,2-bis(acrylamido)acetic acid (4.210 g, 20.0 mmol); lithium hydroxide monohydrate (1.695 g, 40.0 mmol); cystamine dihydrochloride (0.704 g, 3.0 mmol); water (18 mL). Yield 68%, $\bar{M}n$ = 8400, PDI = 1.25.

^{1}H NMR (D_2O): δ (ppm) = 1.52-1.60 (br, NCH$_2$CH$_2$C$\underline{H}_2$); 1.71-1.77 (br, NCH$_2$C$\underline{H}_2$); 2.64-2.76 (br, NHCOC$\underline{H}_2$); 2.92-2.94 (m, C$\underline{H}_2$S); 3.08-3.20 (m, NCOCH$_2$C$\underline{H}_2$N); 3.34-3.47 (br, NC$\underline{H}_2$CH$_2$CH$_2$ and NC$\underline{H}_2$CH$_2$S); 5.51-5.56 (s, C$\underline{H}$COOH).

^{13}C NMR (D_2O): δ (ppm) = 18.5 (C$\underline{H}_2$S); 22.3 (NCH$_2$CH$_2$C$\underline{H}_2$); 25.0 (NCH$_2$C$\underline{H}_2$); 29.0 (NHCOC$\underline{H}_2$); 40.4 (CH$_2$C$\underline{H}_2$NH); 49.1 (NC$\underline{H}_2$CH$_2$CONH); 52.5 (NC$\underline{H}_2$CH$_2$CH$_2$CH$_2$NH); 54.8 (NC$\underline{H}_2$CH$_2$S); 56.0 (C$\underline{H}$COOH); 155.1 (H$_2$NC=NH); 171.3 (NHCO); 173.5 (COOH).

4.3. ISA23-SH

2-methylpiperazine (1.431 g, 14.0 mmol); 2,2-bis(acrylamido)acetic acid (4.210 g, 20.0 mmol), lithium hydroxide monohydrate (1.102 g, 26.0 mmol); cystamine dihydrochloride (0.704 g, 3.0 mmol); water (7.5 mL). Yield 66%, $\bar{M}n$ = 9200, PDI = 1.73.

^{1}H NMR (D_2O): δ (ppm) = 1.28 (d, CH$_3$); 2.55-2.65 (m, NHCOC$\underline{H}_2$); 2.80-2.90 (m, C$\underline{H}_2$S); 2.97-3.10 (m, NCOCH$_2$C$\underline{H}_2$N); 3.20-3.61 (br, NC$\underline{H}_2$C$\underline{H}_2$N, NC$\underline{H}_2$C$\underline{H}$N and NC$\underline{H}_2$CH$_2$S); 5.48 (s, C$\underline{H}$COOH).

^{13}C NMR (D_2O): δ (ppm) = 14.0 (C$\underline{H}_3$); 20.0 (C$\underline{H}_2$SH); 30.6 (CO$\underline{C}$H$_2$CH$_2$N); 48.8 (N$\underline{C}$H$_2$CH$_2$N); 49.6 (NCH$_2$C$\underline{H}_2$N); 52.4 (NCOCH$_2$C$\underline{H}_2$N); 55.4 (N$\underline{C}$H$_2$CHN); 56.1 (N$\underline{C}$H$_2$CH$_2$S); 56.2 (NCH$_2$C$\underline{H}$N); 58.3 (C$\underline{H}$COOH); 171.9 (NHC=O); 173.1 (COOH).

5. In vitro analysis of PAA targeting to mosquito stages of Plasmodium

5.1. Plasmodium falciparum gametocyte culture and targeting assay

Gametocytes of the *P. falciparum* NF54 strain were obtained from continuously maintained cultures of asexual blood stage parasites, setting up flasks at 1% parasitaemia and 3% hematocrit. Gametocytes began to form in significant numbers in blood culture following daily medium change. All operations were performed on a warming plate set to 37/38 °C in order to minimize heat loss to cultures during the time they were out of the incubator. Smears and an exflagellation test were performed on culture days 4, 7, 10, and 14. For the exflagellation test, a few µL of the culture were spun down and, after discarding the supernatant, the pellet was taken up in 5 µL of ookinete medium and added to a disposable counting slide; after 20 min incubation at room temperature the slide was observed under the microscope with the 40× objective. For targeting assays, 10 mL of a *P. falciparum* stage V gametocyte culture was centrifuged (37 °C, 5 min, 500 g), and the culture pellet was taken up in 3 mL of incomplete RPMI medium and added (1:1 *v/v*) to a heparin solution in the same buffer. Samples were incubated in the presence of 0.25 mg/mL PAA-FITC for 90 min at 37 °C, and the cultures were subsequently spun down and washed 3 times with incomplete RPMI medium. Smears were fixed with 4% paraformaldehyde, stained with DAPI, and examined by fluorescence confocal microscopy.

5.2. Plasmodium berghei ookinete culture and targeting assay

Ookinete culture medium consisted of 16.4 g/L RPMI supplemented with 2% *w/v* $NaHCO_3$, 0.05% *w/v* hypoxanthine, 100 μM xanthurenic acid, 50 U/mL penicillin, 50 μg/mL streptomycin (Invitrogen), 25 mM HEPES, pH 7.4. Complete medium was prepared just before use by supplementing with heat-inactivated fetal bovine serum (FBS, Invitrogen) to a final concentration of 20%. Six days prior to performing the targeting assay, a mouse was treated intraperitoneally with 10 μg/mL phenylhydrazine (PHZ) to induce reticulocytosis. Three days after PHZ treatment the mouse was inoculated by intraperitoneal injection of 200 μL of blood containing ca. 5×10^7 *P. berghei* mCherry (a kind gift from Dr. D. Vlachou) pBRCs extracted by cardiac puncture from a donor mouse that had been infected intraperitoneally 3 days before with 200 μL of a cryopreserved *P. berghei* suspension just thawed. Three days later, 1 mL of infected blood was collected by cardiac puncture onto 30 mL ookinete medium, and incubated for 24 h at 19-21 °C with 70-80% relative humidity. For ookinete targeting assays, 100 μL of 0.25 mg/mL PAA-FITC were added to 100 μL of culture and incubated in the dark for 90 min under orbital stirring (300 rpm). The samples were centrifuged for 1.5 min at 800 g and washed 3× with PBS. Fixed cell slides were prepared by adding 0.5 μL FBS to 0.5 μL pellet and by fixing the smear with 4% paraformaldehyde for 15 min. After performing 3 washing steps with PBS, slides were mounted with Vectashield® DAPI-containing media (Vector Laboratories, UK). All work involving laboratory animals was performed in accordance with the EU regulations 'EU Directive 86/609/EEC' and within the regulations of the United Kingdom Animals (Scientific Procedures) Act 1986.

5.3. P. berghei oocyst culture and targeting assay

After performing direct *Anopheles stephensi* feeding on malaria-infected mice as decribed above, for oocyst targeting assay mosquitoes were dissected for midguts on day 10 post-feeding. After anesthetizing the mosquitoes with CO_2 and keeping them on ice, they were added to ~300 μL incomplete RPMI medium and the midguts were removed under a dissecting microscope and carefully collected onto a 24-well plate containing 500 μL incomplete RPMI medium (5 midguts/well). The guts were transferred to a well containing PAA-FITC dissolved in incomplete RPMI medium at 0.25 mg/mL, and incubated for 90 min at room temperature with gentle stirring. Samples were then washed 2 times with PBS, and fixed with 4% paraformaldehyde for 15 min. After fixation, 2 washing steps with PBS were performed, and the slides were finally prepared by transferring the midguts to a slide containing a few μL of Vectashield antifade mounting medium containing DAPI.

5.4. P. berghei sporozoite culture and targeting assay

Six days prior to feeding female *A. stephensi* mosquitoes, a mouse was treated intraperitoneally with PHZ as described above, and three days after treatment the mouse was infected by intraperitoneal injection with *P. berghei* mCherry pBRCs (a kind gift from Dr. D. Vlachou). The selected female mosquitoes were not fed with sugar in the 24 h preceding the blood feed but were kept hydrated with water. On the day of the feed, the parasitemia and gametocytemia of the mouse were recorded, and an exflagellation test was also performed. Subsequently the mouse was anesthetized and placed on the netting of the mosquito cage. The feed was maintained for 30 min at 19-21 °C in the dark. After feeding, as there was a pool of sticky blood on the bottom of the cage, the pot was laid on its side overnight at 19-21 °C with 70-80% humidity. On day 1 post-feeding, the mosquitoes were anesthetized with CO_2 and kept on ice while the unfed ones were removed. Mosquitoes were then fed with 5% glucose/0.05% 4-aminobenzoic acid every 2 days and maintained for 21 days at 19-21 °C and 70-80% humidity.

For sporozoite targeting assays, mosquitoes were dissected for salivary glands on day 21 post-feeding. Glands were sliced from the head and transferred to an eppendorf tube containing 50 μL of incomplete RPMI medium. After centrifugation for 10 min at 2350 g, the pellet was taken up in 100 μL of 0.2 mg PAA-FITC/mL incomplete RPMI and incubated for 90 min at 37 °C with gentle stirring. Samples were finally centrifuged for 5 min at 2350 g and washed 3 times with incomplete RPMI. When the last wash was completed, the pellet was taken up in Hoechst 33342 solution (0.05 μg/mL)

and a 5-min centrifugation step at 2350 g was performed. The pellet was finally taken up in incomplete RPMI and the slides containing live cells were prepared for confocal microscopy analyses.

Supplementary Figures

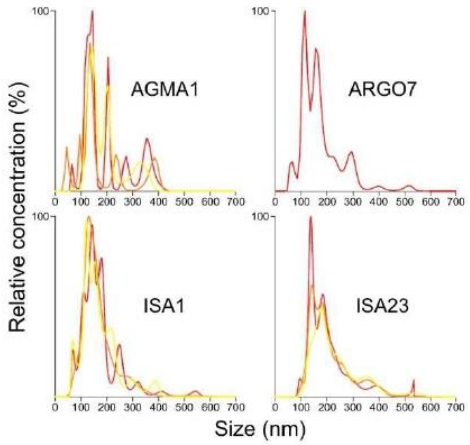

Figure S1. Nanoparticle tracking analysis of PAAs.

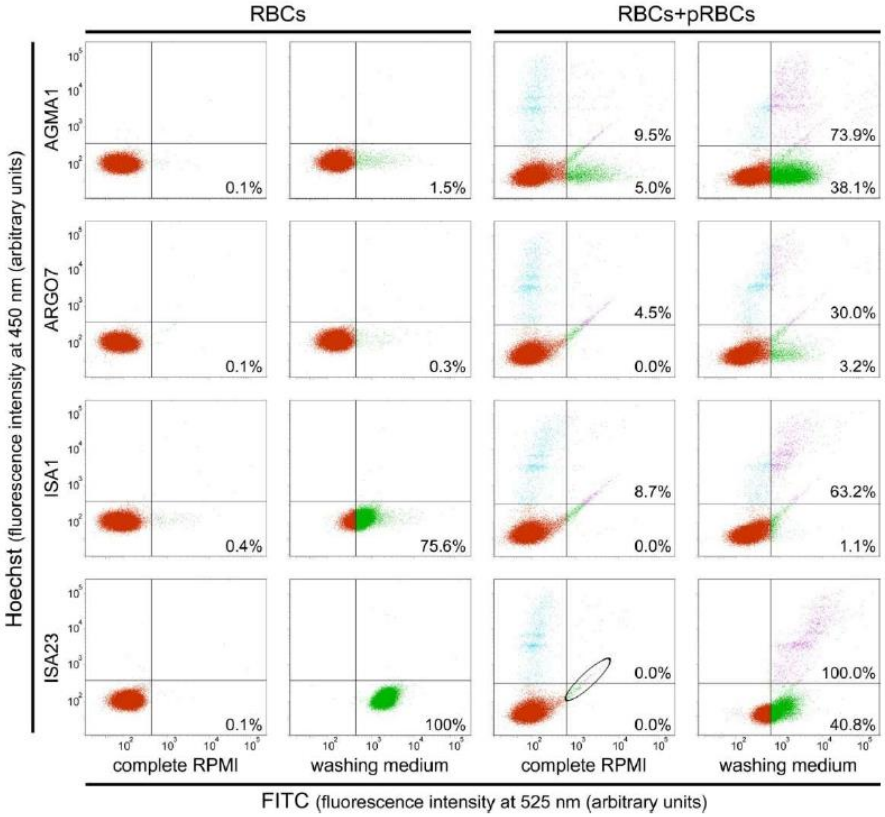

Figure S2. Flow cytometry analysis of the interaction of PAAs-FITC with RBCs and pRBCs in complete and incomplete RPMI (washing medium). The upper areas correspond to pRBCs (Hoechst fluorescence) and the right-hand areas correspond to PAA-bound cells (FITC fluorescence). Percentage values indicate the fraction of PAA-bound pRBCs (upper right areas) and RBCs (lower right areas). Unspecific fluorescence events (encircled for information only in the ISA23/RBCs+pRBCs/complete RPMI sample) were removed from the counting.

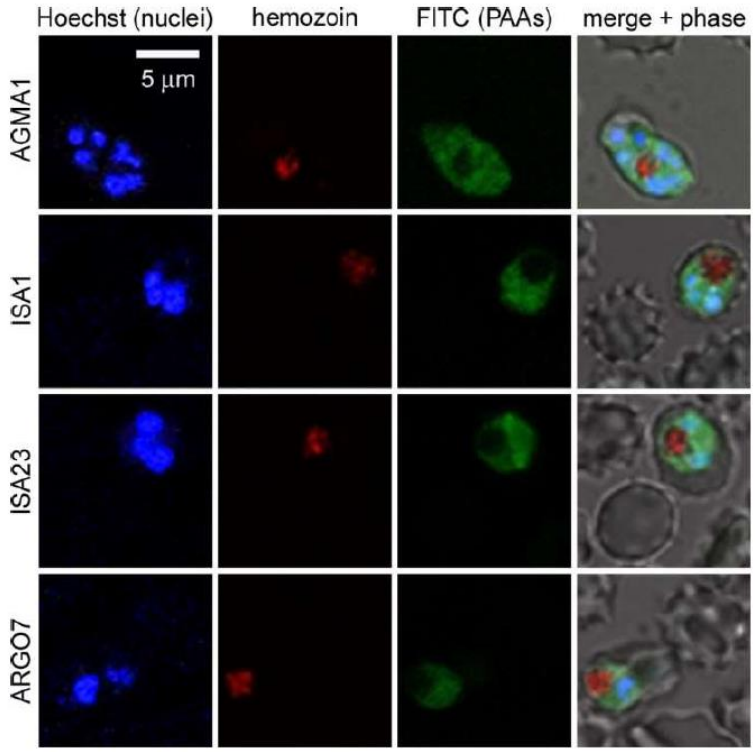

Figure S3. Confocal fluorescence microscopy targeting study of PAAs to *P. falciparum*-containing pRBCs. FITC-labeled polymers were added to living *P. falciparum* cultures of the 3D7 strain in incomplete RPMI and after 90 min of incubation the samples were processed for confocal fluorescence microscopy detection of fluorescein (PAAs), Hoechst (pRBCs), and the reflection of hemozoin crystals in pRBCs.

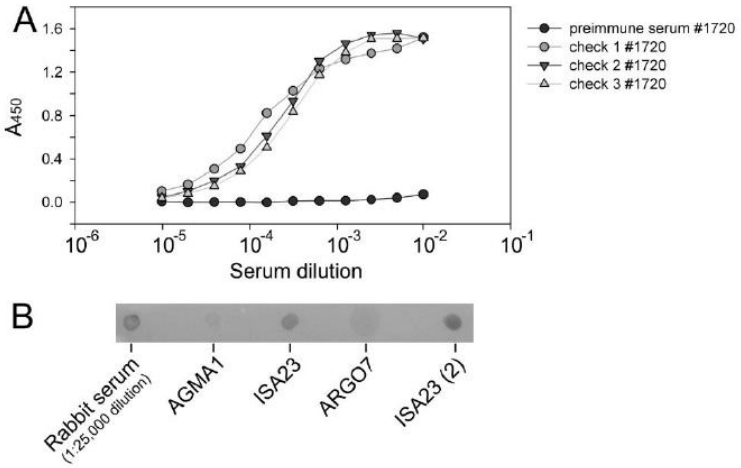

Figure S4. Generation of rabbit polyclonal antibodies against ISA23. (A) Titer determination at days 52, 73, and 93 after the initial immunization (check 1, 2 and 3, respectively). (B) Dot-blot assay to test the specificity of ISA23 antiserum. ISA23 and ISA23 (2) correspond to two different batches synthesized separately.

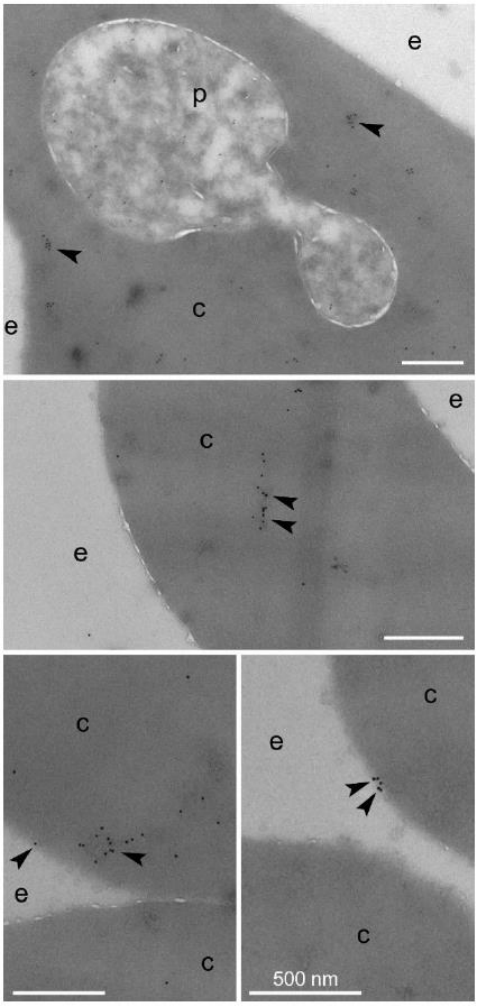

Figure S5. ImmunoTEM analysis of the subcellular localization of ISA23 in *P. falciparum* ring stages. Living pRBCs were treated overnight with ISA23, washed, and processed for immunoTEM. e, extracellular area; c, pRBC cytosol; p, *Plasmodium*. Size bars represent 500 nm.

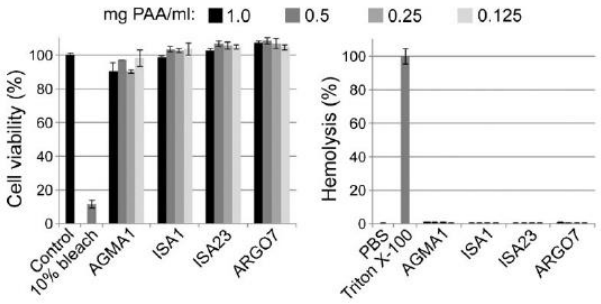

Figure S6. PAA cytotoxicity and hemolysis assays.

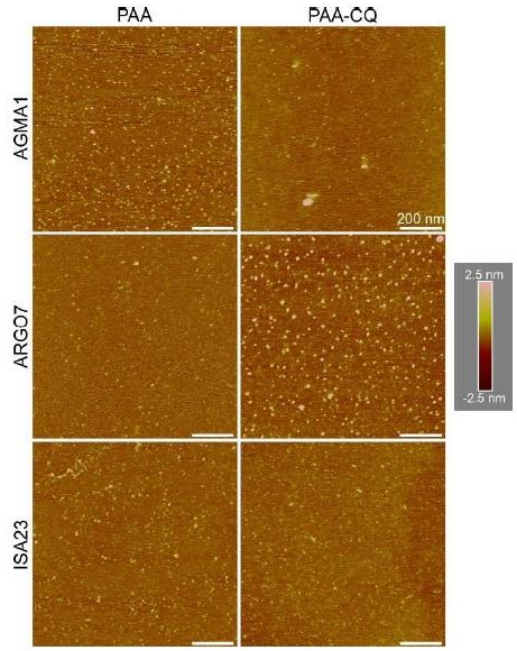

Figure S7. AFM images on mica of PAAs and of PAA-CQ complexes.

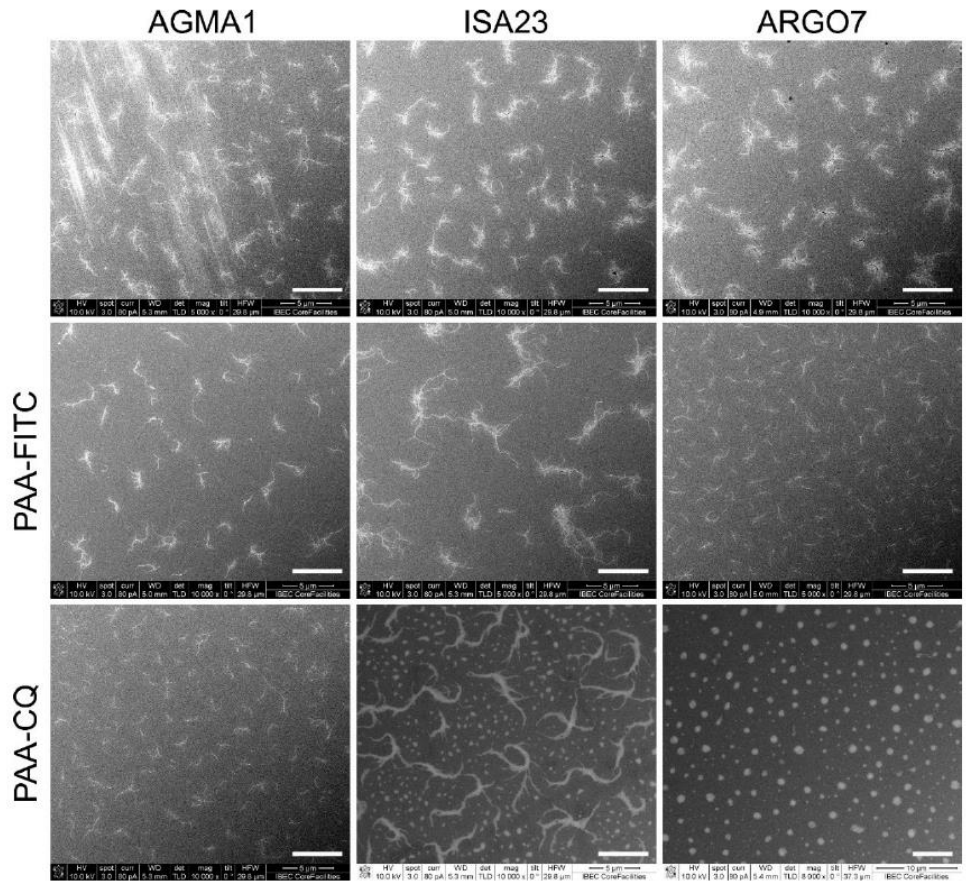

Figure S8. SEM analysis of PAAs, before (upper panels) and after the introduction of FITC groups (PAA-FITC) and the incorporation of CQ (PAA-CQ). The scale bar corresponds to 5 μm.

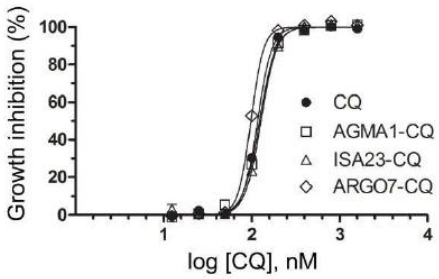

Figure S9. Growth inhibition assay of the effect on *in vitro P. falciparum* cultures of PAA-encapsulated CQ.

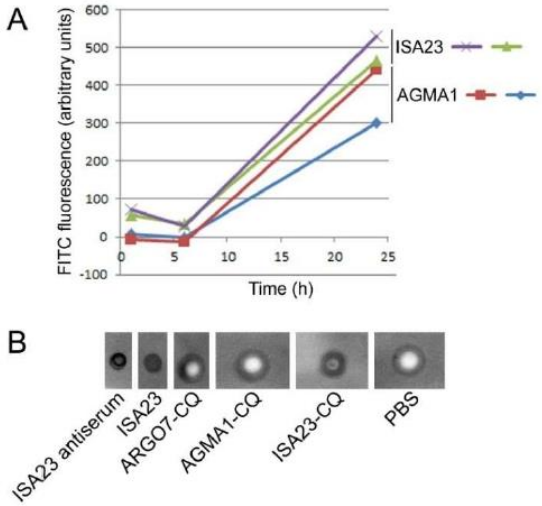

Figure S10. Detection in blood of orally administered PAAs. (A) Detection of FITC fluorescence in the plasma of mice orally-fed PAA-FITC. (B) Dot-blot assay of plasma samples obtained from mice orally-fed PAAs; for detection was used ISA23 antiserum, 3 μL of which directly spotted at a 1:25,000 dilution is shown as a control. ISA23 (3 μL of a 3 mg/mL solution) and PBS are also included as positive and negative controls, respectively.

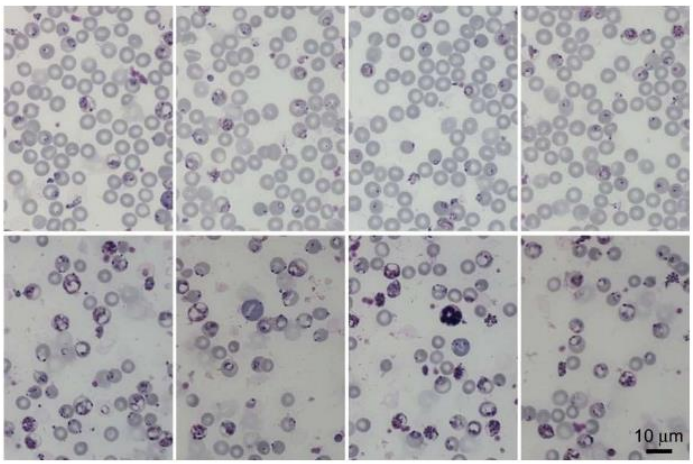

Figure S11. Microscopic images of blood smears prepared on days 3 and 5 post-infection (upper and lower row, respectively) from control *P. yoelii*-infected naïve mice left untreated.

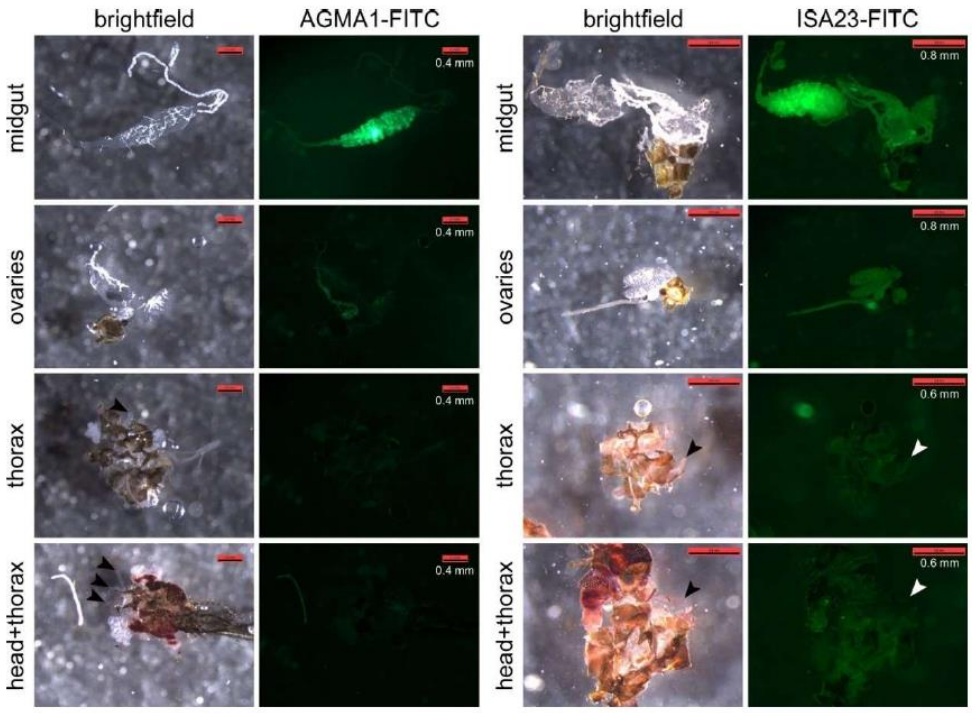

Figure S12. Direct delivery of PAAs to *Anopheles gambiae*. Fluorescein-labeled AGMA1 or ISA23 were diluted in the sugar meal provided to the mosquitoes during three or five days before proceeding to dissection and observation by fluorescence microscopy. The arrowheads indicate salivary glands.

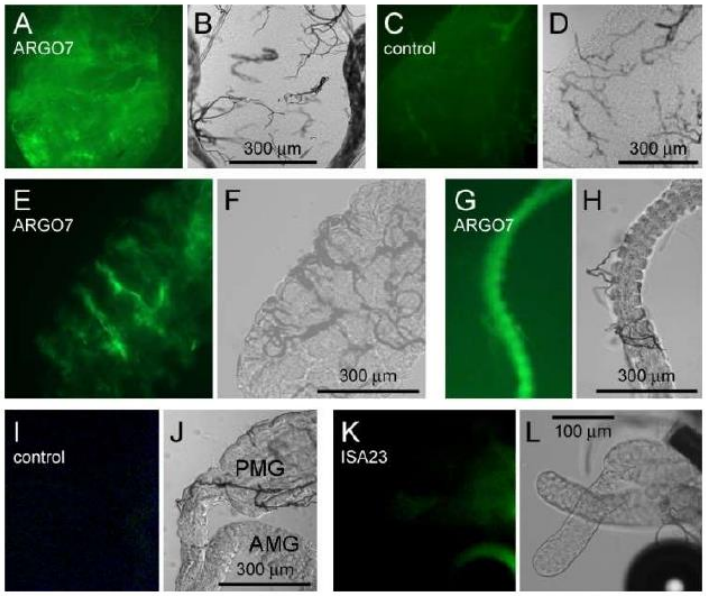

Figure S13. Direct delivery of PAAs to *Anopheles gambiae*. Fluorescein-labeled PAAs were diluted in the sugar meal provided to the mosquitoes during three or five days before proceeding to dissection and observation by fluorescence microscopy. (A) Posterior midgut from mosquito fed with ARGO7-FITC for three days. (C) Posterior midgut from control mosquitoes fed only with sugar. (E,G) Midguts (E, posterior midgut; G, anterior midgut) dissected from mosquitoes fed with ARGO7-FITC for five days. (I) Midgut from control mosquitoes fed only with sugar. Anterior midgut (AMG) and posterior midgut (PMG) are indicated. (K) Salivary glands dissected from mosquitoes fed with ISA23-FITC. Panels B, D, F, H, J and L are brightfield images of each fluorescence image immediate to the left.

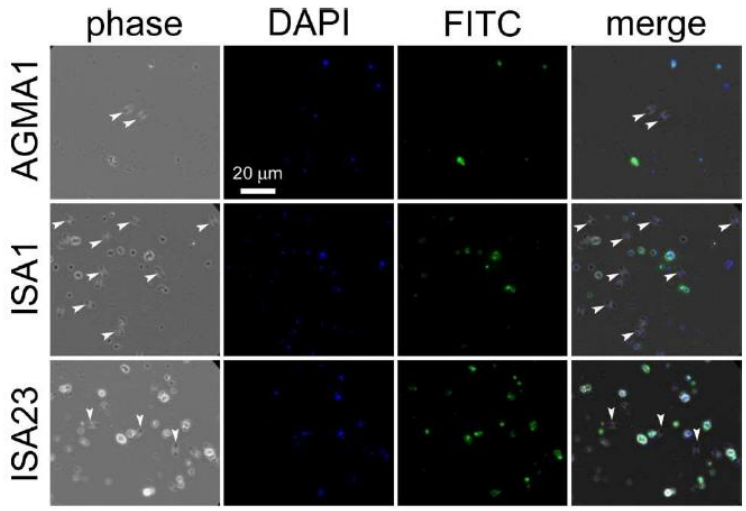

Figure S14. Targeting assay of PAA-FITC to *P. falciparum* gametocytes. Some gametocytes are indicated with arrowheads.

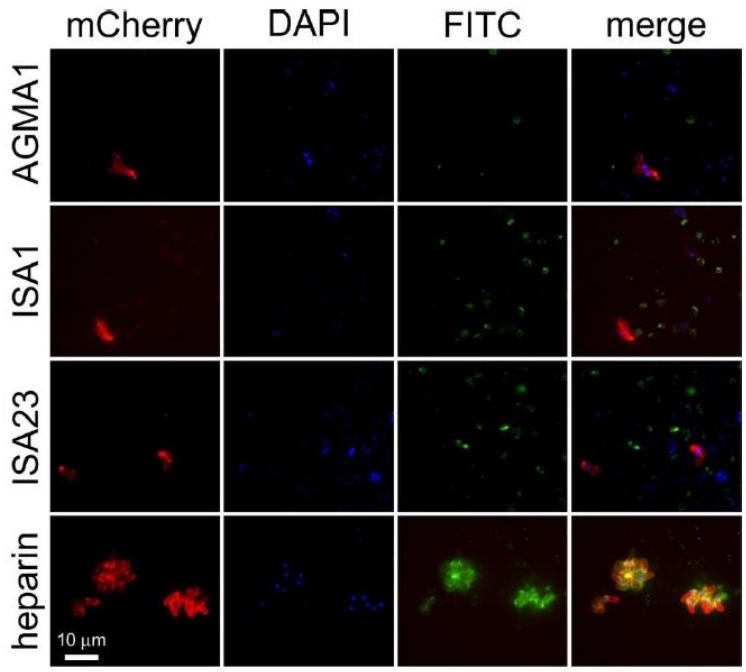

Figure S15. Targeting assay of PAA-FITC to *P. berghei* ookinetes expressing the mCherry marker. Heparin-FITC targeting is shown as a positive control [5].

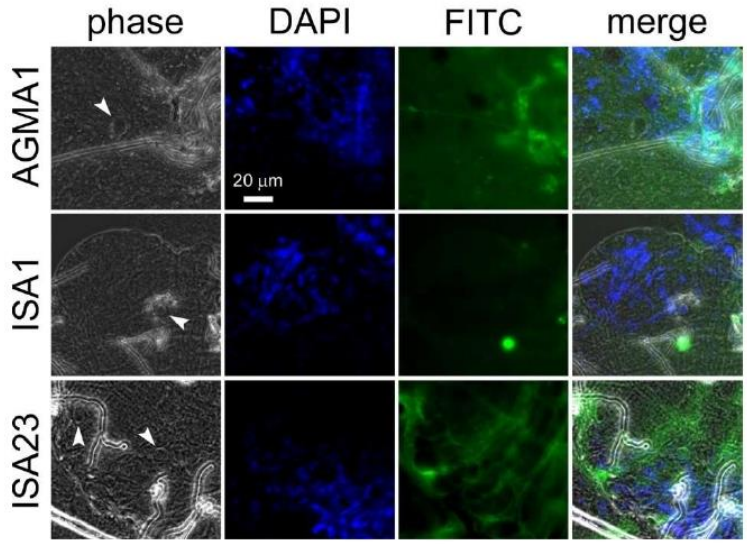

Figure S16. Targeting assay of PAA-FITC to *P. berghei* oocysts (indicated with arrowheads).

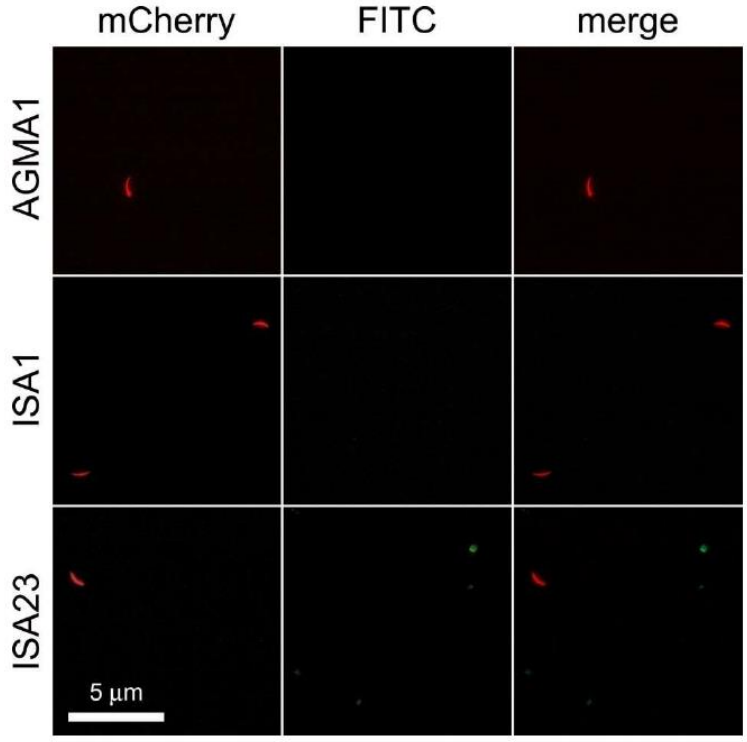

Figure S17. Targeting assay of PAA-FITC to *P. berghei* sporozoites expressing the mCherry marker.

Table S1. Proteins from the *P. falciparum* 3D7 strain identified in affinity chromatography columns and binding more than one PAA. Proteins potentially involved in extracellular interactions are highlighted in yellow and those involved in protein folding are shadowed in grey.

UniProtKB	Subcellular location	Molecular function	Biological process
37 common proteins to all 4 PAAs			
14-3-3 protein [C0H4V6_PLAF7]	cytoplasm / nucleus	histone binding	-
Adenosine deaminase [Q8IJA9_PLAF7]	cytosol	adenosine deaminase activity	adenosine catabolic process, hypoxanthine salvage, inosine biosynthetic process, purine ribonucleoside monophosphate biosynthetic process, response to drug
Adenosylhomocysteinase [SAHH_PLAF7]	cytosol	adenosylhomocysteinase activity / NAD binding	one-carbon metabolic process, S-adenosylhomocysteine catalytic process, S-adenosylmethionine cycle
Conserved *Plasmodium* protein [O96127_PLAF7]	-	-	-
DNA/RNA-binding protein Alba 4 [Q8IDM3_PLAF7]	cytoplasm / nucleus	DNA binding / RNA binding	-
Elongation factor 1-alpha [Q8I0P6_PLAF7]	intracellular (plasma membrane)	GTPase activity / GTP binding / translation elongation factor activity	translational elongation
Elongation factor 1-gamma, putative [Q8IDV0_PLAF7]	cytoplasm / nucleus	glutathione transferase activity / translation elongation factor	glutathione metabolic process, translational elongation
Elongation factor 2 [Q8IKW5_PLAF7]	-	GTPase activity / GTP binding / translation elongation factor activity	-
Enolase [ENO_PLAF7]	cytoplasm	magnesium ion binding / phosphopyruvate hydratase activity	activation of immune response / autophagosome assembly / glycolytic process / transcription

Eukaryotic initiation factor 4A [Q8IKF0_PLAF7]	cytoplasm / nucleus	3-5 DNA/RNA helicase activity, ATPase activity, ATP binding	regulation of gene expression, regulation of translational initiation, RNA secondary structure unwinding, translational initiation.
Fructose-bisphosphate aldolase [ALF_PLAF7]	cytoplasm	actin binding, fructose-bisphosphate aldolase activity	actin polymerization or depolymerization / glycolytic process
Glyceraldehyde-3-phosphate dehydrogenase [Q8IKK7_PLAF7]	cytosol / membrane	glyceraldehyde-3-phosphate dehydrogenase / NAD and NADP binding	gluconeogenesis / glycolytic process
Glycophorin-binding protein [GBP_PLAF7]	host cell cytoplasm	-	involved in erythrocyte invasion
Heat shock protein 110 [Q8IC01_PLAF7]	cytoplasm	ATP binding	-
Heat shock protein 70 [Q8IB24_PLAF7]	cytoplasm / nucleus	ATP binding / heat shock protein binding	-
Heat shock protein 70 [K7NTP5_PLAF7]	-	ATP binding	-
Heat shock protein 90 [Q8IC05_PLAF7]	-	ATPase activity / ATP binding / unfolded protein binding	protein folding / response to stress
Hypoxanthine phosphoribosyltransferase [Q8IJS1_PLAF7]	cytoplasm	guanine phosphoribosyltransferase activity / hypoxanthine phosphoribosyltransferase activity / metal ion binding / nucleotide binding	IMP salvage / purine ribonucleoside salvage
Inositol-3-phosphate synthase [Q8I3Y8_PLAF7]	cytoplasm	inositol-3-phosphate synthase activity	inositol biosynthetic process / phospholipid biosynthetic process

Karyopherin beta [Q8I3M5_PLAF7]	cytoplasm / nuclear membrane / nuclear periphery / nuclear pore / nuclear pore central transport channel	nuclear localization sequence binding / protein domain specific binding / protein heterodimerization activity / protein transport activity	NLS-bearing protein import into nucleus / nucleocytoplasmic transport / protein import into nucleus, translocation / ribosomal protein import into nucleus
L-lactate dehydrogenase [Q76NM3_PLAF7]	-	L-lactate dehydrogenase activity	glycolytic process
M17 leucyl aminopeptidase [Q8IL11_PLAF7]	cytosol	aminopeptidase activity / identical protein binding / manganese ion binding / metalloexopeptidase activity	-
M1-family alanyl aminopeptidase [Q8IEK1_PLAF7]	cytoplasm / food vacuole / integral component of membrane / microneme / nucleus	aminopeptidase activity / metalloaminopeptidase activity / peptide binding / zinc ion binding	peptide catabolic process / proteolysis
Ornithine aminotransferase [OAT_PLAF7]	cytoplasm	identical protein binding / ornithine-oxo-acid transaminase activity / pyridoxal phosphate binding	L-proline biosynthetic process / ornithine metabolic process
Phosphoethanolamine N-methyltransferase [Q8IDQ9_PLAF7]	Golgi apparatus	phosphoethanolamine N-methyltransferase activity	phosphatidylcholine biosynthetic process
Phosphoglycerate kinase [PGK_PLAF7]	-	ATP binding / phosphoglycerate kinase activity	glycolytic process
Phosphoglycerate mutase [Q8IIG6_PLAF7]	cytosol	2,3-bisphosphoglycerate-dependent phosphoglycerate mutase activity / phosphoglycerate mutase activity	gluconeogenesis / glycolytic process / regulation of pentose-phosphate shunt
Phosphotransferase [C6KT76_PLAF7]	cytosol	ATP binding / fructokinase activity / glucokinase activity / glucose binding / hexokinase activity / mannokinase activity	cellular glucose homeostasis / glycolytic process

Probable ATP-dependent 6-phosphofructokinase [Q8I2Z8_PLAF7]	cytoplasm	6-phosphofructokinase activity / ATP binding / diphosphate-fructose-6-phosphate 1-phosphotransferase activity / metal ion binding	fructose 6-phosphate metabolic process
Proteasome subunit alpha type [Q8IBI3_PLAF7]	cytoplasm / nucleus	endopeptidase activity / threonine-type endopeptidase activity	proteasome-mediated ubiquitin-dependent protein catabolic process / ubiquitin-dependent protein catabolic process
Pyruvate kinase [C6KTA4_PLAF7]	cytoplasm	kinase activity / magnesium ion binding / potassium ion binding / pyruvate kinase activity	protein homotetramerization
Receptor for activated kinase C [Q8IBA0_PLAF7]	cytosol	kinase activity / protein kinase C binding	-
S-adenosylmethionine synthase [Q7K6A4_PLAF7]	cytosol	ATP binding / metal ion binding / methionine adenosyltransferase activity / protein homodimerization activity	one-carbon metabolic process / S-adenosylmethionine biosynthetic process
Serine-repeat antigen protein [SERA_PLAF7]	parasitophorous vacuole (extracellular space / lysosomes / symbiont-containing vacuole)	cysteine-type endopeptidase activity / cysteine-type peptidase activity	immunoglobulin production / proteolysis / proteolysis involved in cellular protein catabolic process / regulation of immune response
STI1-like protein [STI1L_PLAF7]	cytosol	-	-
T-complex protein 1 subunit alpha [Q8II43_PLAF7]	cytoplasm	ATP binding / protein binding involved in protein folding / unfolded protein binding	de novo protein folding / chaperone-mediated protein folding / protein folding

Thioredoxin peroxidase 1 [Q8IL80_PLAF7]	cytosol	antioxidant activity / protein dimerization activity / thioredoxin peroxidase activity	cell redox / DNA protection / response to heat / response to oxidative stress
30 common proteins to AGMA1, ISA1 and ARGO7			
Actin-1 [ACT1_PLAF7]	cytoskeleton	ATP binding / structural constituent of cytoskeleton	actin polymerization-dependent cell motility involved in migration of symbiont in host / cytoskeleton organization
ATP-dependent RNA helicase [Q9TY94_PLAF7]	cytoplasm / nucleolus / nucleus / spliceosomal complex	ATP binding / ATP-dependent RNA helicase activity / RNA binding	cellular response to DNA damage stimulus / mRNA export from nucleus / mRNA splicing, via spliceosomes / regulation gene expression / RNA secondary structure unwinding
Cell division cycle protein 48 homologue, putative [C6KT34_PLAF7]	-	ATP binding / hydrolase activity	cell division
EMP1-trafficking protein [Q8IBF2_PLAF7]	transmembrane (integral component of membrane)	-	-
Erythrocyte membrane protein 3 [O96124_PLAF7]	transmembrane (cytoplasm integral component of membrane/ Maurer's cleft/ symbiont-containing vacuole)	-	-
Falcilysin [Q76NL8_PLAF7]	apicoplast / food vacuole	metal ion binding / metalloendopeptidase activity	hemoglobin catabolic process
Glutathione reductase [GSHR_PLAF7]	cytoplasm (apicoplast/ cytoplasm)	electron transfer activity / flavin adenine dinucleotide binding / glutathione-disulfide reductase activity / thioredoxin-disulfide reductase activity	cell redox homeostasis / response to oxidative stress / response to oxygen radical

Glycerophosphodiester phosphodiesterase, putative [Q8IM31_PLAF7]	cytosol / food vacuole / symbiont-containing vacuole	glycerophosphodiester phosphodiesterase activity	lipid metabolic process
GTP-binding nuclear protein [Q7KQK6_PLAF7]	nucleus	GTPase activity / GTP binding	intracellular protein transport / protein import into nucleus / regulation of cell cycle / ribosomal subunit export from nucleus / RNA export from nucleus
Haloacid dehalogenase-like hydrolase [Q8IJ74_PLAF7]	cytoplasm	metal ion binding / sugar-phosphatase activity	dephosphorylation / negative regulation of isopentenyl diphosphate biosynthetic process, methylerythritol 4-phosphate pathway
Haloacid dehalogenase-like hydrolase, putative [Q8I5F4_PLAF7]	-	hydrolase activity	-
Heat shock protein 70 [Q8I2X4_PLAF7]	endoplasmic reticulum	ATP binding	-
Mature parasite-infected erythrocyte surface antigen [Q8I492_PLAF7]	host cell plasma membrane	-	-
Obg-like ATPase 1 [Q8IBM9_PLAF7]	cytoplasm	ATPase activity / ATP binding / GTP binding / ribosomal large subunit binding / ribosome binding	signal transduction
Peptidase, putative [Q8IKT5_PLAF7]	cytosol / food vacuole	metal ion binding / metalloaminopeptidase activity / protein homodimerization activity	hemoglobin catabolic process / proteolysis
Probable inorganic pyrophosphatase [IPYR_PLAF7]	cytoplasm	inorganic diphosphatase activity / magnesium ion binding	phosphate-containing compound metabolic process

Protein DJ-1 [C6KTB1_PLAF7]	cytosol	hydroxyethylthiazole kinase activity / peptidase activity	protein folding / thiamine biosynthetic process
Pyridoxal 5'-phosphate synthase subunit Pdx1 [PDX1_PLAF7]	cytoplasm / cytosol	catalytic activity / glutaminase activity / identical protein binding / pyridoxal 5'-phosphate synthase	pyridoxal phosphate biosynthetic process / pyridoxine biosynthetic process / response to singlet oxygen / vitamin B6 biosynthetic process
Ring-exported protein 1 [Q8I2G1_PLAF7]	transmembrane (cytoplasm/ host cell membrane/ integral component of membrane/ Maurer's cleft)	-	-
S-antigen protein [SANT_PLAF7]	parasitophorous vacuole (symbiont-containing vacuole)	-	-
Serine repeat antigen 3 [O96165_PLAF7]	extracellular space / lysosome	cysteine-type endopeptidase activity / cysteine-type peptidase activity	immunoglobulin production / proteolysis / proteolysis involved in cellular protein catabolic process / regulation of immune response
Serine repeat antigen 4 [O96164_PLAF7]	extracellular space / lysosome / symbiont-containing vacuole	cysteine-type endopeptidase activity / cysteine-type peptidase activity	immunoglobulin production / proteolysis / proteolysis involved in cellular protein catabolic process / regulation of immune response
Serine repeat antigen 7 [O96163_PLAF7]	extracellular space / lysosome	cysteine-type endopeptidase activity / cysteine-type peptidase activity	immunoglobulin production / proteolysis / proteolysis involved in cellular protein catabolic process / regulation of immune response
Serine repeat antigen 9 [Q8I3C0_PLAF7]	extracellular space / lysosome	cysteine-type endopeptidase activity	immunoglobulin production / proteolysis involved in cellular protein catabolic process / regulation of immune response

Surface protein P113 [Q8ILP3_PLAF7]	transmembrane (integral component of membrane/ symbiont-containing vacuole membrane)	-	-
T-complex protein 1 subunit beta [O97247_PLAF7]	cytoplasm	protein binding involved in protein folding / unfolded protein binding	-
T-complex protein 1 subunit delta [C0H5I7_PLAF7]	cytoplasm	ATP biding / protein binding involved in protein folding / unfolded protein binding	de novo protein folding / chaperone-mediated protein folding / protein folding
T-complex protein 1 subunit eta [TCPH_PLAF7]	cytoplasm	ATP biding / protein binding involved in protein folding / unfolded protein binding	de novo protein folding / chaperone-mediated protein folding / protein folding
T-complex protein 1 subunit gamma [Q8I5C4_PLAF7]	cytoplasm	ATP biding / protein binding involved in protein folding / unfolded protein binding	de novo protein folding / chaperone-mediated protein folding / protein folding
Tubulin beta chain [TBB_PLAF7]	cytoskeleton (microtube)	GTPase activity / GTP binding / structural constituent of cytoskeleton	microtubule cytoskeleton organization / response to drug
2 common proteins to AGMA1, ISA23 and ARGO7			
High molecular weight rhoptry protein 2 [C0H571_PLAF7]	rhoptry	-	-
Polyadenylate-binding protein [Q8I5H4_PLAF7]	cytoplasm	mRNA binding / poly (A) binding	RNA processing
2 common proteins to AGMA1, ISA1 and ISA23			
Methionine-tRNA ligase [Q8IJ60_PLAF7]	cytoplasm	ATP binding / methionine tRNA ligase activity	methionyl-tRNA aminoacylation
T-complex protein 1 subunit epsilon [O97282_PLAF7]	cytoplasm	ATP binding / protein binding involved in protein folding / unfolded protein binding	de novo protein folding / chaperone-mediated protein folding / protein folding

1 common protein to ISA1, ISA23 and ARGO7			
Triosephosphate isomerase [TPIS_PLAF7]	cytosol	triose-phosphate isomerase activity	fatty acid biosynthetic process / gluconeogenesis / glyceraldehyde-3-phosphate biosynthetic process / glycerol catabolic process / glycolytic process / pentose-phosphate shunt
6 common proteins to AGMA1 and ISA1			
Asparagine-tRNA ligase [O96198_PLAF7]	cytoplasm	asparagine-tRNA ligase activity / ATP binding / nucleic acid binding	asparaginyl-tRNA aminoacylation
Ethanolamine kinase [Q8IIB7_PLAF7]	cytoplasm	ethanolamine kinase activity	lipid metabolic process / phosphatidylcholine biosynthetic process / phosphatidylethanolamine biosynthetic process
Proliferation-associated protein 2g4, putative [Q8ILI2_PLAF7]	-	metalloexopeptidase activity	cell cycle arrest / cell proliferation
Serine hydroxymethyltransferase [Q8I566_PLAF7]	apicoplast / cytoplasm / mitochondrion	glycine hydroxymethyltransferase activity / methyltransferase activity / pyridoxal phosphate binding	D-serine metabolic process / glycine biosynthetic process from serine / one-carbon metabolic process / tetrahydrofolate interconversion
T-complex protein 1 subunit theta [O96220_PLAF7]	cytoplasm	1-phosphatidylinositol-3-phosphate 5-kinase activity / ATP binding	phosphatidylinositol phosphorylation / protein folding / retrograde transport (endosome to Golgi)
Ubiquitin-activating enzyme E1 [Q8I5F9_PLAF7]	cytoplasm	ubiquitin activating enzyme activity	cellular response to DNA damage stimulus / ubiquitin-dependent protein catabolic process

4 common proteins to AGMA1 and ISA23			
Cytoadherence linked asexual protein 3.2 [O77309_PLAF7]	host cell plasma membrane / rhoptry	cell adhesion molecule binding	cytoadherence to microvasculature (mediated by symbiont protein)
Eukaryotic translation initiation factor 3 subunit M [Q8I1Q5_PLAF7]	cytoplasm (eukaryotic 43S preinitiation complex)	translation initiation factor activity	cytoplasmic translation initiation / formation of translation preinitiation complex / regulation of translational initiation
Importin subunit alpha [Q8IAW0_PLAF7]	cytosol / nuclear pore / nuclear pore central transport channel / nucleoplasm	nuclear import signal receptor activity / nuclear localization sequence binding / protein domain specific binding / protein heterodimerization activity / protein transport activity	NLS-bearing protein import into nucleus / nuceocytoplasmic transport
Rab GDP dissociation inhibitor [Q8I501_PLAF7]	intracellular	GTPase activator activity / Rab GDP-dissociation inhibitor activity	protein transport / small GTPase mediated signal transduction / vesicle-mediated transport
20 common proteins to AGMA1 and ARGO7			
101 kDa malaria antigen [ABRA_PLAF7]	merozoite cell surface / parasitophorous vacuole	-	-
60S acidic ribosomal protein P0 [Q8II61_PLAF7]	cytosolic large ribosomal subunits	structural constituent ribosome	ribosome biogenesis / translation
Acyl-CoA synthetase [Q8I6Z1_PLAF7]	-	AMP binding / decanoate-CoA ligase activity / long-chain fatty acid-CoA ligase activity	fatty acid metabolic process
ADP-ribosylation factor 1 [ARF1_PLAF7]	Golgi apparatus	GTP binding	protein ADP-ribosylation / protein transport / vesicle-mediated transport
Alpha/beta hydrolase, putative [Q8IK20_PLAF7]	membrane	acylglycerol lipase activity / lipase activity	lipid metabolic process

Duffy binding-like merozoite surface protein [Q8IJ52_PLAF7]	cell surface / integral component of membrane	host cell surface binding / receptor activity	entry into host cell / pathogenesis
Glutamate-tRNA ligase, putative [Q8IDK7_PLAF7]	cytoplasm	ATP binding / glutamate-tRNA ligase activity	glutamyl-tRNA aminoacylation
GTPase-activating protein, putative [Q8I3A9_PLAF7]	-	-	-
High molecular weight rhoptry protein 3 [Q8I395_PLAF7]	rhoptry	-	entry into host cell
Merozoite surface protein P41 [PF41_PLAF7]	merozoite cell surface / cell membrane	miscellaneous	miscellaneous
Nucleosome assembly protein [Q8I608_PLAF7]	cytoplasm / nucleus	histone binding	nucleosome assembly
Parasitophorous vacuolar protein 1 [Q8II72_PLAF7]	symbiont-containing vacuole	-	-
PRE-binding protein [Q8IJS7_PLAF7]	nucleus	DNA binding transcription factor activity / double-stranded DNA binding / RNA binding	regulation of transcription (DNA-templated)
Proliferating cell nuclear antigen [PCNA_PLAF7]	nucleus	DNA binding / DNA polymerase processivity factor activity	leading strand elongation / mismatch repair / regulation of DNA replication / translesion synthesis
Proteasome endopeptidase complex [C6KST3_PLAF7]	nucleus / cytoplasm / proteasome core complex	endopeptidase activity / threonine-type endopeptidase activity	ubiquitin-dependent protein catabolic process
Ribonucleotide reductase small subunit [Q8IM38_PLAF7]	-	ribonuleoside-diphosphate reductase activity	deoxyribonucleotide biosynthetic process
Serine repeat antigen 6 [Q9TY96_PLAF7]	extracellular space / lysosome / symbiont-containing vacuole	cysteine-type endopeptidase activity / cysteine-type peptidase activity	immunoglobulin production / proteolysis

T-complex protein 1 subunit zeta [C6KST5_PLAF7]	cytoplasm	ATP binding / protein binding involved in protein folding / unfolded protein binding	de novo protein folding / chaperone-mediated protein folding / protein folding
Tubulin alpha chain [Q6ZLZ9_PLAF7]	cytoskeleton	GTPase activity / GTP binding / structural constituent of cytoskeleton	microtubule-based process
V-type proton ATPase subunit B [Q6ZMA8_PLAF7]	cell / proton-transporting V-type ATPase (V1 domain)	ATP binding / proton-transporting ATPase activity	ATP hydrolysis coupled proton transport / ATP metabolic process / vacuolar acidification
1 common protein to ISA1 and ARGO7			
1-Cys peroxiredoxin [Q8IAM2_PLAF7]	cytosol	antioxidant activity / peroxidase activity / peroxiredoxin activity	cell redox homeostasis / response to oxidative stress
1 common protein to ISA23 and ARGO7			
Purine nucleoside phosphorylase [Q8I3X4_PLAF7]	-	purine-nucleoside phosphorylase activity	nucleoside metabolic process

Venn diagram showing the distribution of the 142 *Plasmodium* proteins binding the four PAA columns:

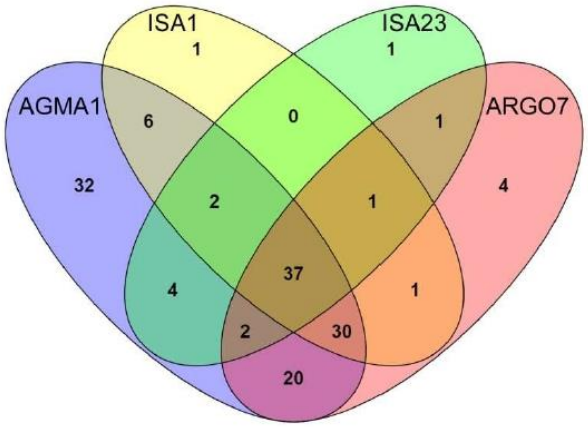

References

1. Ferruti, P.; Ranucci, E.; Trotta, F.; Gianasi, E.; Evagorou, E.G.; Wasil, M.; Wilson, G.; Duncan, R. Synthesis, characterisation and antitumour activity of platinum(II) complexes of novel functionalised poly(amido amine)s. *Macromol. Chem. Phys.* **1999**, *200* (7), 1644-1654, https://doi.org/10.1002/(SICI)1521-3935(19990701)200:7%3C1644::AID-MACP1644%3E3.0.CO;2-P.
2. Ranucci, E.; Ferruti, P.; Lattanzio, E.; Manfredi, A.; Rossi, M.; Mussini, P.R.; Chiellini, F.; Bartoli, C. Acid-base properties of poly(amidoamine)s. *J. Polym. Sci. A Polym. Chem.* **2009**, *47* (24), 6977-6991, http://dx.doi.org/10.1002/pola.23737.
3. Ferruti, P.; Franchini, J.; Bencini, M.; Ranucci, E.; Zara, G.P.; Serpe, L.; Primo, L.; Cavalli, R. Prevailingly cationic agmatine-based amphoteric polyamidoamine as a nontoxic, nonhemolytic, and "stealthlike" DNA complexing agent and transfection promoter. *Biomacromolecules* **2007**, *8* (5), 1498-1504, http://dx.doi.org/10.1021/bm061126c.
4. Ferruti, P.; Mauro, N.; Falciola, L.; Pifferi, V.; Bartoli, C.; Gazzarri, M.; Chiellini, F.; Ranucci, E. Amphoteric, prevailingly cationic L-arginine polymers of poly(amidoamino acid) structure: synthesis, acid/base properties and preliminary cytocompatibility and cell-permeating characterizations. *Macromol. Biosci.* **2014**, *14* (3), 390-400, http://dx.doi.org/10.1002/mabi.201300387.
5. Marques, J.; Valle-Delgado, J.J.; Urbán, P.; Baró, E.; Prohens, R.; Mayor, A.; Cisteró, P.; Delves, M.; Sinden, R.E.; Grandfils, C.; de Paz, J.L.; García-Salcedo, J.A.; Fernàndez-Busquets, X. Adaptation of targeted nanocarriers to changing requirements in antimalarial drug delivery. *Nanomedicine: NBM* **2017**, *13*, 515-525, https://doi.org/10.1016/j.nano.2016.09.010.

Discussion

A. CONTRIBUTION OF POLYMER NANOCARRIERS TO MDA

From 2000 to 2015 the global trends in the burden of malaria indicated a reduction of new cases and deaths (Figure 22A) due to current malaria control efforts programmes. They aimed to control malaria and consisted in symptomatic and preventive treatment with antimalarial drugs including artemisinin-based combination therapies, as well as vector control with indoor residual spraying (IRS) and insecticide-treated bed nets (ITNs) (Figure 22B) (World Health Organisation, 2018). Among these three interventions, ITN was the most effective in reducing the *P. falciparum* parasite rate (PfPR) which is a commonly reported index of malaria transmission intensity (Smith *et al.*, 2007). Nonetheless, from 2015 to 2017 the previous progress in reducing the PfPR had come to a standstill leading to calls for novel ways to prevent the transmission of malaria parasites, especially using tools able to target residual transmission which can be integrated with current interventions, such as targeted malaria elimination eradication that includes mass drug administration (MDA) (von Seidlein *et al.*, 2019).

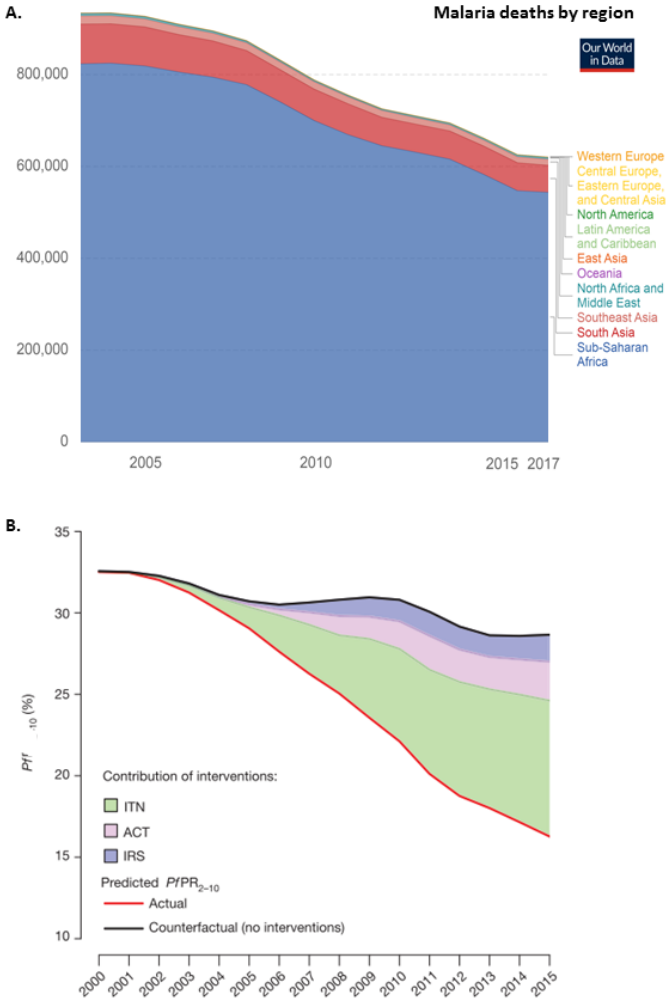

Figure 22. (A) Malaria deaths by region from 2000 to 2017. Figure adapted from Our World in Data (Roser and Ritchie, 2017). **(B) Contribution of intervention** from 2000 to 2015 in Africa. The red line shows the actual prediction and the black line is a 'counterfactual' prediction in a scenario without coverage by ITNs, ACTs or IRS. The coloured regions indicate the relative contribution of each intervention in reducing the PfPR (Bhatt *et al.*, 2015).

In 2015 the WHO recommended the use of MDA as part of a multifaceted approach to accelerate the global eradication of malaria in areas with good access to treatment, effective implementation of vector control and surveillance, and minimal risk of re-introduction of infection (WHO Global Malaria Programme, 2015). The objectives behind these new recommendations were to reduce the transmission of malaria and achieve a rapid reduction of morbidity and mortality (World Health Organization, 2017b), by targeting all the population in a certain area, both asymptomatic and chronic patients. These patients are semi-immune subjects suffering from a long-term malaria infection. MDA can be a key issue in eradication since in these two types of patients parasitemia is lower than the detection threshold, and gametocyte production continues, thereby perpetuating transmission (Nicholas J White, 2008).

MDA has been used in the past, albeit without outstanding results and with a perceived risk of drug resistance related to suboptimal timing, insufficient number of MDA rounds and subtherapeutic doses, which could be overcome with adequate MDA implementation. Nevertheless, the implementation of the MDA timeframe is not straightforward, and in the different settings requires high coverage (> 80 %) in the targeted community and a defined low endemicity area. Likewise, MDA should be carried out in combination with other interventions, with the participation, understanding and acceptance of the community, and the monitoring of the development of possible resistance to the administered drugs (Hetzel and Genton, 2018; Kaehler *et al.*, 2018; Zuber and Takala-Harrison, 2018). While the optimal mode of MDA implementation remains to be determined, it has been demonstrated that it can temporarily reduce the prevalence of parasites in certain areas (Newby *et al.*, 2015).

One of the most relevant factors contributing to MDA failure is non-adherence to dosing regimens. In order to counteract this, oral treatment should be the first choice of administration since it is directly related to patient compliance (Yamanaka and Leong, 2008), the risk of infection is very low, it is reliable, easy to use, it is generally less expensive than intravenous treatment and is not invasive, and is, thus, painless (Ensign, Cone and Hanes, 2012). However, neither is this administration route ideal. As mentioned before, to maintain the therapeutic range for an extended period of time after oral administration, conventional dosages have limitations (Dilnawaz, 2017), in that they require the use of drug delivery systems (DDSs) such as dendrimers and PAAs, which can serve as nanocarriers for oral antimalarial treatment.

Orally administered encapsulated drugs should be > 20 nm and < 100 nm in size to avoid filtration by the kidney and specific sequestration by sinusoids in the spleen and fenestra of the liver, being nanoparticles between 50 to 100 nm the ones displaying the lowest blood clearance rates (Alexis *et al.*, 2008). This can be more easily accomplished with dendrimers than with PAA, since dedrimeric polymers can be highly controlled during synthesis, obtaining monodisperse particles of a chosen size range (Liu and Fréchet, 1999), excluding polydispersity, and therefore, different particles size behaviour, as was observed in the past with some PAAs, where it was detected that the lager the polymer average weight the higher parasite growth inhibition (Urbán, Ranucci and Fernàndez-Busquets, 2015).

In article 1 the HDLDBC nanocarriers encapsulating CQ had a size of around 11 to 17 nm and the DHP nanocarriers were around 12 to 20 nm, and both were, consequently, likely filtered by the kidney (Venturoli and Rippe, 2005). Since HDLDBC and DHP did not show unspecific toxicity and haemolysis *in vitro* up to 0.15 mg/mL or *in vivo* up to 120 mg/mL for HDLDBC and 37.5 mg/mL for DHP, it would be key to synthesise new dendrimers with sizes larger than 50 nm, since this might improve their pharmacokinetics and *in vivo* performance. Moreover, *in vivo* oral administration of these encapsulations must be tested in order to compare the activity of the encapsulated drugs with the free drug. Conversely, we observed dendrimers incorporated by both erythrocytes and endothelial cells; however, HDLDBC and DHP behaved differently, and their different localisations within endothelial cells should be taken into account for two reasons. First for pharmacokinetic studies, both dendrimers are incorporated in endothelial cells, HUVEC cells, which could significantly affect the overall polymer concentrations in blood. Second, dendrimers could be used to encapsulate drugs to treat other intracellular parasites which infect endothelial cells like *Trypanosoma cruzi* .

On the other hand, linear polymers showed no toxicity *in vivo* after oral administration even though the encapsulations did not improve the free drug. Actually, PAAs dissolved in simulated fasted-state gastric fluid was slowly degraded up to 19 h exhibiting a regular distribution of hydrolysis products corresponding to multiples of the mass of the main building block (Figure 14). Another demonstration of the slow degradation of PAAs was the detection of PAA-FITC in the blood stream 24 h post administration, despite the rapid GI transit time and gastric emptying. Therefore, PAAs could be good carriers with a sufficiently large size to slowly degrade to non-toxic products in the GIT by releasing the drug gradually like a depot (a formulation that allows slow release and gradual absorption) (Cabral-Miranda *et al.*, 2017). PAAs could, for example, be used to encapsulate ivermectin, a promising vector control strategy administered orally to humans with a plasma half-life of 18 hours (González Canga *et al.*, 2008). Hence, ivermectin PAAs encapsulations could increase ivermectin half-life after oral administration by gradually releasing the drug over a longer period of time, therefore reducing the number of repeated doses necessary for MDA.

Furthermore, both carriers have the capacity to encapsulate more than one drug at the same time. This approach goes in line with new antimalarial formulation methods contemplating, the use of combinations of two or more drugs in a single medicinal dosage. These new formulations could provide innovative medicinal products, improve therapeutic outcomes and enhance patient compliance (Balducci *et al.*, 2016).

Conversely, as mentioned earlier it is more cost effective to improve classical drugs than to discover new ones. Therefore, nanocarrier strategy search can follow two approaches depending on whether it targets *Plasmodium* infected red blood cells (pRBCs) passively or actively (Basore *et al.*, 2015). In passive targeting there is a natural selection and accumulation of certain carriers in the targeted cell or tissue depending on the inner physicochemical, pharmacological and/or pathophysiological properties of the nanocarrier. With this targeting, uptake by macrophages is extremely common due to their phagocytic properties, whereas RBCs are phagocytically and endocytically inactive (Goodyer *et al.*, 1997; Santos-Magalhães and Mosqueira, 2010; Thakkar and Brijesh, 2016). Passive targeting can

also be achieved by surface modifications of the nano-drug delivery system with the help of hydrophilic polymers such as poly(ethyleneglycol) (PEG) which delays phagocytosis, resulting in a prolonged drug half-life (Gref *et al.*, 1995). On the other hand, active targeting happens when uptake is facilitated by a specific interaction between the delivery system and the cell, through optional surface-functionalization nanocarriers with targeting molecules such as peptides and aptamers, or antibodies (Garnett, 2001). This mechanism generally avoids macrophages and can deliver high drug concentrations to pRBCs, and is therefore considered a valuable strategy to avoid the development of drug resistance (Thakkar and Brijesh, 2016). Two examples of targeted nanocarriers are liposomes engineered with antibodies (known as immunoliposomes) or with heparin. Immunoliposomes with a monoclonal antibody against the erythrocyte surface protein glycophorin A target infected and non-infected RBCs (Moles *et al.*, 2015). Heparin-functionalized liposomes specifically target pRBCs with comparable specificity as but at a significantly lower cost than immunoliposomes (Marques *et al.*, 2014).

Hence, to discover nanocarrier that reaches the parasite through passive targeting, the best choice is to perform cell targeting high throughput screening (HTS) analysed by cytometry, combined with haemolysis assays to discard NPs toxic for red blood cells. This strategy allows the analysis of the natural selection and accumulation inside pRBCs of a huge amount of samples. Equally, a more in depth understanding of the natural entering process is required to find molecules which actively enter pRBCs. Thus, experiments using targeted transport inhibitors and channel blockers will contribute to understanding how solutes and other molecules are uptaken. This deeper understanding will contribute to identifying new targeting molecules to add on the surface of the nanocarrier or the polymer in order to allow their entry into a specific cell type. Moreover, since chloroquine (CQ) has already shown to be a very efficient drug it would be interesting to work with CQ-resistant strains once the nanocarriers are chosen and loaded with antimalarial drugs.

B. SOCIOECONOMIC FACTORS AS TREATMENT LIMITATIONS

Treatment failure is a great concern not only for MDA but also in the eradication of malaria, since non-treated uncomplicated malaria perpetuates transmission and can evolve to severe malaria and death within 24 - 48h (World Health Organization, 2015a). Biomedical approaches have greatly contributed to the reduction of the disease; however, the persistence of treatment failure requires acknowledgement of other factors, beyond parasitological and pharmacological perspectives, that also interfere with the treatment process. Indeed, there is an erroneous assumption that failure mainly depends on drug resistance, whereas this factor only accounts for 10 % of treatment failures (Huijben and Paaijmans, 2018). From a positive point of view, the research community is slowly starting to recognise these non-biomedical factors. Nonetheless, extensive research addressed to analyse the socioeconomic factors related to treatment failure, which are key drivers of health disparities between and within countries, are necessary to understand and reverse this situation (Anyanwu *et al.*, 2017), and draw relevant conclusions about their individual implications (Bruxvoort *et al.*, 2014).

Treatment failure is a broad and complex process, where prominent factors are involved for instance availability of funds for meaningful research and existence of patents. Nevertheless, many causal factors can also interfere, and these can be classified into two different groups depending on whether they intervene during the process of accessing the treatment or during the treatment *per se* (Figure 23). A reliable understanding of these causal factors, the role they play in determining human behaviour and how they interact with one another is essential to contribute to eradicate malaria.

Pre-treatment phase

The main pre-treatment factors are universal access to prevention (ITNs), diagnosis (RDT) and treatment (first or second line treatment). In addition, economic factors such as drug price or household income, as well as patient background including education or beliefs can also affect patient outcomes (Figure 23). Interestingly, in 2015, Amponsah and colleagues reported that around 28 % of the patients interviewed claimed to be cured by prayer rather than by the medicine taken (Amponsah, Vosper and Marfo, 2015), hence this should be known, understood and revert in elimination programmes.

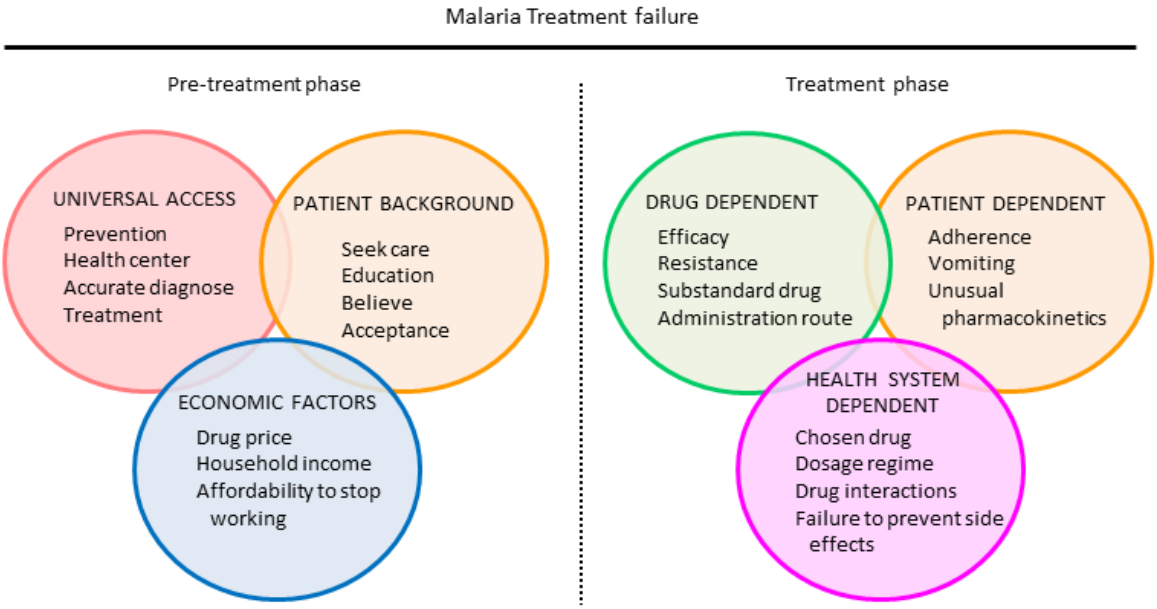

Figure 23. Malaria treatment failure. Some of the factors related to failure are divided into two groups: pre-treatment and during treatment (MacE *et al.*, 2011; Bruxvoort *et al.*, 2014; Amponsah, Vosper and Marfo, 2015; Aspinall, 2015; World Health Organization, 2015a).

Treatment phase

Once the patient accesses the health system, other factors interfere, such as the choice of an adequate drug by the physician, its dose and frequency of administration, and the recommended treatment duration. Sub-optimal treatment is one of the major and most widespread causes of failure and can be related to the evolution of resistance, severe malaria and death. Possible solutions for an

inadequate adherence are clear guidelines, education of health workers and the community, fixed dose combinations (now being used for the majority of ACTs), shorter regimes, and paediatric friendly pills (Aspinall, 2015; World Health Organization,2015a). The oral route of administration should be chosen whenever possible in order to reduce treatment failure since it is patient-friendly, painless, easy to self-administer, cheaper than the parental route (Yamanaka and Leong, 2008), and often does not require maintaining the cold chain which is a significant aspect to take into account in malaria endemic countries. In fact, the cold chain is also mandatory for vaccines (Healer *et al.*, 2017).

Likewise, drug price has an impact on patient adherence and delays seeking for treatment in repetitive malarial infections, however it is hard to capture the true burden of disease as data systems are often of poor quality and reporting is frequently incomplete. Moreover, it can be very challenging to determine the cost of malaria treatment for children and adults from heterogeneous sources, inputs, methods, studies and times. However, overall the annual per capita cost of malaria control to the health system during the period 2006 to 2015, ranged from $ 0.11 to $ 39.06 (median: $ 2.21), whereas for malaria elimination it ranged from $ 0.18 to $ 27.0 (median: $ 3.0) representing 6 % of a household's total expenses on health (Shretta, Avanceña and Hatefi, 2016; Shretta *et al.*, 2019). The general perception of the cost of antimalarial treatment is high, and therefore, new antimalarial drugs should not increment health systems costs. In fact, there have been different attempts, at different levels, to reduce or maintain drug prices; one example is the pre-packaging strategy which dispenses the exact amount of treatment tablets to be administered orally, avoiding left-overs (Yeboah-Antwi *et al.*, 2001). Other completely different strategies have been aimed at reducing the price at a molecular level; for example, by adapting target molecules to the malaria environment replacing monoclonal antibodies by cheaper options such as heparin, and thereby reducing the final cost of the potential treatment by about 10-fold (Marques *et al.*, 2017). In this line, we suggest the use of cheap materials such as polymers, either PAA or dendrimers, for nanocarriers production, which would put an end to the stigma of nanomedicine being expensive. Previous analyses by our group concluded that the synthesis of PAA is inexpensive (Urbán *et al.*, 2014); the cost of the synthesis of 1 g of two hybrid dendritic-linear-dendritic block copolymers was estimated to be 14 and 67 €, respectively, which adds less than 0.5 € to the *in vitro* IC_{50} of PQ and CQ. This cost could be reduced with the production of larger batches (Movellan *et al.*, 2014). Moreover, the participation of the pharmaceutical industry in collaboration with public agencies in the production of antimalarial drugs for low-income countries, would make production costs and scale ups more affordable, especially with the use of this type of materials (Urbán and Fernàndez-Busquets, 2014).

C. PAAs AS TRANSMISSION-BLOCKING NANOCARRIERS

Despite many years of research and a substantial number of available antimalarial drugs, the ideal drug treatment remains to be found and should be: (i). parasite-specific, (ii). able to reach the site of action independently of the parasite proteins transport, (iii). act quickly, (iv). be stable, v. be safe for patients, (vi). be able to be used in combination therapy, (vii). reduce the development of resistance and side effects, and finally, (viii). be easy and cheap to produce (World Health Organization, 2015a; Meier, Erler and Beitz, 2018).

Most of the current antimalarial treatments, available or under study, were designed to be parasite specific towards asexual stages with the aim of alleviating symptoms. However, lately the focal research point has moved towards targeting other parasite stages, such as the two bottlenecks present in the *Plasmodium* life cycle in which the amount of parasite is much lower than in the rest of the cycle, making them priority targets (Aly, Vaughan and Kappe, 2009). These two bottlenecks occur during transmission between hosts. The first one, which is responsible for relapses, occurs after the inoculation of the parasites in the body and during liver stages in which there are around 100 sporozoites. The second one is responsible for transmission and occurs during mosquito parasite development, with the presence of around 50 to 100 ookinetes resulting in about 5 oocysts per mosquito, which become sporozoites in the salivary glands immediately before inoculation. Yet, it is true that a few cells to be reached per individual is counterbalanced by a large mosquito population (Sinden *et al.*, 2012).

Malaria eradication will only occur by breaking the transmission of the disease, rather than curing individual patients. Nevertheless, to date, no compound, targeting mosquito stages, and thus blocking malaria transmission without killing the mosquito, has been developed. Since eradicating a species might have unpredicted consequences on the ecosystem with potential undesirable side effects (Paaijmans and Fernàndez-Busquets, 2014), the malaria agenda is willing to hear about new strategies to discover mosquito-friendly drugs to break the transmission cycle. This caused a change in malaria research and screening for mosquito targeting activity became a priority over blood-stage activity (Burrows *et al.*, 2017). Moreover even compound libraries that had previously demonstrated schizonticide activity were re-examined (Sinden, 2017). Consequently, future drugs will combine different active molecules or dual activity drugs, having complementary modes of action. These should ideally consist of fast-acting and long-lasting schizonticides, and transmission-blocking components, which should be stable and exert inhibition over several days and reduce the probability of selecting resistant mutants to any drug (Delves *et al.*, 2012).

Nevertheless, the development of new drugs based on new chemical entities would take too long to be useful in the malaria eradication agenda. The traditional drug development process takes at least 15 years taking into account basic research, drug discovery, pre-clinical, clinical trials phase I, II and III and Food and Drug Administration (FDA) or European Medicine Agency (EMA) review (Olliaro and Yuthavong, 1999). Moreover, after these years there is still the last phase, the indefinite post-marketing surveillance. Moreover, outcomes are unpredictable with only around 1 compound ever reaching the end of the process after the screening of 5000 to 10000 compounds (Matthews, Hanison and Nirmalan, 2016).

Therefore, directly attacking mosquito stages with encapsulated drugs may eventually be a more suitable strategy to fight malaria, although it is a largely unexplored avenue in antimalarial drug development. Confocal fluorescence microscopy examination of entire or dissected *Anopheles atroparvus* mosquitoes 24 h post ingestion of ISA23-FITC showed the presence of the polymer in the midgut (Figure 24 B), and also in the thorax and around the salivary glands three days' post ingestion.

Specific binding to mosquito stages of *P. berghei* was not observed; however, PAAs accumulated in the midgut where gametogenesis, zygote formation and differentiation to ookinete, occur (Figure 24 A). On the other hand, ookinete development to oocyst occurs after the ookinete crosses intracellularly the epithelial cells (Baton and Ranford-Cartwright, 2005). And ISA23 was observed to accumulate inside epithelial cells (Figure 24 C), thus, parasite development could be stoped in this stage by using ISA23 nanocarrier to deliver antimalarial drugs inside epithelial mosquito cells. Therefore, PAAs are potential nanocarriers of drugs against *Plasmodium* mosquito stages, although a deeper understanding of the interaction between parasites, PAAs and antimalarial drugs is essential. For instance, the previous results would need to be confirmed by repeating the experiments with antibodies against PAAs in order to rule out the possibility that the signal observed comes from the PAA *per se* and not from the cleaved FITC. Additional information about the specific localization of PAAs over time, their longevity, the efficacy of the nanovector reaching the targeted location, and the possible effects on the mosquito life span are essential to develop a potential antimalarial nanocarrier. More information on the encapsulated drugs is also required, including the ideal dose, drug stability, temperature-related drug release rate, antimalarial effect on mosquito stages, and IC_{50}, among others.

In addition, targeting efficacy can be improved, with surface targeting molecules which have already proved their binding to ookinetes such as heparin (Marques *et al.*, 2017). Recent studies focusing on the characterization of membrane proteins from mosquito stages are revealing a number of new potential targets such as P230 and P48/45 on the gametocyte membrane (Acquah *et al.*, 2019), and perforin-like protein 4 (PPLP4) on the ookinete surface (Deligianni *et al.*, 2018).

Targeting mosquito stages should be ecofriendly, economically viable and harmless to humans if we compare with insecticides (Rai *et al.*, 2017). For example, drugs could be delivered in attractive traps for mosquitoes, hanged on the walls of dwellings in malaria endemic areas (Paaijmans and Fernàndez-Busquets, 2014). Sugar is an essential source of energy for female mosquitoes; thus, sugar meal traps could be combined with other traps emitting human volatiles with blood-like substances and containing a mixture of encapsulated drugs. Besides, traps have a fixed volume and therefore, they can contain a highly concentrated drug against *Plasmodium* gametes, ookinetes, oocyts or sporozoites such as atovaquone or pyrimethamine (Delves *et al.*, 2012), protected and stabilized against extreme conditions thanks to the polymers.

Mosquito-specific DDSs avoid harmful effects to humans and are aimed at drug delivery directly to mosquito stages. This contributes to a reduction in both the costs of product development by simplification or bypassing preclinical assays and clinical trials, and of the bench-to-bed time of future antimalarial medicines which would obviate the frequent delay of years in the deployment of new medicines (Fernàndez-Busquets, 2016).

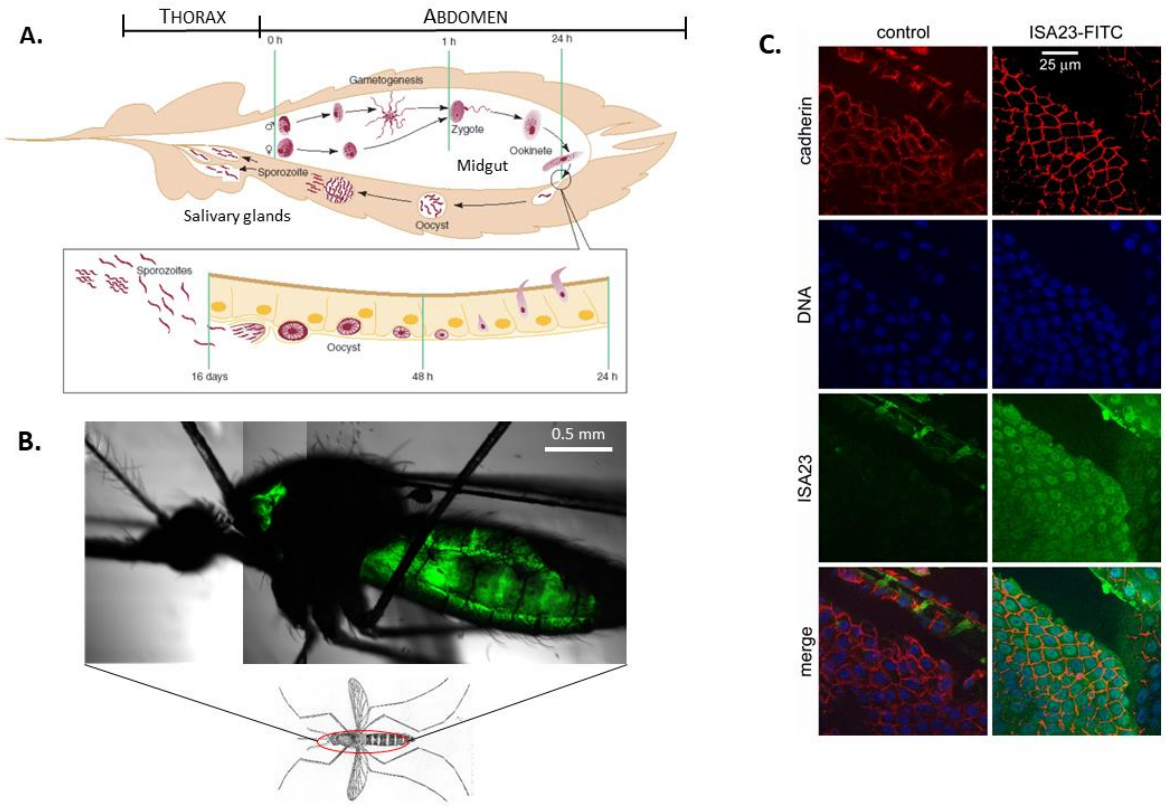

Figure 24. (A) *Plasmodium* mosquito stages. Figure adapted from (Riehle *et al.*, 2003). **(B) Confocal microscopy images of *A. atroparvus* fed with ISA23-FITC (488 nm).** Five-day-old female mosquitoes (F1 generation) were kept in the dark and allowed to feed on a sugar-water solution containing ISA23-FITC for 48 h (*unpublished data*). **(C) Confocal microscopy images of *A. gambiae* dissected midguts fed with ISA23.** Mosquitoes were allowed to feed on sugar meals containing ISA23 for seven days. Then midguts were dissected and processed for immunolabeling using an antibody against ISA23 (generated at IBEC) and a cadherin antibody to label the midgut epithelial cell membrane. DNA was stained with TO-PRO (*unpublished data*).

D. POLYMER NANOCARRIERS AGAINST OTHER INTRACELLULAR PARASITES

Intracellular parasitic diseases other than malaria, such as leishmaniasis, Chagas disease or toxoplasmosis, also linked to socio-economical and geographical factors, are a major concern in most developing countries. The parasites responsible for these diseases, *Leishmania*, *Trypanosoma cruzi* and *Toxoplasma gondii*, respectively, together with *Plasmodium*, have developed specific molecular parasite-host cell interactions to invade host cells, evade the host immune system, and undergo intracellular replication, all of which are essential processes for their survival and completion of their life cycle (Walker et al., 2014). Actually, for the life cycle to be completed, parts of the development occur inside another host different than the human host. For instance, *T. cruzi* develops inside blood-feeding triatomine insects (de Fuentes-Vicente *et al.*, 2018), whereas *T. gondii* has a range of intermediate hosts, which are generally warm-blooded animals including birds and rodents among others, in which the parasite establishes a long-life, latent infection inside the tissues of these animals (Dubey, 2016).

Plasmodium and *Toxoplasma* are apicomplexan parasites, while *Leishmania* and *T. cruzi* are kinetoplastid parasites characterised by the presence of at least one of the life cycle stages of a

kinetoplast and a flagellum. *T. cruzi* and *Leishmania* can mainly invade macrophages but *T. cruzi* can also invade non-phagocytic cells. Conversely, *Toxoplasma* can invade nucleated type cells of the long living tissue such as muscle and neuronal cells, and cells from the intestinal tract (Webster, 2010; David Sibley, 2011).

Along the manuscript, the treatment and the challenges of fighting malaria and leishmaniasis have been mentioned. This last section of the Discussion will focus on toxoplasmosis and Chagas disease. The first line treatment of *T. gondii* is the combination of pyrimethamine and sulfadiazine which can be replaced by clindamycin, and alternative treatments are atovaquone or azythromicin combined with the first line treatment (Katlama *et al.*, 1996). Some of these drugs are antimalarial, and although both *Plasmodium* and *Toxoplasma* are apicomplexan parasites, analysis of the *Toxoplasma* genome, life cycle, hosts, etc. has highlighted large differences between these two parasites (Holland Alday and Stone Doggett, 2017). Moreover, most of these drug combinations cause severe side effects in patients with *Toxoplasma* and mostly in patients suffering from encephalitis, leading to treatment discontinuation. The presence of side effects and the differences between *Plasmodium* and *Toxoplasma* suggest that more specifically designed drugs would be more efficient (Webster, 2010). First line treatment for *T. cruzi* includes benznidazole and nifurtimox, which are given orally and cause high toxicity. Unfortunately, to date no alternative treatment is available (Barrett and Croft, 2012; Walker *et al.*, 2014).

Despite the high prevalence of toxoplasmosis and Chagas disease, there is currently only a handful of first line treatments available for these disease, with scarce or inexistent alternatives for toxoplasma and Chagas disease, respectively. Moreover, most of these treatments are characterised by severe side effects due to the accumulation of toxic derivative products. They also increase parasitic resistance, making it imperative to develop new products with low toxicity while maintaining high antiparasitic efficacy (Bermudez *et al.*, 2016).

Up to now, no pharmaceutical treatment has the ability to cross biological barriers, reach a specific target, or minimise the toxic side effects of toxoplasmosis or Chagas diseases, similarly to what occurs with malaria and leishmaniasis. Consequently, it has become crucial to optimise the treatments currently available. Branquinho *et al*. in their study worked with mice suffering from chronic Chagas, which involves possible irreversible heart damage, and obtained better intravenously treatment with encapsulated drug than with free drug. The carrier used was a biodegradable polymeric nanocapsule, which, moreover, had the capability to shield and deliver the drug and protect against the side effects of the free form (Branquinho *et al.*, 2017). For *Toxoplasma*, several nanoparticles are under study, such as chitosan and silver NPs (Gaafar *et al.*, 2014), nanosuspensions (Dunay *et al.*, 2004) and polylactide polymeric nanocapsules (Dalençon *et al.*, 1997) encapsulating atovaquone, which presents low solubility. In all cases, the encapsulations presented better efficacy than the free drugs in rodent models.

Additional investigation on ISA23 should be carried out since according to fluorescence microscopy analysis it can be incorporated by macrophages, at least those of the tumour mouse cell line (RAW 264.7) 90 min after incubation. ISA23 is the only PAA of the four tested which is predominantly anionic, suggesting higher affinity for macrophages lipid bilayers and interacting with cell membranes and vesicular extracellular structures. Consequently, ISA23 could be a novel nanocarrier to treat intracellular parasites other than *Plasmodium*, such as *Leishmania* and *T. cruzi*, which also infect macrophages. Taking into account that *T. gondii* infects nucleated cells, it might be interesting to explore the behaviour of ISA23 with other cell types. Moreover, ISA23 could also be used to treat common coinfections of these 4 pathogens.

On the other hand, the two branched polymers investigated, DHP-bMPA and HDLDBC-bGMPA, were incorporated by human umbilical vein endothelial cells (HUVEC) in different locations. DHP-bMPA was found exclusively in the nucleus, whereas HDLDBC-bGMPA was in the cytosol (Figure 25 B). When *T. cruzi* invades non-phagocytic cells such as HUVEC cells, it seems to be found in the border between the nucleus and the cytosol but with a cytosolic localisation (Figure 25 A) (Libisch *et al.*, 2018). Therefore, HDLDBC-bGMPA, a new hybrid dendritic-linear-dendritic block copolymer that self-assembles in micelles is worth exploring for the delivery of drugs to fight Chagas disease to the target site more efficiently and with less toxicity.

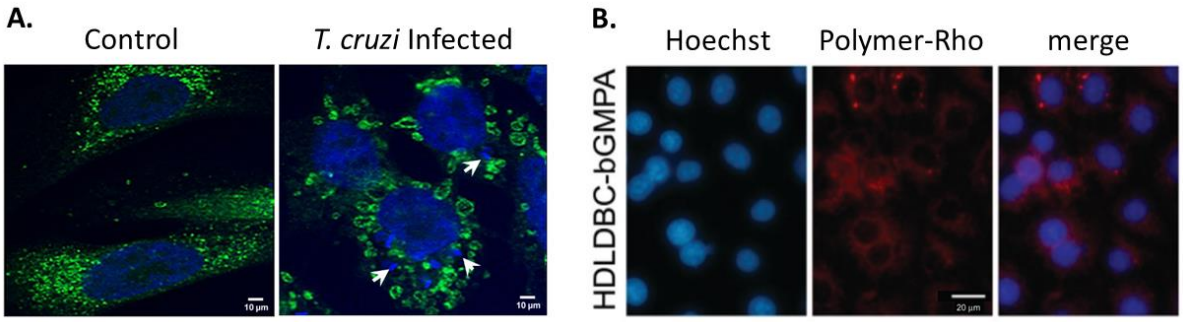

Figure 25. (A) Confocal microscopy images of HUVEC cells infected with *T. cruzi* shown by white arrows. For the experiments anti-cytochrome c antibody (dilution 1/100) and DAPI were used for DNA staining 24 hours post ingestion (Libisch *et al.*, 2018). (B) Fluorescence microscopy images of HUVEC incubated with HDLDBC-bGMPA, which shows a cytosolic localization (Martí Coma-Cros *et al.*, 2019).

Therefore, it can be concluded that PAAs and dendrimers have potential as nanocarriers of drugs for the treatment of diverse parasitic diseases.

CONCLUSIONS

The conclusions of this thesis are the following ones:

1.1 Different linear (PAA-based) and branched (dendrimer-based) polymers have been identified that do not cause unspecific toxicity in HUVEC cells and neither haemolysis in red blood cells, in concentrations much higher than those required for *in vivo* experiments.

1.2 A size decrease of dendrimeric polymers from >150 nm to <30 nm contributed to the reduction of unspecific toxicity. However, increasing size to 50 nm and improving drug release (as much as 35% of CQ remained stably encapsulated) might ameliorate the pharmacokinetics and the antimalarial activity of the encapsulations.

2.1 Different types of linear and branched polymers targeted pRBCs:

- Dendrimeric DHP-bMPA targeted specifically pRBCs (vs. RBCs) whereas HDLDBC-bGMPA targeted both.
- All PAA-based linear polymers behaved similarly in terms of pRBC (vs. RBC) specific targeting.

2.2 Specific targeting can be improved by functionalizing nanocarriers with targeting molecules like heparin. AGMA1 *in vitro* showed a concentration-dependent decrease of *P. falciparum* invasion rate, suggesting a potential antimalarial activity of AGMA1 similar to that described for heparin (i.e. binding to merozoites leading to invasion inhibition).

2.3 DHP-bMPA and HDLDBC-bGMPA also bind *P. falciparum* merozoites *in vitro*.

2.4 DHP-bMPA and HDLDBC-bGMPA have been observed to be internalized in HUVEC cells, whereas the PAA ISA23 has been shown to enter macrophages, which opens perpectives for these polymers to be applied to the treatment of other intracellular parasitic diseases such as Leishmaniasis, Chagas disease and Toxoplasmosis, or to coinfections of it/these with malaria.

3. The mechanism of specific pRBC vs. RBC targeting of linear PAA-based polymers might be based on a generalized adhesiveness to *Plasmodium*-specific proteins.

4.1 After intravenous administration to *P. yoelii*-infected mice of dendrimer-based polymers, HDLDBC-bGMPA showed better performance than DHP-bMPA, most likely due to its capacity to target both infected and non-infected RBCs observed in in vitro assays.

4.2 Oral administration of encapsulations in the PAA-based linear polymers AGMA1, ISA23 and ARGO7 slightly improved CQ activity relative to the free drug.

5. PAAs accumulate in the midgut of *Anopheles stephensi* and *Anopheles gambiae* mosquitoes, where part of the parasite development process occurs. Thus PAAs are potential nanocarriers of drugs against specific mosquito stages, to be delivered directly to the insect.

References

Acquah, F. K. *et al.* (2019) 'Transmission-Blocking Vaccines: Old Friends and New Prospects', *Infection and Immunity*. Edited by A. T. Maurelli, 87(6), pp. 1–19.

Aditya, N. P. *et al.* (2013) 'Advances in nanomedicines for malaria treatment', *Advances in Colloid and Interface Science*. Elsevier B.V., 201–202, pp. 1–17.

Agrawal, P., Gupta, U. and Jain, N. K. Ã. (2007) 'Glycoconjugated peptide dendrimers-based nanoparticulate system for the delivery of chloroquine phosphate', *Biomaterials*, 28, pp. 3349–3359.

Akhoundi, M. *et al.* (2016) 'A Historical Overview of the Classification, Evolution, and Dispersion of Leishmania Parasites and Sandflies', *PLoS Neglected Tropical Diseases*, 10(3), pp. 1–40.

Albrecht, L. *et al.* (2011) 'var gene transcription and PfEMP1 expression in the rosetting and cytoadhesive Plasmodium falciparum clone FCR3S1.2', *Malaria Journal*, 10(1), p. 17.

Alexis, F. *et al.* (2008) 'Factors affecting the clearance and biodistribution of polymeric nanoparticles', *Molecular Pharmaceutics*, 5(4), pp. 505–515.

Almela, M. J. *et al.* (2012) 'Activity of Clinically Relevant Antimalarial Drugs on Plasmodium falciparum Mature Gametocytes in an ATP Bioluminescence "'Transmission Blocking'" Assay', *PLoS ONE*, 7(4), pp. 1–8.

Alonso, M. J. (2004) 'Nanomedicines for overcoming biological barriers', *Biomedicine and Pharmacotherapy*, 58(3), pp. 168–172.

Aly, A. S. I., Vaughan, A. M. and Kappe, S. H. I. (2009) 'Malaria Parasite Development in the Mosquito and Infection of the Mammalian Host', *Annual Review of Microbiology*, 63(1), pp. 195–221.

Amaratunga, C. *et al.* (2016) 'Dihydroartemisinin-piperaquine resistance in Plasmodium falciparum malaria in Cambodia: A multisite prospective cohort study', *The Lancet Infectious Diseases*. Elsevier Ltd, 16(3), pp. 357–365.

Amponsah, A. O., Vosper, H. and Marfo, A. F. A. (2015) 'Patient Related Factors Affecting Adherence to Antimalarial Medication in an Urban Estate in Ghana', *Malaria Research and Treatment*, 2015, pp. 1–8.

Anand, P. *et al.* (2007) 'Bioavailability of Curcumin : Problems and Promises reviews Bioavailability of Curcumin : Problems and Promises', *Molecular Pharmacology*, 4(November), pp. 807–818.

Angulo-Barturen, I. *et al.* (2008) 'A murine model of falciparum-malaria by in vivo selection of competent strains in non-myelodepleted mice engrafted with human erythrocytes', *PLoS ONE*, 3(5).

Anyanwu, P. E. *et al.* (2017) 'Exploring the role of socioeconomic factors in the development and spread of anti-malarial drug resistance: a qualitative study', *Malaria Journal*. BioMed Central, 16(1), pp. 1–15.

Araújo, C. C. and Leon, L. L. (2001) 'Biological activities of Curcuma longa L.', *Memorias do Instituto Oswaldo Cruz*, 96(5), pp. 723–8.

Arnold, L. *et al.* (2011) 'Further improvements of the P. falciparum humanized mouse model', *PLoS ONE*, 6(3).

Ashley, E. A., Pyae Phyo, A. and Woodrow, C. J. (2018) 'Malaria', *The Lancet*, 391.

Ashley, E. and White, N. (2014) 'The duration of Plasmodium falciparum infections', *Malaria Journal*, 13(1), p. 500.

Aspinall, A. (2015) 'Adherence to antimalarial treatments in the real world – does it really matter ?', *Medicine for Malaria Venture*, pp. 19–21.

Attlmayr, B. *et al.* (2006) 'In vitro antimalarial drug resistance in Southeastern Bangladesh', *Wiener klinische Wochenschrift*, 118(S3), pp. 58–61.

Auparakkitanon, S. *et al.* (2003) 'Antimalarial 9-Anilinoacridine Compounds Directed at Hematin', *Antimicrobial Agents and Chemotherapy*, 47(12), pp. 3708–3712.

Baer, K. *et al.* (2007) 'Release of Hepatic Plasmodium yoelii Merozoites into the Pulmonary Microvasculature', 3(11).

Bailey, J. W. *et al.* (2013) 'Guideline: The laboratory diagnosis of malaria', *British Journal of Haematology*, 163(5), pp. 573–580.

Baird, J. K. (2004) 'Chloroquine Resistance in Plasmodium vivax', *Antimicro. Agents Chemo.*, 48(11), pp. 4075–4083.

Bakar, N. A. *et al.* (2010) 'Digestive-vacuole genesis and endocytic processes in the early intraerythrocytic stages of Plasmodium falciparum', *Journal of Cell Science*, 123(3), pp. 441–450.

Balducci, A. G. *et al.* (2016) 'From tablets to pharmaceutical nanotechnologies: Innovation in drug delivery strategies for the administration of antimalarial drugs', *Journal of Drug Delivery Science and Technology*. Elsevier Ltd, 32, pp. 167–173.

Bannister, L. H. *et al.* (2000) 'A Brief Illustrated Guide to the Ultrastructure of Plasmodium falciparum Asexual Blood Stages', *Molecular Approaches to Malaria*, 4758(1998), pp. 427–433.

Barber, B. E. *et al.* (2017) 'The Treatment of Plasmodium knowlesi Malaria', *Trends in Parasitology*. Elsevier Ltd, 33(3), pp. 242–253.

Barrett, M. P. and Croft, S. L. (2012) 'Management of trypanosomiasis and leishmaniasis', *British Medical Bulletin*, 104(1), pp. 175–196.

Basore, K. *et al.* (2015) 'How do antimalarial drugs reach their intracellular targets?', *Frontiers in Pharmacology*, 6(MAY), pp. 1–7.

Baton, L. A. and Ranford-Cartwright, L. C. (2005) 'How do malaria ookinetes cross the mosquito midgut wall?', *Trends in Parasitology*, 21(1), pp. 22–28.

Belachew, E. B. (2018) 'Immune Response and Evasion Mechanisms of Plasmodium falciparum Parasites', *Journal of Immunology Research*, 2018.

Bell, D. *et al.* (2016) 'Development of new malaria diagnostics: matching performance and need', *Malaria Journal*. BioMed Central, 15(1), pp. 1–12.

Bennis, I. *et al.* (2018) 'Psychosocial burden of localised cutaneous Leishmaniasis: A scoping review', *BMC Public Health*. BMC Public Health, 18(1), pp. 1–12.

Bermudez, J. *et al.* (2016) 'Current drug therapy and pharmaceutical challenges for Chagas disease', *Acta Tropica*, 156, pp. 1–16.

Bern, C. *et al.* (2006) 'Liposomal Amphotericin B for the Treatment of Visceral Leishmaniasis', *Clinical Infectious Diseases*, 43(7), pp. 917–924.

Besteiro, S. *et al.* (2007) 'Protein turnover and differentiation in Leishmania', *International Journal for Parasitology*, 37(10), pp. 1063–1075.

Bhatt, S. *et al.* (2015) 'The effect of malaria control on Plasmodium falciparum in Africa between 2000 and 2015.', *Nature*, 526(7572), pp. 207–211.

Bhatt, S. *et al.* (2016) 'The effect of malaria control on Plasmodium falciparum in Africa between 2000 and 2015', 526(7572), pp. 207–211.

Biamonte, M. A., Wanner, J. and Le Roch, K. G. (2013) 'Recent advances in malaria drug discovery', *Bioorganic and Medicinal Chemistry Letters*. Elsevier Ltd, 23(10), pp. 2829–2843.

Blanazs, A., Armes, S. P. and Ryan, A. J. (2009) 'Self-Assembled Block Copolymer Aggregates: From Micelles to Vesicles and their Biological Applications', *Macromolecular Rapid Communications*, 30, pp. 267–277.

Boggild, A. K. *et al.* (2007) 'Atovaquone-Proguanil: Report From the Cdc Expert Meeting on Malaria

Chemoprophylaxis (II)', *The American journal of tropical medicine and hygiene*, 76(2), pp. 208–223.

Boyle, M. *et al.* (2010) 'Interactions with heparinlikemolecules during erythrocyte invasion by Plasmodium falciparum merozoites', *Blood*, 115(22), pp. 4559–4568.

Branquinho, R. T. *et al.* (2017) 'Biodegradable Polymeric Nanocapsules Prevent Cardiotoxicity of Anti-Trypanosomal Lychnopholide', *Scientific Reports*. Nature Publishing Group, 7(August 2016), pp. 1–13.

Bruni, N. *et al.* (2017) 'Nanostructured delivery systems with improved leishmanicidal activity: A critical review', *International Journal of Nanomedicine*, 12, pp. 5289–5311.

Bruxvoort, K. *et al.* (2014) 'How patients take malaria treatment: A systematic review of the literature on adherence to antimalarial drugs', *PLoS ONE*, 9(1).

Buffet, P. A. *et al.* (2018) 'Review article The pathogenesis of Plasmodium falciparum malaria in humans : insights from splenic physiology stages of the parasite that develop inside', *Blood Journal*, 117(2), pp. 1–3.

Bugno, J., Hsu, H. and Hong, S. (2015) 'Recent advances in targeted drug delivery approaches using dendritic polymers', *Biomaterials Science*, 3(7), pp. 1025–1034.

Burrows, J. N. *et al.* (2017) 'New developments in anti-malarial target candidate and product profiles', *Malaria Journal*. BioMed Central, 16(1), pp. 1–29.

Cabral-Miranda, G. *et al.* (2017) 'Microcrystalline Tyrosine (MCT®): A Depot Adjuvant in Licensed Allergy Immunotherapy Offers New Opportunities in Malaria', *Vaccines*, 5(4), p. 32.

Calderón, M. *et al.* (2007) 'Synthesis and Characterization of Dendronized Polymers', *Macromolecular Symposia*, 258, pp. 53–62.

Carlson, J. (1993) 'Erythrocyte rosetting in Plasmodium falciparum malaria--with special reference to the pathogenesis of cerebral malaria.', *Scandinavian journal of infectious diseases. Supplementum*, 86, pp. 1–79.

Carlton, J. M. *et al.* (2002) 'Genome sequence and comparative analysis of the model rodent malaria parasite Plasmodium yoelii yoelii', *Nature*, 419(6906), pp. 512–519.

Carter, R. and Diggs, C. (1977) 'Plasmodia of rodents', *Parasitic Protozoa Academic Press, New York*, III, pp. 359–465.

Chaccour, C., Hammann, F. and Rabinovich, N. R. (2017) 'Ivermectin to reduce malaria transmission I. Pharmacokinetic and pharmacodynamic considerations regarding efficacy and safety', *Malaria Journal*. BioMed Central, 16(1), pp. 1–16.

Chaccour, C. J. *et al.* (2013) 'Ivermectin to reduce malaria transmission: a research agenda for a promising new tool for elimination', *Malaria Journal*, 12(1), p. 153.

Chalapareddy, S. and Desai, S. A. (2017) 'Malaria parasite proteins involved in nutrient channels at the host erythrocyte membrane: advances and questions for future research.', *International journal of current multidisciplinary studies*, 3(3), pp. 619–623.

Chango, A. and Abdennebi-Najar, L. (2011) 'Folate metabolism pathway and Plasmodium falciparum malaria infection in pregnancy', *Nutrition Reviews*, 69(1), pp. 34–40.

Chen, J. *et al.* (2010) 'Insights into the role of heme in the mechanism of action of antimalarials', *ACS Chemical Biology*, 50(5), pp. 294–306.

Chinappi, M. *et al.* (2010) 'On the mechanism of chloroquine resistance in Plasmodium falciparum', *PLoS ONE*, 5(11).

Coelho, C. H. *et al.* (2017) 'Advances in malaria vaccine development: Report from the 2017 malaria vaccine symposium', *npj Vaccines*. Springer US, 2(1).

Couvreur, P. and Vauthier, C. (2006) 'Nanotechnology: Intelligent Design to Treat Complex Disease',

Pharmaceutical Research, 23(7), pp. 1417–1450.

Cowman, A. F. *et al.* (2017) 'Review The Molecular Basis of Erythrocyte Invasion by Malaria Parasites', *Cell Host and Microbe*. Elsevier Inc., 22(2), pp. 232–245.

Cowman, A. F. and Crabb, B. S. (2006) 'Invasion of red blood cells by malaria parasites', *Cell*, 124(4), pp. 755–766.

Craig, A. G. *et al.* (2012) 'The role of animal models for research on severe malaria', *PLoS Pathogens*, 8(2).

Dahl, E. L. and Rosenthal, P. J. (2007) 'Multiple antibiotics exert delayed effects against the Plasmodium falciparum apicoplast', *Antimicrobial Agents and Chemotherapy*, 51(10), pp. 3485–3490.

Dalençon, F. *et al.* (1997) 'Atovaquone and rifabutine-loaded nanocapsules: formulation studies', *International Journal of Pharmaceutics*, 153(1), pp. 127–130.

Date, A. A., Hanes, J. and Ensign, L. M. (2016) 'Nanoparticles for oral delivery: Design, evaluation and state-of-the-art', *Journal of Controlled Release*, 240, pp. 504–526.

Date, A. A., Joshi, M. D. and Patravale, V. B. (2007) 'Parasitic diseases: Liposomes and polymeric nanoparticles versus lipid nanoparticles', *Advanced Drug Delivery Reviews*, 59(6), pp. 505–521.

David Sibley, L. (2011) 'Invasion and intracellular survival by protozoan parasites', *Immunological Reviews*, 240(1), pp. 72–91.

Deligianni, E. *et al.* (2018) 'Essential role of Plasmodium perforin-like protein 4 in ookinete midgut passage', *PLOS ONE*. Edited by T. Spielmann, 13(8), p. e0201651.

Delves, M. *et al.* (2012) 'The activities of current antimalarial drugs on the life cycle stages of plasmodium: A comparative study with human and rodent parasites', *PLoS Medicine*, 9(2).

Deng, C. *et al.* (2018) 'Large-scale Artemisinin – Piperaquine Mass Drug Administration With or Without Primaquine Dramatically Reduces Malaria in a Highly Endemic Region of Africa', (May), pp. 1–7.

Dennis, E., Peoples, V. and Johnson, F. (2015) 'Utilizing Nanotechnology to Combat Malaria', *Journal of Infectious Diseases & Therapy*, 03(04).

Desai, S. A. (2012) 'Ion and nutrient uptake by malaria parasite-infected erythrocytes', *Cellular Microbiology*, 14(7), pp. 1003–1009.

Desai, S. A. (2014) 'Why do malaria parasites increase host erythrocyte permeability ?', *Trends in Parasitology*. Elsevier Ltd, 30(3), pp. 151–159.

Desai, S. A. et al. (2000) 'A voltage-dependent channel involved in nutrient uptake by red blood cells infected with the malaria parasite. (news article on page 949', *Nature 406: 1001-1005*, 406(August), pp. 1001–1005.

Desai, S. A. and Miller, L. H. (2015) 'Protein–export pathway illuminated', *NIH Public Access*, 511(7511), pp. 541–542.

Dilnawaz, F. (2017) 'Polymeric Biomaterial and Lipid Based Nanoparticles for Oral Drug Delivery', *Current Medicinal Chemistry*, 24(22), pp. 2423–2438.

Dubey, J. P. (2016) *Toxoplasmosis of Animals and Humans*. CRC Press.

Dunay, I. R. *et al.* (2004) 'Atovaquone Maintenance Therapy Prevents Reactivation of Toxoplasmic Encephalitis in a Murine Model of Reactivated Toxoplasmosis', *Antimicrobial Agents and Chemotherapy*, 48(12), pp. 4848–4854.

Ensign, L. M., Cone, R. and Hanes, J. (2012) 'Oral drug delivery with polymeric nanoparticles: The gastrointestinal mucus barriers', *Advanced Drug Delivery Reviews*. Elsevier B.V., 64(6), pp. 557–570.

Esch, K. J. and Petersen, C. A. (2013) 'Transmission and Epidemiology of Zoonotic Protozoal Diseases of

Companion Animals', *Clinical microbiology reviews*, 26(1), pp. 58–85.

Feng, H. *et al.* (2017) 'Block Copolymers: Synthesis, Self-Assembly, and Applications', *Polymers*, 9, p. 494.

Fernàndez-Busquets, X. (2016) 'Novel strategies for Plasmodium -targeted drug delivery', *Expert Opinion on Drug Delivery*. Taylor & Francis, 13(7), pp. 919–922.

Ferruti, P. *et al.* (2000) 'Amphoteric Linear Poly(amido-amine)s as Endosomolytic Polymers : Correlation between Physicochemical and Biological Properties', *Macromolecules*, 33, pp. 7793–7800.

Ferruti, P. *et al.* (2007) 'Prevailingly cationic agmatine-based amphoteric polyamidoamine as a nontoxic, nonhemolytic, and "stealthlike" DNA complexing agent and transfection promoter', *Biomacromolecules*, 8(5), pp. 1498–1504.

Ferruti, P. (2013) 'Poly(amidoamine)s: Past, Present, and Perspectives', *Polymer Chemistry*, 1, pp. 2319–2353.

Ferruti, P. *et al.* (2014) 'Amphoteric , Prevailingly Cationic L-Arginine Polymers of Poly(amidoamino acid) Structure: Synthesis, Acid/Base Properties and Preliminary Cytocompatibility and', *Macromolecular Bioscience*, 14, pp. 390–400.

Ferruti, P., Marchisio, M. A. and Duncan, R. (2002) 'Poly(amido-amine)s: Biomedical Applications', *Macromolecular Rapid Communications*, 23(5), pp. 332–355.

Foote, S. J. and Cowman, a F. (1994) 'The mode of action and the mechanism of resistance to antimalarial drugs.', *Acta tropica*, 56(2–3), pp. 157–171.

Franchini, J. *et al.* (2006) 'Synthesis , Physicochemical Properties , and Preliminary Biological Characterizations of a Novel Amphoteric Agmatine-Based Poly(amidoamine) with RGD-Like Repeating Units', *Biomacromolecules*, 7, pp. 1215–1222.

Frauenrath, H. (2005) 'Dendronized polymers — building a new bridge from molecules to nanoscopic objects', 30, pp. 325–384.

Fu, Y. *et al.* (2012) 'Comparative Histopathology of Mice Infected With the 17XL and 17XNL Strains of Plasmodium yoelii', *Journal of Parasitology*, 98(2), pp. 310–315.

de Fuentes-Vicente, J. A. *et al.* (2018) 'What makes an effective Chagas disease vector? Factors underlying Trypanosoma cruzi -triatomine interactions', *Acta Tropica*, 183, pp. 23–31.

Gaafar, M. R. *et al.* (2014) 'Chitosan and silver nanoparticles: Promising anti-toxoplasma agents', *Experimental Parasitology*, 143, pp. 30–38.

Gallup, J. L. and Sachs, J. D. (1998) 'The economic burden of malaria.', *The American journal of tropical medicine and hygiene*, 64(1–2 Suppl), pp. 85–96.

Gao, C. and Yan, D. (2004) 'Hyperbranched polymers: from synthesis to applications', 29, pp. 183–275.

García-Basteiro, A. L., Bassat, Q. and Alonso, P. L. (2012) 'Approaching the Target: the Path Towards an Effective Malaria Vaccine', *Mediterranean jornal of hematology and infectious diseases*, 4(1).

Garnett, M. C. (2001) 'Targeted drug conjugates: Principles and progress', *Advanced Drug Delivery Reviews*, 53(2), pp. 171–216.

Gbalégba, C. G. N. *et al.* (2018) 'Distribution of Plasmodium spp . infection in asymptomatic carriers in perennial and low seasonal malaria transmission settings in West Africa', *Infectious Diseases of Poverty*. Infectious Diseases of Poverty, 7, p. 39.

Georgiadou, S. P., Makaritsis, K. P. and Dalekos, G. N. (2015) 'Leishmaniasis revisited : Current aspects on epidemiology , diagnosis and treatment', *Journal of Translational Internal Medicine*, 3(2), pp. 43–50.

Gherbawy, Y. *et al.* (2013) 'The Anti-Fasciolasis Properties of Silver Nanoparticles Produced by Trichoderma harzianum and Their Improvement of the Anti-Fasciolasis Drug Triclabendazole', *International Journal of*

Molecular Sciences, 14(11), pp. 21887–21898.

Ghodratollah, S. *et al.* (2015) 'Identification of Leishmania species by kinetoplast DNA-polymerase chain reaction for the first time in Khaf district, Khorasan-e-Razavi province, Iran', *Tropical Parasitology*, 5(1), p. 50.

Gilson, P. R. *et al.* (2017) 'Host cell remodelling in malaria parasites : a new pool of potential drug targets', *International Journal for Parasitology*. Australian Society for Parasitology, 47(2–3), pp. 119–127.

Ginsburg, H. *et al.* (1998) 'Inhibition of glutathione-dependent degradation of heme by chloroquine and amodiaquine as a possible basis for their antimalarial mode of action.', *Biochemical pharmacology*, 56(10), pp. 1305–13.

Ginsburg, H. and Stein, W. D. (2005) 'How many functional transport pathways does Plasmodium falciparum induce in the membrane of its host erythrocyte?', *Trends in Parasitology*, 21(3), pp. 118–121.

Gomes, A. *et al.* (2014) 'N-cinnamoylation of antimalarial classics: Quinacrine analogues with decreased toxicity and dual-stage activity', *ChemMedChem*, 9(2), pp. 305–310.

González Canga, A. *et al.* (2008) 'The Pharmacokinetics and Interactions of Ivermectin in Humans—A Mini-review', *The AAPS Journal*, 10(1), pp. 42–46.

Goodyer, I. D. *et al.* (1997) 'Characterization of macromolecular transport pathways in malaria-infected erythrocytes.', *Molecular and biochemical parasitology*, 87(1), pp. 13–28.

Gref, R. *et al.* (1995) 'The controlled intravenous delivery of drugs using PEG-coated sterically stabilized nanospheres', *Advanced Drug Delivery Reviews*, 16(2–3), pp. 215–233.

Gregoriadis, G. (1988) 'Liposomes as a Drug Delivery System: Optimization Studies', in, pp. 151–159.

van Griensven, J. and Diro, E. (2019) 'Visceral Leishmaniasis Recent Advances in Diagnostic and Treatment Regimens', *Infectious Disease Clinics of North America*. Elsevier Inc, 33(1), pp. 79–99.

Griffiths, P. C. *et al.* (2013) 'Self-Assembled PAA-Based Nanoparticles as Potential Gene and Protein Delivery Systems a', pp. 641–649.

Grimaldi, G. and Tesh, R. B. (1993) 'Leishmaniases of the New World: current concepts and implications for future research.', *Clinical microbiology reviews*, 6(3), pp. 230–250.

Groger, M. *et al.* (2017) 'A systematic review of the clinical presentation, treatment and relapse characteristics of human Plasmodium ovale malaria', *Malaria Journal*. BioMed Central, 16(1), pp. 1–16.

Grüring C1, Heiber A, Kruse F, Ungefehr J, Gilberger TW, S. T. (2011) 'Development and host cell modifications of Plasmodium falciparum blood stages in four dimensions', *Nature Communications*, 25(2), p. 165.

Guizetti, J., Scherf, A. and Biologie, U. De (2013) 'Silence, activate, poise and switch! Mechanisms of antigenic variation in Plasmodium falciparum', *Cellular Microbiology*, 15(5), pp. 718–726.

Guo, Z. (2016) 'Artemisinin anti-malarial drugs in China', *Acta Pharmaceutica Sinica B*. Elsevier, 6(2), pp. 115–124.

Gutiérrez, V. *et al.* (2015) 'New approaches from nanomedicine for treating leishmaniasis', *Chem. Soc. Rev.*, pp. 152–168.

Hauck, T. S. *et al.* (2010) 'Nanotechnology diagnostics for infectious diseases prevalent in developing countries ☆', *Advanced Drug Delivery Reviews*. Elsevier B.V., 62(4–5), pp. 438–448.

Hawker, C. and Fréchet, J. M. (1990) 'Preparation of Polymers with Controlled Molecular Architecture. A New Convergent Approach to Dendritic Macromolecules', *Journal of the American Chemical Society*, 1(2), pp. 7638–7647.

Healer, J. *et al.* (2017) 'Vaccines to Accelerate Malaria Elimination and Eventual Eradication', *Cold Spring Harbor Perspectives in Medicine*, 7(9), p. a025627.

Hemingway, J., Ranson, H., *et al.* (2016) 'Averting a malaria disaster: Will insecticide resistance derail malaria control?', *The Lancet*, 387(10029), pp. 1785–1788.

Hemingway, J., Shretta, R., *et al.* (2016) 'Tools and Strategies for Malaria Control and Elimination: What Do We Need to Achieve a Grand Convergence in Malaria?', *PLoS Biology*, 14(3), pp. 1–14.

Hetzel, M. W. and Genton, B. (2018) 'Mass drug administration for malaria elimination: Do we understand the settings well enough?', *BMC Medicine*. BMC Medicine, 16(1), pp. 1–3.

Hirsh, J. and Fuster, V. (2001) 'Guide to anticoagulant therapy: Heparin: A Statement for Healthcare Professionals From the American Heart Association', *American Heart Association*, 103(24), pp. 2994–3018.

Holland Alday, P. and Stone Doggett, J. (2017) 'Drug Design, Development and Therapy Dovepress Drugs in development for toxoplasmosis: advances, challenges, and current status', *Drug Design, Development and therapy*, 11, pp. 273–293.

Hopkins, H. *et al.* (2007) 'Comparison of Hrp2- and P Ldh-Based Rapid Diagnostic Tests for Malaria With Longitudinal Follow-Up in Kampala , Uganda', *Tropical Medicine*, 76(6), pp. 1092–1097.

Howes, R. E. *et al.* (2016) 'Global epidemiology of Plasmodium vivax', *American Journal of Tropical Medicine and Hygiene*, 95(Suppl 6), pp. 15–34.

Huang, W. *et al.* (2018) 'A malaria vaccine adjuvant based on recombinant antigen binding to liposomes', *Nature Nanotechnology*. Springer US, 13(12), pp. 1174–1181.

Huijben, S. and Paaijmans, K. P. (2018) 'Putting evolution in elimination: Winning our ongoing battle with evolving malaria mosquitoes and parasites', *Evolutionary Applications*, 11(4), pp. 415–430.

Ito, D., Schureck, M. A. and Desai, S. A. (2017) 'An essential dual-function complex mediates erythrocyte invasion and channel-mediated nutrient uptake in malaria parasites', *eLife*, 6, pp. 1–24.

Jadhav, P., Jadhav, M. and Shah, R. (2012) 'Important advances in malaria vaccine research', *Chronicles of Young Scientists*, 3(2), p. 111.

Jones, R. A., Panda, S. S. and Hall, C. D. (2015) 'Quinine conjugates and quinine analogues as potential antimalarial agents', *European Journal of Medicinal Chemistry*. Elsevier Masson SAS, 97(1), pp. 335–355.

Kaehler, N. *et al.* (2018) 'The promise, problems and pitfalls of mass drug administration for malaria elimination: a qualitative study with scientists and policymakers.', *International health*, 3(11).

Kaphingst, K. A., Persky, S. and Lachance, C. (2010) 'Discovery, mechanisms of action and combination therapy of artemisinin', *Expert Review of Anti-Infective Therapy*, 14(4), pp. 384–399.

Kappe, S. H. I. *et al.* (2010) 'That Was Then But This Is Now : Malaria Research in the Time of an', *Science*, 328(May), p. 862.

Karunamoorthi, K. (2014) 'The counterfeit anti-malarial is a crime against humanity: A systematic review of the scientific evidence', *Malaria Journal*, 13(1), pp. 1–13.

Katlama, C. *et al.* (1996) 'Pyrimethamine-Clindamycin vs. Pyrimethamine-Sulfadiazine as Acute and Long-Term Therapy for Toxoplasmic Encephalitis in Patients with AIDS', *Clinical Infectious Diseases*, 22(2), pp. 268–275.

Kavishe, R. A., Koenderink, J. B. and Alifrangis, M. (2017) 'Oxidative stress in malaria and artemisinin combination therapy: Pros and Cons', *FEBS Journal*, 284(16), pp. 2579–2591.

Kesharwani, P., Jain, K. and Jain, N. K. (2014) 'Dendrimer as nanocarrier for drug delivery', *Progress in Polymer Science*. Elsevier Ltd, 39(2), pp. 268–307.

Kiboi, D. M. *et al.* (2009) 'Plasmodium berghei ANKA: Selection of resistance to piperaquine and lumefantrine in a mouse model', *Experimental Parasitology*, 122(3), pp. 196–202.

Kicska, G. a *et al.* (2003) 'Effect of dietary p-aminobenzoic acid on murine Plasmodium yoelii infection.', *The Journal of infectious diseases*, 188(11), pp. 1776–1781.

Kim, B. Y. S., Rutka, J. T. and Chan, W. C. W. (2010) 'Nanomedicine', *New England Journal of Medicine*, 363(25), pp. 2434–2443.

Kirk, K. (2001) 'Membrane transport in the malaria-infected erythrocyte.', *Physiological reviews*, 81(2), pp. 495–537.

Koning-ward, T. F. De *et al.* (2016) 'Plasmodium species : master renovators of their host cells', *Nature Publishing Group*. Nature Publishing Group, 14(8), pp. 494–507.

Krampa, F. *et al.* (2017) 'Recent Progress in the Development of Diagnostic Tests for Malaria', *Diagnostics*, 7(3), p. 54.

Krukemeyer, M., Krenn, V. and Huebner, F. (2015) 'History and Possible Uses of Nanomedicine Based on Nanoparticles and Nanotechnological Progress', *Journal of Nanomedicine & Nanotechnology*, 06(06).

Kulane, A. *et al.* (1992) 'Effect of different fractions of heparin on Plasmodium falciparum merozoite invasion of red blood cells in vitro.', *The American journal of tropical medicine and hygiene*, 46(5), pp. 589–94.

Kumar, C. S. S. R. (2009) 'Nanotechnology tools in pharmaceutical R&D', *Materials Today*. Elsevier Ltd, 12(SUPPL.), pp. 24–30.

Kumar, S. *et al.* (2007) 'Antimalarial drugs inhibiting hemozoin (β-hematin) formation: A mechanistic update', *Life Sciences*, 80(9), pp. 813–828.

Kumar, S. *et al.* (2018) 'Drug targets for resistant malaria: Historic to future perspectives', *Biomedicine & Pharmacotherapy*. Elsevier, 104(3), pp. 8–27.

Kumar, S. and Bandyopadhyay, U. (2005) 'Free heme toxicity and its detoxification systems in human', *Toxicology Letters*, 157(3), pp. 175–188.

Kumari, A., Yadav, S. K. and Yadav, S. C. (2010) 'Biodegradable polymeric nanoparticles based drug delivery systems', *Colloids and Surfaces B: Biointerfaces*, 75(1), pp. 1–18.

Kundu, C. N. *et al.* (2015) 'Anti-malarials are anti-cancers and vice versa - One arrow two sparrows', *Acta Tropica*. Elsevier B.V., 149, pp. 113–127.

Langford, S. *et al.* (2015) 'Plasmodium malariae Infection Associated with a High Burden of Anemia: A Hospital-Based Surveillance Study', *PLoS Neglected Tropical Diseases*, 9(12), pp. 1–16.

Lardeux, F. J. *et al.* (2008) 'A physiological time analysis of the duration of the gonotrophic cycle of Anopheles pseudopunctipennis and its implications for malaria transmission in Bolivia', *Malaria Journal*, 7(1), p. 141.

Lau, Y.-L. *et al.* (2013) 'Acute respiratory distress syndrome and acute renal failure from Plasmodium ovale infection with fatal outcome', *Malaria Journal*. Malaria Journal, 12(1), p. 389.

Lauletta, J. A. *et al.* (2018) 'Visceral leishmaniasis and HIV coinfection: current perspectives', *HIV/AIDS - Research and Palliative Care*, 10, pp. 193–201.

Lavazec, C. (2017) 'Molecular mechanisms of deformability of Plasmodium -infected erythrocytes', *Current Opinion in Microbiology*. Elsevier Ltd, 40, pp. 138–144.

Li, M. *et al.* (2019) 'Composition design and medical application of liposomes', *European Journal of Medicinal Chemistry*, 164, pp. 640–653.

Libisch, M. G. *et al.* (2018) 'Early Trypanosoma cruzi infection triggers mTORC1-mediated respiration increase and mitochondrial biogenesis in human primary cardiomyocytes', *Frontiers in Microbiology*, 9(AUG), pp. 1–14.

Liechty, W. B. *et al.* (2010) 'Polymers for Drug Delivery Systems', *Annual Review of Chemical and Biomolecular Engineering*, 1(1), pp. 149–173.

Liu, H. *et al.* (2014) 'Fluorinated poly(propylenimine) dendrimers as gene vectors', *Biomaterials*. Elsevier Ltd, 35(20), pp. 5407–5413.

Liu, M. and Fréchet, J. M. J. (1999) 'Designing dendrimers for drug delivery', *Pharmaceutical Science and Technology Today*, 2(10), pp. 393–401.

Lockman, P. R. *et al.* (2002) 'Nanoparticle technology for drug delivery across the blood-brain barrier', *Drug Development and Industrial Pharmacy*, 28(1), pp. 1–13.

Lucca, R. M. R. de *et al.* (2015) 'Genotoxic effects of the antimalarial drug Lumefantrine in human lymphocytes in vitro and computational prediction of the mechanism associated with its interaction with DNA', *Environmental and Molecular Mutagenesis*, 56, pp. 556–562.

MacE, K. E. *et al.* (2011) 'Adherence to treatment with artemether-lumefantrine for uncomplicated Malaria in Rural Malawi', *Clinical Infectious Diseases*, 53(8), pp. 772–779.

Maier, A. G. *et al.* (2009) 'Malaria parasite proteins that remodel the host erythrocyte', *Focus on Microbial Host Cell Subversion*, 7(may).

Malaria Vaccine Initiative (2009) 'RTS,S/AS01 Candidate Malaria vaccine Summary for the SAGE meeting', (10), pp. 1–14.

Manfredi, A. *et al.* (2007) 'Polymerization Kinetics of Poly(amidoamine)s in Different Solvents', *Journal of Bioactive and Caompatible Polymers*, 22, p. 219.

Manfredi, A. *et al.* (2017) 'Self-Ordering Secondary Structure of D-Arginine-Derived Polyamidoamino Acids', *ACS Macro Letters*, 6(9), pp. 987–991.

Marchisio, M. A., Longo, T. and Ferruti, P. (1973) 'A selective de-heparinizer filter made of new cross-linked polymers of a poly-amido-amine structure', *Experienta*, 29(1), pp. 93–5.

Maroli, M. *et al.* (2013) 'Phlebotomine sandflies and the spreading of leishmaniases and other diseases of public health concern', *Medical and Veterinary Entomology*, 27(2), pp. 123–47.

Marques, J. *et al.* (2014) 'Application of heparin as a dual agent with antimalarial and liposome targeting activities toward Plasmodium-infected red blood cells', *Nanomedicine: Nanotechnology, Biology, and Medicine*. Elsevier Inc., 10(8), pp. 1719–1728.

Marques, J. *et al.* (2017) 'Adaptation of targeted nanocarriers to changing requirements in antimalarial drug delivery', *Nanomedicine: Nanotechnology, Biology, and Medicine*. The Authors, 13(2), pp. 515–525.

Martí Coma-Cros, E. *et al.* (2019) 'Micelle carriers based on dendritic macromolecules containing bis-MPA Micelle carriers based on dendritic macromolecules containing bis-MPA and glycine for antimalarial drug delivery†', *Biomaterials Science*. Royal Society of Chemistry, 7(4), pp. 1661–1674.

Marti, M. *et al.* (2004) 'Targeting malaria virulence and remodeling proteins to the host erythrocyte', *Science*, 306(5703), pp. 1930–1933.

Matthews, H., Hanison, J. and Nirmalan, N. (2016) '"Omics"-Informed Drug and Biomarker Discovery: Opportunities, Challenges and Future Perspectives', *Proteomes*, 4(3), p. 28.

Mbai, M., Rajamani, S. and January, C. T. (2002) 'The anti-malarial drug halofantrine and its metabolite N - desbutylhalofantrine block HERG potassium channels', 55(August), pp. 799–805.

Meier, A., Erler, H. and Beitz, E. (2018) 'Targeting Channels and Transporters in Protozoan Parasite Infections', *Frontiers in Chemistry*, 6(March), p. 88.

Mhlwatika, Z. and Aderibigbe, B. A. (2018) 'Application of Dendrimers for the Treatment', *Molecules*, 23(9), p. 2205.

Michel, G. *et al.* (2011) 'Importance of worldwide asymptomatic carriers of Leishmania infantum (L. chagasi)

in human', *Acta tropica*, 119, pp. 69–75.

Millholland, M. G. *et al.* (2011) 'The Malaria Parasite Progressively Dismantles the Host Erythrocyte Cytoskeleton for Efficient Egress', *Molecular & Cellular Proteomics*, 10(12), p. M111.010678.

Mohandas, N. and Gallagher, P. G. (2018) 'Red cell membrane : past, present, and future', *Blood Journal*, 112(10), pp. 3939–3949.

Moles, E. *et al.* (2015) 'Immunoliposome-mediated drug delivery to Plasmodium-infected and non-infected red blood cells as a dual therapeutic/prophylactic antimalarial strategy', *Journal of Controlled Release*. Elsevier B.V., 210, pp. 217–229.

Moore, L. R. *et al.* (2006) 'Hemoglobin degradation in malaria-infected erythrocytes determined from live cell magnetophoresis', *The FASEB Journal*, 20(6), pp. 747–749.

Moradin, N. and Descoteaux, A. (2012) 'Leishmania promastigotes: building a safe niche within macrophages.', *Frontiers in cellular and infection microbiology*, 2(September), p. 121.

Morales-Orue, I., Chicas-Sett, R. and Lara, P. C. (2019) 'Nanoparticles as a promising method to enhance the abscopal effect in the era of new targeted therapies', *Reports of Practical Oncology and Radiotherapy*. Greater Poland Cancer Centre, 24(1), pp. 86–91.

Movellan, J. *et al.* (2014) 'Amphiphilic dendritic derivatives as nanocarriers for the targeted delivery of antimalarial drugs', *Biomaterials*, 35(27), pp. 7940–7950.

Munir, M. *et al.* (1980) 'Heparin in the treatment of cerebral malaria.', *Paediatrica Indonesiana*, 20(1–2), pp. 47–50.

Murambiwa, P. *et al.* (2011) 'Anti-malarial drug formulations and novel delivery systems: A review', *Acta Tropica*. Elsevier B.V., 118(2), pp. 71–79.

Mvango, S. *et al.* (2018) 'Nanomedicines for Malaria Chemotherapy: Encapsulation vs. Polymer Therapeutics', *Pharmaceutical Research*. Pharmaceutical Research, 35(12), p. 237.

Na-Bangchang, K. and Karbwang, J. (2009) 'Current status of malaria chemotherapy and the role of pharmacology in antimalarial drug research and development', *Fundamental and Clinical Pharmacology*, 23(4), pp. 387–409.

Najer, A. *et al.* (2014) 'Nanomimics of Host Cell Membranes Block Invasion and Expose Invasive Malaria Parasites', *ACS Nano*, 8(12), pp. 12560–12571.

Najer, A. *et al.* (2016) 'Giant Host Red Blood Cell Membrane Mimicking Polymersomes Bind Parasite Proteins and Malaria Parasites', *Chimia International Journal for Chemistry*, 70(4), pp. 288–291.

Najer, A. *et al.* (2018) 'Challenges in Malaria Management and a Glimpse at Some Nanotechnological Approaches', in Adhikari, R. and Thapa, S. (eds) *Infectious Diseases and Nanomedicine III*. Singapore: Springer Singapore (Advances in Experimental Medicine and Biology), pp. 103–112.

Newby, G. *et al.* (2015) 'Review of mass drug administration for malaria and its operational challenges', *American Journal of Tropical Medicine and Hygiene*, 93(1), pp. 125–134.

Nogueira, E. *et al.* (2015) 'Design of liposomal formulations for cell targeting', *Colloids and Surfaces B: Biointerfaces*. Elsevier B.V., 136, pp. 514–526.

Oakes, R. S. and Jewell, C. M. (2018) 'A plug-and-play approach for malaria vaccination', *Nature Nanotechnology*, 13(12), pp. 1096–1097.

Olliaro, P. L. and Yuthavong, Y. (1999) 'An Overview of Chemotherapeutic Targets for Antimalarial Drug Discovery', *Pharmacology & Therapeutics*, 81(2), pp. 91–110.

Otto, T. D. *et al.* (2014) 'A comprehensive evaluation of rodent malaria parasite genomes and gene

expression', *BMC Biology*, 12(1), p. 86.

Ouattara, A. and Laurens, M. B. (2015) 'Vaccines against malaria', *Clinical Infectious Diseases*, 60(6), pp. 930–936.

Paaijmans, K. and Fernàndez-Busquets, X. (2014) 'Antimalarial drug delivery to the mosquito: an option worth exploring?', *Future Microbiology*, 9(5), pp. 579–582.

Palma, E. *et al.* (2018) 'Antileishmanial Activity of Amphotericin B-loaded-PLGA Nanoparticles: An Overview', *Materials*, 11(7), p. 1167.

Panneerselvam, S. and Choi, S. (2014) 'Nanoinformatics : Emerging Databases and Available Tools', pp. 7158–7182.

Partnership, S. C. T. (2015) 'Efficacy and safety of RTS,S/AS01 malaria vaccine with or without a booster dose in infants and children in Africa: fi nal results of a phase 3, individually randomised, controlled trial', *The Lancet*. Elsevier Ltd, 386(9988), pp. 31–45.

PATH Malaria Vaccine Initiative (2018) 'The RTS,S malaria vaccine'.

Paul, R. E. L. and Brey, P. T. (2003) 'Malaria parasites and red blood cells: from anaemia to transmission.', *Molecules and cells*, 15(2), pp. 139–149.

Pearson, R. *et al.* (2012) 'Dendritic nanoparticles: The next generation of nanocarriers?', *Therapeutic delivery*, 3(8), pp. 941–59.

Pearson, T., Greiner, D. L. and Shultz, L. D. (2008) 'Creation of "Humanized" Mice to Study Human Immunity', *Current protocols in immunology*, 15.

Plapied, L. *et al.* (2011) 'Fate of polymeric nanocarriers for oral drug delivery', *Current Opinion in Colloid and Interface Science*. Elsevier Ltd, 16(3), pp. 228–237.

Portugal, S., Drakesmith, H. and Mota, M. M. (2011) 'Superinfection in malaria: Plasmodium shows its iron will', *EMBO Reports*. Nature Publishing Group, 12(12), pp. 1233–1242.

Prajapati, V. K. *et al.* (2011) 'Targeted killing of leishmania donovani in vivo and in vitro with amphotericin β attached to functionalized carbon nanotubes', *Journal of Antimicrobial Chemotherapy*, 66(4), pp. 874–879.

Prajapati, V. K. *et al.* (2012) 'An oral formulation of amphotericin B attached to functionalized carbon nanotubes is an effective treatment for experimental visceral leishmaniasis', *Journal of Infectious Diseases*, 205(2), pp. 333–336.

Proellocks, N. I. *et al.* (2016) *Malaria Parasite Proteins and Their Role in Alteration of the Structure and Function of Red Blood Cells*, *Advances in Parasitology*. Elsevier Ltd.

Pulkki-Brännström, A.-M. *et al.* (2012) 'Cost and cost effectiveness of long-lasting insecticide-treated bed nets - a model-based analysis', *Cost Effectiveness and Resource Allocation*, 10(1), p. 5.

Ragavan, K. V. *et al.* (2018) 'Advances in biosensors and optical assays for diagnosis and detection of malaria', *Biosensors and Bioelectronics*. Elsevier B.V., 105(November 2017), pp. 188–210.

Rai, M. *et al.* (2017) 'Recent advances in use of silver nanoparticles as antimalarial agents', *International Journal of Pharmaceutics*. Elsevier B.V., 526(1–2), pp. 254–270.

Ramalho, D. B. *et al.* (2018) 'Meglumine antimoniate intralesional infiltration for localised cutaneous leishmaniasis: a single arm, open label, phase II clinical trial', *Memorias do Instituto Oswaldo Cruz*, 113(9), p. e180200.

Rampengan, T. (1991) 'Cerebral malaria in children. Comparative study between heparin, dexamethasone and placebo.', *Paediatrica Indonesiana*, 31(1), pp. 59–66.

Ranucci E, Spagnoli G, Ferruti P, Sgouras D, D. R. (1991) 'Poly(amidoamine)s with potential as drug carriers:

degradation and cellular toxicity.', *Biomaterials Science*, 2(4), pp. 303–15.

Raza, A. *et al.* (2019) 'Solid nanoparticles for oral antimicrobial drug delivery: a review', *Drug Discovery Today*. Elsevier Ltd, 00(1).

Reddy, R. C. *et al.* (2005) 'Curcumin for malaria therapy', *Biochemical and Biophysical Research Communications*, 326(2), pp. 472–474.

Reithinger, R. *et al.* (2007) 'Cutaneous leishmaniasis', *The Lancet Infectious Diseases*, 7(9), pp. 581–596.

Richardson, S. C. W. *et al.* (2001) 'Poly(Amidoamine)s as Potential Nonviral Vectors: Ability to Form Interpolyelectrolyte Complexes and to Mediate Transfection in Vitro', *Biomacromolecules*, 2, pp. 1023–1028.

Richardson, S., Ferruti, P. and Duncan, R. (2009) 'Poly(amidoamine)s as Potential Endosomolytic Polymers: Evaluation In Vitro and Body Distribution in Normal and Tumour-Bearing Animals', *Journal of Drug Targeting*, 6(6), pp. 391–404.

Riehle, M. A. *et al.* (2003) 'Towards genetic manipulation of wild mosquito populations to combat malaria: advances and challenges', *Journal of Experimental Biology*, 206(21), pp. 3809–3816.

Roberts, B. P. *et al.* (2009) 'Molecular Dynamics of Poly(L-lysine) Dendrimers with Naphthalene Disulfonate Caps', *Macromolecules*, 42, pp. 2775–2783.

Roser, M. and Ritchie, H. (2017) 'Malaria', (12).

Sachs, J. and Malaney, P. (2002) 'The economic and social burden of malaria', *Nature*, 415(6872), pp. 680–685.

Santos-Magalhães, N. S. and Mosqueira, V. C. F. (2010) 'Nanotechnology applied to the treatment of malaria', *Advanced Drug Delivery Reviews*. Elsevier B.V., 62(4–5), pp. 560–575.

Schrier, S. L. (2018) 'What does the spleen see?', *Blood*, 120(2), pp. 242–244.

Seeber, F. and Steinfelder, S. (2016) 'Recent advances in understanding apicomplexan parasites', *F1000Research*, 5(0), p. 1369.

von Seidlein, L. *et al.* (2019) 'The impact of targeted malaria elimination with mass drug administrations on falciparum malaria in southeast Asia: A cluster randomised trial', *PLoS Medicine*, 16(2), pp. 1–26.

Selvapandiyan, A., Dey, R. and Gannavaram, S. (2014) 'Generation of growth arrested Leishmania amastigotes : A tool to develop live attenuated vaccine candidates against visceral leishmaniasis', *Vaccine*. Elsevier Ltd, 32(31), pp. 3895–3901.

Shaw, C. and Carter, K. (2014) 'Drug delivery: lessons to be learnt from Leishmania studies.', *Nanomedicine (London, England)*, 9(10), pp. 1531–44.

Shaw, D. L. (2017) 'Is Open Science the Future of Drug Development?', *The Yale journal of biology and medicine*, 90(1), pp. 147–151.

Shretta, R. *et al.* (2019) 'Predicting the cost of malaria elimination in the Asia-Pacific', *Wellcome Open Research*, 4, p. 73.

Shretta, R., Avanceña, A. L. V. and Hatefi, A. (2016) 'The economics of malaria control and elimination: a systematic review', *Malaria Journal*. BioMed Central, 15(1), p. 593.

Sibley, C. H. *et al.* (2001) 'Pyrimethamine–sulfadoxine resistance in Plasmodium falciparum: what next?', *Trends in Parasitology*, 17(12), pp. 582–588.

Sinden, R. E. *et al.* (2012) 'The biology of sexual development of Plasmodium: The design and implementation of transmission-blocking strategies', *Malaria Journal*. BioMed Central Ltd, 11(1), p. 70.

Sinden, R. E. (2017) *Targeting the Parasite to Suppress Malaria Transmission*, *Advances in Parasitology*.

Elsevier Ltd.

Singhal, A. and Gupta, C. M. (1986) 'Antibody-mediated targeting of liposomes to red cells in vivo', *FEBS Letters*, 201(2), pp. 321–326.

Skidmore, M. A. *et al.* (2008) 'Disruption of rosetting in Plasmodium falciparum malaria with chemically modified heparin and low molecular weight derivatives possessing reduced anticoagulant and other serine protease inhibition activities', *Journal of Medicinal Chemistry*, 51(5), pp. 1453–1458.

Slater, A. F. G. (1993) 'Chloroquine: Mechanism of drug action and resistance in plasmodium falciparum', *Pharmacology & Therapeutics*, 57(2–3), pp. 203–235.

Smith, D. L. *et al.* (2007) 'Standardizing estimates of the Plasmodium falciparum parasite rate', *Malaria Journal*, 6(1), p. 131.

Smith, J. D. *et al.* (2014) 'Malaria's Deadly Grip: Cytoadhesion of Plasmodium falciparum infected erythrocytes', *Cellular Microbiology*, 15(12), pp. 1–13.

Sousa-Batista, A. and Rossi-Bergmann, B. (2018) 'Nanomedicines for Cutaneous Leishmaniasis', in *Leishmaniases as Re-emerging Diseases*. InTech.

Sowinska, M. and Urbanczyk-Lipkowska, Z. (2014) 'Advances in the chemistry of dendrimers', *New Journal of Chemistry*, 38(6), p. 2168.

Srinivasan, P. *et al.* (2011) 'Binding of Plasmodium merozoite proteins RON2 and AMA1 triggers commitment to invasion.', *Proceedings of the National Academy of Sciences of the United States of America*, 108(32), pp. 13275–80.

Staines, H. M., Rae, C. and Kirk, K. (2000) 'Increased permeability of the malaria-infected erythrocyte to organic cations', *Biochimica et Biophysica Acta - Biomembranes*, 1463(1), pp. 88–98.

Steverding, D. (2017) 'The history of leishmaniasis', *Parasite & Vectors*. Parasites & Vectors, 10(2), pp. 1–10.

Sugiarto, S. R., Davis, T. M. E. and Salman, S. (2017) 'Pharmacokinetic considerations for use of artemisinin-based combination therapies against falciparum malaria in different ethnic populations', *Expert Opinion on Drug Metabolism & Toxicology*. Taylor & Francis, 13(11), pp. 1115–1133.

Sun, T. *et al.* (2014) 'Engineered Nanoparticles for Drug Delivery in Cancer Therapy', *Angewandte Chemie International Edition*, 53, pp. 12320–12364.

Sundar, S. and Chakravarty, J. (2015) 'An update on pharmacotherapy for leishmaniasis', *Expert Opinion on Pharmacotherapy*, 16(2), pp. 237–252.

Sutherland, C. J. (2016) 'Persistent Parasitism: The Adaptive Biology of Malariae and Ovale Malaria', *Trends in Parasitology*. Elsevier Ltd, 32(10), pp. 808–819.

Taylor, B. J. *et al.* (2014) 'A lab-on-chip for malaria diagnosis and surveillance', *Malaria Journal*, 13, p. 179.

Teixeira, M. C., Carbone, C. and Souto, E. B. (2017) 'Beyond liposomes: Recent advances on lipid based nanostructures for poorly soluble/poorly permeable drug delivery', *Progress in Lipid Research*. Elsevier, 68(August), pp. 1–11.

Teklehaimanot, A. and Mejia, P. (2008) 'Malaria and poverty', *Annals of the New York Academy of Sciences*, 1136, pp. 32–37.

Thakkar, M. and Brijesh, S. (2016) 'Combating malaria with nanotechnology-based targeted and combinatorial drug delivery strategies', *Drug Delivery and Translational Research*. Drug Delivery and Translational Research, 6(4), pp. 414–425.

Tizifa, T. a. *et al.* (2018) 'Prevention Efforts for Malaria', *Current Tropical Medicine Reports*. Current Tropical Medicine Reports, pp. 41–50.

Tomalia, D. A. (1985) 'A New Class of Polymers : Starburst-Dendritic Macromolecules', *Polymer Journal*, 17(June), pp. 117–132.

Torres-Guerrero, E. *et al.* (2017) 'Leishmaniasis: a review', *F1000Research*, 6(5), pp. 1–15.

Tse, E. G., Korsik, M. and Todd, M. H. (2019) 'The past , present and future of anti - malarial medicines', *Malaria Journal*. BioMed Central, pp. 1–21.

Twibanire, J. d'Amour K. and Grindley, T. B. (2014) 'Polyester dendrimers: Smart carriers for drug delivery', *Polymers*, 6(1), pp. 179–213.

Unicef (2007) *Malaria and children: progress and intervention coverage. New York*, *Unicef*.

UNITAID (2014) 'Malaria Diagnostics Technology and Market Landscape, 2014', *Unitaid Secretariat World Health Organization*, 28(July), pp. 1–148.

Urbán, P. *et al.* (2011) 'Study of the efficacy of antimalarial drugs delivered inside targeted immunoliposomal nanovectors', *Nanoscale Research Letters*, 6, pp. 1–16.

Urbán, P. *et al.* (2014) 'Use of poly(amidoamine) drug conjugates for the delivery of antimalarials to Plasmodium', *Journal of Controlled Release*, 177, pp. 84–95.

Urbán, P. and Fernàndez-Busquets, X. (2014) 'Nanomedicine Against Malaria', *Current Medicinal Chemistry*, 21(5), pp. 605–629.

Urbán, P., Ranucci, E. and Fernàndez-Busquets, X. (2015) 'Polyamidoamine nanoparticles as nanocarriers for the drug delivery to malaria parasite stages in the mosquito vector.', *Nanomedicine (London, England)*, 10(22), pp. 3401–14.

Valle-Delgado, J. J., Urbán, P. and Fernàndez-Busquets, X. (2013) 'Demonstration of specific binding of heparin to Plasmodium falciparum-infected vs. non-infected red blood cells by single-molecule force spectroscopy', *Nanoscale*, 5(9), pp. 3673–3680.

Van de Ven, H. *et al.* (2012) 'PLGA nanoparticles and nanosuspensions with amphotericin B: Potent in vitro and in vivo alternatives to Fungizone and AmBisome', *Journal of Controlled Release*, 161(3), pp. 795–803.

Venturoli, D. and Rippe, B. (2005) 'Ficoll and dextran vs. globular proteins as probes for testing glomerular permselectivity: effects of molecular size, shape, charge, and deformability', *American Journal of Physiology-Renal Physiology*, 288(4), pp. F605–F613.

Voit, B. I. and Lederer, A. (2009) 'Hyperbranched and Highly Branched Polymer Architectures - Synthetic Strategies and Major Characterization Aspects', *Chemical Reviews*, 109(11), pp. 5924–5973.

de Vries, H. J. C., Reedijk, S. H. and Schallig, H. D. F. H. (2015) 'Cutaneous Leishmaniasis: Recent Developments in Diagnosis and Management', *American Journal of Clinical Dermatology*, 16(2), pp. 99–109.

Vries, P. J. and Dien, T. K. (1996) 'Clinical pharmacology and therapeutic potential of artemisinin and its derivatives in the treatment of malaria.', *Drugs*, 52(6), pp. 818–36.

Walker, D. M. *et al.* (2014) 'Mechanisms of cellular invasion by intracellular parasites', *Cellular and Molecular Life Sciences*, 71(7), pp. 1245–1263.

Wang, L. *et al.* (2008) 'Synthesis of hybrid linear-dendritic block copolymers with carboxylic functional groups for the biomimetic mineralization of calcium carbonate', *Polymer*. Elsevier Ltd, 49(5), pp. 1199–1210.

Wang, Y. *et al.* (2017) 'Application of nanodiagnostics in point-of-care tests for infectious diseases', *International Journal of Nanomedicine*, 12, pp. 4789–4803.

Webster, J. P. (2010) 'Review of "Toxoplasmosis of Animals and Humans (Second Edition)" by J.P. Dubey', *Parasites & Vectors*, 3(1), p. 112.

Wells, T. N. C., Alonso, P. L. and Gutteridge, W. E. (2009) 'New medicines to improve control and contribute

to the eradication of malaria', *Nature Reviews Drug Discovery*, 8(11), pp. 879–891.

Wells, T. N. C., Van Huijsduijnen, R. H. and Van Voorhis, W. C. (2015) 'Malaria medicines: A glass half full?', *Nature Reviews Drug Discovery*. Nature Publishing Group, 14(6), pp. 424–442.

White, N. J. (2008) 'Plasmodium knowlesi: The Fifth Human Malaria Parasite', *Clinical Infectious Diseases*, 46(2), pp. 172–173.

White, N. J. (2008) 'The role of anti-malarial drugs in eliminating malaria', *Malaria Journal*, 7(S1), p. S8.

WHO (2010) 'Control of the leishmaniases', (March), pp. 22–26.

WHO (2019) 'Leishmaniasis: Key facts'.

WHO Global Malaria Programme (2015) 'The role of mass drug administration , mass screening and treatment , and focal screening and treatment for malaria. WHO reference number: WHO/HTM/GMP/2015.8'.

WHO, R. M. P. (2015) 'Action and investment to defeat malaria 2016-2030. For a malaria free world.', pp. 1–104.

WHO and UNICEF (2015) 'Achieving the malaria MDG target: reversing the incidence of malaria 2000-2015', *Unicef*, p. 32.

Winstanley, P. and Ward, S. (2006) 'Malaria Chemotherapy', *Advances in parasitology*, 61(05).

Wong, W. *et al.* (2017) 'Mefloquine targets the Plasmodium falciparum 80S ribosome to inhibit protein synthesis', *Nature Microbiology*, 2.

World Health Organisation (2017) *World Malaria Report 2017*.

World Health Organisation (2018) *World malaria report 2018*.

World Health Organization (2015a) 'Guidelines for the treatment of Malaria', *Guidelines For The Treatment of Malaria*, pp. 71–88.

World Health Organization (2015b) 'World Malaria Report 2015'.

World Health Organization (2017a) *A Framework for Malaria Elimination*.

World Health Organization (2017b) *Mass Drug Administration for Falciparum Malaria*.

Wu, W. *et al.* (2015) 'Main chain dendronized hyperbranched polymers: convenient synthesis and good second-order nonlinear optical performance†', *Polymer Chemistry*. Royal Society of Chemistry, 6, pp. 4396–4403.

Yamanaka, Y. J. and Leong, K. W. (2008) 'Engineering strategies to enhance nanoparticle-mediated oral delivery.', *Journal of biomaterials science. Polymer edition*, 19(12), pp. 1549–70.

Yardley, V. and Croft, S. L. (2000) 'A comparison of the activities of three amphotericin B lipid formulations against experimental visceral and cutaneous leishmaniasis', *International Journal of Antimicrobial Agents*, 13(4), pp. 243–248.

Yeboah-Antwi, K. *et al.* (2001) 'Impact of prepackaging antimalarial drugs on cost to patients and compliance with treatment TT - Impact du préconditionnement des antipaludiques sur le coût pour le patient et l'observance du traitement TT - Repercusión del preenvasado de los medicament', *Bulletin of the World Health Organization*, 79(5), pp. 394–399.

Zijlstra, E. E. *et al.* (1992) 'Kala-azar: a comparative study of parasitological methods and the direct agglutination test in diagnosis.', *Transactions of the Royal Society of Tropical Medicine and Hygiene*, 86(5), pp. 505–7.

Zuber, J. A. and Takala-Harrison, S. (2018) 'Multidrug-resistant malaria and the impact of mass drug administration', *Infection and Drug Resistance*, 11, pp. 299–306.

ACKNOWLEDGMENTS

Fa molt temps, una mica més de 10 anys, ja vaig clitxar el CRESIB com a lloc on m'agradaria treballar en algun moment de la vida. Durant el màster en indústria farmacèutica i biotecnologia vaig proposar al meu tutor i gran persona el Dr. Jaume Piulats de fer les pràctiques al CRESIB però ell va creure que la institució no era una biotecnològica com a tal. Intent nº 1 fallit. Un cop ja treballava a Advancell, vaig veure una oferta per anar a Moçambic al centre de recerca de Manhiça durant dos mesos, i vaig aplicar, però preferien metges. Intent nº 2 fallit. Així que me'n vaig oblidar durant un temps i els anys varen passar...

Vaig treballant a Advancell fins que va arribar la crisi i ens varen "convidar a anar-nos" a la meitat de la plantilla, però a mi ja m'estava bé, ja tenia altres coses al cap, un postgrau de societats africanes, fer pràctiques a Farmamundi i marxar cap a Londres. Dit i fet. Però quan portava quasi tres anys a Londres va sortir una oferta de feina al CRESIB, si encara CRESIB, és que ja tenim una edat i ja portem un temps per aquí, i semblava que em descrivís!! Això mateix va pensar un bon amic meu el futur doctor Joan Gómez. Vaig enviar el meu CV i la carta de motivació a un tal Dr. Fernàndez Busquets. Em vaig treure un viatge llampec a BCN de la màniga per fer un cafè/entrevista amb ell i així, el 2014, va començar la meva aventura del doctorat en nanomalària. Intent nº 3!! Això diuen, a la tercera va la vençuda, tot i que l'estada a Londres se'm va quedar curta. Qui sap...

Així que gràcies **XAVI** per donar oportunitats no només els estudiants de notes altíssimes, sinó a gent amb perfils diversos i alta motivació. Han estat un plaer tots aquests mesos, anys,... no sempre ha estat fàcil, potser no han anat com tu esperaves en un principi, entre embarassos i baixes maternals, però ens n'hem sortit! Gràcies

Si no arriba a ser pel Cariplo, la Dra. Elisabetta Ranucci i el Dr. Paolo Ferruti, no hi hauria hagut projecte, però mira que m'heu donat mals de cap, en serio. Bye bye PAA!!

Gràcies **JOANA** i **ERNEST** per acollir-me al nanogroup amb els braços oberts, per fer cafetons a l'entrada, per posar-me al dia del grup, per guiar-me en els primers experiments... Joana se te ocurrió irte a Londres de estancia pocos meses después de que yo llegara y dejarme a soles con Ernest, ya te

vale! Por cierto gracias por llevarte polímeros allí. Y me alegro un montón de que estés feliz en Portugal con tu pequeñín, muito obrigada por tudo! Ernest mmmm ets un crack, t'ho he dit sempre, però el teu sarcasme em descol·locava, espero que segueixi tot bé per Austràlia. En realitat, jo no volia que acabessis mai el teu doctorat, però va anar bé que t'anessis perquè així ens vàrem espavilar i perquè tu i l'Arnau junts, quin perill, i quin desordre! **ARNAU** gràcies per ser les meves mans durant l'embaràs de l'Orisha, i no només això, gràcies pel suport durant tots aquests anys, respondre els meus dubtes professionals i també de vida, compartit bons moments, bogeries (això va més per tu) i penes, però sempre amb un gran somriure. Ha estat un gust treballar amb tu, tot i el teu caos. Però t'ho he dit moltes vegades, crec que hem estat un bon equip, tu el científic boig i jo l'organitzada. És fàcil treballar amb tu. **MIRIAM** gracias por ser nano ahora un 50%, ahora un 25%, y ahora…, yo ya me he perdido... Y no sólo por eso, tmb por nuestras conversaciones mañaneras de pañales, cacas, guarderías, dientes,... ¿Qué les harás para cenar hoy? **ELENA** gracias por formar parte del grupo y poner un poco de orden, una bronca de vez en cuando va bien. Por cierto, que estantería de la nevera es la tuya? No hemos compartido muchísimas comidas, pero si conversaciones entre poyatas. Gràcies a tots els Nanos, que heu estat molts i cada un a aportat el seu granet al grup. Tant als antics, **SILVIA**, **AIDA**, **ALBERT**, **LORIN**, **ALEX**, **LAURA** un extra gràcies, **LUCÍA** que montaña aún no has subido? Com els nous, **CARLOTA**, al final 100% nano, **INÉS**, me encantó conocerte aunque hayamos coincidido poco tiempo, **YUN,** vaya crack, yo quiero ver tu artículo acabado, **LÍVIA**, a ver que te depara el futuro, pero con lo hard-worker que eres seguro cosas buenas, **RENÉ**, enjoy your time here. **ALEX** y **ISABEL**, no habéis sido nano, pero más a menos, así que gracias por ayudarme en dos partes de mi doctorado, con los dendrimeros y con los *in vivo*, ha sido muy fácil y ágil trabajar con vosotros, y eso no pasa a menudo!

Gràcies a **TOTS** ELS **ISGLOBALS** de la planta 1 del CEK!! M'ha encantat compartir el meu doctorat en un ambient tant acollidor, de bon rotllo i d'ajuda mútua!!

MARI PONS tu presentaves quan vaig arribar, la veritat és que no vaig anar-hi perquè no sabia ni quina cara tenies... Ara sí! Gràcies pel collaret i per arribar sempre alegre amb notícies del Perú. Parlant de presentacions de tesi, **LAURA MORO** la tuya fue la primera de muchas y gracias por introducirme en el "Dia de la Ciencia", me gustó mucho participar. Que dir dels Epi? Jo vull ser un Epi! Creatius gràcies a la **ELI LA GUAPA**, mira que dir-me mamasitaaa!!, un plaer compartir nom amb una persona com tu, directe i transparent, riallera i amb bona energia, sempre fent activitats extra curriculars, que si forro, que si teatre, ara un soparet, un curs per fer cremes, cheerleader de l'equip de voleibol,..., gaudeix molt del canvi de vida! Centrats (en el lab) gràcies a l'**ORIOL**, con un toque de humor y malícia necesarios de la rubia **ANASTASIA**, molta sabiduria i també molta labia d'en **LUCAS**, with a perfect combination for funny, crazy, surrealistic and indispensable lunches with **HARVIE**, to keep up with the PhD every single day! I tots ben organitzats gràcies a la **NÚRIA**! I gràcies a tots els epis que heu sigut i sou molt acollidors: **CRISTINA**, **SOFIA**, me encanta hablar contigo y que te pasaras por Roses, **CARLA**, **JÚLIA** i **RAFA**.

Old glyco, **SILVIA**, **BORJA**, **MARTA**, **LING** gràcies per marcar les bases de com s'ha de fer un doctorat, que s'ha de treballar cada cap de setmana, de netejar les cabines, incubadors,... quan toca, de donar-nos enveja amb els vostres group-buildings i de compartir els vostres coneixements sobre merozoits. **MARTA** eres genial, siempre con una sonrisa, aunque te despiertes a las 6 o hayas corrido durante 2 h, por darme envidia de todo el deporte que haces y por organizar actividades para toda la planta. Y por escucharme en un momento triste de mi tesi. And new glyco, **NÚRIA**, **JORDI** i **ALEX**, sou molt de l'estil old glyco així que moleu molt!

PHILOSOPIÆ DOCTORS sou de lo millor que m'ha passat aquest any! Se que no us he pogut seguir massa el ritme de cines, sopars, birres, sortides de festa,... però una fa el que pot i els dinars ja feien molt. Gràcies per distreu-re el meu cap quan era necessari!

Que dir de l'altre costat, que faríem sense els Falcis, la old school amb saviesa, sempre al peu del canó i disposats a donar un cop de mà. Així que gràcies! **ALFONS** tens un cor enorme i uns nens preciosos, últimament ens faltava la teva música recorrent el lab, **DIANA** quien recogería el dinero para los regalos, sería un caos, **LAURA** vull enviar unes mostres amb gel sec, on faig seure el nou nano, l'organització en persona, **PAU** ja se pq vas de negre, **RUTH** hem compartit converses interessant a la cuina, **MARTA** super gràcies per organitzar calçotades macro i així poder-nos socialitzar fora del lab, **REBECCA** vaya vuelta de la boda del año! Per cert va ser genial compartir aquell dissabte mig plujós, mig assolellat però tan fantàstic amb molt de vosaltres! M'ho vaig passar molt bé! **AIDA** podria dir moltes coses de tu, però després d'aquella arribada triomfal a cavall m'he quedat sense paraules, només gràcies per convidar-me. I tots els que heu passat, que heu estat moltíssims, **ARIEL** me encantó volverte a ver, **XAVIER** espero que tot estigui anant genial per Holanda, **MERCEDES**, **HIMANCHU**, **ROBERT**, **HAILY**, **GEMMA**, **LAURA DE LA FUENTE** que ya estás!, **PATRICIA**, **ANA MARIA**,...

Vivax, us van desterrar, però segueixen havent coses vostres pel lab. **ALEIX**, **MIRIAM** y **ANA**, gràcies, va ser un guai compartir mesos o anys de doctorat amb vosaltres, hores de ratolins i de cultius. I tots als altres vivax que ja us he perdut la pista.

GER, doctora, gracias por escucharme y compartir, por dejarte llevar por los crazy-nanos a veces, por las conversaciones profundas y no tan profundas,... básicamente por ser como eres. Vaaaa que ya lo tenemos, por lo menos el mamotreto! Por cierto, el mamotreto sobre mi otro PhD, la vida, por ahora lo dejo para más adelante! Y el futuro, seguro que nos convence.

NÚRIA CORTÉS, un gust haver-te conegut tot i que mai hem coincidit massa entre els teus viatges a Can Ruti, USA, els teus cultius que no sé ni on estan,…

SILVIE, it was really enjoyable to share time, space and nice conversations about live with you. I am truly happy you found a very motivational work place to live with your amazing family.

I cap de "nosaltres no existiriem" sense els PI's: **LUÍS**, **ALFRED**, **CARLOTA**, **ALFREDO**, **HERNANDO** y **CARMEN**! Gràcies per voler investigar sobre la malària.

Aquest doctorat no ens podria haver fet sense l'ajuda de la **MARIA**, l'**ANNA** i l'**ELISENDA**, i els seus coneixements de microscòpia confocal, consells de com poder treure imatges perfectes del nostre estimat *Plasmodium*, suggeriments de quines cubetes usar,... gràcies! I tampoc sense l'ajuda de la gent de FACS, la **ISABEL**, les **CRISTINES** i la **SARA**, per deixar-me fer servir els citòmetres sense fer el curs, tenir paciència en ensenyar-me sense tenir una base, "ajudar-nos" a posar a punt la lectura de les parasitèmies dels ratolins,... gràcies! I moltes altres persones de serveis amb les que he hagut de treballar en algun moment.

CANALETA, no sé que faríem a la planta sense tu! Sort que als nano ens has clavat canya, que sinó això hauria estat un descontrol. Gràcies per tocar-nos el crostó quan cal i tenir sempre la mà oberta per ajudar-nos.

I gràcies també a la gent que ha estat al meu costat durant aquests anys fora del lab, compartint la vida, sopars, caps de setmana, els marrons amb els experiments, articles, ratolins,..., estones que abans

eren gintònics i ara són cafetons amb converses interrompudes per personetes de menys d'1 metre,... bàsicament fer-me desconnectar del PhD. **FAMILY**, **SISTER** gràcies per aquesta portada tan guai, les amigues del cole, **NURINS**, **CAROL**, **NÚRIA**, **VERO** i **MARIA** sabeu que ara això ja és per sempre eh!; **CARLA** i **LAURA**, sou genials però ens hem de veure més sovint; **JOAN** i **CINTA**, els meus metges preferits, d'aquí a poc Drs tmb; **ANNITA**, sort que em vas ensenyar a administrar fàrmacs per via oral; la gent de la capoeira, que sempre ha estat el meu moment de desconexió i socialització, dels antics ja quedeu pocs però ... **AVALANCHE**, **NAVY**, **OLGA**, **MAGO**,...

També gràcies al "lado oscuro", a MESA en particular per deixar-me seguir treballant amb la malària, **MARIA** no se que faria sense tu amb la **KATE** so far away! And **EBERÉ**, as I told you, it is kind of scary the amount of things we share, but very nice at the same time. Per suposat gràcies a totes les del 5-2ª de Rosselló 132, no ens coneixem gaire, però crec que sou un equip genial, curiós i interessant. Això si cadascú posa l'aire com li dona la gana!

And last but not least, thanks **MUYI** for bringing excitement to my flat line, you had been like a cardiogram, sometimes you made me high and sometimes you made me down but now we are in standby, thanks for being there all these years, before, during and after my PhD… thanks for moving back to Barcelona when I started, for being patient all these years, thanks for being my walking steak when I need it, and thanks for these amazing children's, **ORISHA** and **AKIN**. And extra thanks for being with them when I had to take care of the mice and the merozoites at untimed hours. That list would never finish, so just THANKS FOR BEING THE MUSIC while you were! Gràcies Orisha i Akin per alegrar-me les tardes, fer que m'oblidi de la feina només passar per la porta de casa, per tornar-me extremadament eficient durant les hores de feina, i per fer-me créixer en l'àmbit personal. Mami, vas a veure els ratolins? ☺